Strategies of Resource Allocation by Diatoms under Dynamic Light

Nerissa Lynn Fisher

PhD by Research

Submitted in fulfillment of the requirements for
the degree of Doctor of Philosophy

Climate Change Cluster
School of Life Sciences
University of Technology Sydney

May 2021

Certificate of original authorship

I, Nerissa Lynn Fisher, declare that this thesis is submitted in fulfillment of the requirements for the award of Doctorate of Philosophy in the Faculty of Science at the University of Technology Sydney.

This thesis is wholly my own work unless otherwise referenced or acknowledged.

In addition, I certify that all information sources and literature used are indicated in the thesis.

This document has not been submitted for qualifications at any other academic institution.

This thesis is supported by the Australian Government Research Training Program.

Signature:

Production Note:
Signature removed
prior to publication.

Nerissa Lynn Fisher

Date: 20th of May 2021

Acknowledgements

Foremost, I would like to thank David Suggett and Peter Ralph for taking me on as a student to complete this research and for your support and guidance throughout this journey.

I am extremely grateful to Kim Halsey for agreeing to be a co-advisor and for always looking at my work critically and thoroughly. Thank you for always being there to remind me that I could do it.

There were many people along the way who have helped keep me grounded and I am extremely grateful for their support. To name a few, Phoebe Argyle, Anna Bramucci, Sam Goyen, Dave Hughes, and James O'Brien were exceptionally invaluable for personal and science-related help. Technical help from Sue Fenech, Helen Price, Graeme Poleweski, Lochlan de Beyer, Scott Allchin and Paul Brooks are well-deserving of recognition. I am particularly grateful to Helen Price for introducing me to canyoning and for being an awesome dive buddy. Graeme Poleweski was an unwavering source of support over this journey and I cannot thank him enough for his kindness and friendship.

Those I was fortunate to meet who enjoyed hiking and camping as much as me, I had the most amazing adventures, incredible memories and friends for life. Thank you, Anne-Marie, Penny, Dave, Anton and Kat for making me feel part of the adventure crew.

I also had lots of support back home that deserve special recognition. Kristina Mojica (T1), thank you for being my rock through all the ups and downs that come with getting a PhD. Pete, Rob, Dana and Margo, I am grateful for your check-ins, listening to my rants and reminding me to stay strong.

It certainly takes a lot of persistence and resilience to finish a PhD. I owe it to my mom, dad and auntie (dearest of them all) for instilling these qualities in me and, of course, for their unconditional love and support. I look forward to whatever journey comes next.

Table of Contents

List of Figures

Chapter 1

Figure 1.3. Energy budgets from nutrient limited cultures of *Dunaliella tertiolecta* and *Thalassiosira weissflogii* (left and middle plots) and light-limited cultures of *Thalassiosira pseudonana* (right plot) at a range of specific growth rates using carbon- and oxygen-based measurements. Components measured to build the energy budgets included gross primary production (GP_{O2} or GPP_{O2}), gross carbon production (GP_C), net primary production (NP_{O2} or $NP_{O2/C}$) and net carbon production (NP_C or NPP_C). Sub-divisions of energy allocation include light dependent respiration (LDR), nitrogen and sulfur (N+S) reduction, mitochondrial respiration, reductants from carbon catabolism which is equivalent to biosynthesis of macromolecules and net carbon production which is equivalent to biomass. Figures adapted from Halsey et al. 2013 (left and middle plots) and Fisher & Halsey 2016 (right plot).

Figure 1.4. Photosynthesis-irradiance (PE) curves showing two fundamental descriptors of photosynthetic status: E_k-dependent variation (A) and E_k-independent variation (B) when photosynthesis is normalised to chlorophyll (subscript b). The PE curve is characterised by a light-saturated maximum rate of photosynthesis (P_{max}), light-limiting slope (α) and light saturation index (E_k).

Figure 1.5. Phases of FRRf method measuring fluorescence transients. Roman numerals represent the different phases and the times found above correlate to the duration of each phase. Single turnover (ST) flashes (Phases I and V) encompass a series of high frequency (0.5-2 μs intervals) flashlets (80-120). Multiple turnover (MT) flashes (Phase III) is similar to ST with more flashlets (~4000) at lower frequency (20-

200 μs intervals). Following each turnover phase (II, IV, and VI), there is a relaxation protocol of 40-80 flashlets at intervals exponentially varying (50 μs–50 ms). Each phase provides information on various fluorescence transients: I and V give variable fluorescence (F_v) from initial (F_o) and maximal (F_m) fluorescence, functional absorption cross-section (σ_{PSII}), and energy transfer between PSII reaction centres, RCII; II and VI give the kinetics of Q_A re-oxidation; IV give kinetics of PQ pool re-oxidation; III gives fluorescence yield under MT conditions thereby allowing the effects of earlier MT excitations on photosynthetic parameters to be quantified (V and VI).

Chapter 2

Figure 2.1. Initial photophysiological monitoring of seven diatoms: *Phaeodactylum tricornutum* (orange inverted triangles), *Chaetoceros muelleri* (yellow circles), *Ditylum brightwellii* (green diamonds), *Thalassiosira rotula* (black Xs), *Thalassiosira pseudonana* (black squares), *Thalassiosira weissflogii* (blue triangles), and *Thalassisosira oceanica* (red circles). (A) Yield of non-photochemical quenching (YNPQ; see Eq 3) with increasing light intensity. (B) Dynamic non-photochemical quenching [1-Q] versus photochemical [1-C], where data points signify responses to stepped increases in light intensity starting from 0 (far right point) to 1304 μmol photons m^{-2} s^{-1} (far left point) for 4 min at each light intensity. Error bars represent the standard error of the mean of at least *n*=3 for independent biological replicates.

Figure 2.2. YNPQ vs. de-epoxidation state (DPS) of the XC for *T. weissflogii* (blue triangles), *T. oceanica* (red circles), and *T. pseudonana* (black squares) under 10 min exposure to growth irradiance (Ig, 85 μmol photons m^{-2} s^{-1}, solid symbols) and high

light (HL, 1200 µmol photons m^{-2} s^{-1}, open symbols). Dashed lines highlight the extent of changes observed between light treatments for each measured parameter. Data averaged from three independent replicates for DPS and at least four independent replicates for YNPQ with errors bars representing SE of the mean.

Figure 2.3. Representative photo-inhibition and recovery time courses for *T. oceanica* (To), *T. pseudonana* (Tp) and *T. weissflogii* (Tw). Black points show individual determinations of F_v'/F_m' or F_v/F_m from FRRf measurements of cultures with PSII repair active (absence of lincomycin). Dashed orange line connects F_v'/F_m' measures taken immediately after exposure to HL (1200 µmol photons m^{-2} s^{-1}) over 0 – 120 min or recovery light (15 µmol photons m^{-2} s^{-1}) at 150 and 180 min, influenced by combined effects of non-photochemical quenching induction and net photo-inactivation (if any). Solid green line connects F_v/F_m taken after 10 min of subsequent dark for HL time points, to allow relaxation of non-photochemical quenching, or taken immediately during the recovery light period. These points were used to fit the Kok model of PSII photo-inactivation countered by repair. Note the different patterns and amplitudes of short-term (10 min) relaxation of non-photochemical quenching, among the species (black dots). The dotted red line shows F_v/F_m data from separate lincomycin treated cultures to show the underlying photo-inactivation in the absence of counteracting repair.

Figure 2.4. Mean YNPQ and YNPQ relaxation amplitude for *T. weissflogii*, *T. oceanica* and *T. pseudonana* after 120 min high light exposure. (A) Mean values of YNPQ vs. the rate constant for PSII repair, k_{REC}, over 120 min HL exposure showing

nonphotochemical quenching measured immediately after light exposure (larger symbols) or after 10 min dark FRRf incubation (smaller symbols) for *T. weissflogii* (Tw, blue triangles), *T. oceanica* (To, red diamonds) and *T. pseudonana* (Tp, black squares). (B) The amplitude of YNPQ relaxation (also green arrows in (A)). Error bars show standard errors of the estimates for 3 or 4 independent biological replicates.

Figure 2.5. Proportions of total photochemical energy (GP_{O2}) allocated to various oxygen pathways over a 20 min incubation under growth irradiance (Ig) and high light (HL). Fractional percentages of GP_{O2} included net oxygen production (Net_{O2}, grey), dark respiration (R_{DARK}, black) and light dependent respiration (LDR, white) in *T. weissflogii*, *T. oceanica*, and *T. pseudonana* under Ig (85 µmol photons m^{-2} s^{-1}) and HL (1200 µmol photons m^{-2} s^{-1}). Data averaged from 2 or 3 independent biological replicates with error bars representing SE of the mean.

Figure 2.6. The yield of non-photochemical quenching (YNPQ) versus light dependent respiration (LDR) as a % of GP_{O2} for *T. weissflogii* (blue triangles), *T. oceanica* (red circles), and *T. pseudonana* (black squares) under 20 min exposure to growth irradiance (Ig, 85 µmol photons m^{-2} s^{-1}, solid data points) and high light (HL, 1200 µmol photons m^{-2} s^{-1}, open data points). Data averaged from 2 or 3 independent replicates for LDR and at least 4 independent replicates for YNPQ. Error bars represent SE of the mean.

Figure 2.7. Energy flux yields including YNPQ (dark blue), YNO (light blue) and YII, which was then further divided into fractions of LDR (white), R_{DARK} (balck) and Net_{O2} (grey), of *T. pseudonana*, *T. oceanica* and *T. weissflogii* under 85 µmol photons m^{-2} s^{-1}

(Ig) and 1200 μmol photons m^{-2} s^{-1} (HL). Data averaged from 3 independent biological replicates and error bars represent SE of the mean.

Figure 2.8. Summary of relative reliance (low to high; light grey to black) on various energy dissipation strategies when subject to transient HL including (i) de-epoxidation state (DPS) of xanthophyll cycle pigments, (ii) induction/relaxation of nonphotochemical quenching (parameterised as YNPQ), (iii) inactivation/repair of PSII and (iv) O_2 consuming pathways (LDR/R_{DARK}) for the three *Thalassiosira* diatom species examined here.

Chapter 3

Figure 3.1. Changes in $E_{k,YII}$ for *T. oceanica* (circles) and *T. weissflogii* (triangles) acclimated to a 12:12 L:D cycle under sinusoidal light with max irradiance of 400 μmol photons m^{-2} s^{-1} (grey solid line). $E_{k,YII}$ was calculated using FRRf-derived YII values collected from a FLC. The spectrally corrected light intensities for FRRf-incubated samples are shown for *T. oceanica* (dotted line) and *T. weissflogii* (dashed line). Sampling occurred along the photoperiod at 1, 3, 6, 9 and 11 hours after the onset of illumination. Error bars represent SE of the mean for at least 3 independent biological replicates.

Figure 3.2. Total respiration ($R_{TOTAL,}$ pmol O_2 [pg Chl *a* h]$^{-1}$) for *T. oceanica* and *T. weissflogii* acclimated to a sinusoidal light regime (maximum 400 μmol photons m^{-2} s^{-1}) at sample time points along the photoperiod. The light incubations representing

variations in LDR ($Sine_{\mu}$ – dotted white, and $Sine_{HL}$ – solid white) were plotted separately and both included the dark respiration (R_{DARK} – black) for each corresponding timepoint. Error bars represent SE of the mean for at least three independent replicates. Note that the R_{DARK} value at each timepoint does not change between light incubation treatments but LDR values do reflect the response to light intensity shifts between treatments ($Sine_{\mu}$ and $Sine_{HL}$) and the y-axis scale is different between species.

Figure 3.3. Respiratory components of gross oxygen production (GP_{O2}): (A,D) total respiration (R_{TOTAL}) as a percentage of gross O_2 production. GP_{O2} separated into the fraction of net oxygen production (Net_{O2}, grey), dark respiration (R_{DARK}, black) and light dependent respiration (LDR, white) under $Sine_{\mu}$ (B,D) and $Sine_{HL}$ (C,F) for *T. oceanica* (A-C) and *T. weissflogii* (D-F) sampled over the photoperiod. Error bars represent SE of the mean for at least three independent replicates.

Figure 3.4. Correlations between YII (dimensionless) and GP_{O2} (pmol [pg Chl *a* h]$^{-1}$) for *T. oceanica* (circles, solid lines) and *T. weissflogii* (inverted triangles, dashed lines) for incubations at $Sine_{\mu}$ and $Sine_{HL}$ over the integrated photoperiod. Lines of best fit were generated using a simple linear regression model where the shaded areas represent the 95% confidence intervals for significant correlations ($p < 0.05$) only. Model parameters are displayed in S3.2 Table.

Figure 3.5. Energy flux yields for the sum of YNPQ (teal), YNO (purple) and YII, which was then further divided using GP_{O2} fractions of LDR (white), R_{DARK} (black) and

Net_{O2} (grey) for *T. oceanica* and *T. weissflogii* exposed to $Sine_{\mu}$ and $Sine_{HL}$. Data averaged from at least 3 independent replicates with error bars representing SE of the mean.

Figure 3.6. Correlations between fluorescence- and oxygen-derived parameters for *T. oceanica* (circles) and *T. weissflogii* (inverted triangles) at growth irradiance ($Sine_{\mu}$) and 3x growth irradiance ($Sine_{HL}$) collated over a 12-h photoperiod. Correlations included R_{TOTAL} to YII (Panel A), YNPQ (Panel B) and YNO (Panel C). Data points represent three individual replicate measures for each sample timepoint (1, 3, 6, 9, 11 h). Regression lines were included for both *T. oceanica* (solid line) and *T. weissflogii* (dashed line) and 95% CI (grey shaded area) displayed only for significant correlations ($p < 0.05$). Model parameters are displayed in S3.2 Table.

Figure 3.7. Correlations between $E_{k,YII}$ and (A) R_{TOTAL}, (B) Net_{O2}, and (C,D) carbon (pg cell-1) for *T. oceanica* (circles) and *T. weissflogii* (inverted triangles). Regression lines with 95% CI (grey shaded area) are displayed only for significant correlations ($p < 0.05$). Model parameters are displayed in S3.2 Table.

Chapter 4

Figure 4.1. (A) PCA of relative metabolite abundances for constant light treatments (24:0 L:D) at high (yellow circles), medium (green circles) and low (blue circles) intensities. (B) PLS-DA of relative metabolite abundances for high and low constant (high and low) and pulse (high – orange triangles, low – purple triangles) light treatments. Light intensities for high, medium and low are 200, 60 and 5 μmol photons

m^{-2} s^{-1}, respectively. Data for relative metabolite abundances was normalised by internal standard then 'metabolite extract biomass'. Explained variances are shown as a percentage in brackets and shaded area is the 95% confidence region. Individual data points represent independent biological replicates (n=4).

Figure 4.2. Significant metabolites (green circles) identified by SAM between constant light treatments (high - HC, medium - MC, low - LC). Significant metabolites determined from an ANOVA are distinguished in bold followed by post-hoc correlations in italics for a significance level of $p < 0.05$.

Figure 4.3. Significant metabolites (green circles) identified by SAM between high and low constant and pulse light treatments (HC – high constant, HP – high pulse, LC – low constant, LP – low pulse). Significant metabolites are distinguished in bold followed by post-hoc analysis generated from an ANOVA ($p < 0.05$).

Figure 4.4. Summary metabolic pathway schematic of metabolites identified using GC-MS with overlaying plots of relative metabolite concentrations for high constant (HC, yellow bars), low constant (LC, blue bars), high pulse (HP, orange bars) and low pulse (LP, purple bars) light treatments.

Figure 4.5. Schematic of the general metabolic changes for significant metabolites in *T. pseudonana* grown under high vs low light intensity for both constant and pulse light dose treatments. Blue indicates upregulation of relative metabolite concentrations for corresponding processes under lower light acclimation and red correlates to processes

with associated significant metabolites that were upregulated under high light acclimation. Black indicates intermediary steps/processes that were not significantly up or down regulated according to the metabolites identified across all light treatments.

Chapter 5

Figure 5.1. Schematic of diatom responses to high light from species found in open ocean (*T. oceanica*) and estuary (*T. weissflogii*) in which coastal diatoms exhibit an intermediate response. The main flow of energy involves light energy harvested at photosystem II (PSII) where excitons are passed along the linear electron transport chain to PSI where NADPH is generated to fuel, in addition to ATP, the Calvin-Benson-Bassham (CBB) cycle. Products generated from the CBB cycle enter the cytoplasm (yellow box) to glycolysis which feeds into the tricarboxylic acid cycle (TCA) cycle in the mitochondria (red box) to build macromolecules to support growth. Alternatively, gluconeogenesis diverts energy away from TCA cycle to build carbon reserves. Sources of energy dissipation from high light before reaching PSII are the yield of constitutive losses via fluorescence and heat (YNO) and the yield of regulated thermal dissipation via nonphotochemical quenching (YNPQ) Once photolysis occurs at the PSII reaction centre, electrons can enter processes of light-dependent respiration (LDR) via oxidase activity within the chloroplast (green box) which can be a way to dissipate excess electrons or generate additional ATP. Additionally, mitochondrial respiration can supplement ATP demands via the catabolism of carbon molecules to supply to the CBB cycle or assimilation of nutrients (i.e. nitrogen, N). Nitrogen is particularly essential to build pigments and proteins that are fundamental components of the nonphotochemical quenching mechanism. The arrow thickness correlates to the

upregulation of pathways by these diatoms under high light as observed in Chapters 2 and 3.

Figure 5.2. Development of energy budget models using cellular currencies – carbon (green background), oxygen (blue background) and fluorescence (yellow background) – from (A) historical, (B) current to (C) proposed future models. Historical energy budget models typically include two cellular currencies and a separate biofractionation of macromolecules. Current energy budgets account for the three cellular currencies but does not include that deeper carbon insight gained from metabolomics. Future energy budgets models could integrate all cellular currencies including the information gained from further partitioning of carbon molecules (e.g. metabolites). Such comprehensive energy budgets will provide more accurate accounting of energy that ultimately is retained in biomass under various environmental stressors. Data adapted from (A) Fisher & Halsey (2016) and (B) Chapters 2 and 3 where sub-fractionations within cellular currencies are measurements that were collected from diatoms in response to light.

List of Tables

Chapter 2

low light recovery (15 μmol photons m^{-2} s^{-1}) (Fig 2.3). Values derived from curve fits (Kok 1956; Campbell & Serôdio 2020) of data from 3 independent replicates. Values in parentheses represent SE of the mean.

Chapter 3

Table 3.1. Exposure light intensities during MIMS analysis for each sampling time point. Incubation treatments either mimicked the growth light intensity ($Sine_{\mu}$,) or were 3.0-fold higher ($Sine_{HL}$). Spectral correction factors (SCF) were applied to account for the light source differences between MIMS (white LED) and FRRf (blue LED) incubations for *T. oceanica* and *T. weissflogii*.

Table 3.2. Cell culture and properties of *Thalassiosira oceanica* and *Thalassiosira weissflogii* during steady-state growth acclimated to a sinusoidal ($Sine_{\mu}$) light regime with a maximum irradiance of 400 μmol photons m^{-2} s^{-1} over a 12:12 L:D photoperiod at 20°C. Values in parentheses are standard error for at least 3 independent biological replicates at each sample time. A two-way ANOVA test comparing species, time and interactive (Species*Time) effects for each property are represented with significant *p*-values (< 0.05) in bold. The test results from a one-way ANOVA are shown using superscripted letters to identify the Bonferroni post-hoc analysis for significance between sample times (h). Letters indicate means that are statistically indistinguishable ($p < 0.05$; ANOVA).

Chapter 4

Table 4.1. Physiological characteristics of *Thalassiosira pseudonana* measured at the time of metabolomics sampling during steady-state acclimated growth to five different light regimes: Constant (high, medium, low), and Pulse (high, low) at 20^{o}C. Values in parentheses represent SE of the mean for at least 3 independent biological replicates for specific growth rate (d^{-1}), cell density (mL^{-1}), Chl *a* ($cell^{-1}$), carbon (pg $cell^{-1}$), nitrogen (pg $cell^{-1}$), C:N, F_v/F_m and σ_{PSII} (nm^2 $PSII^{-1}$). ANOVA or Kruskal-Wallis (KW) test results are presented using F or H-values, respectively, for constant light treatments followed by Tukey post-hoc analysis with differences between individual cell characteristics and light intensity designated by superscripted letters and Student's *t* – test using t-values for pulse light treatments with significant *p* values ($p < 0.05$) in bold. For 2-way ANOVA test results for light treatments of equal PFD (HC-HP, LC-LP) see S4.4 Table.

Table 4.2. Compilation of SAM-identified significant metabolites for the various comparisons of light treatments – constant only (yellow), pulse only (green) and constant+pulse treatments of equal average PFD (blue).

List of Supplementary Figures

Chapter 2

S2.1 Figure. Photophysiological assessment of seven diatoms. Conventional non-photochemical quenching (NPQ; see Eq. 2) capacities of *Phaeodactylum tricornutum* (orange inverted triangles), *Chaetoceros muelleri* (yellow circles), *Ditylum brightwellii* (green diamonds), *Thalassiosira rotula* (black Xs), *Thalassiosira pseudonana* (black squares), *Thalassiosira weissflogii* (blue triangles), and *Thalassisosira oceanica* (red circles) with increasing light intensity. Error bars represent the standard error of the mean of at least n=3 for independent biological replicates.

Chapter 3

S3.1 Figure. Schematic of experimental design including (1) culture growth light regime, (2) sample preparation of sub-culture aliquots inoculated with labelled oxygen ($^{18}O_2$), (3) light treatments used to measure oxygen consumption and production using membrane inlet mass spectrometry (MIMS) and (4) sampling time points across the photoperiod with corresponding incubation irradiances for MIMS treatment samples ($Sine_{\mu}$ and $Sine_{HL}$).

S3.2 Figure. Photon flux of light sources used for fluorescence (blue LED, black circles) and oxygen (white LED, grey squares) incubations and analyzed via FRRf and MIMS, respectively (left panel). Spectrally corrected fluorescence excitation detected at 730 nm of *T. weissflogii* (red dots) and *T. oceanica* (blue dots) weighting blue LED

light to white LED light over photosynthetically active radiation (PAR, 400-700 nm) wavelengths (right panel).

S3.3 Figure. Oxygen consumption in the dark and light by *T. oceanica* (circles) and *T. weissflogii* (triangles) acclimated to growth under 12 hours of sinusoidal light with a maximum intensity of 400 µmol photons m^{-2} s^{-1}. Dark respiration and LDR were measured over the photoperiod at 1, 3, 6, 9 and 11 hours. LDR measurements were completed at $Sine_{LL}$ and $Sine_{HL}$ light incubations for each timepoint as denoted in the "Light Treatment" panel. Remaining panels ('cell number', 'cell volume', 'carbon' and 'chlorophyll *a*') show oxygen consumption measurements normalised to the corresponding parameter. Error bars for 'cell number', 'carbon' and 'chlorophyll *a*' panel graphs represent SEM while the error associated with 'cell volume' normalisations were calculated using the percentage of uncertainty to get the propagation of error for averages from at least three independent biological replicates.

Chapter 4

S4.1 Figure. PCAs of the relative metabolite abundances for (A) pulse (12:12 L:D) treatments at high (HP, 200 µmol photons m^{-2} s^{-1}) and low (LP, 5 µmol photons m^{-2} s^{-1}) light intensities and (B) for constant and pulse (HC – yellow circles, HP – orange squares, LC – blue circles, LP – purple squares) light treatments. Explained variances are shown as a percentage in brackets and shaded area is the 95% confidence region of individual treatment groups. Individual data points represent independent biological replicates (n=4).

S4.2 Figure. Significant metabolites (green circles) identified by SAM between high and low pulse light treatments (HP – high pulse, LP – low pulse). Significant metabolites are distinguished in bold ($p < 0.05$) and a false detection rate (FDR) < 10%.

S4.3 Figure. Summary of annotated differentially expressed genes for those (A) downregulated in constant low light (LC, 5 µmol photons m^{-2} s^{-1}) relative to constant high light (HC, 200 µmol photons m^{-2} s^{-1}) and (B) upregulated in LC compared to HC. Differential expression was determined using the threshold $|FC| > 2$, $p < 0.05$ from three independent biological replicates.

S4.4 Figure. Differentially expressed genes for *T. pseudonana* grown at constant low light (LC, 5 µmol photons m^{-2} s^{-1}) compared to constant high light (HC, 200 µmol photons m^{-2} s^{-1}) conditions showing upregulated (green) and downregulated (red) genes in LC. Right panel figure shows the interplay between processes occurring in the plastid, peroxisome and mitochondrion and left panel figures shows more detailed interactions between glycolysis, fatty acid and branched chain amino acid (BCAA) degradation and TCA cycle where dashed lines represent the glyoxylate cycle two-step bypass. PEPCK = PEP carboxykinase; PPDK = pyruvate-phosphate dikinase; PK = pyruvate kinase; PC = pyruvate carboxylase; PEPC = PEP carboxylase; Pex1,5,19 = peroxins that import proteins into the peroxisomes.

List of Supplementary Tables

Chapter 2

S2.1 Table. Rates of oxygen production and consumption. MIMS analysis of gross oxygen production (GP_{O2}), light dependent respiration (LDR), dark respiration (R_{DARK}), and net oxygen production (Net_{O2}) for *T. weissflogii*, *T. oceanica*, and *T. pseudonana* under 20 min exposure to HL (1200 µmol photons m^{-2} s^{-1}). Data averaged from 3 independent replicates. Values in parentheses are SE of the mean. A 2-way ANOVA test comparing species and light treatment with oxygen measurements (GP_{O2}, Net_{O2}, LDR) and a 1-way ANOVA for R_{DARK} are presented with significant p-values (< 0.05) in bold. Superscripted asterisks (*) or letter identifies the Bonferroni post-hoc analysis for significance between species groups.

S2.2 Table. MIMS analysis of oxygen pathways as a percentage of gross oxygen production (% of GP_{O2}). Fractions (as a %) include light dependent respiration (LDR), dark respiration (R_{DARK}), and net oxygen production (Net_{O2}) for *T. weissflogii*, *T. oceanica*, and *T. pseudonana* under 20 min incubation at Ig (85 µmol photons m^{-2} s^{-1}) and HL (1200 µmol photons m^{-2} s^{-1}). Data averaged from 2 or 3 independent replicates. Values in parentheses are SE of the mean. A 2-way ANOVA comparing species and light treatment with oxygen measurements (R_{DARK}, Net_{O2}, LDR) are presented with significant p-values (< 0.05) in bold. Superscripted asterisks (*) identifies the Fisher's Tukey post-hoc analysis for significance between species groups.

Chapter 3

S3.1 Table. PE curve parameters for *T. oceanica* and *T. weissflogii* grown over 12:12 L:D photoperiod following a sinusoidal light regime with a maximum irradiance of 400 μmol photons m^{-2} s^{-1}. PE curves were collected after 1, 3, 6, 9 and 11 hours following the onset of illumination. YII_{max}, is the maximum fluorescence-derived photochemical conversion at PSII, α is the light-limiting slope, $E_{k,YII}$ is the light saturation index calculated as YII_{max}/α and R^2 represents the goodness of fit. Values in parentheses represent the SE of the mean for at least three independent replicates.

S3.2 Table. Correlation parameters for various comparisons between measures of oxygen (GP_{O2}, R_{TOTAL}, LDR, Net_{O2}), fluorescence (YII, YNPQ, YNO, $E_{k,YII}$) and biomass (carbon, pg $cell^{-1}$) combining replicate (n=3) measurements for all time points over the photoperiod for *T. oceanica* and *T. weissflogii* under $Sine_{\mu}$ and $Sine_{HL}$. Significant correlations ($p < 0.05$) shown in bold.

S3.3 Table. Rates of oxygen production and consumption. MIMS analysis of gross oxygen production (GP_{O2}), light dependent respiration (LDR), dark respiration (R_{DARK}), and net oxygen production (Net_{O2}) for *T. weissflogii* and *T. oceanica* grown under a sinusoidal light regime with a maximum of 400 μmol photons m^{-2} s^{-1} ($Sine_{\mu}$) over a 12:12 L:D cycle. Rates were also collected from a transient exposure to high light that was 3x $Sine_{\mu}$ ($Sine_{HL}$) at the sample time. Samples were collected during the photoperiod at 1, 3, 6, 9 and 11 hours. Data averaged from 3 independent replicates. Values in parentheses are SE of the mean. For direct comparison with oxygen consumption/production rates from Chapter 2 see S2.1 Table.

Chapter 4

S4.1 Table. Cell densities (mL^{-1}), volume of culture (mL) concentrated and preserved for metabolite extraction and the total cells (mL^{-1}) extracted for metabolomics analysis of technical replicates for three constant (high, medium, low) and two pulse (high, low) light treatments.

S4.2 Table. Fold change matrix of average total cell densities extracted for metabolomics analysis between light treatments (Constant – High [HC], Medium [MC], Low [LC] and Pulse – High [HP], Low [LP]) where n = 4 for independent biological replicates. Values in parentheses represent *p* values for independent t-tests.

S4.3 Table. Physiological characteristics of *Thalassiosira pseudonana* during steady-state acclimated growth to four light regimes: Constant (high, low), and Pulse (high, low) at 20°C. Values in parentheses represent SE of the mean for at least 3 independent biological replicates for specific growth rate (d^{-1}), Chl *a* ($cell^{-1}$), carbon ($pg\ cell^{-1}$), nitrogen ($pg\ cell^{-1}$), C:N, F_v/F_m and σ_{PSII} ($nm^2\ PSII^{-1}$). ANOVA or Kruskal-Wallis (KW) test results are presented using F or H-values, respectively, followed by Bonferroni or Dunnett T3 post-hoc analysis, respectively, with differences between individual cell characteristics and light treatment designated by superscripted letters and significant *p* values ($p < 0.05$) in bold.

S4.4 Table. Summary of differentially expressed genes involved in the glyoxylate cycle, TCA cycle, and related pathways. Genes with adjusted *p* value <0.05 in *T.*

pseudonana grown at constant low light (LC, 5 µmol photons m^{-2} s^{-1}) compared to constant high light (HC, 200 µmol photons m^{-2} s^{-1}) conditions.

List of Abbreviations

AA	Amino acids
ADP	Adenosine diphosphate
ANOVA	Analysis of variance
AOX	Mitochondrial alternative oxidase
Ar	Argon
ATP	Adenosine triphosphate
BCAA	Branched chain amino acid
β-Car	Beta carotene
C	Carbon
CBB cycle	Calvin-Bassham-Benson cycle
CCM	Carbon concentrating mechanism
CEF	Cyclic electron flow
Chl	Chlorophyll
CI	Confidence intervals
CO_2	Carbon dioxide
Cyt b_6f	Cytochrome b_6f
DCMU	3-(3,4-dichlorophenyl)-1,1-dimethylurea
Dd	Diadinoxanthin
DHA	Docosahexaenoic acid
DOC	Dissolved organic carbon
DPS	De-epoxidation state
Dt	Diatoxanthin
E	Irradiance
EGT	Endosymbiotic gene transfer
ETC	Electron transport chain
ETR/ETR_{PSII}	Electron transport rate from PSII
FC	Fold change
Fd	Ferredoxin
FDP	Flavodiiron protein
FDR	False discovery rate
FLC	Fluorescence light response curve
FNR	Fd-NADP+ oxidoreductase
FRRf	Fast repetition rate fluorometry
Fuc	Fucoxanthin
GAP	Glyceraldehyde phosphate
GC-MS	Gas chromatography mass spectrometry
GDC	Glycine decarboxylase p-protein
GF/F	Glass fiber filter
GP_C	Gross carbon production
GP_{O2}	Gross oxygen production
GPP	Gross primary production
H^+	proton
HC	High constant
$HgCl_2$	Mercuric chloride
HL	High light
HP	High pulse
HPLC	High-performance liquid chromatography

Ig	Growth irradiance
KCN	Potassium cyanide
KEGG	Kyoto encyclopedia of genes and genomes
KW	Kurskal-Wallis
L:D	Light:Dark
LC	Low constant
LC-MS	Liquid chromatography mass spectrometry
LDR	Light dependent respiration
LED	Light emitting diode
LEDR	Light enhanced dark respiration
LEF	Linear electron flow
LHC	Light harvesting complex
LHCX	Light harvesting complex proteins
LIFT	Light induced fluorescence transient
LL	Low light
LP	Low pulse
MAP	Mehler ascorbate peroxidase
MC	Medium constant
MeOH	Methanol
MIMS	Membrane inlet mass spectrophotometry
MOX	Midstream oxidase
MT	Multiple turnover
N/N_2	Nitrogen/nitrogen gas
NADPH	Nicotinamide adenine dinucleotide phosphate
Net_{O2}	Net oxygen production
NP_C	Net carbon production
NPP	Net primary production
NPQ	Nonphotochemical quenching
NPQ_{NSV}	Stern-Volmer nonphotochemical quenching
NR	Nitrate reductase
O_2	Oxygen
OAA	Oxaloacetate
OEC	Oxygen evolving complex
PAM	Pulse amplitude modulated
PAR	Photosynthetically active radiation
PC	Plastocyanin
PC	Pyruvate carboxylase
PCA	Principle component analysis
PE curve	Photosynthesis-irradiance curve
PEP	Phosphoenolpyruvate
PEPCK/PCK1	Phosphoenolpyruvate carboxykinase
PETC	Photosynthetic electron transport chain
Pex	Peroxin
PFD	Photon flux density
PGA	Phosphoglyceric acid
PGR5	Proton gradient regulation protein
PLS-DA	Partial least squares discriminant analysis
PK	Pyruvate kinase

POC	Particulate organic carbon
PON	Particulate organic nitrogen
PP	Primary productivity
PPDK	Pyruvate-phosphate dikinase
PQ	Plastoquinone
PSI/II	Photosystem I/II
PTOX	Plastid/plastoquinol terminal oxidase
PTS	Peroxisomal targeting signals
QMS	Quadrapole mass spectrometer
R_{DARK}	'Dark' (mitochondrial) respiration
R_{TOTAL}	Total respiration
RC (I/II)	Reaction centre (of PSI/PSII)
RNA	Ribonucleic acid
RuBisCO	Ribulose-1,5-bisphosphate carboxylase
S	Sulfur
SAM	Significance analysis of microarrays
SCF	Spectral correction factor
SE	Standard error
SHAM	Salicylhydroxamic acid
SHMT	Serine hydroxymethyltransferase
$Sine_{HL}$	Sinusoidal high light
$Sine_{\mu}$	Sinusoidal growth irradiance
ST	Single turnover
TCA cycle	Tricarboxylic acid cycle
XC	Xanthophyll cycle
YNPQ	Yield of regulated nonphotochemical quenching
YNO	Yield of constitutive losses via fluorescence and heat
YII	Yield of photochemical conversion at PSII

List of Symbols

μ	Specific growth rate (d^{-1})
[1-C]	Photochemical quenching
[1-Q]	Nonphotochemical quenching
α	Alpha; light limiting slope
σ_{PSII}	Functional absorption cross section of PSII
e^-	Electron
ϕ	Quantum yield
E_k	Light saturation index
$E_{k,YII}$	Light saturation index of photochemical conversion at PSII
F'	Steady-state fluorescence at any point
F_o	Minimum fluorescence from dark acclimated sample
F_m (F_m')	Maximum fluorescence from dark acclimated sample
F_v (F_v')	Variable fluorescence from dark acclimated sample
F_v/F_m	Maximum photochemical efficiency
F_o'	Minimum fluorescence under actinic light
F_m'	Maximum fluorescence under actinic light
F_v'	Variable fluorescence under actinic light
F_v'/F_m'	Maximum PSII efficiency under actinic light
k_{PI}	Photo-inactivation rate constant
k_{REC}	Recovery rate constant
P_{max}	Photosynthetic maximum

Thesis Abstract

Diatoms are the evolutionarily youngest phytoplankton group and considered to be the most productive across diverse ocean, coastal and freshwater environments. Based on their evolutionary history in diverse environments, diatoms have acquired unique diverse mechanisms to cope with fluctuating availability of resources required for cellular maintenance and growth. Yet how these mechanisms actually operate to moderate metabolic functioning by the energetic tracking of light energy to carbon capture – commonly measured as "emergent signatures" or photosynthesis rates via fluorescence, O_2 evolution and/or CO_2 uptake –remains somewhat of a black box.

This thesis addresses the response of diatoms to light, with particular emphasis on the gaps in current energy budgets that quantify trade-offs in O_2 evolution and carbon-assimilation. An initial assessment of a variety of diatom species revealed distinct categories of photo-protective capacities (i.e. nonphotochemical quenching) that correlated with ecological niche, i.e. taxa originating from estuarine, coastal and open ocean environments. Low capacity to dissipate light energy via nonphotochemical quenching by open ocean diatoms was compensated for by an upregulation of midstream oxidase activity highlighting a key trade-off between light harvesting and light utilization strategies. Diurnal monitoring of diatoms with divergent photo-protective capacities further revealed species-specific dynamic respiratory trends, whereby diatoms with high nonphotochemical quenching capacity exhibited more dynamic R_{DARK} while diatoms with low nonphotochemical quenching capacity exhibited more dynamic light-dependent respiration (LDR). Fluorescence-derived measures of photoacclimation ($E_{k,YII}$) were found to be significantly correlated to oxygen cycling and carbon retained as biomass. Subsequent metabolomic profiling provided deeper insight into these processes via the underlying light-driven metabolite

reorganisation. Using the model coastal diatom (*T. pseudonana*), high light metabolic profiles were reflective of pathways that support higher growth rate (e.g. glycolysis and TCA cycle) compared to low light metabolic profiles associated with carbon conserving pathways (e.g. gluconeogenesis and glyoxylate cycle).

Together these outcomes uncovered previously hidden dynamics of energy processing by diatoms – including dynamic respiration rates between taxa and with time of day, which also mapped differences in inherent metabolic pathways as well as "emergent" metabolic signatures (e.g. fluorescence, O_2 and CO_2 measures of primary productivity). Combining information from cellular currencies (fluorescence, oxygen and carbon) thus provides a more robust mechanistic understanding of metabolic processes. This thesis has created a foundation for future research to compile more comprehensive energy budgets and a framework for improved estimates of primary productivity models.

Thesis Structure and Declaration of Contribution

This thesis is comprised of three data chapters (Chapters 2 - 4) with each constructed around an independent experiment. All data chapters have been written in the form of a journal manuscript for peer-review. At the time of thesis submission, Chapter 2 has been published and Chapters 3 and 4 are in final draft for submission and ready for submission/peer review pending availability of funds. Each data chapter introduction is exhaustive thus, to avoid information redundancy, the thesis general introduction (Chapter 1) has focussed on topics not covered in as much depth within data chapter introductions to better develop the outlined aims of the thesis.

Chapter 2: Fisher N.L., Campbell D.A., Hughes D.J., U., Halsey, K.H., Ralph, P.J. and Suggett D.J. 2020. Divergence of energy strategies amongst diatoms. Published in *PLOS ONE*.

NLF, KHH, PJR, DJS designed the experiment. NLF conducted the experiment. NLF collected all samples and processed data for FRRf and MIMS measurements. UK performed HPLC data analysis. DAC created R script to process photo-inactivation and repair rates and provided figures. NLF wrote manuscript first draft. DAC, DJH, KHH, PJR, DJS provided substantial critical contributions and edits.

Chapter 3: Fisher N.L., Halsey K.H., Hughes D.J., Argyle P., Ralph P.J. and Suggett D.J. Contrasting dynamics of light-dependent and -independent respiration from two

Thalassiosira diatoms under diurnal light. Thesis chapter. Intended Journal, *Journal of Phycology*

NLF conceptualised and designed the experiment. KHH, DJH, DJS, NLF finalised the experimental design. NLF conducted the experiment. NLF collected all samples and processed data. NLF wrote manuscript first draft. PA assisted with statistical analyses. KHH, DJH, PJR, DJS provided substantial critical contributions and edits.

Chapter 4: Fisher N.L., Halsey K.H., Suggett D.J., Pombrol M., Ralph P.J., Lutz A., Sogin E.M. and Matthews J.L. Light-dependent metabolic phenotype of the model diatom *Thalassiosira pseudonana*. Submitted for peer review to *Journal of Experimental Botany*

NLF, KHH, PJR, DJS conceptualised and designed the experiment. NLF conducted the experiment. NLF collected and extracted all samples. AL provided protocols for metabolite extraction and initial processing of metabolomics samples. EMS processed metabolomics samples and resources associated with analysis. JLM identified metabolites from processed data and provided guidance for anlayzing metabolomics data. NLF analysed data and created metabolic pathways. MP and KHH provided transcriptomics data. NLF wrote manuscript first draft. KHH made substantial contributions to the written manuscript. JLM, KHH, PJR, DJS, AL, EMS provided critical contributions and edits.

Chapter 1

General Introduction and Thesis Outline

1.1. Phytoplankton

Single-celled prokaryotic and eukaryotic 'drifting' microalgae (collectively termed phytoplankton) are the base of aquatic food webs. They account for approximately 50% of global primary production (PP) (Field et al. 1998; Falkowski & Raven 2007) while comprising a mere 1% of all photosynthetic biomass on Earth (Bidle & Falkowski 2004). Phytoplankton face many pressures not only from the highly unpredictable physical nature of aquatic environments, but also from grazers (i.e. zooplankton) and viruses, while simultaneously competing amongst other phytoplankton species for the same, often limiting, resources that fuel growth (i.e. light and nutrients, Scheffer et al. 2003). As a result of competitive pressure, broad evolutionary divergence in the light-nutrient requirements (e.g. Quigg et al. 2003) amongst the highly dynamic environment of aquatic systems (e.g. Moore et al. 2006) has enabled thousands of phytoplankton taxa to co-exist and thrive in the 'same' niche space, thus overcoming the "paradox of the plankton" (Hutchinson 1961).

The first forms of phytoplankton were cyanobacteria – antecedents of the green and red algal lineages – emerged approximately 2.15 billion years ago (Knoll et al. 2006). Of these lineages, diatoms were the relatively 'late starters', emerging around 180 million years ago (Kooistra et al. 2007), and likely diversified over the last 40 million years when large concentrations of silica were released from terrestrial systems into the oceans (Cermeno et al. 2015). Evolutionary pressures caused by dynamic environments has resulted in the conservation of genes, sometimes a combination of plant and animal (Falkowski et al. 2004; Armbrust et al. 2004), that facilitate fitness via complex mechanisms that allow phytoplankton to sense and respond to changes in abiotic

factors such as light, nutrients, pH, salinity, and temperature. While all phytoplankton groups possess a broad but specialised set of strategies for responding to environmental stressors, the focus of this research will be on this latest group to emerge, diatoms – the engines of the ocean (Armbrust 2009). Specifically, to better understand the complex mechanisms that diatoms have acquired to maximise competitive fitness in marine aquatic environments.

1.1.1. Diatoms

The evolutionary history of diatoms explains the presence of some unique genes that code for various cellular functions that are not observed by the green algal lineage. Indeed, the diatom genome is unlike any other photosynthetic organism sequenced to-date, and even the genomes of geometrically distinct (centric versus pennate) diatoms are quite unique (Bowler et al. 2008). Whole genome sequencing has revealed an explanation for this anomalous set of genes, whereby an endosymbiotic event occurred through a heterotrophic host that first engulfed a cyanobacteria cell giving rise to red algae; this in turn was followed by a second endosymbiotic event where another heterotrophic host engulfed the red algal cell thereby leading to the emergence of diatoms (Rynearson & Palenik 2011; Armbrust 2009) (Fig 1.1). Evidence of green algal genes within the diatom genome suggested that a two-step secondary endosymbiosis event occurred whereby the genes of both red and green algal lineages were retained to form the present-day diatom genome (Moustafa et al. 2009; Bowler et al. 2010; Prihoda et al. 2012) (Fig 1.1).

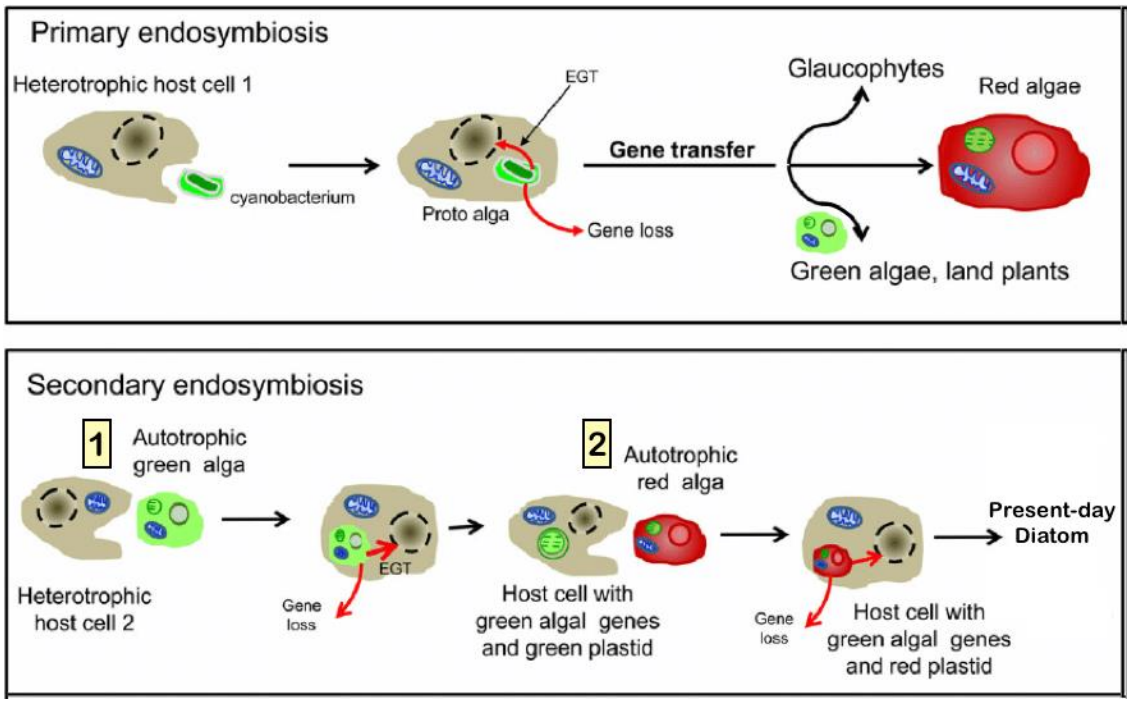

Figure 1.1. Schematic of the hypothesised endosymbiotic events leading to the evolution of diatoms. Primary endosymbiosis lead to the origin of green and red algal lineages as well as Glaucophytes and land plants from the engulfment of a cyanobacteria by a heterotrophic host cell. Secondary endosymbiosis is represented by two events, numbered boxes, where in the first event a green algal cell combined with a heterotrophic host followed by a second event where a red algal cell was subsequently combined leading to present-day diatoms. Red arrows represent gene loss and endosymbiotic gene transfer (EGT) events. Modified from Prihoda et al. 2012.

Diatoms are ubiquitous throughout the world's oceans (Malviya et al. 2016), and their genetic diversity from endosymbiotic events likely explain how diatoms are remarkably equipped to remain competitively fit in some of the most dynamic environments including, but not exclusive to, coastal regions, areas of upwelling (Smetacek 2012), and high latitudes (Armbrust 2009). Diatoms are not solely planktonic and have also

been found to thrive in ecosystems, such as within the sediments of estuarine flats (Barnett et al. 2015) and under sea-ice (Petrou et al. 2010; Croteau et al. 2020), which highlights the importance of looking at eco-diversity when assessing diatom photophysiology and productivity. Collectively, of all phytoplankton groups, diatoms contribute about 40% of the primary production in aquatic ecosystems (Field et al. 1998; Treguer et al. 1995) and nearly 20% global carbon fixation (Falkowski et al. 2000; Kroth et al. 2008; Cermeno et al. 2018). A contributor to diatom success is their opportunistic nature such that when nutrients become more readily available, from upwelling or mixing events, they are able to respond rapidly and are typically the first algal group to bloom (Sarthou et al. 2005; Armbrust 2009). A bloom is sustained only as long as the nutrient supply can support accelerated growth rates and grazing pressures remain lower than phytoplankton division rates (Behrenfeld 2014). During a bloom, carbon dioxide (CO_2) is sequestered from the atmosphere and either gets exported to higher trophic levels via predator consumption or that carbon sinks to the ocean floor when the algal cell dies. Given diatoms are the primary bloom formers in aquatic environments, their prevalence and perseverance under dynamic light conditions make them ideal candidates to assess (photo)physiological mechanisms that underlie their ecological success (Strzepek & Harrison 2004, Lavaud et al. 2007 Dimier et al. 2007; Wilhelm et al. 2014; Wagner et al. 2017; Blommaert et al. 2018; Lacour et al. 2020).

1.2. Aquatic environments

Phytoplankton survival as a ‘drifter’ in an inherently dynamic environment, due to the fluidity of water, is only further complicated by interacting physical, chemical and

biological factors. The ocean is subject to passive diffusion of atmospheric gases, such as CO_2 that can cause waters to acidify, and involve physical processes, such as eddies, waves, currents and vertical mixing within the water column. Nutrient availability in the ocean is patchy, in which open ocean iron levels, as well as nitrogen, are exceedingly low and limit 30-40% of global PP (Moore et al. 2003, 2013). Key factors including temperature (Eppley 1972; Boyd and Doney 2002, 2003; Beardall et al. 2009), nutrients (Moore et al. 2013), and light (Bopp et al. 2001; Gao et al. 2012; Köhler et al. 2018) have broad spatio-temporal variability with latitude and within the water column. Light, nutrients and temperature greatly influence phytoplankton growth, particularly given the ocean climate is changing at unpresented rates (Boyd et al. 2010, 2016; Behrenfeld 2014). Warming is expected to alter the physiological performance of phytoplankton worldwide as each species has varying temperature niche tolerances (Boyd et al. 2015) and the optimum growth temperature has been found to strongly relate to average environmental temperature which is indicative of past adaptation (Tortell et al. 2008). Specifically, it was found that warming waters will likely lead to a decline in tropical phytoplankton as many tropical strains are genetically disadvantaged to survive small increases in temperature (Thomas et al. 2012; Righetti et al. 2019). Phytoplankton cell size also appears to contribute to physiological responses to the environment (Edwards et al. 2015) where smaller cells have shown to maintain higher photosynthetic rates under light limitation (Finkel 2001) and larger cells experienced less photoinhibition under excessive light (Key et al. 2010). Still, there are many unknowns as to how each factor independently and collectively will influence primary productivity (Lewis et al. 2020; Oziel et al. 2020). Still, phytoplankton must acquire both light and nutrients to drive photo- and bio-chemical processes to fuel growth. While the significant contribution of nutrient

availability, temperature and pH to phytoplankton growth is not to be downplayed, the focus of this thesis is the response of diatoms to **light availability (intensity and regime) given its extremely dynamic nature across all aquatic environments. Furthermore, light fuels the primary metabolic reactions that ultimately enables the acquisition of other resources essential for growth and survival**.

Light is only available to drive photochemical reactions within the euphotic zone, characterised by the depths within the water column above 0.1% surface irradiance (Ryther 1956; Kirk 1994, Marra et al. 2014). Light intensity is often defined as photosynthetically active radiation (PAR) and phytoplankton predominantly use wavelengths within the visible spectrum of light (400-700 nm) to drive photosynthesis. Phytoplankton typically have little control over their position within the water column where the light climate shows rapid depth-dependent modifications in light quality and quantity (Austin & Petzold 1986; Mann & Lazier 2006; Hickman et al. 2009). In fact, it is not unusual for a phytoplankton cell to go from complete darkness to full sunlight over the course of minutes (Macintyre et al. 2002). Therefore, phytoplankton must rapidly adjust to sub- and super-saturating light intensities over short timescales (Falkowski 1984, Kirk 1994), such as wave-flickering and wave-lensing (< seconds) that enhance and diffuse sunlight simultaneously in the upper meters of the water column (Hieronymi & Macke 2010). Other influences on light availability occur over longer timescales, including cloud cover (seconds – minutes), vertical mixing (minutes – hours), and daily/seasonal fluctuations associated with solar position (Falkowski 1984). Since phytoplankton are the major contributors of primary productivity (~95%) in marine environments (Geider et al. 2001) they must possess mechanisms to cope

with the dynamic nature of light to maintain photochemical efficiency and support growth. Indeed, diatoms in particular, have been shown to exhibit extreme plasticity in their ability to cope with light fluctuations (Wilhlem et al. 2014; Lacour et al. 2017).

1.3. Photosynthesis

Oxygenic photosynthesis is undeniably one of the most important biological processes on Earth, whereby the conversion of light energy and carbon dioxide (CO_2) produce biochemical energy/reductant (ATP/NADPH) and oxygen (O_2), as a by-product, which has allowed aerobic life to exist as we know it today. Photosynthesis originated ~2.4 billion years ago when oceans covered Earth's surface (Fischer et al. 2016; Blankenship 2010). Photosynthesis is often thought of as a purely light-dependent process; however, there are four phases of photosynthesis and while the first three are light-dependent, the fourth – carbon fixation – is light-independent. The light-dependent phases consist of (1) light energy absorption and delivery by antennae to reaction centres, (2) initiation of electron transfer in reaction centres, and (3) energy stabilisation via electron transfer between photosystems (Blankenship 2010). Despite the fundamental nature of photosynthesis there are still questions about the underlying mechanisms that control photochemical reactions (Nelson & Ben-Shem 2004). I will first briefly discuss the operation of light-dependent and -independent processes in the context of optimal conditions (i.e. light does not super-saturate photosynthesis).

Eukaryotic oxygenic photosynthesis relies on the same basic mechanisms and component embedded within the thylakoid membrane, including a charge separation at photosystem I and II (PSI and PSII, respectively) that are connecting by the electron

transport chain (ETC) whereby the splitting of water at PSII generates excited electrons for the reduction ferredoxin (Fd) and NADP+ at PSI (Fig 1.2). Concurrently, chemiosmotic production of ATP by an ATP-synthase complex is driven by the proton motive force (PMF) from the formation of a pH gradient by the movements of protons (H+) across the thylakoid membrane (Fig 1.2). Ultimately, linear electron flow (LEF) from PSII to PSI produces a fixed ratio of ATP:NADPH that, under optimal conditions, may be sufficient to support the Calvin-Benson-Bassham (CBB) cycle (Allen 2002; Amthor 2010); however, this is an ongoing topic of debate (Kramer & Evans 2011).

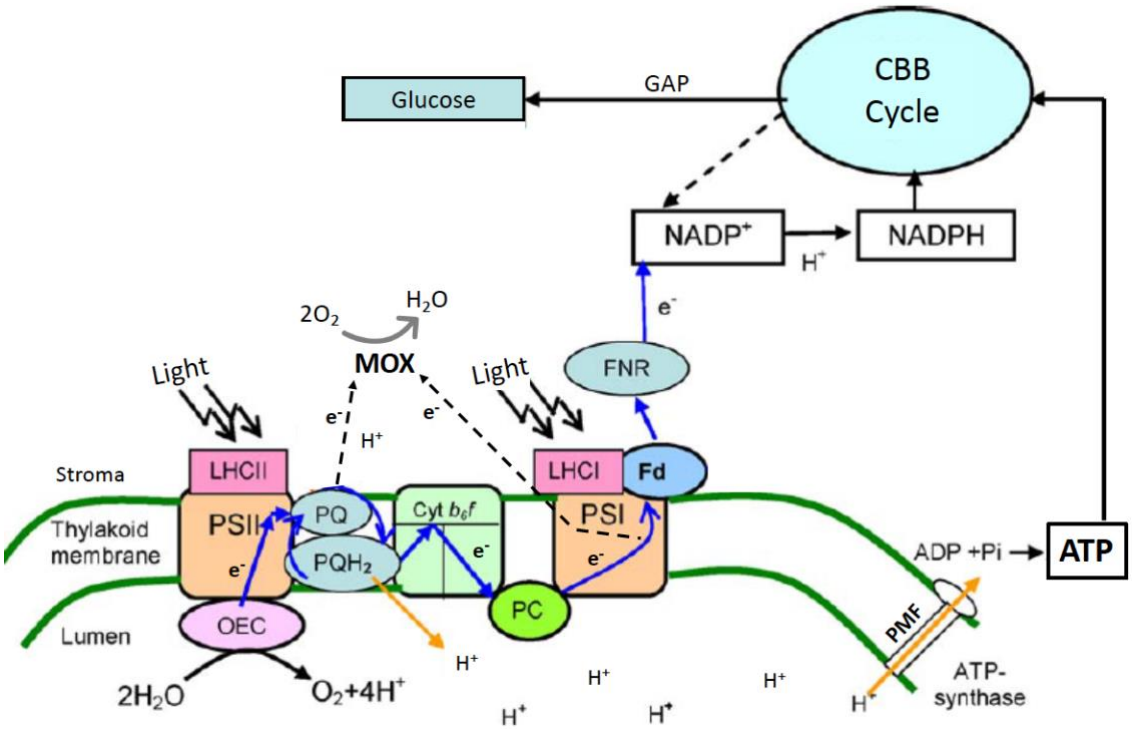

Figure 1.2. Schematic of the thylakoid membrane embedding the components for oxygenic photosynthetic driven by the light energy captured by light harvesting complexes (LHC) of photosystem I and II (PSI and PSII, respectively). Light triggers the photolysis of water by the oxygen evolving complex (OEC) at PSII to initiate linear electron (e^-) flow (LEF, blue line) via plastoquinone (PQ) pool, cytochrome b_6f

complex (Cyt b_6f), plastocyanin (PC), PSI and ferredoxin (Fd). Fd-$NADP^+$ oxidoreductase (FNR) transfers electrons to $NADP^+$ to produce reductant (NADPH). When the photosynthetic electron transport chain is over-excited, processes such as midstream oxidases (MOX, black dashed lines) can alleviate pressure via oxygen consumption. The accumulation of protons (H^+) in the lumen drive a proton motive force (PMF) through ATP-synthase to generate ATP. ATP and NADPH are required to fuel CO_2 fixation by the Calvin-Benson-Bassham (CBB) cycle to make glucose via glyceraldehyde phosphate (GAP) that can be used by other cellular processes. Modified from Allakhverdiev et al. (2010).

The final, light-independent, phase of photosynthesis involves the CBB cycle where inorganic carbon (CO_2) fixation occurs in the stroma of chloroplasts and organic carbon (i.e. glucose) is exported to the cytoplasm where glycolysis occurs. There are three phases of the Calvin Cycle: carboxylation, reduction, and regeneration (Blankenship 2002). Carboxylation depends on the enzyme Ribulose-1,5-bisphosphate carboxylase/oxygenase (RuBisCO) and CO_2 to form phosphoglyceric acid (PGA). This is the only process that functions independently of photochemically generated ATP and NADPH. The reduction phase relies on NADPH and, some, ATP to reduce PGA to glyceraldehyde phosphate (GAP). The final phase requires ATP to regenerate GAP back to RuBisCO; however, some GAP is reserved for starch and glucose synthesis in the chloroplast and cytoplasm, respectively. All phases of photosynthesis are inter-connected and regulated to balance energetic requirements for optimal growth efficiency; however, photo-chemically generated ATP:NADPH ratios are not sufficient to fuel other cellular processes (i.e. synthesis of proteins, nitrogen and sulfur

reduction). Diatoms have demonstrated the ability to tightly regulate photosynthetic and respiratory processes via intracellular signalling between organelles to fulfil energetic cellular requirements (Bailleul et al. 2015; Broddrick et al. 2019).

1.3.1. Balancing cellular energy requirements

Optimal cellular functioning involves tight coupling of processes that have varying ATP:NADPH ratio demands, and these ratios differ amongst species (Raven & Kubler 2002) and physiological status (Behrenfeld et al. 2008; Hughes et al. 2018; Raven et al. 2020). Chloroplasts have rather limited pools of photo-chemically generated ATP and NADPH whereby an imbalance in either pool would result in a cessation of photosynthesis (Cruz et al. 2005; Amthor 2010). For instance, if ADP is limiting then the subsequent build-up of the PMF would inhibit electron transfer to NADP+ and, conversely, limited NADP+ would cause a reduction of photosynthetic carriers thus slowing electron transfer and PMF (i.e. ATP synthesis). Therefore, alternative pathways are needed that generate additional ATP to fuel cellular processes for growth (Behrenfeld et al. 2008) and optimise functioning of metabolic pathways (Bailleul et al. 2015). In fact, there is evidence that cross-talk exists between diatom chloroplasts and mitochondria whereby energetic exchanges of plastid-derived reducing power and mitochondrial ATP can occur to balance cellular demands (Prihoda et al. 2012). Diatoms have a variety of alternative pathways within the chloroplast and mitochondria that can contribute to this re-routing of reductant and ATP (Cardol et al. 2011; Broddrick et al. 2019), particularly to optimise fitness under dynamic light.

1.3.2. Alternative electron pathways in diatoms

Alternative pathways can provide the means to generate energy and/or dissipate energy (e.g. photo-protection, Ralph et al. 2010) and can involve light-dependent or -independent processes. The photosynthetic ETC has a breadth of alternative pathways that effectively employ respiratory processes (i.e. oxygen consumption) as well as cyclic electron pathways that do not consume oxygen. Consumption of oxygen via midstream alternative oxidases (MOXs, Fig 1.2) serves a twofold purpose: as an electron sink to alleviate pressure within ETC and, consequently, as a driver of PMF whereby ATP synthase generates ATP. Examples of MOXs along the photosynthetic ETC include plastid terminal oxidase (PTOX), Mehler reaction, alternative oxidases within the thylakoid membrane and photorespiration (Cardol et al. 2011) that can be teased apart through use of inhibitors (Lewitus and Kana 1995; Bailey et al. 2008):

(1) Mehler activity occurs on the donor side of PSI whereby reduced ferredoxin is used to photo-reduce oxygen which generates ATP but consumes NADPH (Badger et al. 2000). Mehler activity is considered a major contributor of light-dependent respiration (LDR) to either balance cellular ATP:NADPH ratio or supplement photosynthetic ATP under light limitation (Raven & Beardall 2005). Light-induced oxygen uptake by Mehler activity in diatoms has been found to be a significant alternative electron sink, being 20-50% of GP_{O2} at PSII, under balanced (Weger et al. 1989) and unbalanced growth conditions (Claquin et al. 2004; Waring et al. 2010).

(2) Photorespiration involves the oxygenation of RuBisCO that produces unusable products (Wingler et al. 2000) and is an overall inefficient and

energy consuming process (Linka & Weber 2005). Diatoms have evolved CO_2-concentrating mechanisms (CCMs) to counter the low affinity of RuBisCO to CO_2 and thus considered a minor oxygen-consuming process contributing to diatom energy budgets (Beardall 1989; Rost et al. 2003; Claquin et al. 2004).

(3) The specific role of plastid (more accurately plastoquinol) terminal oxidase (PTOX) is contested as there are several processes that appear to be mediated by PTOX activity. In this pathway, a PTOX enzyme catalyzes the reduction of O_2 to H_2O using electrons from an over-reduced PQ pool (Mackey et al. 2008; McDonald et al. 2011) thus operating independently of Cyt b_6f or PSI to establish PMF that generates ATP but not NADPH. This is advantageous for diatoms particularly in low-iron conditions as ATP can be generated without the use of iron-rich Cyt b_6f and PSI (Behrenfeld and Milligan 2013). The targeted location of PTOX explains why it is suspected to have a regulatory role in downstream processes (Khorobrykh et al. 2020). Diatoms have been shown to upregulate PTOX to protect RCII and play a role in acclimation in low-iron or dynamic light environments (Nawrocki et al. 2015; Moreno et al. 2018). Chlororespiration, consumption of O_2 in the dark, and PTOX operate analogously to likely oxidise plastoquinol (Houill-Vernes et al. 2011; Krieger-Liszkay & Feilke 2016).

(4) Another oxygen consuming process is mitochondrial respiration (MR), often referred to as ‘dark’ respiration though this is misleading as MR occurs in the dark and light, concomitantly, with light-dependent respiratory (LDR)

processes. Mitochondrial respiration in diatoms was found to have significant involvement in priming mechanisms that optimise photosynthesis whereby, in the dark, plastid PMF was maintained by the hydrolysis of mitochondria-supplied ATP (Bailleul et al. 2015). Iron-limited diatoms were shown to use mitochondrial respiration in the light as a major sink for reducing equivalents that were photo-chemically generated (Allen et al. 2008). In fact, mitochondrial alternative oxidase (AOX) could be a possible mechanism to re-route photosynthetic electrons towards respiration (Yoshida et al 2007). Mitochondrial respiration can serve as an exclusive source of energy for cellular maintenance and biosynthesis during darkness, provide essential carbon-skeletons for biosynthesis in the light and dark and/or provide energy to supplement photosynthesis during the light (Geider & Osborne 1989). Mitochondrial respiration dynamics in the light are still not well characterised (Raven et al. 2020)

(5) Alternative pathways that do not consume oxygen include cyclic electron flow around PSII and PSI, CEF-PSII and CEF-PSI, respectively. Importantly, CEF-PSII is largely considered a photo-protective measure to avoid damage to PSII as neither ATP nor NADPH are generated from the 'cycling' of electrons from the donor to acceptor side of PSII, which ultimately results in re-oxidation of the PQ pool (Feikema et al. 2006; Lavaud et al. 2007; Wagner et al. 2016). Nitrogen limitation stimulated CEF-PSII activity in *Phaeodactylum tricornutum* (Wagner et al. 2016). Still, this is the most understudied process and could serve additional roles (Miyake & Okamura 2003). CEF-PSI has been observed to contribute to the

regulation of processes governing light acclimation (Iwai et al. 2010) by maintaining a trans-thylakoid pH gradient that also produces ATP (Joilot et al. 2006; Miyake 2010; Cardol et al. 2011) and observed in diatoms (Grouneva et al. 2006). Overall, energy generated from these pathways may largely contribute to the additional resource costs associated with photo-protective mechanisms that dissipate excess excitation energy at PSII.

(6) Flavodiiron proteins (FDPs) have been found in cyanobacteria, green algae and mosses (Allahverdiyeva et al. 2013, 2015) that mediate the protection of PSI from photo-oxidative damage via ROS by safely diverting excess electrons on the donor side of PSI to the photo-reduction of O_2 to H_2O (Ikík et al. 2017). However, diatoms, and all aquatic photoautotrophs in the red plastid lineage, do not encode genes for FDPs (Shimakawa et al. 2019). Indeed, the presence of a protein shown to have a critical role in PSI photo-protection, proton gradient regulation protein (PGR5), via CEF-PSI has been observed in sequenced diatoms, *Thalassiosira pseudonana* and *Phaeodactylum tricornutum* (Grouneva et al. 2011).

1.3.3. Photo-protection capacity of diatoms

As previously mentioned (see section 1.2. “Aquatic light environment”), light in aquatic environments are extremely dynamic, and where cells can go from darkness to exposure to full sunlight in minutes (Falkowski 1984, Macintyre et al. 2002); thus, it is of utmost importance that phytoplankton utilise mechanisms to regulate fluctuations in light that protect the photosynthetic machinery while also maintaining photosynthetic

efficiency. The unique photosynthetic architecture combined with photo-protective mechanisms employed by diatoms is consistent with their plasticity in response to light that leads to their dominance in turbulent environments (Strzepek & Harrison 2004, Goss & Jakob 2010).

Light-harvesting complexes (LHCs) are composed of pigments and proteins that attach to the PSII core to form the antennae which functions as a 'satellite dish' to capture light energy (i.e. photons) and funnel them to photosynthetic reaction centres (RC). Organisation and composition of these light harvesting systems appears quite distinctive for diatoms compared to other phytoplankton (Goss & Jakob 2010; Büchel 2014). Diatoms have unique light harvesting complex (Lhc) proteins (Lhcx) that use fucoxanthin, as the main accessory pigment, to funnel light to chlorophyll *a*, the main light harvesting pigment. This complex is termed fucoxanthin-chlorophyll-proteins (FCPs) (Miloslavina et al. 2009). Additionally, diatoms possess three major sub-groups of the LHC protein family: red alga-like Lhcr (comprise PSI-specific antennae Lhc polypeptides of red algae), Lhcf (comprise PSII antennae Lhc polypeptides named after the main light harvester carotenoid, fucoxanthin) and Lhcx proteins that are mainly involved with nonphotochemical quenching (Lepetit et al. 2012; Büchel 2014; Schober et al. 2019). Lhcr5, a specific Lhcr polypeptide group, is suggested to be involved with the dissipation of heat (i.e. nonphotochemical quenching) in diatoms when bound with a light-dissipating pigment (diatoxanthin, Dt) after increased expression of this protein was observed under high light (Dong et al. 2016) and was not found to be expressed under low light (Grouneva et al. 2016; Schober et al. 2019).

Lhcx proteins have recently been shown to closely interact with the xanthophyll pigment diatoxanthin (Dt) to allow nonphotochemical quenching, whereby – hypothetically – the outer antennae (Lhcx-Dt complex) is disconnected from the PSII core thus leading to a reduction of σPSII, a fluorescence-derived parameter that assesses the functional absorption cross-section of PSII, (Kuzminov & Gorunov 2016; Giovagnetti & Ruban 2017; Xu et al. 2018; Buck et al. 2019). Collectively, nonphotochemical quenching refers to the different phenomena that lead to the reduction of photochemical quenching by PSII, again measured using active chlorophyll fluorescence induction (sections 1.5.2 and 1.5.3). Nonphotochemical quenching is activated by a reduced PQ pool (Lepetit et al. 2013), i.e. acidification of the lumen from the associated build-up of PMF (Muller et al. 2001), to promote de-epoxidation of xanthophyll cycle carotenoids from diadinoxanthin (Dd, light harvesting) to Dt (light dissipating). Although the epoxidase requires NADPH (Goss et al. 2006), this mechanism is particularly cost-beneficial for diatom success in fluctuating light environments as it is the most rapid photo-protective mechanism that can protect PSII compared to the costs associated with damaged photosynthetic machinery (Raven 2011; Campbell & Tyystjärvi 2012; Li et al. 2016). Such photo-protective capacities additionally minimize damage by reactive oxygen species (ROS) via alleviating pressure along the photosynthetic ETC by dissipating photons and/or electrons.

1.3.4. Photo-inactivation and repair rates

Alternative electron pathways and photo-protective mechanisms work to optimise photochemical conversion at PSII and maintain cellular energetic demands of

ATP:NADPH for growth. The intricacies of photo-inactivation, inhibition and/or damage have been detailed in several reviews (Raven 2011, Vass 2012; Campbell & Serôdio 2020); however, there are still many unknowns that, within the context of this thesis, will be considered with greater focus on the energetic implications they have on diatom growth. Noteably, many authors use photo-inactivation, photo-inhibition and photo-damage interchangeably (Campbell & Tyystjärvi 2012). However, some consider photo-inhibition and photo-damage to be separate processes where photo-inhibition is the light-dependent decline of photosynthetic activity (Kok 1956; Vass 2012) and photo-damage refers to the amount of incident visible light that damages the catalytic oxidation of water via the oxygen evolving complex – more specifically the Mn_4Ca cluster (Ohnishi et al. 2005). For the purposes of this thesis, photo-inhibition is used to encompass all light-induced decreases in the quantum yield of photosynthesis from photo-inactivation (i.e. PSII closure driven by increasing light) with counteracting repair rates, all with respect to PSII (see Campbell & Serôdio 2020).

Photo-inactivation of PSII is an inevitable consequence of oxygenic photosynthesis, particularly within dynamic aquatic environments. Diatoms have a wide range of mechanisms at their disposal to limit damage to photosynthetic machinery and, compared to other phytoplankton lineages, show low susceptibility to photo-inactivation though this varies with cell size (Key et al. 2010; Wu et al. 2012; Wu et al. 2015). Photo-inactivation can occur from excess light when the amount of light absorbed by LHCs exceed the capacity of the ETC which can lead to the formation of reactive oxygen species (ROS). This occurs with energy transfer from the triplet state of chlorophyll *a* (P680) to O_2 at PSII, as well as at other sites (i.e. PQ pool and PSI),

where high concentrations of ROS have deleterious consequences (Khorobrykh et al. 2020). While the role of ROS in diatoms still remains largely unexplored (Lepetit & Dietzel 2015), there is some evidence to support ROS playing a signalling function as for plants and green algae (Dietz et al. 2016). The strong oxidative potential of ROS is of interest so long as concentrations are kept low by active scavengers to avoid cell death (Petroutsos et al. 2016; Havaux et al. 2005). Overall, diatoms therefore appear to have sufficient mechanisms in place to keep ROS concentrations low and minimum PSII-inactivation.

Photo-inactivation and repair kinetics overlap (Komenda et al. 2012; Nishiyama et al. 2014) whereby diatoms appear to exhibit trade-offs between coping strategies (Grouneva et al. 2011; Wu et al. 2011, 2012; Lavaud & Goss 2014). One strategy favours cellular investment for instantaneous capacity to repair PSII, which requires concurrent metabolic capacity to support associated protease and chloroplastic ribosomal activity, while the other involves delayed repair of inactive PSII when conditions are conducive for protein investment (Lavaud et al. 2016). The overarching point is that diatoms are well equipped to respond to dynamic light and while responses may be species-specific the ultimate goal is the same – optimise growth through effective cellular maintenance. However, how species-specific differences have evolved to these responses is a key – but still largely underexplored – factor that carries major implications for estimating the contribution of diatoms to primary production over space and time on a global scale.

1.4. Implications for energy budgets/PP models

Energy budgets and primary productivity models account for transfer efficiency of energy from initial photon absorption at PSII to the building of organic carbon cellular constituents. As such, accuracy of energy budgets is ultimately only as good as our ability to track sources and sinks of energy production and consumption. Overall, the efficiency of electron diversion away from carbon assimilation can be high in diatoms in response to growth conditions, and so tight regulation of dissipation mechanisms is necessary to avoid excessive decrease in the overall quantum yield of photosynthesis (Cardol et al. 2011). Diatoms have photo-protective mechanisms such as nonphotochemical quenching that decrease the total light energy that is available for photochemical conversion at PSII (i.e. the total energy available for cellular processes) while oxygen consuming pathways can decrease the fraction of energy remaining for growth. Compared to other phytoplankton groups, diatoms have consistently demonstrated efficient conversion of light energy to growth (Wagner et al. 2006; Jakob et al. 2007; Su et al. 2012). For example, under dynamic light, diatoms of varying photo-protective capacity, *Cyclotella meneghiniana* and *Skeletonema costatum*, utilise ~36% of absorbed light energy for carbon fixation (Su et al. 2012). Here, it was found that the efficiency of biomass production was determined primarily by catabolic metabolism of reduced carbon compounds and not by the efficiency of the photosynthetic reaction or energy dissipation within the chloroplast (Su et al. 2012). For a more completed picture, cellular energy budgets and primary productivity models must account for deviations in linear electron flow (LEF) and CO_2 fixation into biomass from 'losses' via alternative electron pathways and photo-protective mechanisms (e.g. nonphotochemical quenching) – until relatively recently such efforts

did not specifically measure these alternative processes (e.g. LDR or GP_C), but rather were derived.

Most common assessment to date of energy fluxes are from carbon and oxygen incubation-based methods that are highly debated over what is actually being measured along the continuum from gross and net production (Pei & Laws 2013). A particularly informative measure from carbon- and oxygen-based assessments of primary production comes from photosynthesis-irradiance (PE) curves that provide insightful parameterisations of photosynthetic performance. From nitrogen-limited cultures of *Thalassiosira weissflogii* (Halsey et al. 2013) and *Dunaliella tertiolecta* (Halsey et al. 2010) it was shown that only 30% of energy harvested at PSII (i.e. GP_{O2}) was retained as net carbon production (NP_C), or net primary production (NPP). Conversely, from light limited cultures of *Thalassiosira pseudonana* nearly 60% of GP_{O2} was retained into biomass (Fisher & Halsey 2016). more in depth accounting of energy budgets such as these clearly show the divergences not only between algal groups but also between sources of resource limitation (Fig 1.3). As informative and comprehensive as these assessments of energy budgets are, there is a caveat in that there is little data to make connections between the efficiency of conversion of light to energy – e.g. active fluorescence (Suggett et al. 2009; Lin et al. 2016; Hughes et al. 2018) and physiology.

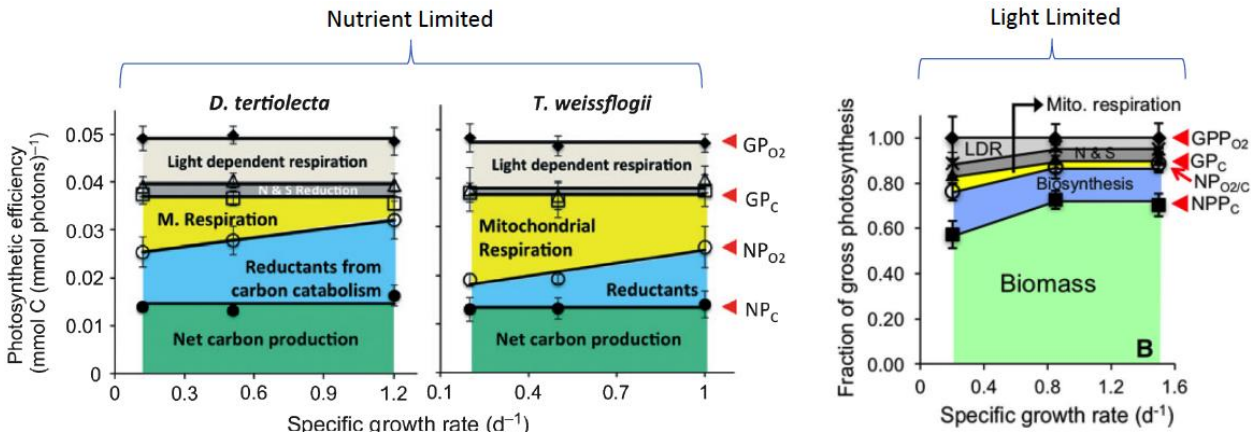

Figure 1.3. Energy budgets from nutrient limited cultures of *Dunaliella tertiolecta* and *Thalassiosira weissflogii* (left and middle plots) and light-limited cultures of *Thalassiosira pseudonana* (right plot) at a range of specific growth rates using carbon- and oxygen-based measurements. Components measured to build the energy budgets included gross primary production (GP_{O2} or GPP_{O2}), gross carbon production (GP_C), net primary production (NP_{O2} or $NP_{O2/C}$) and net carbon production (NP_C or NPP_C). Sub-divisions of energy allocation include light dependent respiration (LDR), nitrogen and sulfur (N+S) reduction, mitochondrial respiration, reductants from carbon catabolism which is equivalent to biosynthesis of macromolecules and net carbon production which is equivalent to biomass. Figures adapted from Halsey et al. 2013 (left and middle plots) and Fisher & Halsey 2016 (right plot).

Many energy budgets are assembled from cultures under steady-state conditions and rarely include a comprehensive set of fluorescence-, oxygen- and carbon-based measurements that would account for all cellular processes associated with energy loss. Florescence has great potential to provide energy allocation information collected more traditionally from incubation-based measures of oxygen and carbon. Still, energy budgets (i.e. Fig 1.3) rarely include fluorescence data. Efforts have gained traction over

the last two decades to link fluorescence-derived parameters (that can be collected from satellites) with current O_2/C-based measures to ultimately improve primary productivity models (Suggett et al. 2009; Trampe et al. 2015; Schuback et al. 2015, 2019; Hughes et al. 2018), but not yet within the framework of energy budgets – addressing this gap is a key feature of this thesis.

1.4.1. Photosynthesis-irradiance (PE) curves

Photosynthesis-irradiance (PE) curves are important because they provide a relatively standardised means of distinguishing between light-limited and light-saturated photosynthesis (MacIntyre et al. 2002), particularly from steady state growth under actinic light. Parameters retrieved from PE curves are the light-limited slope, α, the light-saturated maximum rate of photosynthesis, P_{max} (MacIntyre et al. 2002; Behrenfeld et al. 2004), and the light-saturation index, E_k (= P_{max}/α) (Talling 1957; Platt et al. 1977) (Fig 1.4), which together form the framework for global productivity models (Behrenfeld et al. 2004; Slisbe and Kromkamp 2012; Bouman et al. 2018).

PE curves are inherently a 'shape' function (Fig 1.4) that vary with environmental conditions (e.g. temperature and nutrients) as well as the "currency" (carbon, oxygen, or, more recently, fluorescence) measured. Moore et al. (2006) showed that E_k was much higher for fluorescence-derived ETR than ^{14}C-uptake rates, likely because ^{14}C-uptake saturated with light faster than light harvesting (i.e. ETR) capacity since alternative pathways that can be activated to dissipate excess electrons along the ETC to maintain maximal light harvesting efficiency at PSII (section 1.3.2). Phytoplankton are constantly working to optimise towards E_k (achieved through sensing the redox

state of the photosynthetic ETC, e.g. Escoubas et al. 1995). As such, phytoplankton are constantly photo-physiologically fine-tuning between light limitation, governed by increasing antennae size and/or number of reaction centres, and light saturation, governed by all downstream processes for the "currency" (i.e. electrons, oxygen, carbon) being measured (Hughes et al. 2018).

Behrenfeld et al. (2004) described variability in PE curves associated with variations in E_k. One form of PE curves was associated with independent changes in α^* and P^*_{max} that alter E_k (termed "E_k-dependent variability") and the other having parallel changes in α^* and P^*_{max} that did not change E_k (termed "E_k-independent variability") (Fig 1.4). Here, "*" symbolises chlorophyll-normalised values because of the specificity to phytoplankton and readily measured variable within the field (MacIntyre et al. 2002). An additional justification is that chlorophyll *a* is detectable and estimated from satellite imaging (Behrenfeld et al. 2002). E_k-dependent variability is a well-known characteristic of photoacclimation responses; where E_k varies as a result of changes in the concentration of light harvesting pigment that is regulated separately from the processes downstream of photosynthetic electron transport (Behrenfeld et al. 2004). However, it was not until the work of Halsey et al. (2010) that E_k-independent variability was found to be the result of changes in growth rate dependent carbon metabolism under varying degrees of nutrient limitation.

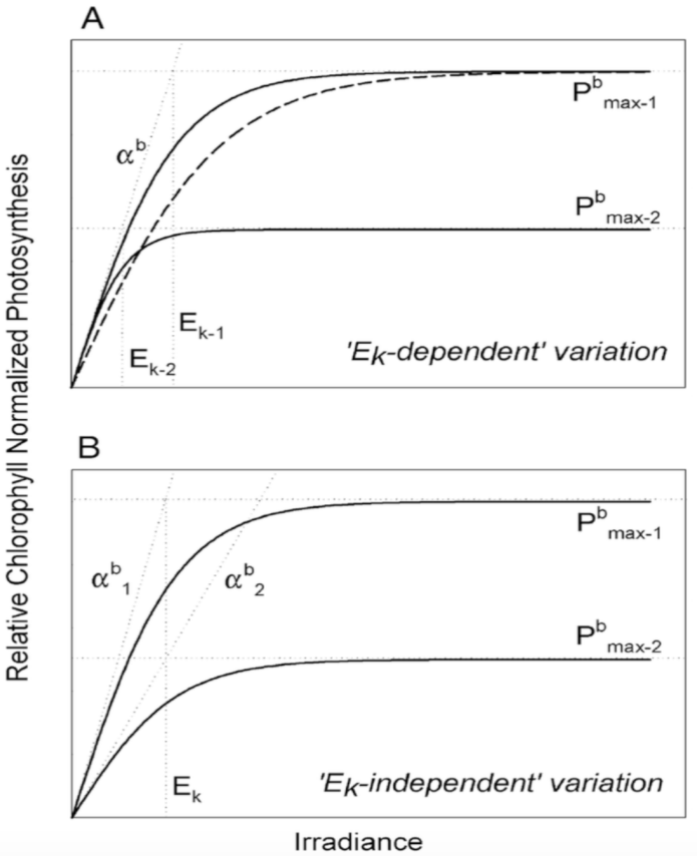

Behrenfeld et al. 2004

Figure 1.4. Photosynthesis-irradiance (PE) curves showing two fundamental descriptors of photosynthetic status: E_k-dependent variation (A) and E_k-independent variation (B) when photosynthesis is normalised to chlorophyll (subscript b). The PE curve is characterised by a light-saturated maximum rate of photosynthesis (P_{max}), light-limiting slope (α) and light saturation index (E_k).

Fisher & Halsey (2016) further found inconsistencies within PE curve parameters when measuring with different photosynthetic currencies. From labelled oxygen generated PE curves, where the cell has just harvested the total amount of energy available for downstream processes, P_{max} and α measurements were higher and E_k best represented

the growth irradiance of the culture. Comparing these results to short-term ^{14}C-uptake rates, P_{max} and α were lower and E_k overestimated the irradiance at which the culture was photo-acclimated suggesting that this currency-based method leads to misinterpretations of the light intensity in which cells are acclimated (i.e. E_k).

PE curves are therefore useful because the derivation and interpretation of their parameters mentioned above can be easily applied to models of PP, and how PP can be predicted from complex changes in the environment. Especially, with the use of fluorescence-derived E_k values, the potential to find correlations between oxygen- and carbon-based measures of photosynthesis would be extremely valuable in providing insight into phytoplankton physiological adjustments under dynamic environments to improve the accuracy of PP models.

1.5. Measurements of primary production

1.5.1. Isotopes as markers

Steemann-Nielsen introduced the ^{14}C technique in 1952 to measure phytoplankton production as CO_2-uptake. This method was hailed as an approach that overcame the sensitivity problem encountered with conventional gas exchange (O_2) measurements from light-dark bottle methods that are still used today (Riley 1939). Much debate followed over whether ^{14}C-uptake measures gross, net, or an intermediate rate of PP (Lloyd et al. 1977; Williams et al. 1996; Laws et al. 2000; Marra 2009; Beardall et al 2009), until Halsey et al (2010) revealed that short-term (20 min) incubations provided good estimates of gross carbon production (GP_C) and longer incubations (24 hours)

were more closely related to net PP. In an extensive review of ^{14}C uptake studies, it is clear that ^{14}C-uptake measurements have consistently underestimated gross PP (Pei & Laws 2013). Nonetheless, the radioactive tracer ^{14}C has been instrumental in determining the biochemical pathways of CO_2 fixation (Bassham & Calvin 1957), generating photosynthetic irradiance (PE) curves that are fundamental in making broader-scale estimates of aquatic PP (e.g. Behrenfeld & Falkowski 1997).

Another useful isotope in evaluating the roles of respiration, photorespiration, and other non-carbon respiratory pathways (e.g., the Mehler reaction, midstream oxidases, and the malate valve) is the oxygen isotope, $^{18}O_2$ (Weger et al. 1989; Geider & Osborne 1992; Kana 1990). This isotope is useful because it allows for the direct evaluation of gross PP (as gross O_2 production, GP_{O2}) (Bender et al. 1987; Grande et al. 1989) and respiration in illuminated algae (Radmer & Ollinger 1980) whereby respiration can be estimated from the consumption of $^{18}O_2$ while simultaneously measuring photosynthesis from the evolution of $^{16}O_2$ (Peltier & Thibault 1985) using instruments such as membrane inlet mass spectrometers (MIMS) (e.g. Kana 1994; Suggett et al. 2009; Fisher & Halsey 2016; Ferrón et al. 2016; Burlacot et al. 2020). The use of inhibitors (e.g. DCMU – Weger et al. 1989, Kana et al 2004; cyanide, KCN – Weger et al. 1989, Kana 1993; SHAM – Møller et al. 1988 and propyl gallate – Bailey et al. 2008) has also allowed the contributions of various respiratory processes in the light vs dark to be teased apart (Lewitus & Kana 1995) though inhibitors can be undermined by the possibility of compensatory processes (Raven et al. 2020). Similarly, chlorophyll concentrations are more closely related to gross PP than net PP, and over the past two decades, the triple oxygen isotope method has become more advanced and has helped provide good estimates of gross PP in the field (Juranek & Quay 2013).

Much progress has been made in developing an incubation-free method to derive net PP from phytoplankton carbon measurements (Graff et al. 2012, 2015) that can be combined with models of growth rate. Ultimately, ^{14}C methods can provide estimates of GP_C and net PP whereas $^{18}O_2$ and $^{16}O_2$ can measure gross PP and net oxygen production (Net_{O2},), respectively. The real goal lies in developing a single, high resolution method that can provide accurate measures of PP, where currently the most attractive candidate is fluorescence.

1.5.2. Fluorescence as a bio-optical tool

The light reactions of photosynthesis involve light absorption and energy dissipation by the two photosystems. Fluorescence occurs when light is emitted at a longer wavelength, thus lower energy, out of the cell to avoid photochemical damage of the reaction centre. Under ambient environmental conditions, all Chl *a*-containing organisms emit some amount of fluorescence (about 3% of all light absorbed) - almost exclusively from photosystem II (PSII) – as a result of inherent inefficiencies of light capture by "open" reaction centres. The reaction centre is "closed" when the electron that was lost at P680/P700 from the excitation of light energy has not been replenished. When this happens, fluorescence increases as more energy is dissipated away from the reaction centres.

The ubiquitous nature of chlorophyll fluorescence emissions from primary producers, and its connection to photosynthetic activity, has resulted in a vast technological push to detect fluorescence from both in situ and remote sensors. Such longer wavelength

fluorescence emissions can be captured by a photo-diode within the fluorometer and can be easily measured in laboratory and field settings to acquire a suite of photophysiological parameters in real time (e.g. Suggett et al. 2010). Importantly, chlorophyll fluorescence methods avoid the problems of traditional methods (above), since gross photosynthesis (GP_{O2}) can be continuously measured non-invasively and in real time without affecting their physiological state (Kolber et al. 1998; Greene et al. 1992). Strictly, chlorophyll fluorescence induction returns the photochemical efficiency of charge separation at PSII (and the so-called "Electron Transport Rate", ETR_{PSII}) (Kolber & Falkowski 1993). As such, gross PP from fluorescence has the potential to differ from GP_{O2} under circumstances that disconnect ETR from the rate of water splitting (e.g. cyclic electron flow around PSII) (Prasil et al. 1996). Even so, ETR_{PSII} have been widely used to describe productivity on their own (e.g. Suggett et al. 2006) and in combination with other currency measures of photosynthesis (C/O_2) (Suggett et al. 2009; Lawrenz et al. 2013; Schuback et al. 2015, 2019). In the latter case, the aim is to resolve the decoupling amongst photosynthetic currencies measured and provide evidence of alternative energetic flows via fluorometry. Fluorescence can also provide important parameters, such as the pool of active verses total PSII, to quantify the photosynthetically generated energy that is available for cellular metabolic processes.

Sources of variability in the relationship between photosynthesis and fluorescence can be generalised by three categories: (1) methodological error associated with "benchmark" measurements of PP (e.g. ^{14}C and $^{18}O_2$) and/or irradiance; (2) temporal discrepancies obtaining rates of photosynthesis (hours) versus fluorescence (seconds); and (3) dynamic environmental factors, such as light, temperature, nutrients, and

species composition (Chamberlin & Marra 1992). Many studies have shown that nutrient stress does not impair photochemical efficiencies (Behrenfeld & Milligan 2013; Silsbe et al. 2015) leading to the misinterpretation that fluorescence measurements provide a universal diagnostic of algal metabolic health. Indeed, how variable photochemical efficiencies (and in turn ETRs) are over space and time, and how this translates to metabolic activity, remains largely unexplored.

1.5.3. Developments measuring fluorescence

Pulse amplitude modulated (PAM) fluorometry are commonly used to measure multiple turnover (MT) of PSII to assess photosynthetic efficiencies (F_v/F_m) and is more commonly used in terrestrial systems (Schreiber et al. 1986), and/or laboratory settings where marine phytoplankton biomass is high (Krompkamp & Peene 1999; Gilbert et al. 2000; Juneau & Harrison 2005). In the latter case, PAM- based approaches have often been routinely employed for assessing the physiology (Petrou et al. 2010) and productivity (Morelle & Claquin 2018) of diatoms. We recognised the advancements and modifications to PAM fluorometry that now include the ability to collect ETR under relatively low chlorophyll yields; however, my research will focus on improving interpretations of Fast Repetition Rate fluorometry (FRRf) signatures – which commonly measure single turnover (ST) of PSII – in response to variable light environments as it is more commonly used in by the oceanographic community, and so provides a means to bridge laboratory and field data that is not confounded by ST versus MT peculiarities (e.g. Suggett et al. 2003).

FRRf delivers single flashlets of light at supersaturating levels over very short timescales (50-200 μs) to achieve measurements of F_v/F_m and the functional absorption cross section of PSII (σ_{PSII}) from a single turnover (ST), followed by prolonged pulses of light to relax the reduced PQ pool (Kolber et al. 1998) (Fig 1.5). ST refers to the excitation and closure of all PSII reaction centres through a series of rapid flashes whereby Q_A is reduced once. The PSII reaction centre remains "closed" until the transfer of photochemically-generated electrons from Q_A to Q_B. This closure, lasting around 1000 μs, results in the increased fluorescence yield captured by the fluorometer. A main advantage of the ST protocol compared to solely MT measurements (as with PAM fluorometry) is that it does not increase the redox state of the plastoquinone (PQ) pool, which itself can modify the fluorescence yields generated from PSII (Suggett et al. 2003). It is this culmination of information gained from ST and MT measures that has made FRRf the preferred method for oceanographers in addition to the high sensitivity of this instrument (Hughes et al. 2018).

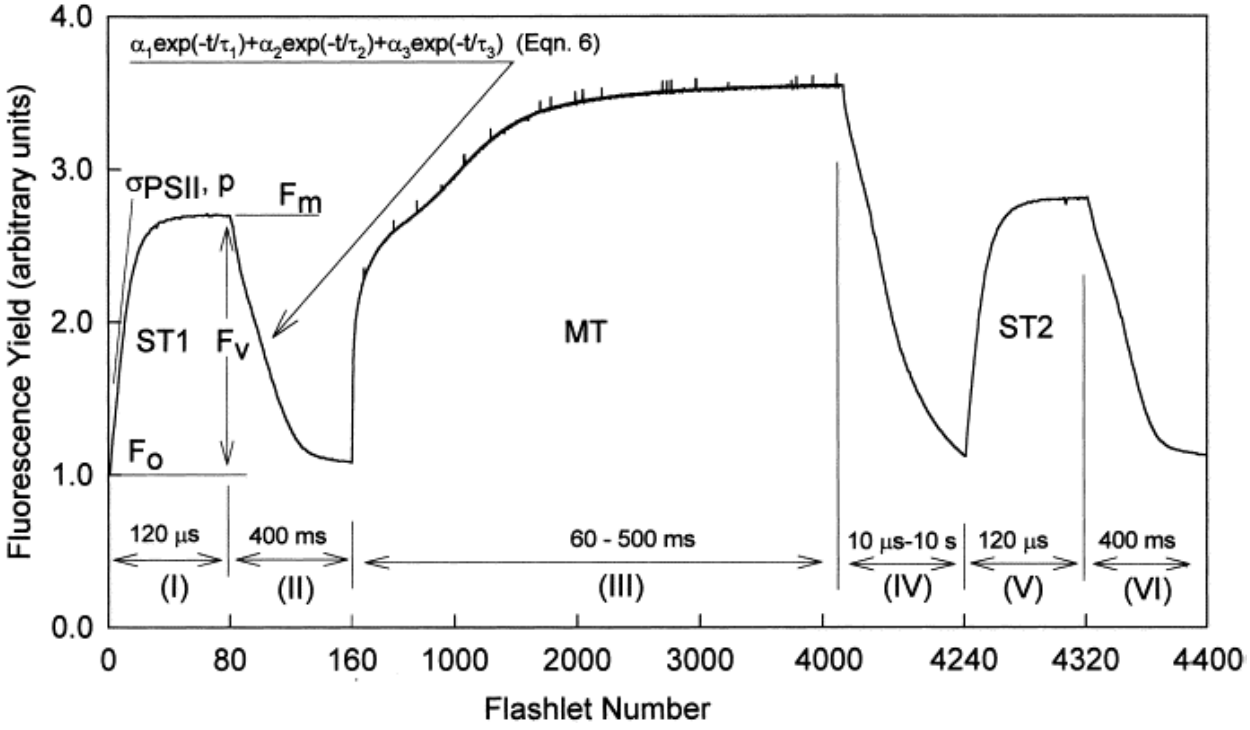

Kolber et al. 1998

Figure 1.5. Phases of FRRf method measuring fluorescence transients. Roman numerals represent the different phases and the times found above correlate to the duration of each phase. Single turnover (ST) flashes (Phases I and V) encompass a series of high frequency (0.5-2 µs intervals) flashlets (80-120). Multiple turnover (MT) flashes (Phase III) is similar to ST with more flashlets (~4000) at lower frequency (20-200 µs intervals). Following each turnover phase (II, IV, and VI), there is a relaxation protocol of 40-80 flashlets at intervals exponentially varying (50 µs–50 ms). Each phase provides information on various fluorescence transients: I and V give variable fluorescence (F_v) from initial (F_o) and maximal (F_m) fluorescence, functional absorption cross-section (σ_{PSII}), and energy transfer between PSII reaction centres, RCII; II and VI give the kinetics of Q_A re-oxidation; IV give kinetics of PQ pool re-oxidation; III gives fluorescence yield under MT conditions thereby allowing the effects of earlier MT excitations on photosynthetic parameters to be quantified (V and VI).

FRRf was originally developed by oceanographers to operate under the characteristically low chlorophyll yields of the open ocean. As such, historically, much of our knowledge of chlorophyll fluorescence characteristics of phytoplankton in natural marine settings, including diatoms, comes from FRRf. Most FRRf protocols use ETRs measured at various light levels to produce a PE curve (i.e. "fluorescence-light response curve", FLC) but this still presents the same problem as ^{14}C-based measurements of lengthy incubations. My research used cutting-edge Light-Induced Fluorescence Transient (LIFT)-FRRf instrumentation (Keller et al. 2019) to assess photophysiological characteristics.

1.6. Metabolomics: advancements towards connecting omics and physiology

While photosynthesis measurements describe the outcome of operation of photosynthetic pathways, "omics" techniques provide high-throughput data generating methods that allow for comprehensive insight into nearly all components within the cell and how they function cohesively (Jamers et al. 2009) without depending on a cellular 'currency' metric (i.e. fluorescence, carbon or oxygen). Any given 'omics' technique answers a different question at different scales of operation: genomics outlines what can happen (giving the genetic potential) (e.g. Armbrust et al. 2004), transcriptomics explains what appears to be happening (giving information about what genes are being expressed but not necessarily translated) (e.g. Ashworth et al. 2013), proteomics demonstrates what makes it happen (showing which proteins are being expressed) (e.g. Dong et al. 2016), and metabolomics informs what has happened and is currently happening (giving pool sizes of compounds produced) (e.g. Heal et al. 2019).

Metabolites are molecules synthesised by enzymatic reactions leading to the biological processes, including responses to environmental change, that contribute to an organism's phenotype, collectively referred to as the metabolome (Goulitquer et al. 2012), and arguably the least employed 'omics platform to date with diatoms. As such, my research used metabolomics for comprehensive and quantitative analysis of diatom biosynthetic processes in response to different dynamic light regimes to ultimately find connections between more traditional measures of cellular currencies (i.e. fluorescence, carbon and oxygen).

Metabolites have long been a useful tool for gaining a snapshot of cell physiology at a specific point in time as they are the end products of cellular regulatory processes. Metabolite concentrations are the ultimate response of biological systems to genetic and environmental changes (Fiehn 2002). Environmental stressors can alter the production and degradation of metabolites thus understanding how such stressors will affect the metabolome of primary producers is significant. However, the vastness and diversity of the metabolome make it technologically impossible to analyze all metabolites in an organism using a single analysis technique (Jamers et al. 2009; Huseby et al. 2012); thus, a combination of methods are necessary but may change as technology advances make differentiating metabolites more efficient and precise (e.g. LC-MS and GC-MS; Hillyer et al. 2016). The methods currently in use still need refinement but ultimately better databases ("libraries"), similar to genomic and proteomic databases, need to be established as there is a surplus of unknown metabolites. As with any "omics"-related discipline, metabolomics is strongly

dependent on the availability and quality of a wide variety of resources that can be used to interpret data more effectively (Goulitquer et al. 2012).

With the advances in genome sequencing technology, more phytoplankton genomes are being completed which in combination with a detailed metabolic profile will greatly enhance our current understanding of the metabolic processes that phytoplankton use to interact with their environment and the evolution of those underlying metabolic pathways (Fernie et al. 2012). Though phytoplankton metabolomics is still in the beginning stages of development, there have been some significant breakthroughs. Ultimately, metabolomics can only improve current ecosystems models and may even bridge the substantial gaps in our present knowledge archive to provide clarification for fundamental topics including defining metabolic pathways that algal species utilise to adapt to dynamic environment while remaining competitively fit and photosynthetically efficient.

At present, it is possible to determine metabolite profiles distinctive for taxonomic and environmental variation but much more difficult to describe detailed cellular mechanisms that would help to better understand metabolic pathways that lead to physiological and ecological differences of different algae (Klueth et al. 2015). Developing metabolomics that can be applied to diatoms will be a critical step in this study to highlight different energy allocation strategies through the up/down regulation or presence/absence of metabolites under various light treatments.

1.7. Thesis Roadmap, Aim & Objectives

Diatoms are incredibly diverse – both functionally and taxonomically – often thriving in physically dynamic environments where light availability is particularly variable. While past research has well established that diatoms have evolved an array of strategies to optimise light harvesting for photosynthesis (Wagner et al. 2006; Wilhelm et al. 2014; Halsey & Jones 2015; Fisher & Halsey 2016), it remains generally unknown how plasticity in light harvesting mechanisms operate in concert with changes in metabolic processes (i.e. photosynthesis and respiration) to ensure growth and/or survival as light availability alters. Therefore, **the overall aim of this thesis is to advance our understanding of diatom "metabolic strategies" that contribute to the maintenance of efficient photosynthetic functioning**. To address this broad aim, I conducted a series of experiments to examine the effect of transient high light exposure, sinusoidal light climates, and influence of light-dark cycles on key diatom species. I applied a suit of state-of-the-art techniques including active chlorophyll fluorometry (with and without inhibitors) and various mass spectrometers to track light utilisation strategies, and, for the first time, metabolomics to resolve how processes operate collectively to enable cellular regulation under dynamic light.

The specific aims of this project are:

<u>Aim 1:</u> Identify energy dissipation mechanisms employed by diatoms under transient exposure to high light. Given the high diversity of diatoms, an initial photophysiological screening of seven diatoms, ranging in size, shape and ecological niche, revealed major differences amongst diatoms in their response to increasing light. From this screening, three diatoms (*Thalassiosira weissflogii*, *Thalassiosira oceanica*,

and *Thalassiosira pseudonana*) that represented the range of diatom responses were selected for further in-depth characterisation of the mechanisms employed to explain this photophysiological variation (Chapter 2), including photochemical pigment conversion, photosynthetic reaction centre turnover, photochemical excitation pressure and simultaneous oxygen production/consumption.

Chapter 2 has been published: Fisher NL, Campbell DA, Hughes DJ, Kuzhiumparambil U, Halsey KH, Ralph PJ, Suggett DJ (2020) Divergence of photosynthetic strategies amongst marine diatoms. PLoS ONE 15(12): e0244252. https://doi.org/10.1371/journal.pone.0244252.

Aim 2: Determine the dynamic contribution of light-dependent O_2-consumption to mitigate excitation pressure over a diel cycle for diatoms with known differences in photo-protection capacities. Models of ocean primary productivity and cellular energy budgets often assume a constant rate of respiration because it is a difficult parameter to measure and interpret. Building on the findings of Chapter 2, where mechanisms to dissipate excess photochemically generated energy was vastly different, one diatom showed clear dependence on light dependent O_2-consumption (respiration) (e.g. *Thalassiosira oceanica*) while another showed much less reliance (e.g. *Thalassiosira weissflogii*) – however, this was based on a single time point from a transient shift to high light. Thus, for Chapter 3 these diatoms were selected to evaluate respiration over a diel cycle to determine whether these 'preferences' were maintained throughout more dynamic – sinusoidal – light regime that occur in nature, and/or whether respiration dependency can be explained by intensity (as time of day). We also

aimed to find links between fluorescence-derived assessments of photo-protective capacity and measures of oxygen in the light, which is rarely seen in the literature.

Aim 3: Resolve deeper changes to the metabolome of *Thalassiosira pseudonana* under varying light dosage and intensity. While research in Chapters 2-3 focussed on *T. weissflogii* and *T. oceanica*, Chapter 4 changes to focus on the sequenced centric diatom *T. pseudonana*. Since the genome was sequenced (Armbrust et al. 2004), *T. pseudonana* has been a model organism for 'omics' studies to complement physiological research. Given that much knowledge has been gained for this diatom taxa, we chose to use this species to more deeply mine metabolic changes through the metabolome. This added to the work in Chapter 2, where *T. pseudonana* employed a more generalised strategy of light harvesting and dissipation (compared to all other taxa) under high light. Given the scarcity of light-driven metabolomics studies for diatoms, using this model diatom taxon was a logical choice to explore the metabolic changes, for the first time, focusing solely on responses to light availability in concert to observed physiology. Chapters 2 and 3 depend on measures of cellular currencies whereas metabolic profiles are not reliant on these measures and thus provide a wholesome snapshot of a cell's response to environmental stimuli. This chapter therefore specifically asked what key (and rapid) metabolic "switches" were evident to support *T. pseudonana*'s generalised response to high light exposure allowing ecological success in natural waters.

Chapter 4 has been submitted for peer-review: Fisher NL, Halsey KH, Suggett DJ, Pombrol M, Ralph PJ, Lutz A, Sogin EM and Matthews JL. Light-dependent metabolic

phenotype of the model diatom *Thalassiosira pseudonana*. Submitted to *Journal of Experimental Botany*

The knowledge gained by addressing these three aims is then considered in Chapter 5 where my findings are synthesised and future directions for diatom energy allocation strategies are discussed.

1.8. References

Allakhverdiev, S. I., Thavasi, V., Kreslavski, V. D., Zharmukhamedov, S. K., Klimov, V. V., Ramakrishna, S., … Carpentier, R. (2010). Photosynthetic hydrogen production. *Journal of Photochemistry and Photobiology C: Photochemistry Reviews*, *11*, 101–113. https://doi.org/10.1016/j.jphotochemrev.2010.07.002

Allahverdiyeva, Y., Mustila, H., Ermakova, M., Bersanini, L., Richaud, P., Ajlani, G., … Aro, E. M. (2013). Flavodiiron proteins Flv1 and Flv3 enable cyanobacterial growth and photosynthesis under fluctuating light. *Proceedings of the National Academy of Sciences of the United States of America*, *110*(10), 4111–4116. https://doi.org/10.1073/pnas.1221194110

Allahverdiyeva, Y., Suorsa, M., Tikkanen, M., & Aro, E. M. (2015). Photo-protection of photosystems in fluctuating light intensities. *Journal of Experimental Botany*, *66*(9), 2427–2436. https://doi.org/10.1093/jxb/eru463

Allen, J. F. (2002). Photosynthesis of ATP—electrons, proton pumps, rotors, and poise. *Cell*, *110*(3), 273-276.

Allen, A. E., LaRoche, J., Maheswari, U., Lommer, M., Schauer, N., Lopez, P. J., ... & Bowler, C. (2008). Whole-cell response of the pennate diatom Phaeodactylum tricornutum to iron starvation. *Proceedings of the National Academy of Sciences*, *105*(30), 10438-10443.

Amthor, J. S. (2010). From sunlight to phytomass: On the potential efficiency of converting solar radiation to phyto-energy. *New Phytologist*, *188*(4), 939–959. https://doi.org/10.1111/j.1469-8137.2010.03505.x

Armbrust, E. V. (2009). The life of diatoms in the world's oceans. *Nature*, *459*(7244), 185–192. https://doi.org/10.1038/nature08057

Armbrust, E. V., Berges, J. A., Bowler, C., Green, B. R., Martinez, D., Putnam, N. H., … Rokhsar, D. S. (2004). The genome of the diatom Thalassiosira pseudonana: Ecology, evolution, and metabolism. *Science*, *306*(5693), 79–86. https://doi.org/10.1126/science.1101156

Ashworth, J., Coesel, S., Lee, A., Armbrust, E. V., Orellana, M. V., & Baliga, N. S. (2013). Genome-wide diel growth state transitions in the diatom Thalassiosira pseudonana. *Proceedings of the National Academy of Sciences of the United States of America*, *110*(18), 7518–7523. https://doi.org/10.1073/pnas.1300962110

Austin, R. W., & Petzold, T. J. (1986). Spectral dependence of the diffuse attenuation coefficient of light in ocean waters. *Optical Engineering*, *25*(3), 253471.

Badger, M. R., Von Caemmerer, S., Ruuska, S., Nakano, H., Laisk, A., Allen, J. F., … Griffiths, H. (2000). Electron flow to oxygen in higher plants and algae: Rates and control of direct photoreduction (Mehler reaction) and rubisco oxygenase. *Philosophical Transactions of the Royal Society B: Biological Sciences*, *355*(1402), 1433–1446. https://doi.org/10.1098/rstb.2000.0704

Bailey, S., Melis, A., Mackey, K. R. M., Cardol, P., Finazzi, G., van Dijken, G., … Grossman, A. (2008). Alternative photosynthetic electron flow to oxygen in marine Synechococcus. *Biochimica et Biophysica Acta - Bioenergetics*, *1777*(3), 269–276. https://doi.org/10.1016/j.bbabio.2008.01.002

Bailleul, B., Berne, N., Murik, O., Petroutsos, D., Prihoda, J., Tanaka, A., … Finazzi, G. (2015). Energetic coupling between plastids and mitochondria drives CO 2 assimilation in diatoms. *Nature*, *524*(7565), 366–369. https://doi.org/10.1038/nature14599

Barnett, A., Méléder, V., Blommaert, L., Lepetit, B., Gaudin, P., Vyverman, W., … Lavaud, J. (2015). Growth form defines physiological photoprotective capacity in intertidal benthic diatoms. *ISME Journal*, *9*(1), 32–45. https://doi.org/10.1038/ismej.2014.105

Bassham, J. A., & Calvin, M. (1957). The path of carbon in photosynthesis. Prentice-Hall, NJ.

Beardall, J. (1989). Photosynthesis and photorespiration in marine phytoplankton. *Aquatic Botany*, *34*(1-3), 105-130.

Beardall, J., Ihnken, S., & Quigg, A. (2009). Gross and net primary production: Closing the gap between concepts and measurements. *Aquatic Microbial Ecology*, *56*(2–3), 113–122. https://doi.org/10.3354/ame01305

Behrenfeld, M. J., & Milligan, A. J. (2013). Photophysiological Expressions of Iron Stress in Phytoplankton. *Annual Review of Marine Science*, *5*, 217–246. https://doi.org/10.1146/annurev-marine-121211-172356

Behrenfeld, M. J., & Falkowski, P. G. (1997). Photosynthetic rates derived from satellite-based chlorophyll concentration. *Limnology and Oceanography*, *42*(1), 1–20. https://doi.org/10.4319/lo.1997.42.1.0001

Behrenfeld, M. J., Marañón, E., Siegel, D. A., & Hooker, S. B. (2002). Photoacclimation and nutrient-based model of light-saturated photosynthesis for quantifying oceanic primary production. *Marine Ecology Progress Series*, *228*, 103–117. https://doi.org/10.3354/meps228103

Behrenfeld, M. J., Prasil, O., Babin, M., & Bruyant, F. (2004). In search of a physiological basis for covariations in light-limited and light-saturated photosynthesis. *Journal of Phycology*, *40*(1), 4–25. https://doi.org/10.1046/j.1529-8817.2004.03083.x

Behrenfeld, M. J., Halsey, K. H., & Milligan, A. J. (2008). Evolved physiological responses of phytoplankton to their integrated growth environment. *Philosophical Transactions of the Royal Society B: Biological Sciences*, *363*(1504), 2687–2703. https://doi.org/10.1098/rstb.2008.0019

Behrenfeld, M. J. (2014). Climate-mediated dance of the plankton. *Nature Climate Change*, *4*(10), 880–887. https://doi.org/10.1038/nclimate2349

Bender, M., Grande, K., Johnson, K., Marra, J., Williams, P. J. L. B., Sieburth, J., … Heinemann, K. (1987). A comparison of four methods for determining planktonic community production. *Limnology and Oceanography*, *32*(5), 1085–1098. https://doi.org/10.4319/lo.1987.32.5.1085

Bidle, K. D., & Falkowski, P. G. (2004). Cell death in planktonic, photosynthetic microorganisms. *Nature Reviews Microbiology*, *2*(8), 643–655. https://doi.org/10.1038/nrmicro956

Blankenship, R. E. (2002). Molecular Mechanisms of Photosynthesis Blackwell Science. *Maiden, MA*.

Blankenship, R. E. (2010). Early Evolution of Photosynthesis. *Plant Physiology*, *154*(2), 434–438. https://doi.org/10.1104/pp.110.161687

Blommaert, L., Lavaud, J., Vyverman, W., & Sabbe, K. (2018). Behavioural versus physiological photo-protection in epipelic and epipsammic benthic diatoms. *European Journal of Phycology*, *53*(2), 146–155. https://doi.org/10.1080/09670262.2017.1397197

Boyd, P. W., Rynearson, T. A., Armstrong, E. A., Fu, F., Hayashi, K., Hu, Z., … Thomas, M. K. (2013). Marine Phytoplankton Temperature versus Growth Responses from Polar to Tropical Waters - Outcome of a Scientific Community-Wide Study. *PLoS ONE*, *8*(5). https://doi.org/10.1371/journal.pone.0063091

Bopp, L., Monfray, P., Aumont, O., Dufresne, J. L., Le Treut, H., Madec, G., … Orr, J. C. (2001). Potential impact of climate change on marine export production. *Global Biogeochemical Cycles*, *15*(1), 81–99. https://doi.org/10.1029/1999GB001256

Bouman, H. A., Platt, T., Doblin, M., Figueiras, F. G., Gudmundsson, K., Gudfinnsson, H. G., … Sathyendranath, S. (2018). Photosynthesis-irradiance parameters of marine phytoplankton: Synthesis of a global data set. *Earth System Science Data*, *10*(1), 251–266. https://doi.org/10.5194/essd-10-251-2018

Bowler, C., Allen, A. E., Badger, J. H., Grimwood, J., Jabbari, K., Kuo, A., … Grigoriev, I. V. (2008). The Phaeodactylum genome reveals the evolutionary history of diatom genomes. *Nature*, *456*(7219), 239–244. https://doi.org/10.1038/nature07410

Bowler, C., Vardi, A., & Allen, A. E. (2010). Oceanographic and biogeochemical insights from diatom genomes. *Annual Review of Marine Science*, *2*(1), 333–365. https://doi.org/10.1146/annurev-marine-120308-081051

Boyd, P. W., & Doney, S. C. (2002). Modelling regional responses by marine pelagic ecosystems to global climate change. *Geophysical Research Letters*, *29*(16), 53-1-53–54. https://doi.org/10.1029/2001gl014130

Boyd, P. W., Strzepek, R., Fu, F., & Hutchins, D. A. (2010). Environmental control of open-ocean phytoplankton groups: Now and in the future. *Limnology and Oceanography*, *55*(3), 1353–1376. https://doi.org/10.4319/lo.2010.55.3.1353

Boyd, P. W., Cornwall, C. E., Davison, A., Doney, S. C., Fourquez, M., Hurd, C. L., … McMinn, A. (2016). Biological responses to environmental heterogeneity under future ocean conditions. *Global Change Biology*, *22*(8), 2633–2650. https://doi.org/10.1111/gcb.13287

Broddrick, J. T., Du, N., Smith, S. R., Tsuji, Y., Jallet, D., Ware, M. A., … Allen, A. E. (2019). Cross-compartment metabolic coupling enables flexible photoprotective mechanisms in the diatom Phaeodactylum tricornutum. *New Phytologist*, *222*(3), 1364–1379. https://doi.org/10.1111/nph.15685

Büchel, C. (2014). *Fucoxanthin-Chlorophyll-Proteins and Non-Photochemical Fluorescence Quenching of Diatoms*. 259–275. https://doi.org/10.1007/978-94-017-9032-1_11

Buck, J. M., Sherman, J., Bártulos, C. R., Serif, M., Halder, M., Henkel, J., … Lepetit, B. (2019). Lhcx proteins provide photo-protection via thermal dissipation of absorbed light in the diatom Phaeodactylum tricornutum. *Nature Communications*, *10*(4167). https://doi.org/10.1038/s41467-019-12043-6

Burlacot, A., Burlacot, F., Li-Beisson, Y., & Peltier, G. (2020). Membrane Inlet Mass Spectrometry: A Powerful Tool for Algal Research. *Frontiers in Plant Science*, *11*(September), 1–15. https://doi.org/10.3389/fpls.2020.01302

Campbell, D. A., & Tyystjärvi, E. (2012). Parameterization of photosystem II photo-inactivation and repair. *Biochimica et Biophysica Acta - Bioenergetics*, *1817*(1), 258–265. https://doi.org/10.1016/j.bbabio.2011.04.010

Campbell, D. A., & Serôdio, J. (2020). Photoinhibition of Photosystem II in Phytoplankton: Processes and Patterns. In *Photosynthesis in Algae: Biochemical and Physiological Mechanisms* (pp. 329-365). Springer, Cham.

Cardol, P., Forti, G., & Finazzi, G. (2011). Regulation of electron transport in microalgae. *Biochimica et Biophysica Acta - Bioenergetics*, *1807*(8), 912–918. https://doi.org/10.1016/j.bbabio.2010.12.004

Cermeño, P., Falkowski, P. G., Romero, O. E., Schaller, M. F., & Vallina, S. M. (2015). Continental erosion and the Cenozoic rise of marine diatoms. *Proceedings of the National Academy of Sciences of the United States of America*, *112*(14), 4239–4244. https://doi.org/10.1073/pnas.1412883112

Chamberlin, S., & Marra, J. (1992). Estimation of photosynthetic rate from measurements of natural fluorescence: analysis of the effects of light and temperature. *Deep Sea Research Part A, Oceanographic Research Papers*, *39*(10), 1695–1706. https://doi.org/10.1016/0198-0149(92)90024-N

Claquin, P., Kromkamp, J. C., & Martin-Jezequel, V. (2004). Relationship between photosynthetic metabolism and cell cycle in a synchronized culture of the marine alga Cylindrotheca fusiformis (Bacillariophyceae). *European Journal of Phycology*, *39*(1), 33–41. https://doi.org/10.1080/0967026032000157165

Croteau, D., Guérin, S., Bruyant, F., Ferland, J., Campbell, D. A., Babin, M., & Lavaud, J. (2020). Contrasting nonphotochemical quenching patterns under high light and darkness aligns with light niche occupancy in Arctic diatoms. *Limnology and Oceanography*, 1–15. https://doi.org/10.1002/lno.11587

Cruz, J. A., Avenson, T. J., Kanazawa, A., Takizawa, K., Edwards, G. E., & Kramer, D. M. (2005). Plasticity in light reactions of photosynthesis for energy production and photo-protection. *Journal of Experimental Botany*, *56*(411), 395–406. https://doi.org/10.1093/jxb/eri022

Dietz, K. J., Turkan, I., & Krieger-Liszkay, A. (2016). Redox- and reactive oxygen species-dependent signaling into and out of the photosynthesizing chloroplast. *Plant Physiology*, *171*(3), 1541–1550. https://doi.org/10.1104/pp.16.00375

Dong, H. P., Dong, Y. L., Cui, L., Balamurugan, S., Gao, J., Lu, S. H., & Jiang, T. (2016). High light stress triggers distinct proteomic responses in the marine diatom Thalassiosira pseudonana. *BMC Genomics*, *17*(1), 1–14. https://doi.org/10.1186/s12864-016-3335-5

Edwards, K. F., Thomas, M. K., Klausmeier, C. A., & Litchman, E. (2015). Light and growth in marine phytoplankton: Allometric, taxonomic, and environmental

variation. *Limnology and Oceanography*, *60*(2), 540–552. https://doi.org/10.1002/lno.10033

Eppley, R. W. (1972). Temperature and phytoplankton growth in the sea. *Fish. bull*, *70*(4), 1063-1085.

Escoubas, J. M., Lomas, M., LaRoche, J., & Falkowski, P. G. (1995). Light intensity regulation of cab gene transcription is signaled by the redox state of the plastoquinone pool. *Proceedings of the National Academy of Sciences of the United States of America*, *92*(22), 10237–10241. https://doi.org/10.1073/pnas.92.22.10237

Falkowski, P. G. (1984). Physiological responses of phytoplankton to natural light regimes. *Journal of Plankton Research*, *6*(2), 295–307. https://doi.org/10.1093/plankt/6.2.295

Falkowski, P., Scholes, R. J., Boyle, E., Canadell, J., Canfield, D., Elser, J., … Steffen, W. (2000). The global carbon cycle: A test of our knowledge of earth as a system. *Science*, *290*(5490), 291–296. https://doi.org/10.1126/science.290.5490.291

Falkowski, P. G., Katz, M. E., Knoll, A. H., Quigg, A., Raven, J. A., Schofield, O., & Taylor, F. J. R. (2004). The evolution of modern eukaryotic phytoplankton. *Science*, *305*(5682), 354–360. https://doi.org/10.1126/science.1095964

Falkowski, P. G., & Raven, J. A. (2013). *Aquatic photosynthesis*. Princeton University Press.

Feikema, W. O., Marosvölgyi, M. A., Lavaud, J., & Van Gorkom, H. J. (2006). Cyclic electron transfer in photosystem II in the marine diatom Phaeodactylum tricornutum. *Biochimica et Biophysica Acta (BBA)-Bioenergetics*, *1757*(7), 829-834.

Fernie, A. R., Obata, T., Allen, A. E., Araújo, W. L., & Bowler, C. (2012). Leveraging metabolomics for functional investigations in sequenced marine diatoms. *Trends in Plant Science*, *17*(7), 395–403. https://doi.org/10.1016/j.tplants.2012.02.005

Ferrón, S., del Valle, D. A., Bjöorkman, K. M., Quay, P. D., Church, M. J., & Karl, D. M. (2016). Application of membrane inlet mass spectrometry to measure aquatic gross primary production by the18O in vitro method. *Limnology and Oceanography: Methods*, *14*(9), 610–622. https://doi.org/10.1002/lom3.10116

Fiehn, O. (2002). Fiehn Plant mol biol 2002_review link between genotypes to phenotypes.pdf. *Plant Molecular Biology*, *48*, 155–171.

Field, C. B., Behrenfeld, M. J., Randerson, J. T., & Falkowski, P. (1998). Primary production of the biosphere: Integrating terrestrial and oceanic components. *Science*, *281*(5374), 237–240. https://doi.org/10.1126/science.281.5374.237

Fischer, W. W., Hemp, J., & Johnson, J. E. (2016). Evolution of Oxygenic Photosynthesis. *Annual Review of Earth and Planetary Sciences*, *44*, 647–683. https://doi.org/10.1146/annurev-earth-060313-054810

Fisher, N. L., & Halsey, K. H. (2016). Mechanisms that increase the growth efficiency of diatoms in low light. *Photosynthesis Research*, *129*(2), 183–197. https://doi.org/10.1007/s11120-016-0282-6

Finkel, Z. V., Beardall, J., Flynn, K. J., Quigg, A., Rees, T. A. V., & Raven, J. A. (2010). Phytoplankton in a changing world: Cell size and elemental stoichiometry. *Journal of Plankton Research*, *32*(1), 119–137. https://doi.org/10.1093/plankt/fbp098

Gao, K., Xu, J., Gao, G., Li, Y., Hutchins, D. A., Huang, B., … Riebesell, U. (2012). Rising CO2 and increased light exposure synergistically reduce marine primary productivity. *Nature Climate Change*, *2*(7), 519–523. https://doi.org/10.1038/nclimate1507

Geider, R. J., & Osborne, B. A. (1992). Using isotopes to measure gas exchange. In *Algal Photosynthesis* (pp. 32-70). Springer, Boston, MA.

Geider, R. J., & Osborne, B. A. (1989). Respiration and microalgal growth: a review of the quantitative relationship between dark respiration and growth. *New Phytologist*, *112*(3), 327–341. https://doi.org/10.1111/j.1469-8137.1989.tb00321.x

Gilbert, M., Domin, A., Becker, A., & Wilhelm, C. (2000). Estimation of primary productivity by chlorophyll a in vivo fluorescence in freshwater phytoplankton. *Photosynthetica*, *38*(1), 111-126.

Giovagnetti, V., & Ruban, A. V. (2017). Detachment of the fucoxanthin chlorophyll a/c binding protein (FCP) antenna is not involved in the acclimative regulation of photo-protection in the pennate diatom Phaeodactylum tricornutum. *Biochimica et Biophysica Acta - Bioenergetics*, *1858*(3), 218–230. https://doi.org/10.1016/j.bbabio.2016.12.005

Goss, R., & Jakob, T. (2010). Regulation and function of xanthophyll cycle-dependent photo-protection in algae. *Photosynthesis Research*, *106*(1–2), 103–122. https://doi.org/10.1007/s11120-010-9536-x

Goss, R., Ann Pinto, E., Wilhelm, C., & Richter, M. (2006). The importance of a highly active and ΔpH-regulated diatoxanthin epoxidase for the regulation of the PS II antenna function in diadinoxanthin cycle containing algae. *Journal of Plant Physiology*, *163*(10), 1008–1021. https://doi.org/10.1016/j.jplph.2005.09.008

Goulitquer, S., Potin, P., & Tonon, T. (2012). Mass spectrometry-based metabolomics to elucidate functions in marine organisms and ecosystems. In *Marine Drugs* (Vol. 10). https://doi.org/10.3390/md10040849

Graff, J. R., Milligan, A. J., & Behrenfeld, M. J. (2012). The measurement of phytoplankton biomass using flowcytometric sorting and elemental analysis of carbon. *Limnology and Oceanography: Methods*, *10*(NOVEMBER), 910–920. https://doi.org/10.4319/lom.2012.10.910

Graff, J. R., Westberry, T. K., Milligan, A. J., Brown, M. B., Dall'Olmo, G., van Dongen-Vogels, V., … Behrenfeld, M. J. (2015). Analytical phytoplankton carbon measurements spanning diverse ecosystems. *Deep-Sea Research Part I: Oceanographic Research Papers*, *102*, 16–25. https://doi.org/10.1016/j.dsr.2015.04.006

Grande, K. D., Marra, J., Langdon, C., Heinemann, K., & Bender, M. L. (1989). Rates of respiration in the light measured in marine phytoplankton using an 18O isotope-labelling technique. *Journal of Experimental Marine Biology and Ecology*, *129*(2), 95–120. https://doi.org/10.1016/0022-0981(89)90050-6

Greene, R. M., Geider, R. J., Kolber, Z., & Falkowski, P. G. (1992). Iron-induced changes in light harvesting and photochemical energy conversion processes in eukaryotic marine algae. *Plant Physiology*, *100*(2), 565–575. https://doi.org/10.1104/pp.100.2.565

Grouneva, I., Jakob, T., Wilhelm, C., & Goss, R. (2006). Influence of ascorbate and pH on the activity of the diatom xanthophyll cycle-enzyme diadinoxanthin de-epoxidase. *Physiologia Plantarum*, *126*(2), 205–211. https://doi.org/10.1111/j.1399-3054.2006.00613.x

Grouneva, I., Rokka, A., & Aro, E. M. (2011). The thylakoid membrane proteome of two marine diatoms outlines both diatom-specific and species-specific features of the photosynthetic machinery. *Journal of Proteome Research*, *10*(12), 5338–5353. https://doi.org/10.1021/pr200600f

Grouneva, I., Muth-Pawlak, D., Battchikova, N., & Aro, E. M. (2016). Changes in relative thylakoid protein abundance induced by fluctuating light in the diatom thalassiosira pseudonana. *Journal of Proteome Research*, *15*(5), 1649–1658. https://doi.org/10.1021/acs.jproteome.6b00124

Halsey, K. H., & Jones, B. M. (2015). Phytoplankton Strategies for Photosynthetic Energy Allocation. *Annual Review of Marine Science*, *7*(1), 265–297. https://doi.org/10.1146/annurev-marine-010814-015813

Halsey, K. H., Milligan, A. J., & Behrenfeld, M. J. (2010). Physiological optimization underlies growth rate-independent chlorophyll-specific gross and net primary production. *Photosynthesis Research*, *103*(2), 125–137. https://doi.org/10.1007/s11120-009-9526-z

Halsey, K. H., O'Malley, R. T., Graff, J. R., Milligan, A. J., & Behrenfeld, M. J. (2013). A common partitioning strategy for photosynthetic products in evolutionarily distinct phytoplankton species. *New Phytologist*, *198*(4), 1030–1038. https://doi.org/10.1111/nph.12209

Havaux, M., Guedeney, G., Hagemann, M., Yeremenko, N., Matthijs, H. C. P., & Jeanjean, R. (2005). The chlorophyll-binding protein IsiA is inducible by high light and protects the cyanobacterium Synechocystis PCC6803 from photooxidative stress. *FEBS Letters*, *579*(11), 2289–2293. https://doi.org/10.1016/j.febslet.2005.03.021

Heal, K. R., Kellogg, N. A., Carlson, L. T., Lionheart, R. M., & Ingalls, A. E. (2019). Metabolic Consequences of Cobalamin Scarcity in the Diatom Thalassiosira pseudonana as Revealed Through Metabolomics. *Protist*, *170*(3), 328–348. https://doi.org/10.1016/j.protis.2019.05.004

Hieronymi, M., & Macke, A. (2010). Spatiotemporal underwater light field fluctuations in the open ocean. *Journal of the European Optical Society*, *5*, 1–8. https://doi.org/10.2971/jeos.2010.10019s

Hickman, A. E., Holligan, P. M., Moore, C. M., Sharples, J., Krivtsov, V., & Palmer, M. R. (2009). Distribution and chromatic adaptation of phytoplankton within a shelf sea thermocline. *Limnology and Oceanography*, *54*(2), 525-536.

Hillyer, K. E., Dias, D. A., Lutz, A., Wilkinson, S. P., Roessner, U., & Davy, S. K. (2017). Metabolite profiling of symbiont and host during thermal stress and bleaching in the coral Acropora aspera. *Coral Reefs*, *36*(1), 105–118. https://doi.org/10.1007/s00338-016-1508-y

Houille-Vernes, L., Rappaport, F., Wollman, F. A., Alric, J., & Johnson, X. (2011). Plastid terminal oxidase 2 (PTOX2) is the major oxidase involved in chlororespiration in Chlamydomonas. *Proceedings of the National Academy of Sciences of the United States of America*, *108*(51), 20820–20825. https://doi.org/10.1073/pnas.1110518109

Hughes, D. J., Campbell, D. A., Doblin, M. A., Kromkamp, J. C., Lawrenz, E., Moore, C. M., … Suggett, D. J. (2018). Roadmaps and Detours: Active Chlorophyll- a Assessments of Primary Productivity Across Marine and Freshwater Systems. *Environmental Science and Technology*, *52*(21), 12039–12054. https://doi.org/10.1021/acs.est.8b03488

Huseby, S., Degerlund, M., Zingone, A., & Hansen, E. (2012). Metabolic fingerprinting reveals differences between northern and southern strains of the cryptic diatom Chaetoceros socialis. *European Journal of Phycology*, *47*(4), 480–489. https://doi.org/10.1080/09670262.2012.741714

Hutchinson, G. E. (1961). *THE PARADOX OF THE PLANKTON * New Haven , Connecticut Osborn Zoological Laboratory , The problem that I wish to discuss in the present contribution is raised by the very paradoxical situation of the plankton , particularly the phyto- plankton , of relativ*. *XCV*(882), 137–145.

Ilík, P., Pavlovič, A., Kouřil, R., Alboresi, A., Morosinotto, T., Allahverdiyeva, Y., … Shikanai, T. (2017). Alternative electron transport mediated by flavodiiron

proteins is operational in organisms from cyanobacteria up to gymnosperms. *New Phytologist*, *214*(3), 967–972. https://doi.org/10.1111/nph.14536

Iwai, M., Takizawa, K., Tokutsu, R., Okamuro, A., Takahashi, Y., & Minagawa, J. (2010). Isolation of the elusive supercomplex that drives cyclic electron flow in photosynthesis. *Nature*, *464*(7292), 1210–1213. https://doi.org/10.1038/nature08885

Jakob, T., Wagner, H., Stehfest, K., & Wilhelm, C. (2007). A complete energy balance from photons to new biomass reveals a light- and nutrient-dependent variability in the metabolic costs of carbon assimilation. *Journal of Experimental Botany*, *58*(8), 2101–2112. https://doi.org/10.1093/jxb/erm084

Jamers, A., Blust, R., & De Coen, W. (2009). Omics in algae: Paving the way for a systems biological understanding of algal stress phenomena? *Aquatic Toxicology*, *92*(3), 114–121. https://doi.org/10.1016/j.aquatox.2009.02.012

Joliot, P., Joliot, A., & Johnson, G. (2006). Cyclic electron transfer around photosystem I. In *Photosystem I* (pp. 639-656). Springer, Dordrecht.

Juneau, P., & Harrison, P. J. (2005). Comparison by PAM fluorometry of photosynthetic activity of nine marine phytoplankton grown under identical conditions. *Photochemistry and Photobiology*, *81*(3), 649–653. https://doi.org/10.1562/2005-01-13-RA-414.1

Juranek, L. W., & Quay, P. D. (2013). Using triple isotopes of dissolved oxygen to evaluate global marine productivity. *Annual Review of Marine Science*, *5*, 503–524. https://doi.org/10.1146/annurev-marine-121211-172430

Kana, T. (1990). Light-dependent oxygen cycling measured by an oxygen-18 isotope dilution technique. *Marine Ecology Progress Series*, *64*, 293–300. https://doi.org/10.3354/meps064293

Kana, T. M. (1993). Rapid oxygen cycling in Trichodesmium thiebautii. *Limnology and Oceanography*, *38*(1), 18–24. https://doi.org/10.4319/lo.1993.38.1.0018

Kana, T. M., Darkangelo, C., Hunt, M. D., Oldham, J. B., Bennett, G. E., & Cornwell, J. C. (1994). Membrane lnlet Mass Spectrometer for Rapid Environmental Water Samples. *Response*, *66*(23), 4166–4170. Retrieved from http://pubs.acs.org/doi/abs/10.1021/ac00095a009

Keller, B., Vass, I., Matsubara, S., Paul, K., Jedmowski, C., Pieruschka, R., … Muller, O. (2019). Maximum fluorescence and electron transport kinetics determined by light-induced fluorescence transients (LIFT) for photosynthesis phenotyping. *Photosynthesis Research*, *140*(2), 221–233. https://doi.org/10.1007/s11120-018-0594-9

Key, T., McCarthy, A., Campbell, D. A., Six, C., Roy, S., & Finkel, Z. V. (2010). Cell size trade-offs govern light exploitation strategies in marine phytoplankton.

Environmental Microbiology, *12*(1), 95–104. https://doi.org/10.1111/j.1462-2920.2009.02046.x

Khorobrykh, S., Havurinne, V., Mattila, H., & Tyystjärvi, E. (2020). Oxygen and ROS in photosynthesis. *Plants*, *9*(1), 1–61. https://doi.org/10.3390/plants9010091

Kirk, J. T. 0. (1994). Characteristics of the light field in highly turbid waters: A Monte Carlo study. *Limnology and Oceanography*, *39*(3), 702–706. https://doi.org/10.4319/lo.1994.39.3.0702

Klueter, A., Crandall, J. B., Archer, F. I., Teece, M. A., & Coffroth, M. A. (2015). Taxonomic and environmental variation of metabolite profiles in marine dinoflagellates of the genus Symbiodinium. *Metabolites*, *5*(1), 74–99. https://doi.org/10.3390/metabo5010074

Knoll, A. H., Javaux, E. J., Hewitt, D., & Cohen, P. (2006). Eukaryotic organisms in Proterozoic oceans. *Philosophical Transactions of the Royal Society B: Biological Sciences*, *361*(1470), 1023–1038. https://doi.org/10.1098/rstb.2006.1843

Köhler, J., Wang, L., Guislain, A., & Shatwell, T. (2018). Influence of vertical mixing on light-dependency of phytoplankton growth. *Limnology and Oceanography*, *63*(3), 1156–1167. https://doi.org/10.1002/lno.10761

Kok, B. (1956). On the inhibition of photosynthesis by intense light. *Biochim. Biophys. Acta*. 21, 234–244. https://doi.org/10.2514/3.29809

Kolber, Z., & Falkowski, P. G. (1993). Use of active fluorescence to estimate phytoplankton photosynthesis in situ. *Limnology and Oceanography*, *38*(8), 1646–1665. https://doi.org/10.4319/lo.1993.38.8.1646

Kolber, Z. S., Prasil, O., & Falkowski, P. G. (1998). Measurements of variable chlorophyll fluorescence using fast repetition rate techniques: defining methodology and experimental protocols. *Biochimica et Biophysica Acta - Bioenergetics*, *1367*, 88–106. Retrieved from papers2://publication/uuid/C591C675-7666-49B5-AB3C-16E2C3FCFD57

Komenda, J., Sobotka, R., & Nixon, P. J. (2012). Assembling and maintaining the Photosystem II complex in chloroplasts and cyanobacteria. *Current Opinion in Plant Biology*, *15*(3), 245–251. https://doi.org/10.1016/j.pbi.2012.01.017

Kooistra, W. H. C. F., Gersonde, R., Medlin, L. K., & Mann, D. G. (2007). The Origin and Evolution of the Diatoms. Their Adaptation to a Planktonic Existence. In *Evolution of Primary Producers in the Sea*. https://doi.org/10.1016/B978-012370518-1/50012-6

Krieger-Liszkay, A., & Feilke, K. (2016). The dual role of the plastid terminal oxidase PTOX: Between a protective and a pro-oxidant function. *Frontiers in Plant Science*, *6*(JAN2016), 2015–2017. https://doi.org/10.3389/fpls.2015.01147

Kromkamp, J., & Peene, J. (1999). Estimation of phytoplankton photosynthesis and nutrient limitation in the Eastern Scheldt estuary using variable fluorescence. *Aquatic Ecology*, *33*(1), 101–104. https://doi.org/10.1023/A:1009900124650

Kroth, P. G., Chiovitti, A., Gruber, A., Martin-Jezeque, V., Mock, T., Parker, M. S., … Bowler, C. (2008). A model for carbohydrate metabolism in the diatom Phaeodactylum tricornutum deduced from comparative whole genome analysis. *PLoS ONE*, *3*(1). https://doi.org/10.1371/journal.pone.0001426

Kramer, D. M., & Evans, J. R. (2011). The importance of energy balance in improving photosynthetic productivity. *Plant Physiology*, *155*(1), 70–78. https://doi.org/10.1104/pp.110.166652

Kuzminov, F. I., & Gorbunov, M. Y. (2016). Energy dissipation pathways in Photosystem 2 of the diatom, Phaeodactylum tricornutum, under high-light conditions. *Photosynthesis Research*, *127*(2), 219–235. https://doi.org/10.1007/s11120-015-0180-3

Lacour, T., Babin, M., & Lavaud, J. (2020). Diversity in Xanthophyll Cycle Pigments Content and Related Nonphotochemical Quenching (NPQ) Among Microalgae: Implications for Growth Strategy and Ecology. *Journal of Phycology*, *56*(2), 245–263. https://doi.org/10.1111/jpy.12944

Lacour, L., Ardyna, M., Stec, K. F., Claustre, H., Prieur, L., Poteau, A., … Iudicone, D. (2017). Unexpected winter phytoplankton blooms in the North Atlantic subpolar gyre. *Nature Geoscience*, *10*(11), 836–839. https://doi.org/10.1038/NGEO3035

Lavaud, J., Strzepek, R. F., & Kroth, P. G. (2007). Photo-protection capacity differs among diatoms: possible consequences on the spatial distribution of diatoms related to fluctuations in the underwater light Climate. *Limnology and Oceanography*, *52*(3), 1188–1194. https://doi.org/10.2307/4499689

Lavaud, J., & Goss, R. (2014). The Peculiar Features of Non-Photochemical Fluorescence Quenching in Diatoms and Brown Algae. Non-Photochemical Quenching and Energy Dissipation in Plants, Algae and Cyanobacteria, pp.421 - 443, 10.1007/978-94-017-9032-1_20. hal-01096599

Lawrenz, E., Silsbe, G., Capuzzo, E., Ylöstalo, P., Forster, R. M., Simis, S. G. H., … Suggett, D. J. (2013). Predicting the Electron Requirement for Carbon Fixation in Seas and Oceans. *PLoS ONE*, *8*(3). https://doi.org/10.1371/journal.pone.0058137

Laws, E. A., Landry, M. R., Barber, R. T., Campbell, L., Dickson, M. L., & Marra, J. (2000). Carbon cycling in primary production bottle incubations: Inferences from grazing experiments and photosynthetic studies using 14C and 18O in the Arabian Sea. *Deep-Sea Research Part II: Topical Studies in Oceanography*, *47*(7–8), 1339–1352. https://doi.org/10.1016/S0967-0645(99)00146-0

Lepetit, B., Goss, R., Jakob, T., & Wilhelm, C. (2012). Molecular dynamics of the diatom thylakoid membrane under different light conditions. *Photosynthesis Research*, *111*(1–2), 245–257. https://doi.org/10.1007/s11120-011-9633-5

Lepetit, B., Sturm, S., Rogato, A., Gruber, A., Sachse, M., Falciatore, A., … Lavaud, J. (2013). High light acclimation in the secondary plastids containing diatom phaeodactylum tricornutum is triggered by the redox state of the plastoquinone pool. *Plant Physiology*, *161*(2), 853–865. https://doi.org/10.1104/pp.112.207811

Lepetit, B., & Dietzel, L. (2015). Light signaling in photosynthetic eukaryotes with "green" and "red" chloroplasts. *Environmental and Experimental Botany*, *114*, 30–47. https://doi.org/10.1016/j.envexpbot.2014.07.007

Lewis, K. M., Van Dijken, G. L., & Arrigo, K. R. (2020). Changes in phytoplankton concentration now drive increased Arctic Ocean primary production. *Science*, *369*(6500), 198–202. https://doi.org/10.1126/science.aay8380

Lewitus, A. J., & Kana, T. M. (1995). Light Respiration in Six Estuarine Phytoplankton Species: Contrasts Under Photoautotrophic and Mixotrophic Growth Conditions. *Journal of Phycology*, *31*(5), 754–761. https://doi.org/10.1111/j.0022-3646.1995.00754.x

Li, G., Woroch, A. D., Donaher, N. A., Cockshutt, A. M., & Campbell, D. A. (2016). A Hard Day's Night: Diatoms Continue Recycling Photosystem II in the Dark. *Frontiers in Marine Science*, *3*(November), 1–10. https://doi.org/10.3389/fmars.2016.00218

Lin, H., Kuzminov, F. I., Park, J., Lee, S. H., Falkowski, P. G., & Gorbunov, M. Y. (2016). Phytoplankton: The fate of photons absorbed by phytoplankton in the global ocean. *Science*, *351*(6270), 264–267. https://doi.org/10.1126/science.aab2213

Linka, M., & Weber, A. P. M. (2005). Shuffling ammonia between mitochondria and plastids during photorespiration. *Trends in Plant Science*, *10*(10), 461–465. https://doi.org/10.1016/j.tplants.2005.08.002

Lloyd, N. D. H., & Canvin, D. T. (1977). Photosynthesis and photorespiration in sunflower selections. *Canadian Journal of Botany*, *55*(24), 3006–3012. https://doi.org/10.1139/b77-338

Macintyre, H. L., Kana, T. M., Anning, T., & Geider, R. J. (2002). Photoacclimation of photosynthesis irradiance response curves and photosynthetic pigments in microalgae and cyanobacteria. *Journal of Phycology*, *38*(1), 17–38. https://doi.org/10.1046/j.1529-8817.2002.00094.x

Mackey, K. R. M., Paytan, A., Grossman, A. R., & Bailey, S. (2008). A photosynthetic strategy for coping in a high-light, low-nutrient environment. *Limnology and Oceanography*, *53*(3), 900–913. https://doi.org/10.4319/lo.2008.53.3.0900

McDonald, A. E., Ivanov, A. G., Bode, R., Maxwell, D. P., Rodermel, S. R., & Hüner, N. P. A. (2011). Flexibility in photosynthetic electron transport: The physiological role of plastoquinol terminal oxidase (PTOX). *Biochimica et Biophysica Acta - Bioenergetics*, *1807*(8), 954–967. https://doi.org/10.1016/j.bbabio.2010.10.024

Malviya, S., Scalco, E., Audic, S., Vincent, F., Veluchamy, A., Poulain, J., … Bowler, C. (2016). Insights into global diatom distribution and diversity in the world's ocean. *Proceedings of the National Academy of Sciences of the United States of America*, *113*(11), E1516–E1525. https://doi.org/10.1073/pnas.1509523113

Mann, K. H., & Lazier, J. R. N. (2006). Vertical Structure of the Open Ocean: Biology of the Mixed Layer. Dynamics of Marine Ecosystems.

Marra, J. (2009). Net and gross productivity: Weighing in with 14C. *Aquatic Microbial Ecology*, *56*(2–3), 123–131. https://doi.org/10.3354/ame01306

Marra, J. F., Lance, V. P., Vaillancourt, R. D., & Hargreaves, B. R. (2014). Resolving the ocean's euphotic zone. *Deep-Sea Research Part I: Oceanographic Research Papers*, *83*, 45–50. https://doi.org/10.1016/j.dsr.2013.09.005

Miloslavina, Y., Grouneva, I., Lambrev, P. H., Lepetit, B., Goss, R., Wilhelm, C., & Holzwarth, A. R. (2009). Ultrafast fluorescence study on the location and mechanism of non-photochemical quenching in diatoms. *Biochimica et Biophysica Acta - Bioenergetics*, *1787*(10), 1189–1197. https://doi.org/10.1016/j.bbabio.2009.05.012

Miyake, C. (2010). Alternative electron flows (water–water cycle and cyclic electron flow around PSI) in photosynthesis: molecular mechanisms and physiological functions. *Plant and Cell Physiology*, *51*(12), 1951-1963.

Møller, I. M., Bérczi, A., van der Plas, L. H., & Lambers, H. (1988). Measurement of the activity and capacity of the alternative pathway in intact plant tissues: identification of problems and possible solutions. *Physiologia Plantarum*, *72*(3), 642-649.

Moore, C. M., Mills, M. M., Arrigo, K. R., Berman-Frank, I., Bopp, L., Boyd, P. W., … Ulloa, O. (2013). Processes and patterns of oceanic nutrient limitation. *Nature Geoscience*, *6*(9), 701–710. https://doi.org/10.1038/ngeo1765

Moore, C. M., Suggett, D. J., Hickman, A. E., Kim, Y. N., Tweddle, J. F., Sharples, J., ... & Holligan, P. M. (2006). Phytoplankton photoacclimation and photoadaptation in response to environmental gradients in a shelf sea. *Limnology and Oceanography*, *51*(2), 936-949.

Moore, C. M., Suggett, D., Holligan, P. M., Sharples, J., Abraham, E. R., Lucas, M. I., … Hydes, D. J. (2003). Physical controls on phytoplankton physiology and production at a shelf sea front: a fast repetition-rate fluorometer based study. *Marine Ecology Progress Series*, *259*, 29–45. Retrieved from papers://64c875cb-35e9-49cc-86a7-69f7bda703f6/Paper/p9

Morelle, J., & Claquin, P. (2018). Electron requirements for carbon incorporation along a diel light cycle in three marine diatom species. *Photosynthesis Research*, *137*(2), 201–214. https://doi.org/10.1007/s11120-018-0491-2

Moreno, C. M., Lin, Y., Davies, S., Monbureau, E., Cassar, N., & Marchetti, A. (2018). Examination of gene repertoires and physiological responses to iron and light limitation in Southern Ocean diatoms. *Polar Biology*, *41*(4), 679–696. https://doi.org/10.1007/s00300-017-2228-7

Moustafa, A., Beszteri, B., Maier, U. G., Bowler, C., Valentin, K., & Bhattacharya, D. (2009). Genomic footprints of a cryptic plastid endosymbiosis in diatoms. *Science*, *324*(5935), 1724–1726. https://doi.org/10.1126/science.1172983

Müller, P., Li, X. P., & Niyogi, K. K. (2001). Update on Photosynthesis Non-Photochemical Quenching. A Response to Excess Light Energy 1. *Plant Physiology*, *125*(April), 1558–1566.

Nawrocki, W. J., Tourasse, N. J., Taly, A., Rappaport, F., & Wollman, F.-A. (2015). The Plastid Terminal Oxidase: Its Elusive Function Points to Multiple Contributions to Plastid Physiology. *Annual Review of Plant Biology*, *66*(1), 49–74. https://doi.org/10.1146/annurev-arplant-043014-114744

Nelson, N., & Ben-Shem, A. (2004). The complex architecture of oxygenic photosynthesis. *Nature Reviews Molecular Cell Biology*, *5*(12), 971–982. https://doi.org/10.1038/nrm1525

Nielsen, E. S. (1952). The Use of Radio-active Carbon (C14) for Measuring Organic Production in the Sea. *ICES Journal of Marine Science*, *18*(2), 117–140. https://doi.org/10.1093/icesjms/18.2.117

Nishiyama, Y., & Murata, N. (2014). Revised scheme for the mechanism of photoinhibition and its application to enhance the abiotic stress tolerance of the photosynthetic machinery. *Applied Microbiology and Biotechnology*, *98*(21), 8777–8796. https://doi.org/10.1007/s00253-014-6020-0

Ohnishi, N., Allakhverdiev, S.I., Takahashi, S., Higashi S., Watanabe, M., Nishiyama, Y., Murata, N. (2005). Two-step mechanism of photodamage to Photosystem II: step 1 occurs at the oxygen-evolving complex and step 2 occurs at the photochemical reaction center. *Biochemistry*, 44, 8494–8499.

Oziel, L., Baudena, A., Ardyna, M., Massicotte, P., Randelhoff, A., Sallée, J. B., … Babin, M. (2020). Faster Atlantic currents drive poleward expansion of temperate phytoplankton in the Arctic Ocean. *Nature Communications*, *11*(1), 1–8. https://doi.org/10.1038/s41467-020-15485-5

Pei, S., & Laws, E. A. (2013). Does the 14C method estimate net photosynthesis? Implications from batch and continuous culture studies of marine phytoplankton. *Deep-Sea Research Part I: Oceanographic Research Papers*, *82*, 1–9. https://doi.org/10.1016/j.dsr.2013.07.011

Peltier, G., & Thibault, P. (1985). O2 uptake in the light in Chlamydomonas: evidence for persistent mitochondrial respiration. *Plant physiology*, *79*(1), 225-230.

Petrou, K., Hill, R., Brown, C. M., Campbell, D. A., Doblin, M. A., & Ralph, P. J. (2010). Rapid photo-protection in sea-ice diatoms from the East Antarctic pack ice. *Limnology and Oceanography*, *55*(3), 1400–1407. https://doi.org/10.4319/lo.2010.55.3.1400

Petroutsos, D., Tokutsu, R., Maruyama, S., Flori, S., Greiner, A., Magneschi, L., … Minagawa, J. (2016). A blue-light photoreceptor mediates the feedback regulation of photosynthesis. *Nature*, *537*(7621), 563–566. https://doi.org/10.1038/nature19358

Platt, T., Denman, K., & Jossby, A. D. (1977). Modelling the productivity of phytoplankton.

Prasil, O., Kolber, Z., Berry, J. A., & Falkowski, P. G. (1996). Cyclic electron flow around Photosystem II in vivo. *Photosynthesis Research*, *48*, 395–410.

Prihoda, J., Tanaka, A., De Paula, W. B. M., Allen, J. F., Tirichine, L., & Bowler, C. (2012). Chloroplast-mitochondria cross-talk in diatoms. *Journal of Experimental Botany*, *63*(4), 1543–1557. https://doi.org/10.1093/jxb/err441

Quigg, A., Finkel, Z. V, Irwin, A. J., Rosenthal, Y., Ho, T., Reinfelder, J. R., … Falkowski, P. G. (2003). The evolutionary inheritance of elemental stoichiometry in marine phytoplankton. *Nature*, *425*, 291–294. https://doi.org/10.1038/nature01953. 1

Radmer, R., & Ollinger, O. (1980). Light-driven Uptake of Oxygen, Carbon Dioxide, and Bicarbonate by the Green Alga Scenedesmus. *Plant Physiology*, *65*(4), 723–729. https://doi.org/10.1104/pp.65.4.723

Ralph, P. J., Wilhelm, C., Lavaud, J., Jakob, T., Petrou, K., & Kranz, S. A. (2010). Chlorophyll a Fluorescence in Aquatic Sciences: Methods and Applications. *Chlorophyll a Fluorescence in Aquatic Sciences: Methods and Applications*. https://doi.org/10.1007/978-90-481-9268-7

Raven, J. A., & Kubler, J. E. (2002). New light on the scaling of metabolic rate with the size of algae. *Journal of Phycology*, *38*, 11–16.

Raven, J. A., & Beardall, J. (2005). Respiration in aquatic photolithotrophs. *Respiration in aquatic ecosystems*, 36-46.

Raven, J. A., Beardall, J., & Quigg, A. (2020). Light-Driven Oxygen Consumption in the Water-Water Cycles and Photorespiration, and Light Stimulated Mitochondrial Respiration. In A. W. D. Larkum, A. R. Grossman, & J. A. Raven (Eds.), *Photosynthesis in Algae: Biochemical and Physiological Mechanisms* (pp. 161–178). https://doi.org/10.1007/978-3-030-33397-3_8

Raven, J. A. (2011). The cost of photoinhibition. *Physiologia Plantarum*, *142*(1), 87–104. https://doi.org/10.1111/j.1399-3054.2011.01465.x

Righetti, D., Vogt, M., Gruber, N., Psomas, A., & Zimmermann, N. E. (2019). Global pattern of phytoplankton diversity driven by temperature and environmental variability. *Science Advances*, *5*(5), 1–11. https://doi.org/10.1126/sciadv.aau6253

Riley, G. A. (1939). Limnological studies in Connecticut. *Ecological Monographs*, *9*(1), 53-94.

Rost, B., Riebesell, U., Burkhardt, S., & Sültemeyer, D. (2003). Carbon acquisition of bloom-forming marine phytoplankton. *Limnology and Oceanography*, *48*(1 I), 55–67. https://doi.org/10.4319/lo.2003.48.1.0055

Ryther, J. H. (1956). Photosynthesis in the Ocean as a Function of Light Intensity. *Limnology and Oceanography*, *1*(1), 61-70.

Rynearson, T. A., & Palenik, B. (2011). Learning to Read the Oceans: Genomics of Marine Phytoplankton. In *Advances in Marine Biology* (pp. 1–40). Retrieved from http://library1.nida.ac.th/termpaper6/sd/2554/19755.pdf

Sarthou, G., Timmermans, K. R., Blain, S., & Tréguer, P. (2005). Growth physiology and fate of diatoms in the ocean: A review. *Journal of Sea Research*, *53*(1-2 SPEC. ISS.), 25–42. https://doi.org/10.1016/j.seares.2004.01.007

Scheffer, M., Szabó, S., Gragnani, A., Van Nes, E. H., Rinaldi, S., Kautsky, N., … Franken, R. J. M. (2003). Floating plant dominance as a stable state. *Proceedings of the National Academy of Sciences of the United States of America*, *100*(7), 4040–4045. https://doi.org/10.1073/pnas.0737918100

Schober, A. F., Río Bártulos, C., Bischoff, A., Lepetit, B., Gruber, A., & Kroth, P. G. (2019). Organelle Studies and Proteome Analyses of Mitochondria and Plastids Fractions from the Diatom Thalassiosira pseudonana. *Plant and Cell Physiology*, *60*(8), 1811–1828. https://doi.org/10.1093/pcp/pcz097

Schuback, N., Schallenberg, C., Duckham, C., Maldonado, M. T., & Tortell, P. D. (2015). Interacting effects of light and iron availability on the coupling of photosynthetic electron transport and CO2-assimilation in marine phytoplankton. *PLoS ONE*, *10*(7), 1–30. https://doi.org/10.1371/journal.pone.0133235

Schuback, N., & Tortell, P. D. (2019). Diurnal regulation of photosynthetic light absorption, electron transport and carbon fixation in two contrasting oceanic environments. *Biogeosciences*, *16*(7), 1381–1399. https://doi.org/10.5194/bg-16-1381-2019

Shimakawa, G., Murakami, A., Niwa, K., Matsuda, Y., Wada, A., & Miyake, C. (2019). Comparative analysis of strategies to prepare electron sinks in aquatic photoautotrophs. *Photosynthesis Research*, *139*(1–3), 401–411. https://doi.org/10.1007/s11120-018-0522-z

Silsbe, G. M., Smith, R. E. H., & Twiss, M. R. (2015). Quantum efficiency of phytoplankton photochemistry measured continuously across gradients of nutrients and biomass in Lake Erie (Canada and USA) is strongly regulated by light but not by nutrient deficiency. *Canadian Journal of Fisheries and Aquatic Sciences*, *72*(5), 651–660. https://doi.org/10.1139/cjfas-2014-0365

Silsbe, G. M., & Kromkamp, J. C. (2012). Modeling the irradiance dependency of the quantum efficiency of photosynthesis. *Limnology and Oceanography: Methods*, *10*(SEPTEMBER), 645–652. https://doi.org/10.4319/lom.2012.10.645

Smetacek, V. (2012). Making sense of ocean biota: How evolution and biodiversity of land organisms differ from that of the plankton. *Journal of Biosciences*, *37*(4), 589–607. https://doi.org/10.1007/s12038-012-9240-4

Strzepek, R. F., & Harrison, P. J. (2004). Photosynthetic architecture differs in coastal and oceanic diatoms. *Nature*, *431*(7009), 689. https://doi.org/10.1038/nature02954

Su, W., Jakob, T., & Wilhelm, C. (2012). The impact of nonphotochemical quenching of fluorescence on the photon balance in diatoms under dynamic light conditions. *Journal of Phycology*, *48*(2), 336–346. https://doi.org/10.1111/j.1529-8817.2012.01128.x

Suggett, D. J., Oxborough, K., Baker, N. R., Macintyre, H. L., Kana, T. M., & Geider, R. J. (2003). Fast repetition rate and pulse amplitude modulation chlorophyll a fluorescence measurements for assessment of photosynthetic electron transport in marine phytoplankton. *European Journal of Phycology*, *38*(4), 371–384. https://doi.org/10.1080/0967026031000161265 5

Suggett, D. J., Moore, C. M., Oxborough, K., & Geider, R. J. (2006). Fast Repetition Rate (FRR) Chlorophyll a Fluorescence Induction Measurements. *Chelsea Technologies Group*, (February 2015), 53. Retrieved from http://www.psi.cz/ftp/publications/kautsky/FRRFmethodsManual.pdf%5Cnpapers://64c875cb-35e9-49cc-86a7-69f7bda703f6/Paper/p289

Suggett, D. J., Moore, C. M., & Geider, R. J. (2010). Chlorophyll a Fluorescence in Aquatic Sciences: Methods and Applications. *Chlorophyll a Fluorescence in Aquatic Sciences: Methods and Applications*. https://doi.org/10.1007/978-90-481-9268-7

Suggett, D. J., Moore, C. M., Hickman, A. E., & Geider, R. J. (2009). Interpretation of fast repetition rate (FRR) fluorescence: Signatures of phytoplankton community structure versus physiological state. *Marine Ecology Progress Series*, *376*, 1–19. https://doi.org/10.3354/meps07830

Talling, J. F. (1957). Photosynthetic characteristics of some freshwater plankton diatoms in relation to underwater radiation. *The New Phytologist*, *56*(1), 29-50.

Thomas, M.K., Kremer, C.T., Klausmeier, C.A., Litchman, E. (2012). A global pattern of termal adaptation in matine phytoplankton. *Science*, DOI: 10.1126/science.1224836.

Tortell, P.D., Payne, C., Gueguen, C., Strzepek, R.F., Boyd, P.W. et al. (2008). Inorganic carbon uptake by Southern Ocean phytoplankton. *Limnology and Oceanography,* 53, 1266-1278.

Trampe, E., Hansen, P. J., & Kühl, M. (2015). A comparison of photosynthesis measurements by o2 evolution,14C assimilation, and variable chlorophyll fuorescence during light acclimatization of the diatom Coscinodiscus granii. *Algae*, *30*(2), 103. https://doi.org/10.4490/algae.2015.30.2.103

Tréguer, P., Nelson, D. M., Van Bennekom, A. J., Demaster, D. J., Leynaert, A., & Quéguiner, B. (1995). The silica balance in the world ocean: A reestimate. *Science*, *268*(5209), 375–379. https://doi.org/10.1126/science.268.5209.375

Vass, I. (2012). Molecular mechanisms of photo-damage in the Photosystem II complex. *Biochimica et Biophysica Acta - Bioenergetics*, *1817*(1), 209–217. https://doi.org/10.1016/j.bbabio.2011.04.014

Wagner, H., Jakob, T., & Wilhelm, C. (2006). Balancing the energy flow from captured light to biomass under fluctuating light conditions. *New Phytologist*, *169*(1), 95–108. https://doi.org/10.1111/j.1469-8137.2005.01550.x

Wagner, H., Jakob, T., Fanesi, A., & Wilhelm, C. (2017). Towards an understanding of the molecular regulation of carbon allocation in diatoms: The interaction of energy and carbon allocation. *Philosophical Transactions of the Royal Society B: Biological Sciences*, *372*(1728). https://doi.org/10.1098/rstb.2016.0410

Wagner, H., Jakob, T., Lavaud, J., & Wilhelm, C. (2016). Photosystem II cycle activity and alternative electron transport in the diatom Phaeodactylum tricornutum under dynamic light conditions and nitrogen limitation. *Photosynthesis Research*, *128*(2), 151–161. https://doi.org/10.1007/s11120-015-0209-7

Waring, J., Klenell, M., Bechtold, U., Underwood, G. J. C., & Baker, N. R. (2010). Light-induced responses of oxygen photoreduction, reactive oxygen species production and scavenging in two diatom species. *Journal of Phycology*, *46*(6), 1206–1217. https://doi.org/10.1111/j.1529-8817.2010.00919.x

Weger, H. G., Herzig, R., Falkowski, P. G., & Turpin, D. H. (1989). Respiratory losses in the light in a marine diatom: measuremetns by short-term mass spectrometry. *Limnology and Oceanography*, *34*(7), 1153–1161.

Wilhelm, C., Jungandreas, A., Jakob, T., & Goss, R. (2014). Light acclimation in diatoms: From phenomenology to mechanisms. *Marine Genomics*, *16*(1), 5–15. https://doi.org/10.1016/j.margen.2013.12.003

Williams, P. J. L. B., Robinson, C., Sondergaard, M., Jespersen, A. M., Bentley, T. L., Lefevre, D., ... & Riemann, B. (1996). Algal 14C and total carbon metabolisms. 2. Experimental observations with the diatom Skeletonema costatum. *Journal of plankton research*, *18*(10), 1961-1974.

Wingler, A., Lea, P. J., Quick, W. P., & Leegood, R. C. (2000). Photorespiration: Metabolic pathways and their role in stress protection. *Philosophical Transactions of the Royal Society B: Biological Sciences*, *355*(1402), 1517–1529. https://doi.org/10.1098/rstb.2000.0712

Wu, H., Cockshutt, A. M., McCarthy, A., & Campbell, D. A. (2011). Distinctive photosystem II photo-inactivation and protein dynamics in marine diatoms. *Plant Physiology*, *156*(4), 2184–2195. https://doi.org/10.1104/pp.111.178772

Wu, H., Roy, S., Alami, M., Green, B. R., & Campbell, D. A. (2012). Photosystem II photo-inactivation, repair, and protection in marine centric diatoms. *Plant Physiology*, *160*(1), 464–476. https://doi.org/10.1104/pp.112.203067

Wu, Y., Li, Z., Du, W., & Gao, K. (2015). Physiological response of marine centric diatoms to ultraviolet radiation, with special reference to cell size. *Journal of Photochemistry and Photobiology B: Biology*, *153*, 1–6. https://doi.org/10.1016/j.jphotobiol.2015.08.035

Xu, K., Lavaud, J., Perkins, R., Austen, E., Bonnanfant, M., & Campbell, D. A. (2018). Phytoplankton σPSII and excitation dissipation; Implications for estimates of primary productivity. *Frontiers in Marine Science*, *5*(AUG). https://doi.org/10.3389/fmars.2018.00281

Yoshida, K., Terashima, I., & Noguchi, K. (2007). Up-regulation of mitochondrial alternative oxidase concomitant with chloroplast over-reduction by excess light.

Chapter 2

Divergence of photosynthetic strategies amongst marine diatoms

Nerissa L. Fisher[1*], Douglas A. Campbell[2], David J. Hughes[1], Unnikrishnan Kuzhiumparambil[1], Kimberly H. Halsey[3], Peter J. Ralph[1], David J. Suggett[1]

[1] Climate Change Cluster, University of Technology Sydney, Ultimo, New South Wales, Australia

[2] Department of Biology, Mount Allison University, Sackville, New Brunswick, Canada

[3] Department of Microbiology, Oregon State University, Corvallis, Oregon, USA

*Corresponding author: Nerissa.Fisher@uts.edu.au

Published 28 December 2020 in *PLOS ONE* as: Fisher, N. L., Campbell, D. A., Hughes, D. J., Kuzhiumparambil, U., Halsey, K. H., Ralph, P. J., & Suggett, D. J. (2020). Divergence of photosynthetic strategies amongst marine diatoms. *PloS one*, *15*(12), e0244252.

2.1. Abstract

Marine phytoplankton, and in particular diatoms, are responsible for almost half of all primary production on Earth. Diatom species thrive from polar to tropical waters and across light environments that are highly complex to relatively benign, and so have evolved highly divergent strategies for regulating light capture and utilisation. It is increasingly well established that diatoms have achieved such successful ecosystem dominance by regulating excitation energy available for generating photosynthetic energy via highly flexible light harvesting strategies. However, how different light harvesting strategies and downstream pathways for oxygen production and consumption interact to balance excitation pressure remains unknown. We therefore examined the responses of three diatom taxa adapted to inherently different light climates (estuarine *Thalassioisira weissflogii*, coastal *Thalassiosira pseudonana* and oceanic *Thalassiosira oceanica*) during transient shifts from a moderate to high growth irradiance (85 to 1200 μmol photons m^{-2} s^{-1}). Transient high light exposure caused *T. weissflogii* to rapidly downregulate PSII with substantial nonphotochemical quenching, protecting PSII from inactivation or damage, and obviating the need for induction of O_2 consuming (light-dependent respiration, LDR) pathways. In contrast, *T. oceanica* retained high excitation pressure on PSII, but with little change in RCII photochemical turnover, thereby requiring moderate repair activity and greater reliance on LDR. *T. pseudonana* exhibited an intermediate response compared to the other two diatom species, exhibiting some downregulation and inactivation of PSII, but high repair of PSII and induction of reversible PSII nonphotochemical quenching, with some LDR. Together, these data demonstrate a range of strategies for balancing light harvesting and utilisation across diatom species, which reflect their adaptation to sustain photosynthesis under environments with inherently different light regimes.

2.2. Introduction

Diatoms account for the majority of marine primary production (Tréguer et al. 1995; Armburst 2009) and are ubiquitous across aquatic environments (Malviya et al. 2016), from tropical to polar regions, and from highly dynamic coastal and upwelling habitats to more stable oceanic waters. Adaptation of diatoms to these environments has resulted in their evolution of photosynthetic machinery optimised to very different light regimes caused by short-term (e.g. clouds, sun flecks, diel cycle) and long-term (e.g. seasonal) processes, as well as positioning relative to water column thermal and nutrient gradients (Lavaud & Goss 2014; Wilhelm et al. 2014). Whilst the overall success of diatoms appears driven by complex acclimation processes trending towards a light level that is close to an average irradiance within the mixed layer of a given water body (Behrenfeld et al. 2005; Westberry et al. 2008), routine exposure to stochastic high light episodes requires dynamic photo-protective capacity (Lavaud et al. 2007; Dimier et al. 2007; Zhu & Green 2010; Goss & Jakob 2010).

Diatoms use multiple processes to regulate photosynthesis, including modifying the ultrastructure (and thus the excitonic connectivity) of pigments and proteins, which together regulate the flow of excitation energy reaching the electron carrier system (Lavaud et al. 2007; Lavaud & Lepetit 2013). Failure to regulate excess excitation energy either as photons reaching the reaction centre or as harvested energy (i.e. electrons) within the electron transport chain can increase the probability of photo-inactivation of photosystem II (PSII, Campbell & Serôdio 2020), likely from the generation of reactive oxygen species (Waring et al. 2010), ultimately leading to a

decrease in net primary productivity and growth. It is therefore paramount that photoautotrophs have mechanisms to dissipate excess light energy and photo-protect the photosystems, and associated metabolism, while maintaining photosynthesis to support growth. One of the most important mechanisms for rapid (on the order of seconds to minutes) regulation of photochemistry under high light is non-photochemical quenching (see Goss & Lepetit 2015 review), parameterised herein as a yield, YNPQ (equivalent to ΦNPQ, Klughammer & Schreiber 2008 and conceptually similar to [1-Q], Suggett et al. 2015), whereby excitation energy in excess of the photosynthetic capacity, is safely dissipated as heat by light harvesting pigment complexes associated with PSII (LHCII, Holt et al. 2004; Lavaud et al. 2004). YNPQ is a regulated process and contrasts with unregulated non-photochemical quenching, parameterised by YNO (equivalent to ΦNO, Klughammer & Schreiber 2008). YNO comprises constitutive thermal losses (Klughammer & Schreiber 2008) as well as intrinsic losses (*sensu* Kramer et al. 2004).

As with all algae, light harvesting pigments in diatoms are connected to the PSII reaction centres (RCIIs) with an embedded oxygen evolving complex (OEC) that splits water to release electrons for use in photochemistry. Alterations in carotenoid pigment composition are regulated through the xanthophyll cycle (XC) and interact with particular photo-protective light harvesting complex protein isoforms (LHCXs) to lower the energetic transfer efficiency from antennae pigments to RCII (Barnett et al. 2015; Dong et al. 2016; Lepetit et al. 2017; Taddei et al. 2018). When light is transiently in excess, induction of nonphotochemical quenching occurs whereby the accumulation of a proton gradient, and consequently ΔpH, across the thylakoid membrane drives the de-epoxidation of XC pigments, via two evolutionarily divergent

protection pathways, diadinoxanthin (Dd, light harvesting) to diatoxanthin (Dt, photo-protective) (Perkins et al. 2018) which dominates in diatoms and/or violaxanthin to zeaxanthin (Lohr & Wilhelm 1999; Grouneva et al. 2006; Lepetit et al. 2012) which dominates in green lineages.

Exposure to high light triggers synthesis of LHCX isoforms that localise closely to the RCII core, resulting in core complex associated non-photochemical quenching (Barnett et al. 2015; Taddei et al. 2018; Blommaert et al. 2017). Sustained high light exposure, in turn, drives accumulation of accessory pigments (Taddei et al. 2018), which may also result from the continued accumulation of LHCXs (Lavaud & Lepetit 2013; Lepetit et al. 2017; Gao et al. 2018) generating longer-lived, more slowly reversible, forms of nonphotochemical quenching. Nevertheless, diatoms typically maintain a constitutive capacity to build substantial but reversible nonphotochemical quenching through the XC (Lavaud & Lepetit 2013). Recent work using mutants of the pennate diatom *P. tricornutum* (Buck et al. 2019) showed that all capacity for rapidly reversible nonphotochemical quenching can be explained by LHCXs and the XC operating in concert and that, at least for *P. tricornutum*, longer-lived nonphotochemical quenching generally signifies the build-up of photo-inhibition that can only be reversed through turnover of PSII protein subunits (Campbell et al. 2013). An additional process – detachment of LHCXs from the RCIIs to invoke "super quenching"– appears to be a relatively minor process in *P. tricornutum*, suggesting that the energy trapping efficiency of the antenna does not out-compete that of the RCIIs (Giovagnetti & Ruban 2107; Kuzminov & Gorbunov 2016). In other diatoms, however, antennae detachment appears to sustain nonphotochemical quenching (Miloslavina et al. 2009; Lepetit et al.

2010; Lepetit et al. 2013) with photo-inactivation and repair (Lacour et al. 2018; Campbell & Serôdio 2020).

Dynamic light regimes appear to select for phytoplankton taxa with different strategies of nonphotochemical quenching to optimise cell growth and survival, as demonstrated in a recent comparative assessment of various microalgal species and ecotypes (Lacour et al. 2020). Environments characterised by particularly large light fluctuations include shallow waters that are inhabited by both benthic diatoms and pelagic estuarine/coastal diatoms. Interestingly, the strategies used to deal with dynamic high light are quite different within niche-specific diatom groups, whereby non-motile benthic diatoms employ rapidly reversible nonphotochemical quenching through XC – presumably to cope with more variable light fields (Lavaud et al. 2007; Derks & Bruce 2018) – whereas motile benthic diatoms preferentially employ slower, sustained non-photochemical quenching (Barnett et al. 2015; Blommaert et al. 2017). This pattern has been further confirmed comparing Artic diatoms (Croteau et al. 2020). Within pelagic species, the coastal taxon *Skeletonema costatum* exhibits inherently less capacity for sustained non-photochemical quenching than the estuarine taxon *Phaeodactylum tricornutum*, but these alternate managements of excitation pressures are compensated by different capacities for PSII repair (Lavaud et al. 2016). Here, maintaining a greater proportion of "active" PSIIs but lower capacity for non-photochemical quenching, presumably, places more pressure on electron carriers downstream of PSII to dissipate the transient accumulation of excessive excitation energy within the photosynthetic electron transport chain.

Microalgae exposed to supra-optimal light can further deal with excessive excitation energy through "alternative electron flows" downstream of PSII (e.g. (Perkins et al. 2018; Cardol et al. 2011; Alric & Johnson 2017; Hughes et al. 2018a). Numerous alternative electron pathways have been described, including electron cycles around PSII (Lavaud et al. 2002a; Onno Feikema et al. 2006; Wagner et al. 2016) and PSI (Schreiber 2004) that do not consume O_2, or alternative midstream terminal oxidase (MOX, Behrenfeld et al. 2008) pathways downstream of PSII (e.g. plastid terminal oxidase, PTOX, Bailey et al. 2008; Nawrocki et al. 2015) or of PSI (Mehler-Ascorbate-Peroxidase, Asada 1999; Weger et al. 1989; Flavodiiron proteins, Allahverdiyeva et al. 2015) that consume electrons and O_2. It has been suggested that such up-regulation of alternative electron flow directly feeds back to non-photochemical quenching generation at PSII by generating ΔpH – a key trigger of antennae-based non-photochemical quenching processes (Nawrocki et al. 2015). In spite of the potential importance of these electron pathways, relatively little is known as to whether they operate to sustain photo-protective capacity in diatoms.

Mehler Ascorbate Peroxidase activity (Mehler for brevity) is an alternative electron sink following PSI, consuming O_2 to ultimately re-generate H_2O (e.g. [54,56]) and appears to be a significant route of total O_2 uptake in the light amongst diatoms (Fisher & Halsey 2016). For example, 60% oxygen uptake via Mehler activity was observed for *Thalassiosira pseudonana* (Kromkamp & Peene 2001) and *Cylindrotheca* (Calquin et al. 2004). However, other reports have suggested a significant role for mitochondrial alternative oxidase (AOX; e.g. *Thalassiosira weissflogii*, Weger et al. 1989), which can, in turn, supply energy to chloroplast-protective processes (Murik et al. 2019). Photorespiration related to RUBISCO oxidase function is often considered a negligible

source of energy dissipation in diatoms as they have evolved carbon concentrating mechanisms (Raven et al. 2000; Giordano et al. 2005). Importantly, Mehler, but not AOX, directly supports chloroplast proton motive force pathways that directly contribute to signalling photo-protection through the light harvesting apparatus (see Hughes et al. 2018a). At present, it remains unexplored whether and how the modulation of O_2 consumption, as a means to balance excess excitation pressure, can be reconciled with differential capacities for non-photochemical protection amongst diatoms.

Here we initially examined allocation of excitation energy to non-photochemical vs. photochemical pathways across a broad panel of diatoms to uncover divergent strategies. We then analyzed three representative diatom taxa (*Thalassioisira weissflogii*, *Thalassiosira pseudonana*, *Thalassiosira oceanica*) from ecologically distinct light environments (estuarine, coastal, open ocean, respectively) to determine their balance of photo-protective strategies through XC versus PSII repair capacity, and whether species with higher capacities for non-photochemical quenching exhibited lower reliance on induction of light-dependent O_2 consumption (light-dependent respiration, LDR). We therefore screened *T. weissflogii*, *T. pseudonana* and *T. oceanica* for (i) pigment content and de-epoxidation activity, (ii) PSII photo-inactivation and repair rate constants, and (iii) LDR upon transient exposure to high light, relative to the growth irradiance. Together these data demonstrate that diatom species from different ecological niches have highly divergent energy allocation strategies to cope with high light exposure.

2.3. Materials and Methods

2.3.1. Culture conditions and growth

Seven diatoms, including *Phaeodactylum tricornutum* (CCMP 632), *Chaetoceros muelleri* (CCMP 1316), *Ditylum brightwellii* (CS 131), *Thalassiosira rotula* (CCMP 3264), *Thalassiosira pseudonana* (CCMP 1335), *Thalassiosira weissflogii* (CCMP 1336), and *Thalassisosira oceanica* (CCMP 1005), were initially screened for their response characteristics using chlorophyll fluorescence metrics. All species were grown as semi-batch cultures using f/2+Si medium (Guillard 1975) supplemented with Na_2SeO_3 at 0.17 µM concentration (Fisher & Halsey 2016). Nitrate and phosphate concentrations in the media reservoir were 250 and 50 µM, respectively (Laws & Bannister 1980). Cultures were grown over 12:12 L:D cycle under 85 µmol photons m^{-2} s^{-1} at 20°C and maintained in exponential phase for 7-10 generations before sampling. Light was supplied by cool-white fluorescent tubes and intensities were measured using a LI-COR photometer (LI-250A, Nebraska, USA) equipped with a 4π spherical quantum sensor. Data were collected from independent biological replicates for cells maintained under exponential phase of growth.

2.3.2. Photophsyiology

Photophysiological assessment was performed using a FastOcean Fast Repetition Rate fluorometer (FRRf; S/N: 12-8679-007) fitted with a FastACT laboratory base unit (Chelsea Technologies Group Ltd, London, U.K), largely as per previous protocols (Suggett et al. 2015; Hughes et al. 2018b). A protocol cumulatively applying 100 flashlets (1 µs flashlets with 2 µs intervals) was used to drive single turnover (ST) closure of RCIIs to generate a fluorescence induction curve. This induction was immediately followed by a relaxation phase of 40 flashlets (1 µs flash with 50 µs

intervals). The biophysical model of Kolber et al. (1998) was then fitted to the generated fluorescence transient to extract minimal (F_o) and maximum (F_m) fluorescence, the functional absorption cross section of PSII (σ_{PSII}, nm^2 PSII^{-1}) and the lifetime for re-opening of PSII (τ, µs). All ST measurements were performed using blue excitation LED (450 nm) and a total of 40 induction/relaxation sequences were conducted per acquisition, with 150 ms intervals between sequences. Samples were taken from growth light cultures and shifted to low light (<10 µmol photons m^{-2} s^{-1}) for 5 min to relax non-photochemical quenching processes before fluorescence measurements were made. Values of σ_{PSII} and maximum PSII photochemical efficiency (F_v/F_m, dimensionless) were then immediately measured on samples transferred to darkness, with F_v/F_m calculated as:

$$\frac{F_v}{F_m} = \frac{F_m - F_o}{F_m} \quad (1)$$

Fluorescence-light response curves (FLCs) were performed in triplicate over 12 light steps of increasing irradiance ranging from 0-1304 µmol photons m^{-2} s^{-1}, provided by a cool white LED array housed within the fluorometer optical head with each light step lasting for 4 min. At each light step, non-photochemical quenching (NPQ) was calculated following the conventional Bilger & Bjorkman (1990) Stern-Volmer equation (see S2.1 Fig):

$$NPQ = (F_m - F_m{}')/F_m{}' \quad (2)$$

where the prime ($'$) notation represents fluorescence measurements under actinic light. We used the approach of Serôdio *et al.* (2005) where the maximum achieved value of F_m' throughout the FLC was used as a proxy for F_m in order to offset any down-regulation of fluorescence through dark-driven plastoquinone (PQ) pool reduction. However, values of NPQ determined through Eq 2 are unbounded, thus we calculated a

complementary parameter that describes the yield of regulated non-photochemical quenching (YNPQ; see Klughammer & Schreiber 2008), and generates a parameter bounded between 0 and 1:

$$YNPQ = \left(\frac{F\prime}{F_{m}\prime}\right) - \left(\frac{F\prime}{F_{m}}\right) \quad (3)$$

where F' is the fluorescence measurement under actinic light and F_m was again taken as the maximum value of F_m' achieved throughout the FLC. Additional fluorescence yield parameters were further calculated following (Klughammer & Schreiber 2008; Genty & Harbinson 2006) to describe the partitioning of absorbed excitation energy at PSII to include photochemical conversion (YII), non-regulated nonphotochemical quenching (YNO) to complement regulated nonphotochemical quenching (YNPQ) such that

$$YII + YNO + YNPQ = 1 \quad (4)$$

$$YII = (F_m' - F')/F_m' \quad (5)$$

$$YNO = F'/F_m \quad (6)$$

To initially identify trade-offs in allocations of excitation energy to photochemical versus non-photochemical pathways, we also calculated the fraction of open RCIIs responsible for photochemical quenching [1-C] to plot vs. dynamic non-photochemical quenching [1-Q] under each actinic light intensity following equations from Suggett et al. (2015) (Eq 7 and 8). Both [1-C] and [1-Q] decrease in value from 1 to 0 with increasing extents of quenching, and the product of [1-C] and [1-Q] is equivalent to the PSII photochemical efficiency normalised to F_v/F_m,

$$[1 - C] = (F_m{}' - F')/(F_m{}' - F_o{}') \quad (7)$$

$$[1 - Q] = ((F_m{}' - F_o{}')/F_m{}')/(F_v/F_m) \quad (8)$$

Where F_o' (fluorescence minimum under actinic light) is estimated as per Oxborough and Baker (1997):

$$F_o' = F_o/[(F_v/F_m) + (F_o/F_m')] \quad (9)$$

Measurements were performed for each species using at least three independent samples collected during acclimated exponential growth. Methods described from this point onwards apply to only the three selected diatoms (*Thalassiosira pseudonana*, *Thalassiosira oceanica*, *Thalassiosira weissflogii*) that span highly divergent photophysiological responses.

2.3.3. Growth and biomass

Small aliquots from each culture were preserved daily (within 2 hours illumination) with glutaraldehyde (25%, Sigma-Aldrich) for later cell counting on a flow cytometer (CytoFlex S, Beckman Coulter, Miami, FL USA). Samples were counted for 60 s at a rate of 30 µL min^{-1}. Specific growth rates (divisions $[day]^{-1}$) were calculated as $\mu = \ln(N_2/N_1)/(t_2-t_1)$, where μ is the specific growth rate (day^{-1}), N_1 and N_2 are the cell concentrations (mL^{-1}) at time 1 (t_1) and time 2 (t_2), respectively. Cell volume was calculated from the same sample used for cell count determinations using shape-specific geometric formulas from Sun & Liu (2003) via an imaging compound light microscope (Nikon). From independent cultures, 10 images were taken at random and cellular dimensions recorded for five cells per image using Infinity software (Lumenera Corporation, Ontario, Canada).

On sampling days, two aliquots each of 5-8 mL culture were filtered onto a 25 mm glass fiber filter (Whatman GF/F) and stored overnight at -20°C in 90% acetone to extract chlorophyll *a*. Absorption was measured using a spectrophotometer (Aligent Technologies, Cary 60 UV-Vis) set at wavelengths 630, 657, 664, and 750 nm and chlorophyll *a* concentration was calculated according to Ritchie (2006). Cellular

particulate organic carbon (POC, units of pg C mL^{-1}) was also measured in duplicate for each biological replicate, by filtering two aliquots each of 5 mL onto pre-combusted filters (Whatman GF/F). POC samples were stored at -20°C until analysis on an elemental analyzer (LECO, Baulkham Hill, Australia) using culture filtrate (5 mL) as the blank. Net primary productivity (NPP) was calculated as the product of specific growth rate (μ) and cellular POC (C), whereby NPP = μ · C. Contributions from DOC were assumed to be negligible (<5% of total energy budget) for diatom cultures (*T. pseudonana*, Fisher & Halsey 2016).

2.3.4. PSII photo-inactivation and repair

Two subsamples (25 mL each) were initially collected from cultures. Using approaches adopted from Campbell *et al.* (2013), lincomycin hydrochloride (95%, Sigma-Aldrich), an inhibitor of chloroplast protein synthesis, and thus PSII repair, was added to one subsample to a final concentration of 500 μg mL^{-1} while the second subsample (control) received no lincomycin hydrochloride addition (Key et al. 2010). After an initial dark incubation (10 min) of both subsamples to allow incorporation of inhibitor, photophysiology was repeatedly tracked via FRRf. Over a subsequent 120 min incubation at 1200 μmol photons m^{-2} s^{-1}, 2 mL of fresh sample was taken for FRRf measurements at 30, 60 and 120 min. Each of these FRRf samples received consecutive induction flashlets every 10 s for a duration of 10 min without actinic light to capture short-term recovery of the PSII photochemical efficiency (F_v'/F_m') resulting from relaxation of non-photochemical quenching as opposed to slower recovery from photo-inactivation. After the 120 min incubation at 1200 μmol photons m^{-2} s^{-1}, subsamples were transferred to low light (~15 μmol photons m^{-2} s^{-1}) for a total of 60 min to capture recovery. Recovery at 15 μmol photons m^{-2} s^{-1} was used instead of complete darkness

since diatom PSII repair is stimulated by light intensities well below photosynthetic saturation (Wu et al. 2012; Li et al. 2016). Measures of FRRf from five induction flashlets taken at 10 s intervals were completed after 30 and 60 min, hereafter referred to as 150 and 180 min, respectively, for consistency in assessment of this time-course experiment. Estimation of photo-inactivation and recovery of PSII were plotted from changes in F_v'/F_m' or F_v/F_m following each treatment time point.

Values of F_v'/F_m' or F_v/F_m from the sub-cultures treated with lincomycin and exposed to 1200 µmol photons m^{-2} s^{-1} (4 time points over 120 min) were fit with exponential decay curves to estimate the apparent first order rate constant for photo-inactivation of PSII under applied irradiance, k_{PI} (s^{-1}). From k_{PI} we then calculated the susceptibility to photo-inactivation generalised across irradiance levels, as a target size functional absorption cross section for photo-inactivation of PSII, $\sigma_I = k_{PI}$/photons m^{-2} s^{-1}. The apparent first order rate constant for PSII repair, k_{REC} (s^{-1}) (Kok 1956) was then estimated following (Campbell & Serôdio 2020; Oliver et al. 2013; Campbell & Tyystjärvi 2012) using subsamples without lincomycin, across the entire treatment trajectory of initial exposure to 1200 µmol photons m^{-2} s^{-1} (4 time points) and then recovery at 15 µmol photons m^{-2} s^{-1} (2 time points). For fitting of k_{REC} we used the σ_I value for each species determined in the presence of lincomycin, on the simplifying assumption that the primary photo-inactivation of PSII is the same in the absence or the presence of PSII repair. Within each species each replicate time-course followed a similar trajectory and therefore k_{PI} and k_{REC} were fit using points pooled from 3-4 replicate trajectories for each species, using the nlsLM fitting function from the minpack.lm package (Elzhov et al. R package v1.2-1) running under R (R Core Team)

and RStudio (RStudio Team). Figures were then generated using ggplot2 (Wickman 2016).

2.3.5. Pigment analysis

High performance liquid chromatography (HPLC) was used to determine concentrations of XC pigments (chlorophyll *a* and *c*, fucoxanthin, diadinoxanthin (Dd), diatoxanthin (Dt), and beta-carotene) in the diatom cultures. In triplicate for each species, 50 mL of culture were incubated in a 20°C waterbath at growth irradiance (Ig, 85 µmol photons m^{-2} s^{-1}) and high light (HL, 1200 µmol photons m^{-2} s^{-1}) for 10 min. Culture was then immediately filtered onto a GF/F filter at volumes to saturate the filter with material (25-40 mL) and thus maximise biomass for pigment signal detection. Filters were flash frozen in liquid nitrogen and stored at -80°C until extraction. Extraction of samples were carried out following Heukelem & Thomas (2001) with slight modifications. Filters were placed into 15 mL tubes containing chilled acetone, sonicated (30 s) and then vortexed for 30 s (x3) under cold, dark conditions to limit pigment degradation, and then stored at 4°C overnight. Pigment extracts were then filtered through a 0.2 µM PTFE 13 mm syringe filter and stored in -80°C until analysis. An Agilent 1290 HPLC system equipped with a binary pump with integrated vacuum degasser, thermostatted column compartment modules, Infinity 1290 autosampler and PDA detector was used for the analysis. Column separation was performed using an Agilent's Zorbax Eclipse XDB C8 HPLC 4.6 mm × 150 mm and guard column using a gradient of TBAA: Methanol mix (30:70) (solvent A) and Methanol (Solvent B) as follows: 0–22 min, from 5 to 95% B; 22–29 min, 95% B; 29-31 min, 5% B; 31-40 min, column equilibration with 5% B. Column temperature was maintained at 55°C. A complete pigment spectrum from 270 to 700 nm was recorded using PDA detector with

3.4 nm bandwidth. The de-epoxidation state (DPS) of XC pigments, particularly diadinoxanthin (Dd) de-epoxidation and diatoxanthin (Dt) epoxidation was determined as Dt $(Dd\text{-}Dt)^{-1}$ (Grouneva et al. 2009) as diatoms have a dominant Dd-Dt cycle and minor violaxanthin-antheraxanthin-zeaxanthin cycle (Lavaud et al. 2002b; Goss et al. 2006; Raven 2011), compared to the dominant violaxanthin-antheraxanthin-zeaxanthin cycle in green algae and vascular plants (Stransky & Hager 1970; Horton & Ruban 1992; Zhu & Green 2010).

2.3.6. Membrane inlet mass spectrometry (MIMS)

Aliquots of 60 mL of culture were sparged with N_2 gas for 20 min to remove $^{16}O_2$, and 50 mL of the sparged sample was then transferred to a gas-tight syringe and directly enriched with labelled oxygen ($^{18}O_2$, Marshall Isotopes Ltd., Israel) and mixed vigorously by shaking for 3 min to allow the $^{18}O_2$ gas bubble to equilibrate with the solution. $^{18}O_2$-Labelled culture was then divided between four 12 mL exetainer vials (LabCo Ltd., UK) for the following treatments: time zero (T_0), dark, growth irradiance (Ig, 85 µmol photons m^{-2} s^{-1}) and high light (HL, 1200 µmol photons m^{-2} s^{-1}). The T_0 samples were fixed immediately with 200 µL 0.2 M mercuric chloride ($HgCl_2$) to cease biological activity. Ig and HL vials were incubated under the specified light intensity for 20 min at 20°C then subsequently fixed in the same manner as T_0. Fixed samples were stored at room temperature under darkness for later analysis on a membrane inlet mass spectrometer (MIMS, Bay Instruments, Maryland, USA).

Set up and analysis using the MIMS was undertaken following Kana et al. (1994) modified by Suggett et al. (2009). In brief, samples were pumped through stainless steel capillary tubing, submerged in a waterbath (20°C), then over a semi-permeable

microbore silicone membrane (Silastic®, DuPont), where gas exchange occurred. Gases flowed through a U-shaped manifold membrane inlet system, resting in a liquid N_2 cryotrap, and attached to a Prisma QMS-200 (Pfeiffer) quadrapole mass spectrometer with a closed ion source and electron multiplier detector for recording mass/charge (m/z) ratios of 32 ($^{16}O_2$), 36 ($^{18}O_2$), and 40 (Ar). Discrete measurements of ion currents were recorded using QuikData software (Bay Instruments, Maryland, USA). Calibration of the MIMS was performed at the beginning and end of sampling and subsequently (~30 min) between sampling.

Rates of oxygen production/consumption were calculated from the difference between signal outputs, $^{16}O_2$ and $^{18}O_2$, for T_0 and light treatment (Dark, Ig, HL) incubation samples before scaling to hourly rates (as per Suggett et al. 2009a). Corrected $^{16}O_2$ signals in the light were assumed to be gross oxygen production (GP_{O2}). Net oxygen production (Net_{O2}) was calculated as the difference between GP_{O2} and total respiration, including dark (R_{DARK}) and light dependent respiration (LDR). R_{DARK} is the $^{18}O_2$ signal from the dark sample and LDR is the difference between R_{DARK} and $^{18}O_2$ signal from each light treatment (Ig or HL). It is important to note that studies with continuous (i.e. real-time) MIMS sampling (Waring et al. 2010; Halsey et al. 2010, 2013; McKew et al. 2013; Du et al. 2018) are able to establish highly accurate rates of oxygen consumption/production, whereas discrete measurements (Suggett et al. 2009a; Brading et al. 2011; Ferrón et al. 2016) – and as per our study –likely underestimate 'true' rates. A 20 min incubation was chosen to minimise the $^{16}O_2$ consumed by respiration while allowing enough time for generation of detectable oxygen signals via MIMS. Without real-time rate information (i.e. continuous measuring) it is impossible to determine when $^{16}O_2$ exceeds $^{18}O_2$ and therefore a portion of this $^{16}O_2$ signal is likely to be

consumed; as such, GP_{O2} is thus likely an underestimate of true $^{16}O_2$ production. However, by this justification, $^{18}O_2$ consumption (respiration) is also likely an under-(conservative) estimate of true values. Having this consistency in assessing the values derived from MIMS provided confidence that the trends observed are accurate; however, the true concentration values may be underestimated. Due to the sensitive nature of MIMS sampling, at least five replicates (and two measurements per replicate) were collected for each species.

2.3.7. Statistics

Differences in cellular properties between species were assessed using one-way analysis of variance (ANOVA) followed by Bonferroni's multiple comparison test where prerequisite assumptions of normality and homoscedasticity were satisfied (tested for using Levene's and Shapiro-Wilk tests respectively). If the assumption of normality was violated, data were either square-root or arcsine-square-root transformed and the distribution of residuals re-tested. If either assumption continued to be violated despite transformation, differences between species were instead evaluated using non-parametric ANOVA on ranks (Kruskal-Wallis test), followed by Dunn's post-hoc test. Two-way ANOVA followed by Bonferroni's multiple comparison test was used to evaluate the significance of the effect of species and light treatment on photobiological characteristics (pigments and DPS) (Ananda & Weerahandi 1997). Residuals of all variables exhibited normal distribution, although assumptions of homoscedasticity were violated for specific variables: Dd, Dt, GP_{O2}, Net_{O2} and LDR. ANOVAs were performed using IBM SPSS Statistics v26, while Sigmaplot v12.5 was used for data transformation and Kruskal-Wallis tests. As the variable YNPQ exhibited neither normal distribution or equal variance across sample groups, a permutation univariate

ANOVA was performed using the PERMANOVA+ add-on (Anderson et al. 2008) in the PRIMER (v6) statistical package (PRIMER-E Ltd, UK). A resemblance matrix computed from Euclidean distance was used for the PERMANOVA procedure, and the test comprised a two-factor design (species and light treatment), type I (sequential) sum of squares and 9999 permutations under the reduced model. The significance level for all tests performed was set at $p < 0.05$.

2.4. Results

2.4.1. Initial photophysiological assessment

Excitation allocation strategies were investigated in diatoms species with different ecological niches; specifically, the coastal pennate *Phaeodactylum tricornutum*, coastal small centric *Chaetoceros muelleri*, coastal large centric *Ditylum brightwellii*, and four centric species of the *Thalassiosira* genus ranging in cell size from smallest to largest: coastal *T. pseudonana,* open ocean *T. oceanica,* esturaine *T. weissflogii,* coastal *T. rotula*. Cells were grown under 85 µmol photons m^{-2} s^{-1} and FRRf-response light curves were used to determine YNPQ (Eq 3, Fig 2.1A) and the proportion of energy directed to [1-C] (photochemistry, Eq 7) versus [1-Q] (photo-protection, Eq 8) (Fig 2.1B). The taxa fell into three excitation allocation strategies: (i) relatively fast/substantial, (ii) relatively slow/negligible accumulation of nonphotochemical quenching vs. declines of [1-Q], and (iii) an intermediary response.

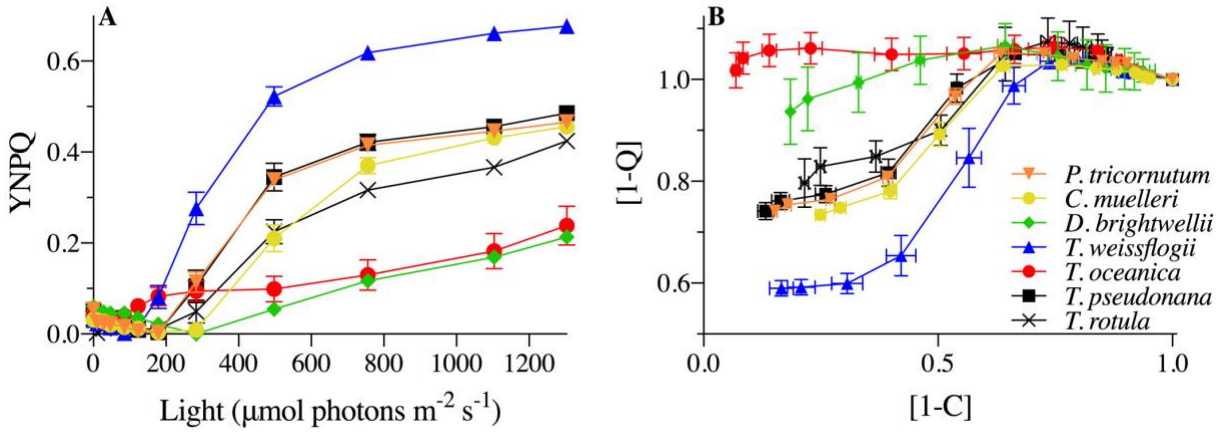

Figure 2.1. Initial photophysiological monitoring of seven diatoms: *Phaeodactylum tricornutum* (orange inverted triangles), *Chaetoceros muelleri* (yellow circles), *Ditylum brightwellii* (green diamonds), *Thalassiosira rotula* (black Xs), *Thalassiosira pseudonana* (black squares), *Thalassiosira weissflogii* (blue triangles), and *Thalassisosira oceanica* (red circles). (A) Yield of non-photochemical quenching (YNPQ; see Eq 3) with increasing light intensity. (B) Dynamic non-photochemical quenching [1-Q] versus photochemical [1-C], where data points signify responses to stepped increases in light intensity starting from 0 (far right point) to 1304 µmol photons m^{-2} s^{-1} (far left point) for 4 min at each light intensity. Error bars represent the standard error of the mean of at least *n*=3 for independent biological replicates.

T. weissflogii, *T. oceanica* and *T. pseudonana*, were chosen as representative candidates of the three strategies observed to subsequently examine the diversity of mechanisms utilised by these related diatoms under dynamic light to maintain photosynthetic efficiency. Under the stepwise progression of increasing actinic light intensity, *T. oceanica*, the open ocean species, initiated negligible nonphotochemical quenching (parameterised as YNPQ, Fig 2.1A). In contrast, *T. weissflogii*, an estuarine native species, rapidly initiated nonphotochemical quenching at relatively low light

intensity (~120 µmol photons m^{-2} s^{-1}) and to a higher capacity. *T. pseudonana*, a coastal species, exhibited an intermediate response, initiating nonphotochemical quenching once reaching a light intensity of ~200 µmol photons m^{-2} s^{-1}. A similar pattern was observed when comparing [1-C] and [1-Q] (Fig 2.1B). Here [1-Q] showed limited short-term change in response to a progressive decrease in [1-C] (RCII closure) under increasing light in *T. oceanica*. In contrast *T. weissflogii* showed strong induction of [1-Q] as [1-C] dropped below 0.6 with increasing light. Values greater than 1 for [1-Q] are attributed to the effects of chlororespiration under very low light/darkness (Lavaud et al. 2002a; Serôdio et al. 2005). Overall, increased reliance on non-photochemical quenching generally corresponded with decreased photochemical quenching, tracking the remaining fraction of RCIIs engaged in photochemistry, across these three species.

2.4.2. Cell characteristics for selected *Thalassiosira* species

Cellular growth rates increased with decreasing cell size from *T. weissflogii* to *T. pseudonana* (Table 2.1). Chl *a*:C and C:N were not statistically different among the three species and are consistent with previous reports for *T. pseudonana* (Fisher & Halsey 2016), *T. weissflogii* (Chl *a* and µ, Walter et al. 2015; Lomas 2004), and *T. oceanica* (Bucciarelli et al. 2013). Net primary production (NPP in units of µmol C (mg Chl h)$^{-1}$) in *T. oceanica* and *T. pseudonana* were not statistically distinguishable from NPP in *T. weissflogii* (Table 2.1). Consistent with previous reports for diatoms grown under steady-state nutrient replete conditions, values of FRRf-based maximum photochemical efficiency (F_v/F_m, dimensionless) were generally higher (and the effective absorption cross section for PSII photochemistry, σ_{PSII}, smaller) for the larger *T. weissflogii* compared to the smaller *T. oceanica* and *T. pseudonana* (Suggett et al. 2009b).

Table 2.1. Cell characteristics of *Thalassiosira weissflogii, Thalassiosira oceanica*, and *Thalassiosira pseudonana* from exponential steady state growth under 85 µmol photons m^{-2} s^{-1} at 20°C. Data shown are the mean of independent biological replicates where n=3 for growth rate (d^{-1}), Chl *a* ($cell^{-1}$) and net primary production (NPP), n=4 for cell concentration (mL^{-1}), carbon (pg $cell^{-1}$), C:N, F_v/F_m and σ_{PSII} (nm^2 $PSII^{-1}$) and n=20 for cell volume. Values in parentheses are SE of the mean. ANOVA or Kruskal-Wallis (KW) test results comparing species and individual cell characteristics are presented using F or H-values, respectively, with significant *p*-values ($p < 0.05$) in bold. Superscripted letters indicate differences between species groups identified by Bonferroni post-hoc analysis.

Species	Growth rate (d^{-1})	Cells mL^{-1} ($x10^5$)	Cell volume (μm^3)	Chl *a* $cell^{-1}$ (pg)	C $cell^{-1}$ (pg)	Chl:C ($x10^{-2}$) (µg μg^{-1})	C:N	NPP (µmol C (mg Chl h)$^{-1}$)	F_v/F_m	σ_{PSII} (nm^2 $PSII^{-1}$)
Thalassiosira weissflogii	0.68 (0.05)	1.40^a (0.03)	1243.10^b (62.26)	5.66^b (0.20)	158.91^b (23.24)	4.32 (0.17)	3.82 (0.13)	67.62 (16.91)	0.58^b (0.01)	2.29^a (0.16)
Thalassiosira oceanica	0.80 (0.02)	3.62^a (0.18)	159.62^a (19.38)	1.03^a (0.01)	56.13^a (3.23)	2.92 (0.48)	5.23 (0.87)	88.36 (17.94)	0.55^a (0.00)	3.98^b (0.17)
Thalassiosira pseudonana	0.94 (0.03)	12.68^b (0.27)	99.82^a (1.77)	0.60^a (0.03)	7.92^a (0.70)	4.11 (0.35)	4.68 (0.80)	84.41 (13.62)	0.56^a (0.00)	3.01^a (0.21)
ANOVA or KW (F/H, *p*)	H=5.4 $p>0.05$	H=9.8 ***p<0.05***	F=601.0 ***p<0.05***	F=46.6 ***p<0.05***	F=28.1 ***p<0.05***	F=5.1 $p>0.05$	F=1.2 $p>0.05$	H=0.6 $p>0.05$	F=34.9 ***p<0.05***	F=17.2 ***p<0.05***

2.4.3. Photophysiology strategy

Contents of accessory chlorophyll and carotenoids were normalised to Chl *a* and were largely similar for samples incubated for 10 min under HL (1200 µmol photons m^{-2} s^{-1}) compared to those at the growth irradiance (Ig, 85 µmol photons m^{-2} s^{-1}) (Table 2.2) within each species. Chl *c*, fucoxanthin and β-carotene, while not influenced by short-term high light ($p > 0.05$), were different among species ($p < 0.05$) with fucoxanthin:Chl *a* highest in *T. oceanica* compared to *T. pseudonana* and *T. weissflogii* (Table 2.2). Most notably, extent of XC, determined as the de-epoxidation state (DPS, see methods *'Pigment Analysis'*), differed between light treatments where all species exhibited an increase in DPS, (as a decrease in Dd:Chl *a*; and corresponding increase in Dt:Chl *a*) from Ig to HL. *T. pseudonana* exhibited the lowest DPS under Ig but also the greatest difference in DPS between Ig and HL (Table 2.2).

Table 2.2. Xanthophyll cycle pigments under growth irradiance (Ig) and transient short-term shift to high light (HL). Diadinoxanthin (Dd), diatoxanthin (Dt), and accessory pigments, Chlorophyll *c* (Chl *c*), fucoxanthin (Fuc), and Beta-carotene (β-Car) were all normalised to Chl *a* for *T. weissflogii*, *T. oceanica*, and *T. pseudonana* under Ig (85 µmol photons m^{-2} s^{-1}) and HL (1200 µmol photons m^{-2} s^{-1}) incubation for 10 min. Data averaged from 3 independent replicates. Value in parentheses represent SE of the mean.

Species	Light	Normalised to Chl *a* (μg mL^{-1})					DPS
		Chl *c*	Fuc	β-Car	Dd	Dt	
T. weissflogii	Ig	0.028 (0.002)	0.533 (0.007)	0.021 (0.001)	0.034 (0.002)	0.012 (0.004)	0.243 (0.076)
	HL	0.027 (0.002)	0.525 (0.003)	0.021 (0.001)	0.026 (0.002)	0.028 (0.004)	0.509 (0.031)
T. oceanica	Ig	0.053 (0.002)	0.959 (0.016)	0.017 (0.001)	0.032 (0.001)	0.008 (0.001)	0.205 (0.013)
	HL	0.049 (0.005)	0.953 (0.034)	0.018 (0.000)	0.027 (0.004)	0.027 (0.007)	0.492 (0.080)
T. pseudonana	Ig	0.033 (0.005)	0.659 (0.006)	0.019 (0.000)	0.049 (0.007)	0.005 (0.003)	0.079 (0.031)
	HL	0.031 (0.004)	0.650 (0.008)	0.020 (0.000)	0.036 (0.004)	0.025 (0.011)	0.372 (0.072)

Increases in DPS from Ig to HL generally accompanied increases in non-photochemical quenching (parameterised as YNPQ, Fig 2.2) for all species, but, importantly, the extent of DPS did not show comparable correlations with YNPQ across species. *T. weissflogii* exhibited much higher nonphotochemical quenching than *T. oceanica* ($p < 0.001$) despite similar DPS. Whilst *T. pseudonana* had lower total DPS, the corresponding increases of DPS and YNPQ from Ig to HL were more similar to those of *T. weissflogii* (dashed lines, Fig 2.2). Thus, the extent to which nonphotochemical quenching induction accompanied DPS accumulation appeared to differ among these three species but was not explicitly tested in our analysis.

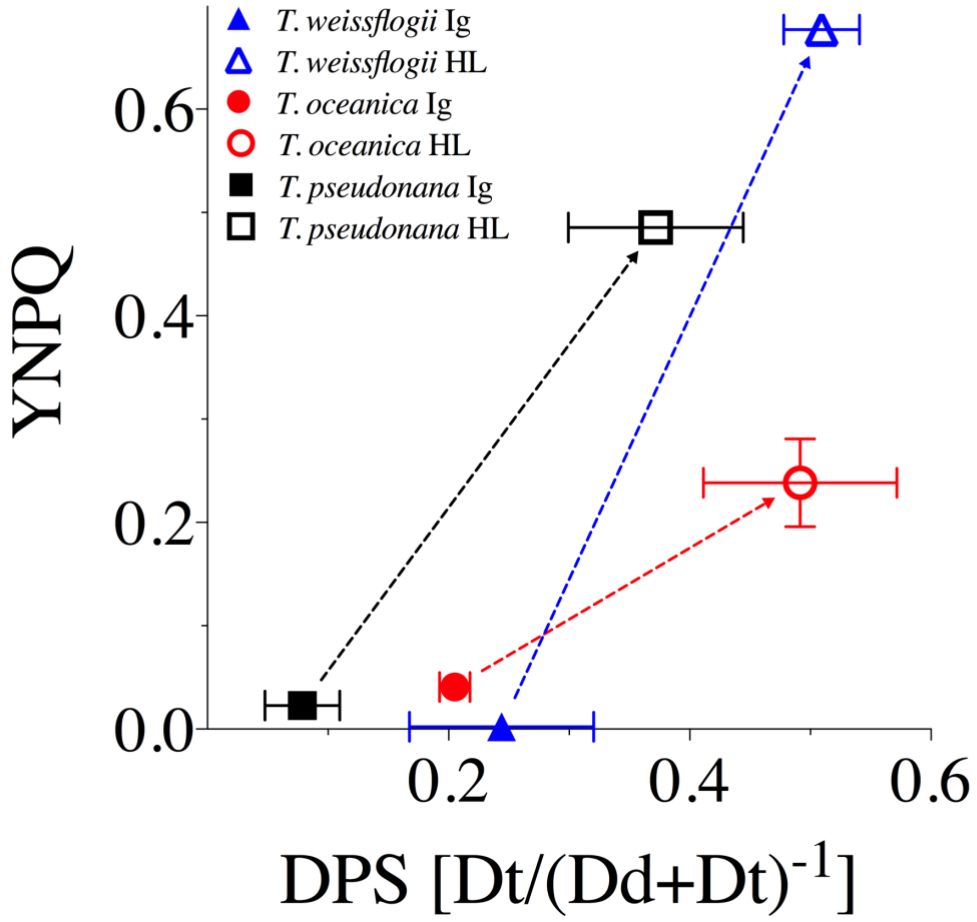

Figure 2.2. YNPQ vs. de-epoxidation state (DPS) of the XC for *T. weissflogii* (blue triangles), *T. oceanica* (red circles), and *T. pseudonana* (black squares) under 10 min exposure to growth irradiance (Ig, 85 µmol photons m^{-2} s^{-1}, solid symbols) and high light (HL, 1200 µmol photons m^{-2} s^{-1}, open symbols). Dashed lines highlight the extent of changes observed between light treatments for each measured parameter. Data averaged from three independent replicates for DPS and at least four independent replicates for YNPQ with errors bars representing SE of the mean.

2.4.4. PSII photo-inactivation and repair

We examined the extent of PSII photo-inactivation and capacity for repair by exposing the cells to HL (1200 µmol photons m^{-2} s^{-1}) for 120 min, followed by a recovery period at 15

µmol photons m^{-2} s^{-1} (Fig 2.3). All three species exhibited a drop in F_v'/F_m' and F_v/F_m over the initial 30-60 min of HL exposure. *T. oceanica* and *T. pseudonana* then stabilised F_v'/F_m' and F_v/F_m, reflecting the induction of PSII repair. Upon the down-shift to15 µmol photons m^{-2} s^{-1} all species showed initial rapid recoveries, as photo-inactivation dropped to very low rates, and PSII repair continued for 30 min until all species had recovered to near-initial levels of F_v/F_m.

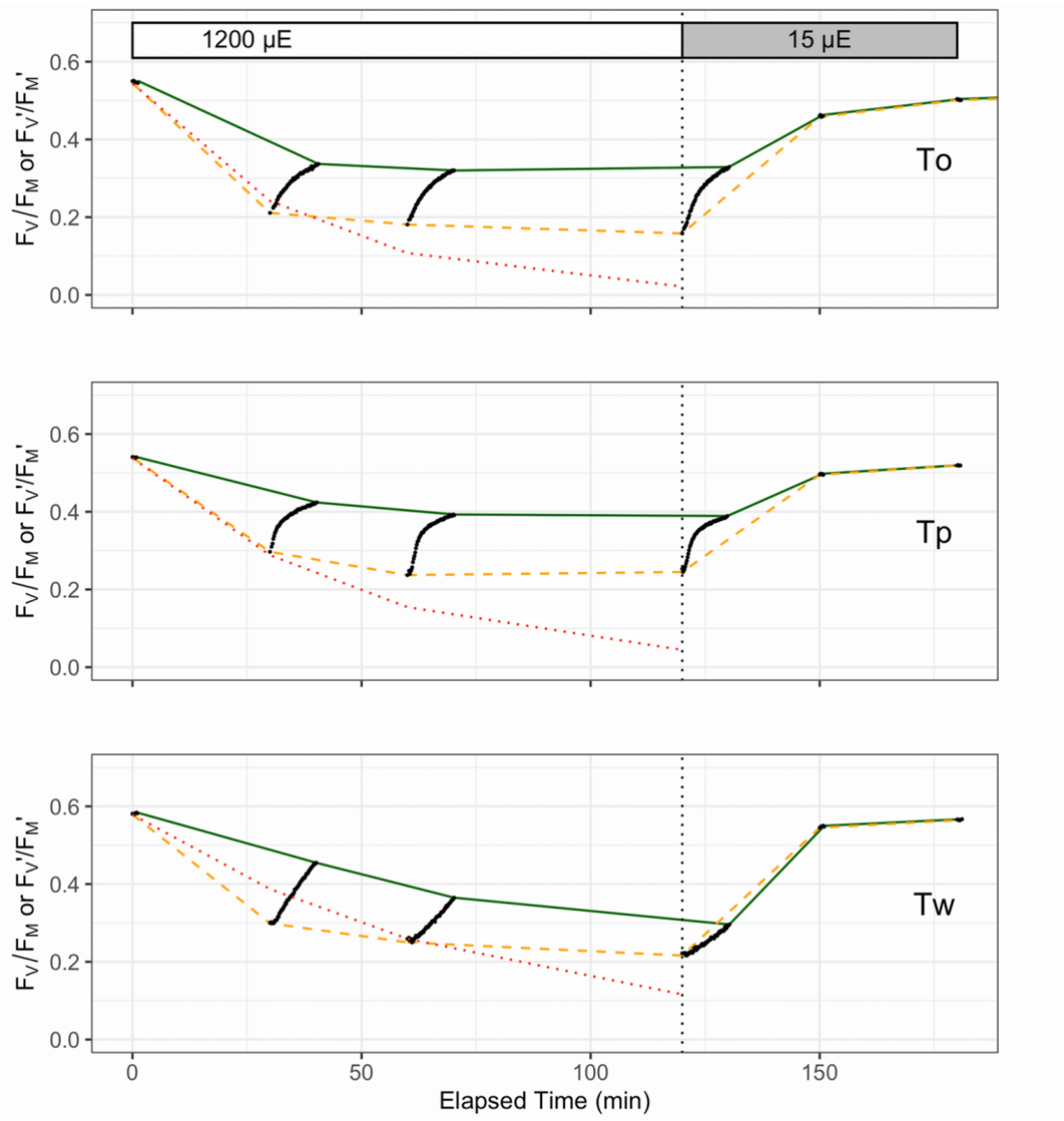

Figure 2.3. Representative photo-inhibition and recovery time courses for *T. oceanica* (To), *T. pseudonana* (Tp) and *T. weissflogii* (Tw). Black points show individual determinations of F_v'/F_m' or F_v/F_m from FRRf measurements of cultures with PSII repair active (absence of lincomycin). Dashed orange line connects F_v'/F_m' measures taken immediately after exposure to HL (1200 µmol photons m^{-2} s^{-1}) over 0 – 120 min or recovery light (15 µmol photons m^{-2} s^{-1}) at 150 and 180 min, influenced by combined effects of non-photochemical quenching induction and net photo-inactivation (if any). Solid green line connects F_v/F_m taken after 10 min of subsequent dark for HL time points, to allow relaxation of non-photochemical quenching, or taken immediately during the recovery light period. These points were used to fit the Kok model of PSII photo-inactivation countered by repair. Note the different patterns and amplitudes of short-term (10 min) relaxation of non-photochemical quenching, among the species (black dots). The dotted red line shows F_v/F_m data from separate lincomycin treated cultures to show the underlying photo-inactivation in the absence of counteracting repair.

In parallel with the effects of photo-inactivation and repair, Fig 2.3 shows the kinetically overlapping influences of nonphotochemical quenching induction upon F_v'/F_m' (orange dashed line) measured immediately after exposure to treatment or recovery light. Systematic photophysiological assessment of samples removed over the 120 min HL exposure and subsequently subjected to a 10 min dark period before fluorometric assessment highlighted the influence of nonphotochemical quenching on PSII function. This is particularly evident in *T. oceanica* and *T. pseudonana* where initial F_v'/F_m' largely relaxed to higher F_v/F_m (through relaxation of nonphotochemical quenching), tracked with the black dots connecting the orange dashed and green solid lines, respectively (see Fig 2.3), over the entire 120 min in HL.

In contrast, *T. weissflogii* showed a progressive decrease in the relaxation amplitude over 120 min HL indicative of sustained (longer lived) nonphotochemical quenching, consistent with the failure of *T. weissflogii* to fully counter photo-inactivation through induction of repair (Wu et al. 2012). It is thus difficult to discriminate between the kinetically overlapping processes of photo-inactivation and sustained downregulation of PSII.

Replicate time courses for PSII photo-inactivation in the presence of lincomycin were fit for each species to extract the rate constant for photo-inactivation, k_{PI}. These k_{PI} values determined for each species in the absence of PSII repair were then inputted into fit models (Kok 1956; Cambell & Serôdio 2020) using data captured from culture samples with PSII repair, in order to estimate the apparent first order rate constant for PSII repair, k_{REC} (Table 2.3). As expected (Key et al. 2010), the susceptibility to photo-inactivation (k_{PI}) decreased with increasing diatom cell size from the smaller *T. oceanica* and *T. pseudonana* to the larger *T. weissflogii* (Table 2.3). The rate constant for the counteracting PSII repair process (k_{REC}) also decreased with increasing cell size from *T. pseudonana* to *T. weissflogii*, but was also low in the offshore *T. oceanica*, consistent with patterns of higher capacity for PSII repair observed previously for onshore versus offshore diatoms (Campbell et al. 2013).

Table 2.3. Rate constants for PSII photo-inactivation (k_{PI}) and repair (k_{REC}) for *T. oceanica*, *T. pseudonana* and *T. weissflogii*, after acclimated growth at 85 µmol photons m^{-2} s^{-1}, followed by treatment for 120 min under HL (1200 µmol photons m^{-2} s^{-1}) then low light recovery (15 µmol photons m^{-2} s^{-1}) (Fig 2.3). Values derived from curve fits (Kok 1956; Campbell & Serôdio 2020) of data from 3 independent replicates. Values in parentheses represent SE of the mean.

Species	k_{PI} (s^{-1})	k_{REC} (s^{-1})
T. oceanica	4.50e-04 (2.28e-05)	5.48e-04 (6.68e-05)
T. pseudonana	3.46e-04 (1.30e-05)	1.50e-03 (1.35e-04)
T. weissflogii	2.23e-04 (9.14e-06)	3.16e-04 (3.35e-05)

The extent of nonphotochemical quenching induction after 120 min of HL, and then relaxation over the subsequent 10 min dark period, were next compared with the PSII repair rates. Interestingly, all species started with similar values of induced YNPQ of ~0.45 - 0.5 (Fig 2.4) under the high light treatment. This contrasts with the much lower values of YNPQ observed for *T. oceanica* compared to *T. weissflogii* from shorter incubations (Figs 2.1, 2.2), highlighting that *T. weissflogii* rapidly builds a rapid but sustained nonphotochemical quenching whereas *T. oceanica* more slowly builds nonphotochemical quenching over time. However, differences in YNPQ between the beginning and end of the 10 min dark incubation (Fig 2.4A), and hence the amplitude of nonphotochemical quenching relaxation (Fig 2.4B), increased with PSII repair capacity. Thus, *T. pseudonana* had the highest PSII repair capacities and maintained a large amplitude of nonphotochemical quenching relaxation whereas *T. oceanica* and, particularly, *T. weissflogii* show sustained nonphotochemical quenching (Fig 2.4) albeit with slower induction for *T. oceanica* (Fig 2.1).

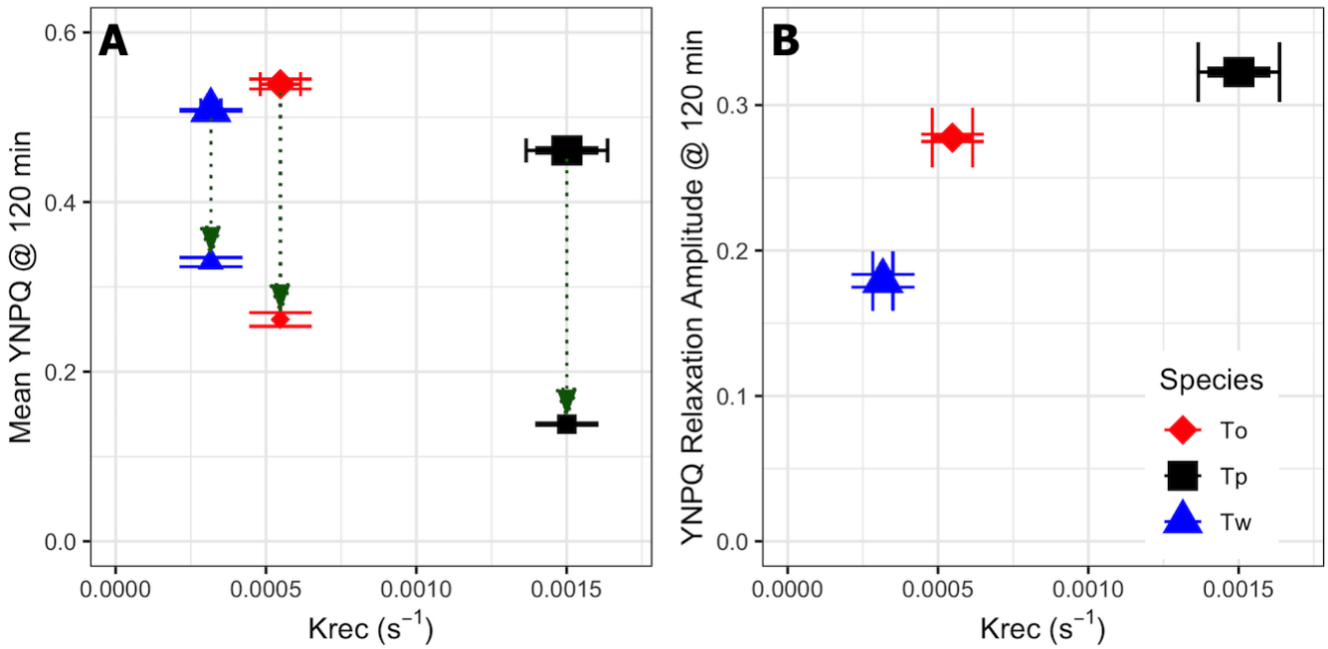

Figure 2.4. Mean YNPQ and YNPQ relaxation amplitude for *T. weissflogii*, *T. oceanica* and *T. pseudonana* after 120 min high light exposure. (A) Mean values of YNPQ vs. the rate constant for PSII repair, k_{REC}, over 120 min HL exposure showing nonphotochemical quenching measured immediately after light exposure (larger symbols) or after 10 min dark FRRf incubation (smaller symbols) for *T. weissflogii* (Tw, blue triangles), *T. oceanica* (To, red diamonds) and *T. pseudonana* (Tp, black squares). (B) The amplitude of YNPQ relaxation (also green arrows in (A)). Error bars show standard errors of the estimates for 3 or 4 independent biological replicates.

2.4.5. Light-driven O_2 consumption

Cell normalised measurements of gross O_2 production (GP_{O2}; pmol cell^{-1} h^{-1}) via MIMS were consistent across light treatments where there was higher production under HL than Ig for all three species ($p < 0.05$, S2.1 Table). However, *T. weissflogii* GP_{O2} was significantly higher from both *T. oceanica* and *T. pseudonana* (Bonferroni post-hoc $p < 0.0001$). Measurements of energy losses are shown in Fig 2.5 as the fraction of GP_{O2} allocated to respiration in the

dark (R_{DARK}) and in the light (LDR), with the remainder being net O_2 production (Net_{O2}). Extent of LDR (% of GP_{O2}) was comparable for all species under Ig but not HL; specifically, %LDR for *T. weissflogii* decreased from 11.8% at Ig to 8.1% at HL but increased from an average of 10.5% at Ig to 16.6% at HL for the other two species, with *T. oceanica* exhibiting the highest LDR increase from Ig to HL. Patterns of $\%R_{DARK}$ were more variable across species and treatment, whereby $\%R_{DARK}$ in *T. weissflogii* and *T. pseudonana* was 16.6 - 21.7% regardless of irradiance and $\%R_{DARK}$ in *T. oceanica* was always <10% (Fig 2.5, S2.2 Table). This trend was supported by Fisher's Tukey post-hoc analysis where *T. oceanica* differed from both *T. weissflogii* ($p = 0.017$) and *T. pseudonana* ($p = 0.033$; see S2.2 Table for full comparisons). Together, the trade-offs in %LDR and $\%R_{DARK}$ from Ig to HL for *T. pseudonana* resulted in unchanged $\%Net_{O2}$, whereas the light-dependent changes in %LDR (but not $\%R_{DARK}$) resulted in an increase and decrease of Net_{O2} from Ig to HL for *T. weissflogii* and *T. oceanica*, respectively (Fig 2.5).

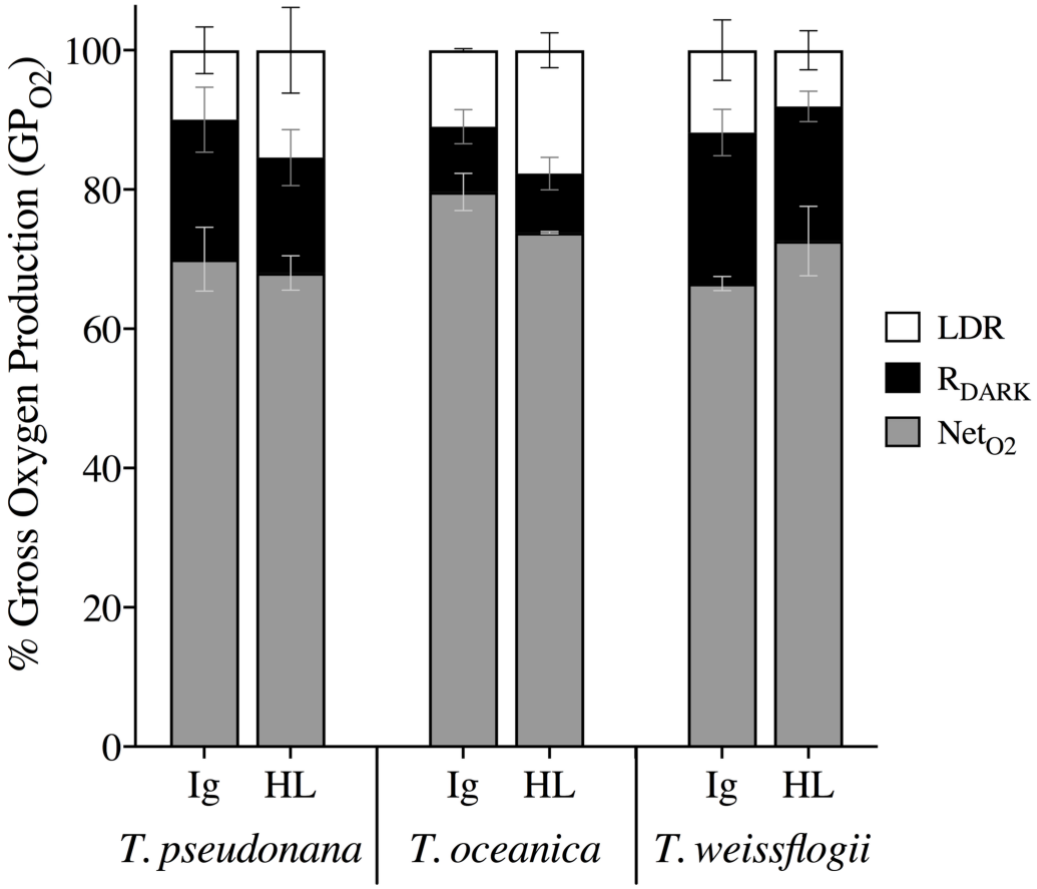

Figure 2.5. Proportions of total photochemical energy (GP_{O2}) allocated to various oxygen pathways over a 20 min incubation under growth irradiance (Ig) and high light (HL). Fractional percentages of GP_{O2} included net oxygen production (Net_{O2}, grey), dark respiration (R_{DARK}, black) and light dependent respiration (LDR, white) in *T. weissflogii*, *T. oceanica*, and *T. pseudonana* under Ig (85 µmol photons m^{-2} s^{-1}) and HL (1200 µmol photons m^{-2} s^{-1}). Data averaged from 2 or 3 independent biological replicates with error bars representing SE of the mean.

2.4.6. Energy excitation fluxes

No variation in %LDR or YNPQ was evident amongst species at Ig; however, %LDR at HL exhibited a negative correlation with YNPQ across the three species (Fig 2.6), where *T.*

oceanica exhibited the highest %LDR despite low capacity for nonphotochemical quenching thus complementing the highest k_{PI} rates observed under HL (Table 2.3). *T. weissflogii* displayed the opposite response with the lowest reliance on LDR and highest YNPQ (Fig 2.6) supporting lowest k_{REC} and k_{PI} rates observed compared to other species (Table 2.3).

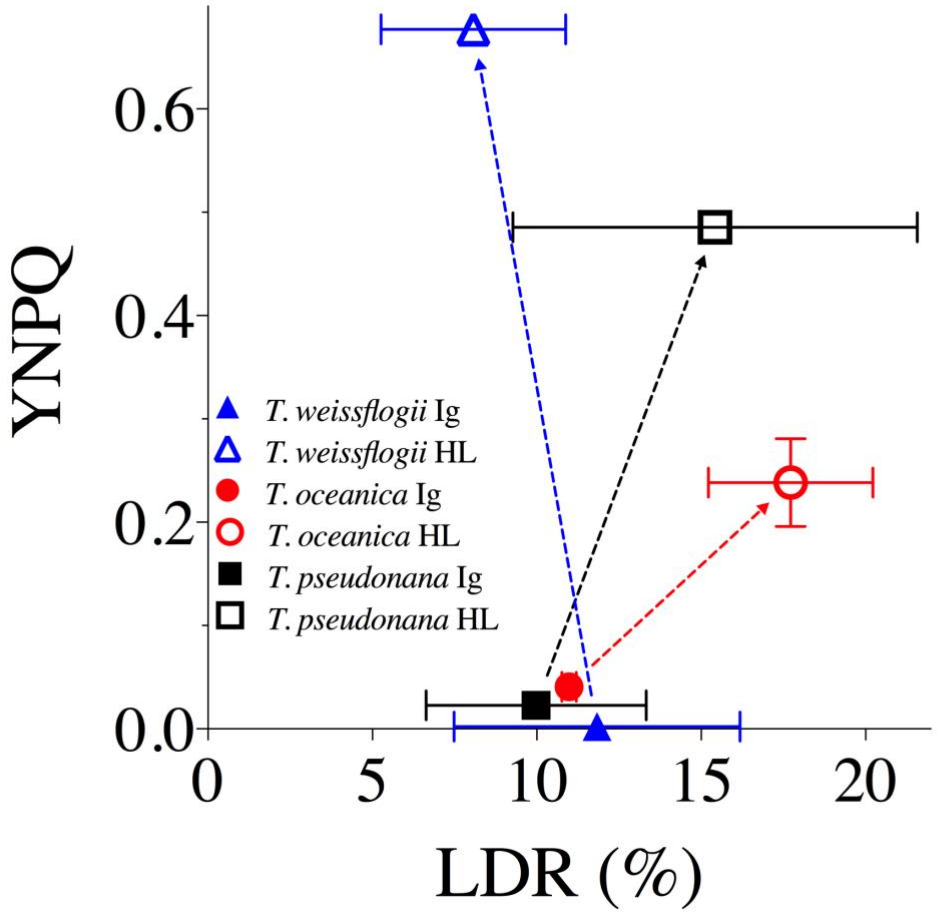

Figure 2.6. The yield of non-photochemical quenching (YNPQ) versus light dependent respiration (LDR) as a % of GP_{O2} for *T. weissflogii* (blue triangles), *T. oceanica* (red circles), and *T. pseudonana* (black squares) under 20 min exposure to growth irradiance (Ig, 85 µmol photons m^{-2} s^{-1}, solid data points) and high light (HL, 1200 µmol photons m^{-2} s^{-1}, open data

points). Data averaged from 2 or 3 independent replicates for LDR and at least 4 independent replicates for YNPQ. Error bars represent SE of the mean.

The collective energy loss yields via YII, YNPQ and YNO (as per Eq 4) revealed clear differences across the species (Fig 2.7). At Ig, the proportion of all absorbed light allocated to photochemical conversion (parameterised as YII, Eq 5) was 0.4 – 0.45; although in *T. pseudonana* YII is significantly higher than in *T. oceanica* (ANOVA for YII across species, $p = 0.022$; Bonferroni post-hoc, $p = 0.03$). Remarkably, for all species under HL only 0.05 of the fluorescence-derived yields for absorbed light energy went to YII (Fig 2.7) (ANOVA, $p = 0.236$), which contradicts (Suggett et al. 2003) showing higher fluxes via pseudo-cyclic electron flow in diatoms. There is a greater proportion of energy flux via YNPQ for *T. weissflogii* (~0.7) under HL while, instead, YNO represents ~0.7 of excitation flux in *T. oceanica*. *T. pseudonana* has balanced YNO and YNPQ at ~0.48 each, once again revealing the divergence of photo-protective strategies employed by these diatoms. Since FRRf-based values of YII appear to, generally, be directly proportional to GP_{O2} in microalgae (e.g. Waring et al. 2010), we further considered the %LDR, $\%R_{DARK}$ and $\%Net_{O2}$ allocations of GP_{O2} to be comparable to YII (Fig 2.7). This demonstrates that a very small fraction of absorbed light ultimately results in 'O_2 recycling' (loss of electrons in the membrane electron transport chain) through %LDR across these diatom species; specifically, 4-6% under Ig and <1% under HL.

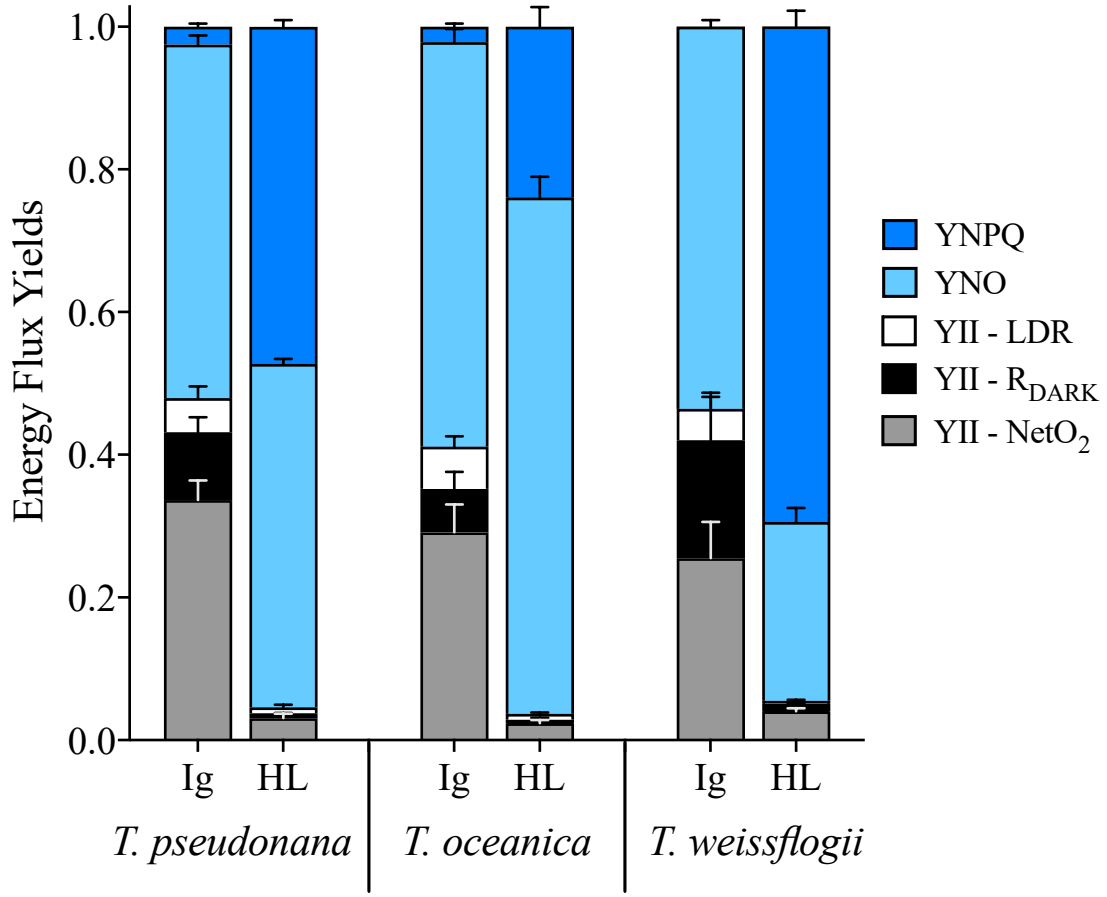

Figure 2.7. Energy flux yields including YNPQ (dark blue), YNO (light blue) and YII, which was then further divided into fractions of LDR (white), R_{DARK} (balck) and Net_{O2} (grey), of *T. pseudonana*, *T. oceanica* and *T. weissflogii* under 85 µmol photons m^{-2} s^{-1} (Ig) and 1200 µmol photons m^{-2} s^{-1} (HL). Data averaged from 3 independent biological replicates and error bars represent SE of the mean.

2.5. Discussion

Diatoms exhibit varying responses to light to thrive across diverse environmental niches (Larkum 2003; Litchman et al. 2004; Edwards et al. 2015; Derks & Bruce 2018; Croteau et al. 2020). Estuarine diatoms (e.g. *T. weissflogii*), exhibit a high capacity to rapidly initiate nonphotochemical quenching whereas oceanic diatoms (e.g. *T. oceanica*) have slower

initiation of nonphotochemical quenching as light intensifies, with coastal diatoms (e.g. *T. pseudonana*), exhibiting an intermediate response (Lavaud et al. 2007; Strzepek & Harrison 2004). Our data confirmed these trends, despite similar rates of NPP across the three diatom representatives when grown under the same conditions of moderate, steady light (Table 2.1). Here, we add to the understanding of adaptive differences in photophysiological trade-offs employed by diatoms shifted to high light through (i) nonphotochemical quenching induction, (ii) reliance on energy consumption downstream of PSII and (iii) utilisation of energetically expensive repair processes to counter damage to the photosynthetic machinery (Fig 2.8). Faster induction of nonphotochemical quenching was accompanied by lower susceptibility to PSII inactivation, while faster relaxation of nonphotochemical quenching corresponded with faster repair, across the three species. The faster nonphotochemical quenching relaxation and PSII repair for *T. pseudonana* was accompanied by greatest change in DPS capacity from Ig to HL. For *T. oceanica*, slower nonphotochemical quenching induction, and greatest susceptibility to PSII inactivation, was in turn accompanied by greater proportion of O_2 evolved from PSII (GP_{O2}) flowing to LDR, and less to R_{DARK}. Thus, under transient high light exposure *T. weissflogii* adopts a strategy of rapid and sustained PSII downregulation, thereby requiring relatively little RCII inactivation/repair, or the need to induce O_2 and electron consuming (LDR) pathways. In contrast, *T. oceanica* appears to not initiate protective mechanisms to alleviate excess excitation pressure on PSII, as evident by relatively little downregulation, inactivation and only moderate repair, but, instead, places greater reliance on LDR to dissipate excess excited energy downstream of PSII. Although these experiments were conducted under nutrient repletion, *T. oceanica* is evolved for low nutrient growth. Limiting reliance upon PSII repair thereby lowers the requirement for mineral nutrient investment into metabolically expensive systems for protein turnover (Campbell et al. 2013; Li et al. 2015). The response for coastal *T. pseudonana* is intermediate, with

moderate downregulation and inactivation of PSII, but high repair of PSII and relaxation of nonphotochemical quenching, and some LDR. These trends show inherent trade-offs in how these different species deploy downregulation and repair of PSII, versus modulating subsequent re-consumption of oxygen and electrons (Fig 2.8).

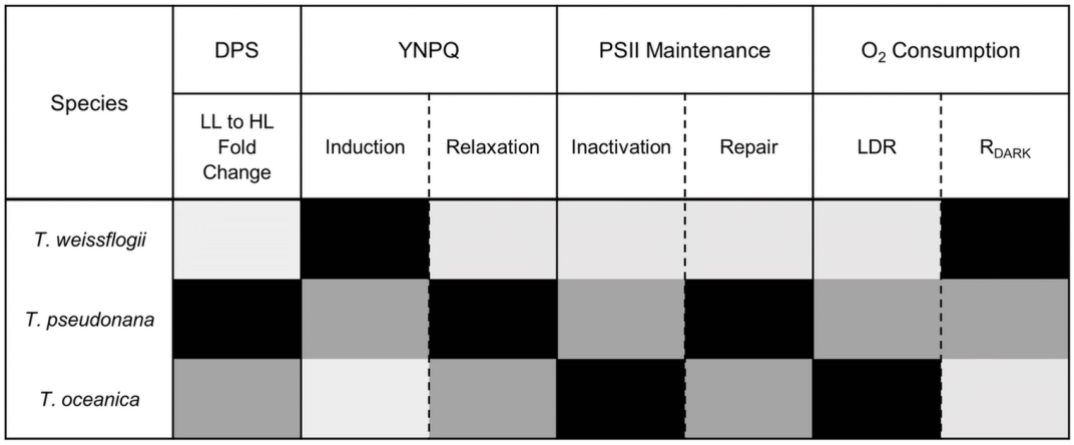

Figure 2.8. Summary of relative reliance (low to high; light grey to black) on various energy dissipation strategies when subject to transient HL including (i) de-epoxidation state (DPS) of xanthophyll cycle pigments, (ii) induction/relaxation of nonphotochemical quenching (parameterised as YNPQ), (iii) inactivation/repair of PSII and (iv) O_2 consuming pathways (LDR/R_{DARK}) for the three *Thalassiosira* diatom species examined here.

In diatoms, activation of nonphotochemical quenching requires both the proton (H^+) gradient across the thylakoid membrane (ΔpH) and xanthophyll cycling (XC), involving the de-epoxidation state (DPS) of diadinoxanthin (Dd, light harvesting pigment) to diatoxanthin (Dt, photo-protective pigment) (Lavaud & Kroth 2006). Dt epoxidation to Dd in *T. pseudonana* was shown to be inhibited at HL due to the presence of a proton gradient, which maintains high concentrations of this photo-protective pigment. Dt epoxidation is also inhibited by complete darkness after HL exposure (Goss et al. 2006). Such inhibition of Dt epoxidation

allows diatoms to re-activate nonphotochemical quenching rapidly if needed, thus avoiding over-reliance on a single photo-protective mechanism (Lavaud & Kroth 2006). Diatoms also benefit from rapid pigment conversion by Dt epoxidase during subsequent transition to low light that is evident through rapid relaxation/reversibility (within 5 min) of a component of nonphotochemical quenching (Goss et al. 2006; Milligan et al. 2012). Such patterns were consistent with those we observed, with all species increasing Dt concentrations under HL (Lacour et al. 2020), however this was not always consistent with a rapidly reversible nonphotochemical quenching. While *T. pseudonana* showed rapidly reversible nonphotochemical quenching, *T. weissflogii* appeared to sustain nonphotochemical quenching upon transition to low light, in parallel with its low capacity for PSII repair (k_{REC}; Table 2.3). Sustained nonphotochemical quenching has been observed to have a linear relationship with Dt whereby at lower acclimated growth irradiances sustained nonphotochemical quenching at the initial dark fluorescence measure was around 5-fold lower than in high-light acclimated *T. gravida* (Lacour et al. 2018). However, recent studies have observed a deviation from this linearity (Croteau et al. 2020), supporting the hypothesis that some portion of Dt is not directly related to nonphotochemical quenching and prevents full relaxation of nonphotochemical quenching (Goss & Lepetit 2015). While our study only obtained Dt concentrations at Ig and a brief (10 min) transient shift to HL, we cannot rule out the effect of Dt on sustained nonphotochemical quenching, and thus fluorescence signals retrieved. However, there was no significant difference in Dt among species at Ig ($p = 0.323$), therefore the trends observed appear robust. Interestingly, *T. oceanica* had slow initiation of nonphotochemical quenching under HL (Fig 2.1A) suggesting that a high content of Dt could be present but disconnected from RCII as was observed by Zhu & Green (2010).

T. oceanica does not rapidly initiate nonphotochemical quenching to dissipate excess incident light energy in the antennae bed and, subsequently, suffers high excitation pressure on the RCIIs that split water and, potentially, higher excitation pressure through the subsequent electron carrier network. Increased 'traffic' of excitation energy was clear from the higher photo-inactivation rates (k_{PI}) for *T. oceanica* compared to the other two species. Previous studies on diatoms have established a link between diatom cell size and susceptibility to photo-inactivation, whereby cell size is inversely proportional to photo-inactivation (Key et al. 2010) and thus larger cells require lower PSII protein turnover (Li et al. 2015). This complements our data of higher PSII repair rates (k_{REC}) for the smaller *T. pseudonana* than the larger *T. weissflogii*. Importantly, cell size may explain some photo-inactivation trends, but protein synthesis and regeneration, that alters in accordance with photosynthetic architecture also needs to be considered (Key et al. 2010; Campbell et al. 2013). It is technically difficult to discriminate between photo-inactivation of PSII and sustained downregulation of PSII, but ecophysiologically (Raven 2011) a sustained suppression of PSII activity imposes opportunity costs on subsequent productivity, whatever the mechanism.

PSII repair comes at a significant cost to the cell where the (re)synthesis of photosynthetic machinery comes at the expense of photosynthetic production (Raven 2011). Chloroplastic protein metabolism for PSII repair saturates at low light and continues during dark periods thus competing with growth for energy generated by photosynthesis (Li et al. 2015; 2016). For *T. oceanica* with the highest k_{PI} (Table 2.3), alternative mechanisms may be employed to obtain additional metabolic energy at the expense of biosynthetic reductant. One source of energy could be PSII-MOX (Behrenfeld et al. 2008; Behrenfeld & Milligan 2013) or PSI-Mehler (Miyake et al. 2012) that consume O_2 and generate a trans-membrane proton gradient to power ATP generation. While specific O_2-consuming pathways were not distinguished in

this study, there was evidence to support a higher reliance on energy sourced from O_2-consuming pathways by *T. oceanica* evidenced by higher LDR as a percentage of GP_{O2} at HL compared to all other species (S2.2 Table, Fig 2.5). The corresponding slower induction of nonphotochemical quenching exhibited by *T. oceanica* confirms previous studies showing a higher dependence on MOX processes. Importantly, such LDR pathways also act to consume excessive oxygen, which in the presence of high excitation pressure increases the chance of reactive oxygen species generation and further PSII – and indeed cellular – damage. Interestingly, *T. weissflogii* exhibited the highest dark respiration (Table 2.3). A recent energetic coupling was found in diatoms between mitochondria and chloroplasts whereby ATP is supplied to the plastid by the mitochondria in the dark via upregulation of mitochondrial alternative oxidase (AOX) (Prihoda et al. 2012; Bailleul et al. 2015; Murik et al. 2019). ATPase in the chloroplast hydrolyses this ATP to ADP which increases H^+ concentration in the lumen that ultimately activates de-epoxidation of Dd to Dt (Goss & Lepetit 2015). Thus, in contrast to *T. oceanica* that is slower to initiate nonphotochemical quenching, our data would suggest *T. weissflogii* relies on "front loading", or priming the photosynthetic apparatus, for rapid HL exposure at any time and in the absence of a light-driven proton motive force by keeping pH and Dt concentrations optimal for photo-protection.

Diatoms exhibit distinct alterations in photosynthetic architecture based on ecological niche, where oceanic diatoms (*T. oceanica*) have been found to have up to 10 PSII:PSI while coastal diatoms generally have 2 PSII:PSI (Strzepek & Harrison 2004). These differences are primarily attributed to iron (Fe) availability, as the requirement for synthesis of PSII, Cyt b_6f, and PSI are 3, 6, and 12 Fe atoms, respectively, but also provide insight into potential evolutionarily conserved species-specific photo-protective strategies amongst diatoms. Fe

availability greatly influences growth rates of diatoms from various habitats whereby *T. pseudonana* and *T. weissflogii* growth rates were lowered by approximately 75% under Fe limitation while *T. oceanica* showed no significant change in growth rate (Maldonado & Price 1996) suggesting an evolutionary predisposition for the Fe-depleted open ocean. Different diatoms are equipped (genetically) to exploit many environments (Armburst 2009; Lommer et al. 2012; Murik et al. 2019). When light is stable and nutrients are limiting, typical of oceanic waters, diatoms appear to focus on upregulating light harvesting to produce more photochemical energy for cellular maintenance as nutrients are the limiting factor for division in these environments (Suggett et al. 2009b). This pattern is consistent with the reliance of *T. oceanica* upon recycling electrons back to O_2 under excess light. This cyclic flux of electrons trades biosynthetic reductant for ATP generation. If inorganic nutrients are limiting, the requirement for ATP for maintenance and nutrient uptake increases relative to the requirement for actual reductive biosynthesis. Conversely, for coastal/estuarine waters, where light is dynamic and nutrients plentiful, diatoms can afford to invest more energy in biosynthesis of macromolecules and division as well as energetically expensive photosynthetic machinery, such as PSI, that are more efficient trapping excitation energy than PSII (Joly & Carpentier 2007). Also, PSI photochemistry incurs a higher Fe requirement compared to ATP generation through MOX pathways (Behrenfeld et al. 2008). The most studied MOX, plastid terminal oxidase (PTOX), was found to be a significant contributor to electron flow in marine *Synechococcus* (Bailey et al. 2008) but absent for several coastal phytoplankton species compared to oceanic species (Mackey et al. 2008; Rusch et al. 2010). Based on our observations, we propose that *T. oceanica* cannot "afford" to synthesise new photosynthetic machinery and instead evolved strategies to allocate harvested light energy towards chemical energy for maintenance and growth while the slowly induced nonphotochemical quenching provides a fail-safe in the event of prolonged light stress.

2.6. Conclusions

In summary, we have built on previous studies demonstrating differences in nonphotochemical quenching amongst diatom species, and strategies in dealing with transient high light exposure (e.g. Lavaud et al. 2007) to elucidate the trade-offs amongst varying energy dissipating strategies from ecologically distinct diatoms. We found that *T. weissflogii* and *T. pseudonana* exhibited capacity to rapidly initiate nonphotochemical quenching at lower light, which corresponded to lower light dependent respiration (LDR) at HL and lower k_{PI}. *T. oceanica*, on the other hand, does not initiate nonphotochemical quenching as a rapid primary response mechanism to dissipate excess light energy and therefore had an accumulation of photochemical energy resulting in higher rates of LDR but also higher k_{PI}. This supports the idea that photo-protective strategies are evolutionarily conserved based on ecological niche for diatoms. These diatoms possess similar core machinery to dissipate excess light energy but have balanced the mechanistic dissipation strategies employed to best suit their respective niche.

2.7. Acknowledgments

Authors would like to thank Tomas Zlamal (Czechglobe Global Change Research Institute CAS, Brno, Czech Republic) for his valuable support setting-up the MIMS. UTS research technical officers, especially Paul Brooks, Scott Allchin, Graeme Poleweski and Sue Fenech, deserve a special acknowledgment for their support and guidance throughout the various experiments.

2.8. References

Allahverdiyeva, Y., Suorsa, M., Tikkanen, M., & Aro, E. M. (2015). Photo-protection of photosystems in fluctuating light intensities. *Journal of Experimental Botany*, *66*(9), 2427–2436. https://doi.org/10.1093/jxb/eru463

Alric, J., & Johnson, X. (2017). Alternative electron transport pathways in photosynthesis: a confluence of regulation. *Current Opinion in Plant Biology*, *37*(i), 78–86. https://doi.org/10.1016/j.pbi.2017.03.014

Ananda, M. M. A., & Weerahandi, S. (1997). Two-Way ANOVA with unequal cell frequencies and unequal variances. *Statistica Sinica*, *7*(3), 631–646.

Anderson, M., Gorley, R., Clarke, K. P. (2008). For PRIMER: guide to software and statistical methods. PRIMER-E. Plymouth, UK.

Armbrust, E. V. (2009). The life of diatoms in the world's oceans. *Nature*, *459*(7244), 185–192. https://doi.org/10.1038/nature08057

Asada, K. (1999). The water-water cylce in chloroplasts: scavenging of active oxygens and dissipation of excess photons. *Annual Review of Plant Physiology and Plant Molecular Biology*, *50*(1), 601–639. https://doi.org/10.1146/annurev.arplant.50.1.601

Bailey, S., Melis, A., Mackey, K. R. M., Cardol, P., Finazzi, G., van Dijken, G., … Grossman, A. (2008). Alternative photosynthetic electron flow to oxygen in marine Synechococcus. *Biochimica et Biophysica Acta - Bioenergetics*, *1777*(3), 269–276. https://doi.org/10.1016/j.bbabio.2008.01.002

Bailleul, B., Berne, N., Murik, O., Petroutsos, D., Prihoda, J., Tanaka, A., … Finazzi, G. (2015). Energetic coupling between plastids and mitochondria drives CO 2 assimilation in diatoms. *Nature*, *524*(7565), 366–369. https://doi.org/10.1038/nature14599

Barnett, A., Méléder, V., Blommaert, L., Lepetit, B., Gaudin, P., Vyverman, W., … Lavaud, J. (2015). Growth form defines physiological photo-protective capacity in intertidal benthic diatoms. *ISME Journal*, *9*(1), 32–45. https://doi.org/10.1038/ismej.2014.105

Behrenfeld, M. J., & Milligan, A. J. (2013). Photophysiological Expressions of Iron Stress in Phytoplankton. *Annual Review of Marine Science*, *5*, 217–246. https://doi.org/10.1146/annurev-marine-121211-172356

Behrenfeld, M. J., Boss, E., Siegel, D. A., & Shea, D. M. (2005). Carbon-based ocean productivity and phytoplankton physiology from space. *Global Biogeochemical Cycles*, *19*(1), 1–14. https://doi.org/10.1029/2004GB002299

Behrenfeld, M. J., Halsey, K. H., & Milligan, A. J. (2008). Evolved physiological responses of phytoplankton to their integrated growth environment. *Philosophical Transactions of the Royal Society B: Biological Sciences*, *363*(1504), 2687–2703. https://doi.org/10.1098/rstb.2008.0019

Bilger, W., & Björkman, O. (1990). Role of the xanthophyll cycle in photo-protection elucidated by measurements of light-induced absorbance changes, fluorescence and photosynthesis in leaves of Hedera canariensis. *Photosynthesis Research*, *25*(3), 173–185. https://doi.org/10.1007/BF00033159

Blommaert, L., Huysman, M. J. J., Vyverman, W., Lavaud, J., & Sabbe, K. (2017). Contrasting NPQ dynamics and xanthophyll cycling in a motile and a non-motile intertidal benthic diatom. *Limnology and Oceanography*, *62*(4), 1466–1479. https://doi.org/10.1002/lno.10511

Brading, P., Warner, M. E., Davey, P., Smith, D. J., Achterberg, E. P., & Suggett, D. J. (2011). Differential effects of ocean acidification on growth and photosynthesis among phylotypes of Symbiodinium (Dinophyceae). *Limnology and Oceanography*, *56*(3), 927–938. https://doi.org/10.4319/lo.2011.56.3.0927

Bucciarelli, E., Ridame, C., Sunda, W. G., Dimier-Hugueney, C., Cheize, M., & Belviso, S. (2013). Increased intracellular concentrations of DMSP and DMSO in iron-limited oceanic phytoplankton Thalassiosira oceanica and Trichodesmium erythraeum. *Limnology and Oceanography*, *58*(5), 1667–1679. https://doi.org/10.4319/lo.2013.58.5.1667

Buck, J. M., Sherman, J., Bártulos, C. R., Serif, M., Halder, M., Henkel, J., … Lepetit, B. (2019). Lhcx proteins provide photo-protection via thermal dissipation of absorbed light in the diatom Phaeodactylum tricornutum. *Nature Communications*, *10*(4167). https://doi.org/10.1038/s41467-019-12043-6

Campbell, D. A., Hossain, Z., Cockshutt, A. M., Zhaxybayeva, O., Wu, H., & Li, G. (2013). Photosystem II protein clearance and FtsH function in the diatom Thalassiosira pseudonana. *Photosynthesis Research*, *115*(1), 43–54. https://doi.org/10.1007/s11120-013-9809-2

Campbell, D. A., & Tyystjärvi, E. (2012). Parameterization of photosystem II photo-inactivation and repair. *Biochimica et Biophysica Acta - Bioenergetics*, *1817*(1), 258–265. https://doi.org/10.1016/j.bbabio.2011.04.010

Campbell, D. A., Serôdio, J. (2020) Photoinhibition of Photosystem II in Phytoplankton: Processes and Patterns. In: Larkum A., Grossmann A., Raven J. (eds) Photosynthesis in Algae: Biochemical and Physiological Mechanisms. *Advances in Photosynthesis and Respiration (Including Bioenergy and Related Processes)*. vol 45. Springer, Cham. https://doi.org/10.1007/978-3-030-33397-3_13

Cardol, P., Forti, G., & Finazzi, G. (2011). Regulation of electron transport in microalgae. *Biochimica et Biophysica Acta - Bioenergetics*, *1807*(8), 912–918. https://doi.org/10.1016/j.bbabio.2010.12.004

Claquin, P., Kromkamp, J. C., & Martin-Jezequel, V. (2004). Relationship between photosynthetic metabolism and cell cycle in a synchronized culture of the marine alga Cylindrotheca fusiformis (Bacillariophyceae). *European Journal of Phycology*, *39*(1), 33–41. https://doi.org/10.1080/0967026032000157165

Croteau, D., Guérin, S., Bruyant, F., Ferland, J., Campbell, D. A., Babin, M., & Lavaud, J. (2020). Contrasting nonphotochemical quenching patterns under high light and darkness aligns with light niche occupancy in Arctic diatoms. *Limnology and Oceanography*, 1–15. https://doi.org/10.1002/lno.11587

Derks, A. K., & Bruce, D. (2018). Rapid regulation of excitation energy in two pennate diatoms from contrasting light climates. *Photosynthesis Research*, *138*(2), 149–165. https://doi.org/10.1007/s11120-018-0558-0

Dimier, C., Corato, F., Tramontano, F., & Brunet, C. (2007). Photo-protection and xanthophyll-cycle activity in three marine diatoms. *Journal of Phycology*, *43*(5), 937–947. https://doi.org/10.1111/j.1529-8817.2007.00381.x

Dong, H. P., Dong, Y. L., Cui, L., Balamurugan, S., Gao, J., Lu, S. H., & Jiang, T. (2016). High light stress triggers distinct proteomic responses in the marine diatom Thalassiosira pseudonana. *BMC Genomics*, *17*(1), 1–14. https://doi.org/10.1186/s12864-016-3335-5

Du, N., Gholami, P., Kline, D. I., DuPont, C. L., Dickson, A. G., Mendola, D., … Greg Mitchell, B. (2018). Simultaneous quantum yield measurements of carbon uptake and oxygen evolution in microalgal cultures. *PLoS ONE*, *13*(6), 1–21. https://doi.org/10.1371/journal.pone.0199125

Edwards, K. F., Thomas, M. K., Klausmeier, C. A., & Litchman, E. (2015). Light and growth in marine phytoplankton: Allometric, taxonomic, and environmental variation. *Limnology and Oceanography*, *60*(2), 540–552. https://doi.org/10.1002/lno.10033

Elzhov, T. V., Mullen, K. M., Spiess, A. N., Bolker, B. minpack. lm: R interface to the Levenberg-Marquardt nonlinear least-squares algorithm found in MINPACK, plus support for bounds. R package version 1.2-1. https://CRAN.R-project.org/package=minpack.lm

Ferrón, S., del Valle, D. A., Bjöorkman, K. M., Quay, P. D., Church, M. J., & Karl, D. M. (2016). Application of membrane inlet mass spectrometry to measure aquatic gross primary production by the18O in vitro method. *Limnology and Oceanography: Methods*, *14*(9), 610–622. https://doi.org/10.1002/lom3.10116

Field, C. B., Behrenfeld, M. J., Randerson, J. T., & Falkowski, P. (1998). Primary production of the biosphere: Integrating terrestrial and oceanic components. *Science*, *281*(5374), 237–240. https://doi.org/10.1126/science.281.5374.237

Fisher, N. L., & Halsey, K. H. (2016). Mechanisms that increase the growth efficiency of diatoms in low light. *Photosynthesis Research*, *129*(2), 183–197. https://doi.org/10.1007/s11120-016-0282-6

Gao, G., Shi, Q., Xu, Z., Xu, J., Campbell, D. A., & Wu, H. (2018). Global warming interacts with ocean acidification to alter PSII function and protection in the diatom Thalassiosira weissflogii. *Environmental and Experimental Botany*, *147*(October 2017), 95–103. https://doi.org/10.1016/j.envexpbot.2017.11.014

Genty B., Harbinson, J. (2006). Regulation of Light Utilization for Photosynthetic Electron Transport. *Photosynth Environ*. 67–99. https://10.1007/0-306-48135-9_3

Giordano, M., Norici, A., & Hell, R. (2005). Sulfur and phytoplankton: Acquisition, metabolism and impact on the environment. *New Phytologist*, *166*(2), 371–382. https://doi.org/10.1111/j.1469-8137.2005.01335.x

Giovagnetti, V., & Ruban, A. V. (2017). Detachment of the fucoxanthin chlorophyll a/c binding protein (FCP) antenna is not involved in the acclimative regulation of photo-protection in the pennate diatom Phaeodactylum tricornutum. *Biochimica et Biophysica Acta - Bioenergetics*, *1858*(3), 218–230. https://doi.org/10.1016/j.bbabio.2016.12.005

Goss, R., Ann Pinto, E., Wilhelm, C., & Richter, M. (2006). The importance of a highly active and ΔpH-regulated diatoxanthin epoxidase for the regulation of the PS II antenna function in diadinoxanthin cycle containing algae. *Journal of Plant Physiology*, *163*(10), 1008–1021. https://doi.org/10.1016/j.jplph.2005.09.008

Goss, R., & Jakob, T. (2010). Regulation and function of xanthophyll cycle-dependent photo-protection in algae. *Photosynthesis Research*, *106*(1–2), 103–122. https://doi.org/10.1007/s11120-010-9536-x

Goss, R., & Lepetit, B. (2015). Biodiversity of NPQ. *Journal of Plant Physiology*, *172*, 13–32. https://doi.org/10.1016/j.jplph.2014.03.004

Grouneva, I., Jakob, T., Wilhelm, C., & Goss, R. (2009). The regulation of xanthophyll cycle activity and of non-photochemical fluorescence quenching by two alternative electron flows in the diatoms Phaeodactylum tricornutum and Cyclotella meneghiniana. *Biochimica et Biophysica Acta - Bioenergetics*, *1787*(7), 929–938. https://doi.org/10.1016/j.bbabio.2009.02.004

Grouneva, I., Jakob, T., Wilhelm, C., & Goss, R. (2006). Influence of ascorbate and pH on the activity of the diatom xanthophyll cycle-enzyme diadinoxanthin de-epoxidase. *Physiologia Plantarum*, *126*(2), 205–211. https://doi.org/10.1111/j.1399-3054.2006.00613.x

Guillard, R. L. (1975). Culture of phytoplankton for feeding marine invertebrates. In *Culture of Marine Invertebrate Animals* (pp. 29–60).

Halsey, K. H., Milligan, A. J., & Behrenfeld, M. J. (2010). Physiological optimization underlies growth rate-independent chlorophyll-specific gross and net primary production. *Photosynthesis Research*, *103*(2), 125–137. https://doi.org/10.1007/s11120-009-9526-z

Halsey, K. H., O'Malley, R. T., Graff, J. R., Milligan, A. J., & Behrenfeld, M. J. (2013). A common partitioning strategy for photosynthetic products in evolutionarily distinct phytoplankton species. *New Phytologist*, *198*(4), 1030–1038. https://doi.org/10.1111/nph.12209

Heukelem, L., & Thomas, C. S. (2001). Computer-assisted high-performance liquid chromatography method development with applications to the isolation and analysis of

phytoplankton pigments. *J. Chromat. A*, *910*(1), 31–49. https://doi.org/10.1016/S0378-4347(00)00603-4

Holt, N. E., Fleming, G. R., & Niyogi, K. K. (2004). Toward an understanding of the mechanism of nonphotochemical quenching in green plants. *Biochemistry*, *43*(26), 8281–8289. https://doi.org/10.1021/bi0494020

Horton, P., & Ruban, A. V. (1992). Regulation of Photosystem II. *Photosynthesis Research*, *34*(3), 375–385. https://doi.org/10.1007/BF00029812

Hughes, D. J., Campbell, D. A., Doblin, M. A., Kromkamp, J. C., Lawrenz, E., Moore, C. M., … Suggett, D. J. (2018). Roadmaps and Detours: Active Chlorophyll- a Assessments of Primary Productivity Across Marine and Freshwater Systems. *Environmental Science and Technology*, *52*(21), 12039–12054. https://doi.org/10.1021/acs.est.8b03488

Hughes, D. J., Varkey, D., Doblin, M. A., Ingleton, T., Mcinnes, A., Ralph, P. J., … Suggett, D. J. (2018). Impact of nitrogen availability upon the electron requirement for carbon fixation in Australian coastal phytoplankton communities. *Limnology and Oceanography*, *63*(5), 1891–1910. https://doi.org/10.1002/lno.10814

Joly, D., & Carpentier, R. (2007). Regulation of energy dissipation in photosystem I by the redox state of the plastoquinone pool. *Biochemistry*, *46*(18), 5534–5541. https://doi.org/10.1021/bi602627d

Kana, T. M., Darkangelo, C., Hunt, M. D., Oldham, J. B., Bennett, G. E., & Cornwell, J. C. (1994). Membrane lnlet Mass Spectrometer for Rapid Environmental Water Samples. *Response*, *66*(23), 4166–4170. Retrieved from http://pubs.acs.org/doi/abs/10.1021/ac00095a009

Key, T., McCarthy, A., Campbell, D. A., Six, C., Roy, S., & Finkel, Z. V. (2010). Cell size trade-offs govern light exploitation strategies in marine phytoplankton. *Environmental Microbiology*, *12*(1), 95–104. https://doi.org/10.1111/j.1462-2920.2009.02046.x

Klughammer, C., & Schreiber, U. (2008). Complementary PS II quantum yields calculated from simple fluorescence parameters measured by PAM fluorometry and the Saturation Pulse method. *PAM Application Notes*, *1*(1), 27–35. https://doi.org/citeulike-article-id:6352156

Kok, B. (1956). On the inhibition of photosynthesis by intense light. *Biochim. Biophys. Acta*. 21, 234–244. https://doi.org/10.2514/3.29809

Kolber, Z. S., Prasil, O., & Falkowski, P. G. (1998). Measurements of variable chlorophyll fluorescence using fast repetition rate techniques: defining methodology and experimental protocols. *Biochimica et Biophysica Acta - Bioenergetics*, *1367*, 88–106. Retrieved from papers2://publication/uuid/C591C675-7666-49B5-AB3C-16E2C3FCFD57

Kramer, D. M., Avenson, T. J., & Edwards, G. E. (2004). Dynamic flexibility in the light reactions of photosynthesis governed by both electron and proton transfer reactions. *Trends in Plant Science*, *9*(7), 349–357. https://doi.org/10.1016/j.tplants.2004.05.001

Kromkamp, J.C., & Peene, J. (2001) Oxygen consumption in the light by unicellular algae. *Science Access.* 3(1).

Kuzminov, F. I., & Gorbunov, M. Y. (2016). Energy dissipation pathways in Photosystem 2 of the diatom, Phaeodactylum tricornutum, under high-light conditions. *Photosynthesis Research*, *127*(2), 219–235. https://doi.org/10.1007/s11120-015-0180-3

Lacour, T., Babin, M., & Lavaud, J. (2020). Diversity in Xanthophyll Cycle Pigments Content and Related Nonphotochemical Quenching (NPQ) Among Microalgae: Implications for Growth Strategy and Ecology. *Journal of Phycology*, *56*(2), 245–263. https://doi.org/10.1111/jpy.12944

Lacour, T., Larivière, J., Ferland, J., Bruyant, F., Lavaud, J., & Babin, M. (2018). The role of sustained photo-protective non-photochemical quenching in low temperature and high light acclimation in the bloom-forming arctic diatom Thalassiosira gravida. *Frontiers in Marine Science*, *5*(OCT). https://doi.org/10.3389/fmars.2018.00354

Larkum, A. W. D. (2003). *Light-Harvesting Systems in Algae*. https://doi.org/10.1007/978-94-007-1038-2_13

Lavaud, J., Van Gorkom, H. J., & Etienne, A. L. (2002a). Photosystem II electron transfer cycle and chlororespiration in planktonic diatoms. *Photosynthesis Research*, *74*(1), 51–59. https://doi.org/10.1023/A:1020890625141

Lavaud, J., Rousseau, B., Van Gorkom, H. J., & Etienne, A. L. (2002b). Influence of the diadinoxanthin pool size on photo-protection in the marine planktonic diatom Phaeodactylum tricornutum. *Plant Physiology*, *129*(3), 1398–1406. https://doi.org/10.1104/pp.002014

Lavaud, J., Rousseau, B., & Etienne, A. L. (2004). General features of photo-protection by energy dissipation in planktonic diatoms (Bacillariophyceae). *Journal of Phycology*, *40*(1), 130–137. https://doi.org/10.1046/j.1529-8817.2004.03026.x

Lavaud, J., & Kroth, P. G. (2006). In diatoms, the transthylakoid proton gradient regulates the photoprotective non-photochemical fluorescence quenching beyond its control on the xanthophyll cycle. *Plant and Cell Physiology*, *47*(7), 1010–1016. https://doi.org/10.1093/pcp/pcj058

Lavaud, J., Strzepek, R. F., & Kroth, P. G. (2007). Photo-protection capacity differs among diatoms: possible consequences on the spatial distribution of diatoms related to fluctuations in the underwater light Climate. *Limnology and Oceanography*, *52*(3), 1188–1194. https://doi.org/10.2307/4499689

Lavaud, J., & Lepetit, B. (2013). An explanation for the inter-species variability of the photo-protective non-photochemical chlorophyll fluorescence quenching in diatoms. *Biochimica et Biophysica Acta - Bioenergetics*, *1827*(3), 294–302. https://doi.org/10.1016/j.bbabio.2012.11.012

Lavaud, J., & Goss, R. (2014). *The Peculiar Features of Non-Photochemical Fluorescence Quenching in Diatoms and Brown Algae*. https://doi.org/10.1007/978-94-017-9032-1_20

Lavaud, J., Six, C., & Campbell, D. A. (2016). Photosystem II repair in marine diatoms with contrasting photophysiologies. *Photosynthesis Research*, *127*(2), 189–199. https://doi.org/10.1007/s11120-015-0172-3

Laws, E. A., & Bannister, T. T. (2004). Erratum: Nutrient- and light-limited growth of Thalassiosira fluviatilis in continuous culture with implications for phytoplankton growth in the ocean (Limnology and Oceanography (1980) 25 (457-473)). *Limnology and Oceanography*, *49*(6), 2316. https://doi.org/10.4319/lo.2004.49.6.2316

Lepetit, B., Gélin, G., Lepetit, M., Sturm, S., Vugrinec, S., Rogato, A., … Lavaud, J. (2017). The diatom Phaeodactylum tricornutum adjusts nonphotochemical fluorescence quenching capacity in response to dynamic light via fine-tuned Lhcx and xanthophyll cycle pigment synthesis. *New Phytologist*, *214*(1), 205–218. https://doi.org/10.1111/nph.14337

Lepetit, B., Goss, R., Jakob, T., & Wilhelm, C. (2012). Molecular dynamics of the diatom thylakoid membrane under different light conditions. *Photosynthesis Research*, *111*(1–2), 245–257. https://doi.org/10.1007/s11120-011-9633-5

Lepetit, B., Sturm, S., Rogato, A., Gruber, A., Sachse, M., Falciatore, A., … Lavaud, J. (2013). High light acclimation in the secondary plastids containing diatom phaeodactylum tricornutum is triggered by the redox state of the plastoquinone pool. *Plant Physiology*, *161*(2), 853–865. https://doi.org/10.1104/pp.112.207811

Lepetit, B., Volke, D., Gilbert, M., Wilhelm, C., & Goss, R. (2010). Evidence for the existence of one antenna-associated, lipid-dissolved and two protein-bound pools of diadinoxanthin cycle pigments in diatoms. *Plant Physiology*, *154*(4), 1905–1920. https://doi.org/10.1104/pp.110.166454

Li, G., Brown, C. M., Jeans, J. A., Donaher, N. A., Mccarthy, A., & Campbell, D. A. (2015). The nitrogen costs of photosynthesis in a diatom under current and future pCO2. *New Phytologist*, *205*(2), 533–543. https://doi.org/10.1111/nph.13037

Li, G., Woroch, A. D., Donaher, N. A., Cockshutt, A. M., & Campbell, D. A. (2016). A Hard Day's Night: Diatoms Continue Recycling Photosystem II in the Dark. *Frontiers in Marine Science*, *3*(November), 1–10. https://doi.org/10.3389/fmars.2016.00218

Liefer, J. D., Garg, A., Campbell, D. A., Irwin, A. J., & Finkel, Z. V. (2018). Nitrogen starvation induces distinct photosynthetic responses and recovery dynamics in diatoms and prasinophytes. *PLoS ONE*, *13*(4), 1–25. https://doi.org/10.1371/journal.pone.0195705

Litchman, E., Klausmeier, C. A., & Bossard, P. (2004). Phytoplankton nutrient competition under dynamic light regimes. *Limnology and Oceanography*, *49*(4part2), 1457–1462. https://doi.org/10.4319/lo.2004.49.4_part_2.1457

Lohr, M., & Wilhelm, C. (1999). Algae displaying the diadinoxanthin cycle also possess the violaxanthin cycle. *Proceedings of the National Academy of Sciences of the United States of America*, *96*(15), 8784–8789. https://doi.org/10.1073/pnas.96.15.8784

Lomas, M. W. (2004). Nitrate reductase and urease enzyme activity in the marine diatom Thalassiosira weissflogii (Bacillariophyceae): Interactions among nitrogen substrates. *Marine Biology*, *144*(1), 37–44. https://doi.org/10.1007/s00227-003-1181-x

Lommer, M., Specht, M., Roy, A. S., Kraemer, L., Andreson, R., Gutowska, M. A., … LaRoche, J. (2012). Genome and low-iron response of an oceanic diatom adapted to chronic iron limitation. *Genome Biology*, *13*(7), R66. https://doi.org/10.1186/gb-2012-13-7-r66

Mackey, K. R. M., Paytan, A., Grossman, A. R., & Bailey, S. (2008). A photosynthetic strategy for coping in a high-light, low-nutrient environment. *Limnology and Oceanography*, *53*(3), 900–913. https://doi.org/10.4319/lo.2008.53.3.0900

Maldonado, M. T., & Price, N. M. (1996). Influence of N substrate on Fe requirements of marine centric diatoms. *Marine Ecology Progress Series*, *141*(1–3), 161–172. https://doi.org/10.3354/meps141161

Malviya, S., Scalco, E., Audic, S., Vincent, F., Veluchamy, A., Poulain, J., … Bowler, C. (2016). Insights into global diatom distribution and diversity in the world's ocean. *Proceedings of the National Academy of Sciences of the United States of America*, *113*(11), E1516–E1525. https://doi.org/10.1073/pnas.1509523113

Mckew, B. A., Davey, P., Finch, S. J., Hopkins, J., Lefebvre, S. C., Metodiev, M. V., … Geider, R. J. (2013). The trade-off between the light-harvesting and photo-protective functions of fucoxanthin-chlorophyll proteins dominates light acclimation in Emiliania huxleyi (clone CCMP 1516). *New Phytologist*, *200*(1), 74–85. https://doi.org/10.1111/nph.12373

Milligan, A. J., Aparicio, U. A., & Behrenfeld, M. J. (2012). Fluorescence and nonphotochemical quenching responses to simulated vertical mixing in the marine diatom Thalassiosira weissflogii. *Marine Ecology Progress Series*, *448*, 67–78. https://doi.org/10.3354/meps09544

Miloslavina, Y., Grouneva, I., Lambrev, P. H., Lepetit, B., Goss, R., Wilhelm, C., & Holzwarth, A. R. (2009). Ultrafast fluorescence study on the location and mechanism of non-photochemical quenching in diatoms. *Biochimica et Biophysica Acta - Bioenergetics*, *1787*(10), 1189–1197. https://doi.org/10.1016/j.bbabio.2009.05.012

Miyake, C., Suzuki, Y., Yamamoto, H., Amako, K., & Makino, A. (2012). O2-enhanced induction of photosynthesis in rice leaves: the Mehler-ascorbate peroxidase (MAP) pathway drives cyclic electron flow within PSII and cyclic electron flow around PSI. *Soil Science and Plant Nutrition*, *58*(6), 718–727. https://doi.org/10.1080/00380768.2012.736078

Murik, O., Tirichine, L., Prihoda, J., Thomas, Y., Araújo, W. L., Allen, A. E., … Bowler, C. (2019). Downregulation of mitochondrial alternative oxidase affects chloroplast function, redox status and stress response in a marine diatom. *New Phytologist*, *221*(3), 1303–1316. https://doi.org/10.1111/nph.15479

Nawrocki, W. J., Tourasse, N. J., Taly, A., Rappaport, F., & Wollman, F.-A. (2015). The Plastid Terminal Oxidase: Its Elusive Function Points to Multiple Contributions to Plastid Physiology. *Annual Review of Plant Biology*, *66*(1), 49–74. https://doi.org/10.1146/annurev-arplant-043014-114744

Oliver, R. L., Whittington, J., Lorenz, Z., & Webster, I. T. (2013). Erratum: The influence of vertical mixing on the photoinhibition of variable chlorophyll-a fluorescence and its inclusion in a model of phytoplankton photosynthesis (Journal of Plankton Research 25 (1107-1129) DOI: 10.1093/plankt/25.9.1107). *Journal of Plankton Research*, *35*(4), 927. https://doi.org/10.1093/plankt/fbt043

Onno Feikema, W., Marosvölgyi, M. A., Lavaud, J., & van Gorkom, H. J. (2006). Cyclic electron transfer in photosystem II in the marine diatom Phaeodactylum tricornutum. *Biochimica et Biophysica Acta - Bioenergetics*, *1757*(7), 829–834. https://doi.org/10.1016/j.bbabio.2006.06.003

Oxborough, K., & Baker, N. R. (1997). Resolving chlorophyll a fluorescence images of photosynthetic efficiency into photochemical and non-photochemical components - Calculation of qP and Fv'/Fm' without measuring Fo'. *Photosynthesis Research*, *54*(2), 135–142. https://doi.org/10.1023/A:1005936823310

Perkins, R., Williamson, C., Lavaud, J., Mouget, J. L., & Campbell, D. A. (2018). Time-dependent upregulation of electron transport with concomitant induction of regulated excitation dissipation in Haslea diatoms. *Photosynthesis Research*, *137*(3), 377–388. https://doi.org/10.1007/s11120-018-0508-x

Prihoda, J., Tanaka, A., De Paula, W. B. M., Allen, J. F., Tirichine, L., & Bowler, C. (2012). Chloroplast-mitochondria cross-talk in diatoms. *Journal of Experimental Botany*, *63*(4), 1543–1557. https://doi.org/10.1093/jxb/err441

R Core Team. R: A language and environment for statistical computing. R Foundation for Statistical Computing, Vienna, Austria. https://www.R-project.org/

Raven, J. A., Kübler, J. E., & Beardall, J. (2000). Put out the light, and then put out the light. *Journal of the Marine Biological Association of the United Kingdom*, *80*(1), 1–25. https://doi.org/10.1017/S0025315499001526

Raven, J. A. (2011). The cost of photoinhibition. *Physiologia Plantarum*, *142*(1), 87–104. https://doi.org/10.1111/j.1399-3054.2011.01465.x

Ritchie, R. J. (2006). Consistent sets of spectrophotometric chlorophyll equations for acetone, methanol and ethanol solvents. *Photosynthesis Research*, *89*(1), 27–41. https://doi.org/10.1007/s11120-006-9065-9

RStudio Team. RStudio: Integrated Development for R. RStudio. PBC. Boston, MA. http://www.rstudio.com/

Rusch, D. B., Martiny, A. C., Dupont, C. L., Halpern, A. L., & Venter, J. C. (2010). Characterization of Prochlorococcus clades from iron-depleted oceanic regions.

Proceedings of the National Academy of Sciences of the United States of America, *107*(37), 16184–16189. https://doi.org/10.1073/pnas.1009513107

Sarthou, G., Timmermans, K. R., Blain, S., & Tréguer, P. (2005). Growth physiology and fate of diatoms in the ocean: A review. *Journal of Sea Research*, *53*(1-2 SPEC. ISS.), 25–42. https://doi.org/10.1016/j.seares.2004.01.007

Serôdio, J., Cruz, S., Vieira, S., & Brotas, V. (2005). Non-photochemical quenching of chlorophyll fluorescence and operation of the xanthophyll cycle in estuarine microphytobenthos. *Journal of Experimental Marine Biology and Ecology*, *326*(2), 157–169. https://doi.org/10.1016/j.jembe.2005.05.011

Stransky, H., & Hager, A. (1970). The carotenoid pattern and the occurrence of the light-induced xanthophyll cycle in various classes of algae. IV. Cyanophyceae and Rhodophyceae. *Arch Mikrobiol*. 72(1), 84-96.

Strzepek, R. F., & Harrison, P. J. (2004). Photosynthetic architecture differs in coastal and oceanic diatoms. *Nature*, *431*(7009), 689. https://doi.org/10.1038/nature02954

Suggett, D. J., Goyen, S., Pettay, D. T., Szabó, M., Warner, M. E., Evenhuis, C., & Ralph, P. J. (2015). Functional diversity of photobiological traits within the genus Symbiodinium appears to be governed by the interaction of cell size with cladal designation. *New Phytologist*, *208*(2), 370–381. https://doi.org/10.1111/nph.13483

Suggett, D. J., MacIntyre, H. L., Kana, T. M., & Geider, R. J. (2009a). Comparing electron transport with gas exchange: Parameterising exchange rates between alternative photosynthetic currencies for eukaryotic phytoplankton. *Aquatic Microbial Ecology*, *56*(2–3), 147–162. https://doi.org/10.3354/ame01303

Suggett, D. J., Moore, C. M., Hickman, A. E., & Geider, R. J. (2009b). Interpretation of fast repetition rate (FRR) fluorescence: Signatures of phytoplankton community structure versus physiological state. *Marine Ecology Progress Series*, *376*, 1–19. https://doi.org/10.3354/meps07830

Suggett, D. J., Oxborough, K., Baker, N. R., Macintyre, H. L., Kana, T. M., & Geider, R. J. (2003). Fast repetition rate and pulse amplitude modulation chlorophyll a fluorescence measurements for assessment of photosynthetic electron transport in marine phytoplankton. *European Journal of Phycology*, *38*(4), 371–384. https://doi.org/10.1080/09670260310001612655

Sun, J., & Liu, D. (2003). Geometric models for calculating cell biovolume and surface area for phytoplankton. *Journal of Plankton Research*, *25*(11), 1331–1346. https://doi.org/10.1093/plankt/fbg096

Taddei, L., Chukhutsina, V. U., Lepetit, B., Stella, G. R., Bassi, R., van Amerongen, H., … Falciatore, A. (2018). Dynamic Changes between Two LHCX-Related Energy Quenching Sites Control Diatom Photoacclimation. *Plant Physiology*, *177*(3), 953–965. https://doi.org/10.1104/pp.18.00448

Tréguer, P., Nelson, D. M., Van Bennekom, A. J., Demaster, D. J., Leynaert, A., & Quéguiner, B. (1995). The silica balance in the world ocean: A reestimate. *Science*, *268*(5209), 375–379. https://doi.org/10.1126/science.268.5209.375

Van Heukelem, L., & Thomas, C. S. (2001). Computer-assisted high-performance liquid chromatography method development with applications to the isolation and analysis of phytoplankton pigments. *Journal of Chromatography A*, *910*(1), 31–49. https://doi.org/10.1016/S0378-4347(00)00603-4

Wagner, H., Jakob, T., Lavaud, J., & Wilhelm, C. (2016). Photosystem II cycle activity and alternative electron transport in the diatom Phaeodactylum tricornutum under dynamic light conditions and nitrogen limitation. *Photosynthesis Research*, *128*(2), 151–161. https://doi.org/10.1007/s11120-015-0209-7

Walter, B., Peters, J., van Beusekom, J. E. E., & St. John, M. A. (2015). Interactive effects of temperature and light during deep convection: a case study on growth and condition of the diatom Thalassiosira weissflogii. *ICES Journal of Marine Science*, *72*(6), 2061–2071. https://doi.org/10.1093/icesjms/fsu218

Waring, J., Klenell, M., Bechtold, U., Underwood, G. J. C., & Baker, N. R. (2010). Light-induced responses of oxygen photoreduction, reactive oxygen species production and scavenging in two diatom species. *Journal of Phycology*, *46*(6), 1206–1217. https://doi.org/10.1111/j.1529-8817.2010.00919.x

Weger, H. G., & Turpin, D. H. (1989). Mitochondrial respiration can support NO3− and NO2− reduction during photosynthesis. *Plant Physiology*, *89*(2), 409–415. https://doi.org/10.1104/pp.89.2.409

Westberry, T., Behrenfeld, M. J., Siegel, D. A., & Boss, E. (2008). Carbon-based primary productivity modeling with vertically resolved photoacclimation. *Global Biogeochemical Cycles*, *22*(2), 1–18. https://doi.org/10.1029/2007GB003078

Wickham, H. (2016). ggplot2: elegant graphics for data analysis. Springer-Verlag. New York. http://www.springer.com/gp/book/9783319242750

Wilhelm, C., Jungandreas, A., Jakob, T., & Goss, R. (2014). Light acclimation in diatoms: From phenomenology to mechanisms. *Marine Genomics*, *16*(1), 5–15. https://doi.org/10.1016/j.margen.2013.12.003

Wu, H., Roy, S., Alami, M., Green, B. R., & Campbell, D. A. (2012). Photosystem II photo-inactivation, repair, and protection in marine centric diatoms. *Plant Physiology*, *160*(1), 464–476. https://doi.org/10.1104/pp.112.203067

Zhu, S. H., & Green, B. R. (2010). Photo-protection in the diatom Thalassiosira pseudonana: Role of LI818-like proteins in response to high light stress. *Biochimica et Biophysica Acta - Bioenergetics*, *1797*(8), 1449–1457. https://doi.org/10.1016/j.bbabio.2010.04.003

2.9. Supplementary Information

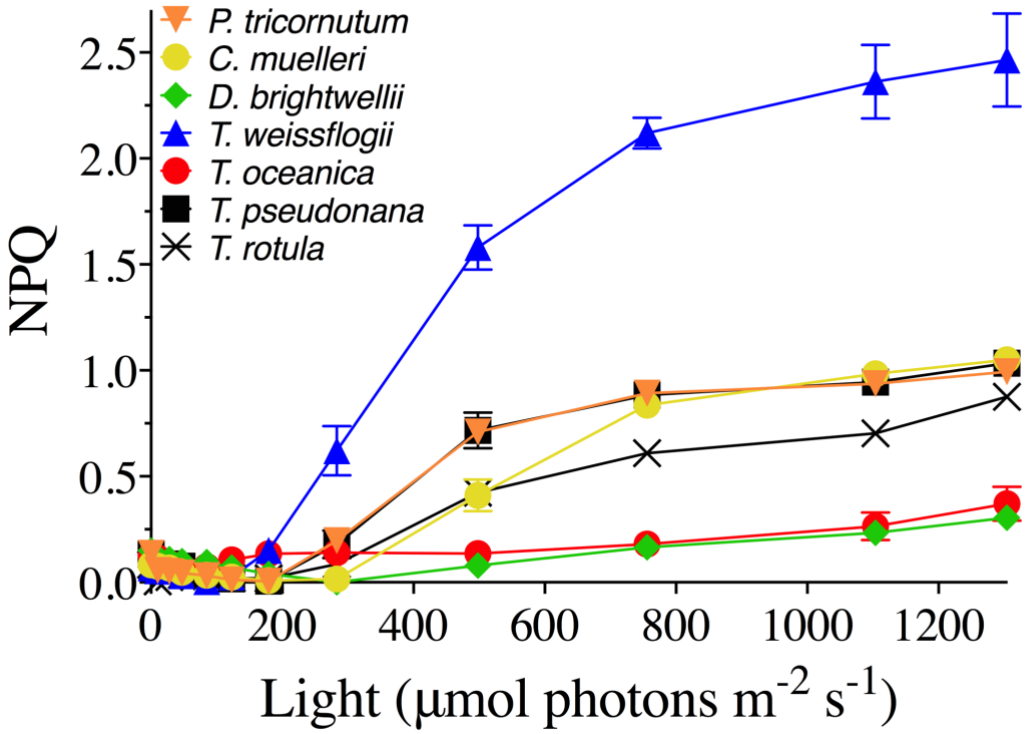

S2.1 Figure. Photophysiological assessment of seven diatoms. Conventional non-photochemical quenching (NPQ; see Eq. 2) capacities of *Phaeodactylum tricornutum* (orange inverted triangles), *Chaetoceros muelleri* (yellow circles), *Ditylum brightwellii* (green diamonds), *Thalassiosira rotula* (black Xs), *Thalassiosira pseudonana* (black squares), *Thalassiosira weissflogii* (blue triangles), and *Thalassisosira oceanica* (red circles) with increasing light intensity. Error bars represent the standard error of the mean of at least n=3 for independent biological replicates.

S2.1 Table. Rates of oxygen production and consumption. MIMS analysis of gross oxygen production (GP_{O2}), light dependent respiration (LDR), dark respiration (R_{DARK}), and net oxygen production (Net_{O2}) for *T. weissflogii*, *T. oceanica*, and *T. pseudonana* under 20 min exposure to HL (1200 µmol photons m^{-2} s^{-1}). Data averaged from 3 independent replicates.

Values in parentheses are SE of the mean. A 2-way ANOVA test comparing species and light treatment with oxygen measurements (GP_{O2}, Net_{O2}, LDR) and a 1-way ANOVA for R_{DARK} are presented with significant p-values (< 0.05) in bold. Superscripted asterisks (*) or letter identifies the Bonferroni post-hoc analysis for significance between species groups. For direct comparison with oxygen consumption/production rates from Chapter 3 see S3.3 Table.

Species	Light	pmol cell^{-1} h^{-1}			
		R_{DARK}	**LDR**	**Net_{O2}**	**GP_{O2}**
T. weissflogii	Ig	0.16^{b} (0.03)	0.06 (0.03)	0.32 (0.12)	0.54 (0.13)
	HL		0.06 (0.02)	0.64 (0.15)	0.86 (0.18)
T. oceanica	Ig	0.02^{a} (0.00)	0.02 (0.00)	0.14 (0.04)	0.18 (0.04)
	HL		0.04 (0.01)	0.14 (0.04)	0.20 (0.05)
T. pseudonana	Ig	0.02^{a} (0.01)	0.01 (0.00)	0.08 (0.01)	0.11 (0.02)
	HL		0.02 (0.01)	0.09 (0.02)	0.13 (0.02)
ANOVA (1-way)	*p*-value	**<0.05**	n/a	n/a	n/a
ANOVA (2-way)	*p*-value	Species	>0.05	**<0.05***	**<0.05***
		Light	>0.05	>0.05	>0.05
		Species*Light	>0.05	>0.05	>0.05

* *T. weissflogii – T. oceanica*/*T. pseudonana*

S2.2 Table. MIMS analysis of oxygen pathways as a percentage of gross oxygen production (% of GP_{O2}). Fractions (as a %) include light dependent respiration (LDR), dark respiration (R_{DARK}), and net oxygen production (Net_{O2}) for *T. weissflogii*, *T. oceanica*, and *T. pseudonana* under 20 min incubation at Ig (85 µmol photons m^{-2} s^{-1}) and HL (1200 µmol photons m^{-2} s^{-1}). Data averaged from 2 or 3 independent replicates. Values in parentheses are SE of the mean. A 2-way ANOVA comparing species and light treatment with oxygen measurements (R_{DARK}, Net_{O2}, LDR) are presented with significant p-values (< 0.05) in bold. Superscripted asterisks (*) identifies the Fisher's Tukey post-hoc analysis for significance between species groups.

Species	Light	% of GP_{O2}		
		R_{DARK}	**LDR**	**Net_{O2}**
T. weissflogii	Ig	21.67 (3.33)	11.83 (4.35)	66.50 (1.02)
	HL	19.33 (2.17)	8.07 (2.81)	72.60 (4.98)
T. oceanica	Ig	9.38 (2.45)	10.98 (0.22)	79.64 (2.66)
	HL	8.46 (2.34)	17.72 (2.50)	73.82 (0.17)
T. pseudonana	Ig	20.02 (4.67)	9.98 (3.35)	69.99 (4.57)
	HL	16.58 (4.03)	15.42 (6.15)	68.01 (2.47)
ANOVA (2-way)	Species	**<0.05***	>0.05	>0.05
	Light	>0.05	>0.05	>0.05
	Species*Light	>0.05	>0.05	>0.05

* *T. oceanica – T. weissflogii/T. pseudonana*

Chapter 3

Contrasting dynamics of light-dependent and -independent respiration from two *Thalassiosira* diatoms under diurnal light

Nerissa L. Fisher[1], Kimberly H. Halsey[2], David J. Hughes[1], Phoebe Argyle[1], Peter J. Ralph[1], David J. Suggett[1]

[1] Climate Change Cluster, University of Technology Sydney, Ultimo, New South Wales, Australia

[2] Department of Microbiology, Oregon State University, Corvallis, Oregon, USA

3.1. Abstract

Autotrophic phytoplankton metabolism fuels carbon drawdown in aquatic systems. Cellular-specific rate measurements of autotrophy for decades have largely focused on capturing the nature and variability of net carbon production. Corresponding losses – through internal O_2 recycling within cells – as "respiration" is commonly assumed to occur at a constant daily rate that is proportional to gross photosynthesis. As such, the dynamics of phytoplankton respiration rates over space and time remains largely unknown, particularly the respective contributions of light-dependent (LDR) versus light-independent (R_{DARK}) respiratory processes that operate concurrently with photosynthesis. Here we used simultaneous measurements of O_2 production and consumption using $^{18}O_2$ and $^{16}O_2$ via membrane inlet mass spectrometry (MIMS) to evaluate the dynamic and species-specific respiratory activities of two diatoms with known differences in photophysiology (i.e. nonphotochemical quenching) and LDR capacity (*Thalassiosira weissflogii*, *Thalassiosira oceanica*) over a sinusoidal photoperiod. In this study, we (1) evaluated total respiration (R_{TOTAL}), as LDR and R_{DARK}, over the photoperiod, (2) compared species-specific dependencies on these respiratory processes and (3) elucidated correlations for incubation-based O_2 measurements with parallel active chlorophyll fluorescence-derived parameters describing the photochemical activity of photosystem II (PSII). Together, these measurements demonstrated trade-offs between energy dissipation strategies (e.g. PSII activity, O_2 production and consumption, and cellular carbon biomass accumulation) with respect to time of day. The extent of R_{TOTAL} as a % of gross O_2 production (GP_{O2}) over the photoperiod ranged from 2.7–12.3% and 7.6–29.4% in *T. weissflogii* and *T. oceanica*, respectively. *T. weissflogii* exhibited dynamic R_{DARK} that followed light intensity and dissipated excess light energy as nonphotochemical quenching, whereas *T. oceanica* preferentially employed LDR to dissipate excess energy to compensate for its low photo-protective capacity. Parallel measurements of $E_{K.YII}$ – the light saturation

index of photochemical conversion - derived from fluorometric assessments, as well as other measures of photobiology (nonphotochemical light dissipation as fluorescence and heat) were correlated with R_{TOTAL} , net O_2 production and carbon per cell, suggesting that high resolution measures of $E_{K,YII}$ over space and time may provide a novel means to support improved functional description– and hence better resolve patterns – of phytoplankton productivity.

3.2. Introduction

Photosynthesis converts light energy to chemical energy via the splitting of water at photosystem II (PSII) via linear electron transport (LEF). These processes in turn drive reductant (e.g. NADPH) and energy (ATP) generation to fuel inorganic CO_2 fixation through the Calvin-Benson-Bassham (CBB) cycle into biomass. For most phytoplankton in the ocean, carbon assimilation is mainly driven by photosynthetic LEF, yet the fixed ratio of ATP:NADPH generated by LEF alone is not flexible enough to balance the variable demand for energy and reductant imposed by CO_2 fixation and other key cellular processes such as nitrogen (N) and sulfur (S) reduction (Allen 2002, Behrenfeld et al. 2008, Hughes et al. 2018a). To meet the energetic requirements of CO_2, N and S assimilation, in addition to biosynthesis of macromolecules (i.e. lipids, amino acids, pigments, proteins) and other demands for gene expression and cell division, various respiratory pathways must operate to supplement ATP and reductant pools (Raven 1988; Asada 1999; Geider & MacIntyre 2002; Wagner et al. 2016). Balancing cellular ATP:NADPH requirements to optimise growth, and hence photosynthesis and respiration processes, is critical in environments where phytoplankton cells are continuously subject to dynamic changes in resource availability (e.g. Behrenfeld et al. 2008, Finazzi et al. 2010, Cardol et al. 2011).

About twice as much CO_2 is assimilated than is ultimately retained in cell biomass (Geider & MacIntyre 2002; Halsey et al. 2011), with the remainder eventually catabolised back to CO_2 via glycolytic processes and mitochondrial respiration. Despite this, we know far less about how phytoplankton respiratory processes and rates vary over time compared to phytoplankton photosynthesis. This is largely due to the fact that photosynthetic O_2 production operates concurrently with respiratory O_2 consumption, making it challenging to experimentally separate these metabolic processes (Weger et al. 1989, Cardol et al. 2011). Laboratory- and field-based studies of phytoplankton respiration typically focus on dark, or mitochondrial, respiration (referred to henceforth as R_{DARK}) under the assumption that R_{DARK} accounts for the majority of the total respiratory budget (Laws 1991). Conventional light-dark (L/D) bottle incubations used to measure gross primary production (e.g. Gaarder & Gran 1927) track O_2 concentrations in the light and dark (i.e. net O_2 production (Net_{O2}) in the light and O_2 consumption in the dark), but this approach assumes R_{DARK} is constant in the light and is unable to capture information about light-dependent respiration (LDR) processes, such as photorespiration, Mehler activity, and midstream oxidase activity. R_{DARK} is known to be dependent on growth rate and physiological status (Laws & Bannister 1980; Waite et al. 1992; Jochem 1999), light intensity (Weger et al. 1989; Manticki et al. 2017), environmental conditions (Lewitus & Kana 1995; Laws et al. 2020) and taxonomy (e.g. Langdon 1993; Kana 1993; Kana et al. 1994; Lewitus & Kana 1995). Compiling such data across algal groups has indeed shown that photosynthesis-to-R_{DARK} ratio is not conserved, varying from 0.10 for cyanobacteria, 0.13 for chlorophytes and 0.16 for prymnesiophytes/diatoms to 0.35 for dinoflagellates (Langdon 1993 and refs within).

Membrane inlet mass spectrometry (MIMS, Hoch & Kok 1963) allows measurements of real-time dissolved isotopic gas concentrations (e.g. $^{18}O_2$ – Kana et al. 1994, 2006; Tortell 2005)

within a water sample containing phytoplankton. MIMS is able to discriminate LDR and R_{DARK}, thus revealing the fundamental role of LDR in phytoplankton energy budgets (Beckmann et al. 2009, Burlacot et al. 2020) that is often overlooked. Furthermore, LDR is often a substantial portion of gross production in the light (Suggett et al. 2009a) and can contribute 20-75% of gross photosynthesis (Lewitus & Kana 1995, Milligan et al. 2007; Halsey et al. 2010, 2011, 2013; Waring et al. 2010, Suggett et al. 2009a; Bailleul et al. 2017; Broddrick et al. 2019). A key LDR process is Mehler Ascorbate Peroxidase (MAP) – or Mehler activity for short – which alone, is estimated to account for ~10% of gross oxygen evolution, GP_{O2} (Raven & Beardall 1990) but can exceed 25% in marine cyanobacteria (Kana 1992, 1993). Nevertheless, the collective respiratory processes of R_{DARK} and LDR, are often simplified to be ~10% of gross O_2 production (GP_{O2}) (Beardall & Raven 1990) in energy budget and primary productivity models, which ultimately confounds the ability to make accurate, realistic, estimates. Furthermore, measures of light-enhanced dark respiration (LEDR) rates have been used to provide estimates of R_{DARK} rates in the light when direct measurement is not possible. LEDR quantifies the increase in $^{16}O_2$ consumption (i.e. R_{DARK}) following transient high light exposure (Falkowski et al. 1985), where rates have shown to increase by 50-140% from steady-state R_{DARK} (Beardall et al. 1994). LEDR is characterised by a short-lived increase of R_{DARK} in the dark after illumination that is proportional to the extent and intensity of light exposure. This 'burst' in R_{DARK} gradually decreases as the products of photosynthesis are metabolised (Weger et al. 1989; Xue et al. 1996; Beardall et al. 1994; Mantikci et al. 2017), eventually reaching the maintenance, or basal, R_{DARK} level. Again, LEDR does not accurately elucidate the contribution of LDR processes (e.g. Mehler and photorespiration) to total respiration (R_{TOTAL}), thus underestimating respiration occurring in the light.

Parameterisation of total phytoplankton respiration is critical for modelling primary production in marine systems (Platt et al. 1991, Marra et al. 2014), as incomplete knowledge of respiration dynamics hinders a deeper understanding of ocean carbon cycling (del Giorgio & Williams 2007, Bailleul et al. 2017). Efforts have accelerated over the past two decades to explore relationships of O_2 and CO_2 fluxes with chlorophyll fluorescence-based descriptors of PSII photochemistry (i.e fluorescence quantum yield of PSII, YII or ϕPSII – Genty et al. 1989), to exploit the rapid, real-time and *in situ* capacities of instruments that can capture chlorophyll fluorescence (Kolber & Falkowski 1995, Suggett et al. 2009a; Du et al. 2018). Coupled analyses of chlorophyll fluorescence and cellular metabolic processes reveals more complete phytoplankton energy budgets (Wagner et al. 2006; Jakob et al. 2007; Lagner et al. 2009; Su et al. 2012; Fratamico et al. 2016; Ware et al. 2020), but few such intensive studies have been conducted over the diurnal cycle (Halsey & Jones 2015). Moreover, the extent that respiratory processes vary over time and contribute to PSII photochemistry and O_2/CO_2 fluxes remains largely unexplored (Fisher & Halsey 2016; also see Chapter 2).

Here we examined respiration in diatoms, one of the most productive (Tréguer et al. 1995; Armburst 2009) and diverse (Malviya et al. 2016) phytoplankton groups, often dominating in physically dynamic environments (Falkowski et al. 2004; Tozzi et al. 2004; Sarthou et al. 2005; Smetacek 2012). We monitored LDR and R_{DARK} using MIMS-based analysis of $^{18}O_2$ and $^{16}O_2$ signals at intervals throughout a sinusoidal photoperiod for two diatom species, *Thalassiosira oceanica* and *Thalassiosira weissflogii*, that we (Chapter 2) and others (Strzepek & Harrison 2004; Lavaud et al. 2007) have previously revealed to exhibit differing energy dissipation strategies under high light exposure. The diurnal respiration trends were not conserved between diatom species but reflected photo-adaptive strategies to optimise growth in differing light environments. Our results reaffirm that respiration is not constant,

with total respiration over the day ranging between 3-32% of GP_{O2}. Trade-offs were observed between respiration processes where *T. weissflogii* exhibits more dynamic daytime R_{DARK} compared to greater LDR variation in *T. oceanica*. Empirical relationships with active chlorophyll fluorescence suggest that measures of oxygen consumption/production and phytoplankton biomass may be predictable, overcoming major obstacles in the promising use of fluorometric technologies to derive productivity.

3.3. Materials and methods

3.3.1. Culture conditions and growth

Semi-turbidostat cultures of *Thalassiosira weissflogii* (CS 871) and *Thalassisosira oceanica* (CCMP 1005) were grown using f/2+Si medium (Guillard 1975) supplemented with Na_2SeO_3 at 0.17 µM concentration (as per Fisher & Halsey 2016). Nitrate and phosphate concentrations were 250 and 50 µM, respectively (Laws & Bannister 1980) to maintain nutrient repletion within the media. Cultures were grown at 20°C over a 12:12 L:D cycle under sinusoidal light with a maximum light intensity of 400 µmol photons m^{-2} s^{-1} ($Sine_{\mu}$) that resulted in an average photon flux density (PFD) of 250 µmol photons m^{-2} s^{-1} throughout the photoperiod. All cultures were acclimated to each growth light regime for at least 7 generations and maintained in exponential growth via dilutions with fresh media. Light was supplied by an array of LEDs (AI Hydra FiftyTwo HD, Aqua Illumination, Ames, Iowa, USA) using the cool white LED channel only (Cree XP-G2, >70 CRI) and intensities were measured using a photometer (LI-COR, LI-250A, Nebraska, USA) attached with a 4π spherical quantum sensor.

Cultures were bubbled with air and diluted with fresh media in proportion to the specific growth rate (1.05 ± 0.04 and 1.0 3± 0.02 for *T. oceanica* and *T. weissflogii*, respectively,

mean ± standard error, n=4) to maintain nutrient repletion and cell density. Specific growth rates (μ, d^{-1}) were calculated as $\ln(N_2/N_1)/(t_2-t_1)$, where N_1 and N_2 are the cell concentrations (mL^{-1}) at time 1 (t_1) and time 2 (t_2), respectively. Aliquots of 0.5 mL from each culture were sampled at one hour into the photoperiod and preserved daily with glutaraldehyde (Sigma-Aldrich) for later cell enumeration on a flow cytometer (CytoFlex S, Beckman Coulter, Miami, FL USA). Samples were counted for 60 s at a rate of 30 µL min^{-1}.

3.3.2. Diurnal cellular and photophysiological characteristics

Experimental and back-up semi-turbidostat cultures were simultaneously maintained in exponential growth phase (as per the light regime described above) in independent vessels to allow acclimation to the light environment and then cultures were intensively sampled over the 12-h photoperiod. Cultures were monitored daily and determined to have reached steady-state when maximum the PSII photochemical efficiency (fluorometric assessment described in detail below) and growth rates were consistent for three consecutive days. At this stage, each culture was periodically sampled over the 12-h photoperiod, with samples drawn at 1, 3, 6, 9 and 11 hours following "lights on". This sampling procedure was repeated for five independent biological replicates for each diatom species.

At each timepoint on sampling days, cellular properties were assessed as follows: (i) single aliquots of 0.5 mL were taken for cell counts as above. Cell volume was calculated from the same sample used for cell count determinations using shape-specific geometric formulas from Sun & Liu (2003) via an imaging compact high-performing inverted microscope (Nikon Eclipse TS100). Five images were taken at random from each replicate and time point, and cellular dimensions recorded per image using Infinity software (Lumenera Corporation, Ontario, Canada). (ii) Duplicate aliquots of 5-8 mL culture, depending on culture density,

were each passed through 25 mm glass fiber filters (Whatman GF/F) then stored overnight at -20°C in 90% acetone for later chlorophyll *a* determination. Absorption was measured using a spectrophotometer (Aligent Technologies, Cary 60 UV-Vis) set at wavelengths 630, 657, 664 and 750 nm to quantify chlorophyll *a* concentration according to Ritchie (2006). (iii) Triplicate 10 mL aliquots were each passed through pre-combusted GF/F filters for particulate organic carbon and nitrogen concentrations where culture filtrate (10 mL) was also collected and analyzed for background subtraction. All samples were flash frozen in liquid nitrogen then stored at -80°C until measured on an elemental analyzer (LECO, Baulkham Hill, Australia) (Chapter 2).

An additional 1-2 mL was drawn at each time point for photophysiological assessment using a benchtop Light Induced Fluorescence Transient-Fast Repetition Rate fluorometer (LIFT-FRRf, Soliense Inc., USA), via a modified protocol of Keller et al. (2019). A single turnover (ST) excitation protocol with a saturation sequence of 100 flashlets (1.6 μs flashlet length with 2.5 μs intervals) followed by a relaxation sequence of 127 flashlets (1.6 μs flashlet length with an initial interval of 20 μs then subsequently increased by an exponential factor of 1.025) was used to drive ST closure of PSII reaction centres (RCII) to generate a fluorescent induction-relaxation curve. All excitation power for ST measurements were performed using only the blue excitation LED (445 nm) and a total of 10 sequences were conducted per acquisition (with 150 ms interval between sequences). A biophysical model (Kolber et al. 1998) was then fit to each acquired fluorescence transient using custom software (Z. Kolber, pers. comm.) to extract minimum (F_0 or F') and maximum (F_m or F_m') fluorescence as well as the effective absorption cross section (σ_{PSII} or σ_{PSII}'; $Å^2$ $quanta^{-1}$) for samples in darkness or under actinic (i.e. ambient) light, respectively. Maximum PSII

photochemical efficiency (F_v/F_m) was determined as (F_m-F_o)/F_m. All samples were low light (<10 μmol photons m^{-2} s^{-1}) acclimated for 10 min prior to LIFT-FRRf measurements.

FRRf-derived fluorescence light response curves (FLCs) were subsequently performed by subjecting each sample to a gradient of increasing actinic light intensity (0, 10, 25, 50, 100, 150, 250, 500, 750 μmol photons m^{-2} s^{-1}) also supplied by blue excitation at 445 nm. While each FLC light step duration was 4 min, only the average of data retrieved within the last 30 s (ca. 5 acquisitions) of each light step was used as indicative of steady state fluorescence (e.g. Suggett et al. 2015). For each light step, we determined the yield of regulated non-photochemical quenching (YNPQ; see Klughammer & Schrieber 2008), which, compared to the unbounded conventional Stern-Volmer measure of nonphotochemical quenching, NPQ_{NSV}, (F_m-F_m')/F_m' (Bilger & Bjorkman 1990), generates a parameter bounded between 0 and 1 following,

$$YNPQ = \frac{F'}{F_{m'}} - \frac{F'}{F_m} \quad (1)$$

where F' is the fluorescence measurement under actinic light and F_m is the maximum fluorescence after a short (5 min) low light incubation. We used the approach of Serôdio et al. (2005) where the maximum achieved fluorescence value (F_m') throughout the FLC was used as a proxy for F_m in order to offset any down-regulation of fluorescence through dark-driven plastoquinone pool reduction (i.e. negative values). Additional fluorescence yield parameters were further calculated following (Klughammer & Schrieber 2008, Genty et al. 1989) to describe the partitioning of absorbed excitation energy at PSII to include photochemical conversion (YII) and non-regulated constitutive losses as heat and fluorescence (YNO) such that,

$$YII + YNO + YNPQ = 1 \quad (2)$$

$$YII = (F_m' - F')/F_m' \quad (3)$$

$$YNO = F'/F_m \quad (4)$$

where F_m was again taken as the maximum value of F_m' achieved throughout the FLC (Serôdio et al. 2005). Finally, we also fit the PSII photochemical efficiency (YII, Eq. 5) from the FLCs to a model describing the light (E, µmol photons m^{-2} s^{-1})-dependent nature of YII (e.g. Suggett et al. 2003; Hennige et al. 2008; Silsbe & Kromkamp 2012) using least-squares non-linear regression (MATLAB™, vR2020a) to retrieve the light saturation intensity of PSII photochemistry ($E_{K,YII}$, µmol photons m^{-2} s^{-1}),

$$YII = [(YII_{max} * E_{k,YII})\ (1 - \exp\ (-E/E_{k,YII}))]/E \quad (5)$$

3.3.3. Membrane inlet mass spectrometry (MIMS)

Aliquots of 70 mL for each sample were sparged with N_2 gas for 5 min to remove $^{16}O_2$; this timing was found to be sufficient to remove >99% $^{16}O_2$ from culture (data not shown) as measured via a fibre optic oxygen sensor spot (OXR430, Pyroscience GmbH, Aachen, Germany) connected to an oxygen data logger (FireSting, Pyroscience, Germany). Approximately 60 mL of N_2-sparged culture was transferred to a gas-tight syringe then enriched with labelled oxygen isotope ($^{18}O_2$, Marshall Isotopes Ltd., Israel) by drawing up a small bubble of $^{18}O_2$ into the syringe and shaking for 3 min to allow equilibration of the $^{18}O_2$ gas bubble with the sparged culture (as per Suggett et al. 2009a; Chapter 2). $^{18}O_2$-Labelled culture was then divided between five 12 mL exetainer vials (LabCo Ltd., UK) for the following treatments: time zero (T_0), dark, growth irradiance matching the sinusoidal growth

light regime ($Sine_{\mu}$) and high light that was three times the sinusoidal growth light irradiance ($Sine_{HL}$) (S3.1 Fig). T_0 was fixed immediately with 150 µL 0.2 M mercuric chloride ($HgCl_2$) to cease biological activity. $Sine_{\mu}$ and $Sine_{HL}$ sample vials were incubated under the treatment time-specific light intensity for 20 min at 20°C then subsequently fixed in the same manner as T_0 (see S3.1 Fig for methods schematic). Fixed samples were stored at room temperature under darkness until analysis via MIMS (Bay Instruments, Maryland, USA). All fixed samples were processed within one week of collection.

3.3.4. MIMS sample processing

Set-up of the MIMS and sample analysis was undertaken following Kana et al. (1994, 2006) modified by Suggett et al. (2009a). In brief, samples were pumped through stainless steel capillary tubing, submerged in a waterbath (20°C), then over a semi-permeable microbore silicone membrane (Silastic®, DuPont) where gas exchange occurred. Gases flowed through a U-shaped manifold membrane inlet system, resting in a liquid N_2 cryotrap, and attached to a Prisma quadrapole mass spectrometer (QMS-200; Pfeiffer) with a closed ion source and electron multiplier detector for recording mass/charge (m/z) ratios of 32 ($^{16}O_2$), 36 ($^{18}O_2$), and 40 (Ar). Discrete measurements of ion currents were recorded using QuikData software (Bay Instruments, Maryland, USA) after gas signals had stabilised then were recorded in triplicate. Calibration of the MIMS was performed, using filtered media equilibrated to atmospheric O_2 concentrations, at the beginning and end of sampling and also throughout (~30 min intervals) to account for instrument drift in the ion current signal. For MIMS sampling, the capillary tubing was placed near the bottom of the exetainer vial and sample time never exceeded 4 min, thus ensuring negligible gas exchange with the atmosphere through diffusion (Kana 1994).

Rates of oxygen production/consumption were calculated using signal ($^{16}O_2$ and $^{18}O_2$) output differences from T_0 and light treatment (Dark, $Sine_{\mu}$, $Sine_{HL}$) samples incubated for 20 min before scaling to hourly rates as per Suggett et al. (2009a). Specifically, corrected $^{16}O_2$ signals in the light were assumed to reflect gross oxygen production (GP_{O2}). Total respiration (R_{TOTAL}) was the corrected $^{18}O_2$ signal for all sample light treatments (Dark, $Sine_{\mu}$, $Sine_{HL}$) after subtracting from T_0. The 'Dark' light treatment ultimately provided concentrations for dark, or mitochondrial, respiration (R_{DARK}) while 'true' light dependent respiration (LDR) was obtained by subtracting the R_{TOTAL} for each light treatment ($Sine_{\mu}$, $Sine_{HL}$) from the 'Dark' treatment (i.e. R_{DARK}) as

$$LDR_{E>0,t} = R_{TOTAL_{E>0,t}} - R_{DARK_t} \quad (6)$$

where E>0 represent the individual sample light treatments under illumination (i.e. $Sine_{\mu}$ and $Sine_{HL}$) at each timepoint over the photoperiod (t). Net oxygen production (Net_{O2}) was thus calculated by factoring in both $^{16}O_2$ and $^{18}O_2$ signals for each light treatment using the following equation:

$$Net_{O_2} = GP_{O_2} - R_{TOTAL} \quad (7)$$

An incubation of 20 min was chosen to minimise the $^{16}O_2$ consumed by respiration, while allowing enough time for generation of detectable oxygen signals via MIMS. We used discrete measures which do not provide real-time rate information as from continuous measures (see Chapter 2). It was thus impossible to determine when $^{16}O_2$ exceeds $^{18}O_2$ and therefore a portion of newly produced $^{16}O_2$ signal is likely to be consumed; as such, GP_{O2} is likely an underestimate of true $^{16}O_2$ production. However, by this justification, $^{18}O_2$

consumption (i.e. respiration) is also likely an under- (conservative) estimate of true values (see Chapter 2). Ensuring this consistency in assessing the values derived from MIMS provided confidence that the trends observed over time and between species are real.

3.3.5. Spectral corrections

In order to explore MIMS-based photosynthesis characteristics (GP_{O2}, LDR) with corresponding FRRf-based measures of photochemical activity (YII, YNPQ) at equivalent light intensities for each time point, we applied a spectral correction factor (SCF) to account for the different actinic light sources used for MIMS (white LED) versus FRRf (445 nm LED) sample incubations as per Hughes et al. (2018b) as.

$$\mathrm{SCF} = \sum \bar{a}_{FRRf} \,/\, \sum \bar{a}_{MIMS} \qquad (8)$$

Values for $\bar{a}_{MIMS}$ or $\bar{a}_{FRRf}$ were determined by weighting the respective actinic spectra with fluorescence excitation spectra (400-700 nm) from previously collected data for these two taxa that were pre-treated with DCMU and fluorescence emission measured at 730 nm (see S3.2 Fig; Suggett et al. 2004), to yield SCF values of ~1.50 and 1.36 for *T. oceanica* and *T. weissflogii*, respectively. FRRf actinic light intensities (E) used for the FLC to retrieve photophysiological parameters (e.g. $E_{K,YII}$, Eq 5) were spectrally weight-adjusted toward the MIMS white LED by dividing the corresponding species SCF for each light step. Once FLC light intensities of FRRf sample incubations were spectrally corrected, we used the corresponding light intensity that most closely matched the light intensity for the MIMS incubation (Table 3.1) for subsequent measurement comparisons.

Table 3.1. Exposure light intensities during MIMS analysis for each sampling time point. Incubation treatments either mimicked the growth light intensity ($Sine_{\mu}$,) or were 3.0-fold higher ($Sine_{HL}$). Spectral correction factors (SCF) were applied to account for the light source differences between MIMS (white LED) and FRRf (blue LED) incubations for *T. oceanica* and *T. weissflogii*.

Sample Time (h)	Light Intensity of Sample Incubations (µmol photons m^{-2} s^{-1})					
	MIMS (white LED)		FRRf (blue LED) spectrally corrected			
	-----	-----	*T. oceanica* (SCF = 1.50)		*T. weissflogii* (SCF = 1.36)	
	$Sine_{\mu}$	$Sine_{HL}$	$Sine_{\mu}$	$Sine_{HL}$	$Sine_{\mu}$	$Sine_{HL}$
1	70	210	75	225	68	204
3	215	645	225	750	204	680
6	400	1200	375	1125	340	1020
9	215	645	225	750	204	680
11	70	210	75	225	68	204

3.3.6. Statistics

Differences in cellular properties between species were assessed using one-way analysis of variance (ANOVA) followed by Bonferroni's multiple comparison test where prerequisite assumptions of normality and homoscedasticity were first satisfied according to Levene's and Shapiro-Wilk tests, respectively. Two-way ANOVA followed by Bonferroni's multiple comparison test was used to evaluate significance of the effect of species and time of day on photobiological characteristics (Ananda & Weerahandi 1997). These ANOVAs were performed using IBM SPSS Statistics v26. To compare the change in oxygen (i.e LDR, R_{DARK}, R_{TOTAL}, Net_{O2} and GP_{O2}) and fluorescence (i.e. YII, YNO and YNPQ) traits over time, individual one-way repeated measures ANOVAs were performed for each trait for each light condition, for each species. When an effect of time was found, pairwise t-tests (with FDR p-value adjustment) were run between each set of time points to establish significant differences. When ANOVA assumptions were not met, a Friedman's non-parametric test was used, followed by post-hoc tests using the posthoc.friedman.nemenyi.test from the PMCMR package in R. To compare overall differences in oxygen and fluorescence-based parameters

between the species and between light levels within each species, one-way ANOVAs were used. Where ANOVA assumptions were not met, a Kruskall-Wallis test was used. Pearsons correlation between fluorescence (e.g. YII, YNO, YNPQ), oxygen (e.g. GP_{O2}, R_{TOTAL}, Net_{O2}) and carbon (e.g. C cell^{-1}) measures were performed in GraphPad Prism v8.4.3 using a simple linear regression model where a line of best-fit and 95% confidence intervals were included to quantify the relationship from individual replicate values (n=3) at each timepoint. The significance level for all tests performed was set at $p < 0.05$.

3.4. Results

3.4.1. Physiological assessments

T. oceanica and *T. weissflogii* were monitored over a 12 h sinusoidal photoperiod at five time points. Cell densities (and hence optical thickness) were consistent throughout the day (Table 3.2). Significant differences were observed between species for all physiological characteristics assessed, except C:N (Table 3.2). C:N increased significantly between 1-3 h and 9-11 h in *T. oceanica* that was driven by increasing C cell^{-1} concentrations over the photoperiod (Table 3.2). For *T. weissflogii,* C:N remained unchanged over the day even though a significant increase in both carbon (C, pg cell^{-1}) and nitrogen (N, pg cell^{-1}) was observed at midday (6 h) (Table 3.2). Maximal PSII photochemical efficiency, F_v/F_m, in *T. oceanica* declined at midday (6 h) from ~0.7 at 1, 3 h to ~0.65 for subsequent time points. Conversely, *T. weissflogii* showed no change in F_v/F_m over the photoperiod. There was no time of day effect for the functional absorption cross section of PSII, σ_{PSII}, for either species, but was significantly larger in *T. oceanica* compared to *T. weissflogii* (Table 3.2) as expected given their respective cell size (Suggett et al. 2009b).

Table 3.2. Cell culture and properties of *Thalassiosira oceanica* and *Thalassiosira weissflogii* during steady-state growth acclimated to a sinusoidal ($Sine_{\mu}$) light regime with a maximum irradiance of 400 µmol photons m^{-2} s^{-1} over a 12:12 L:D photoperiod at 20°C. Values in parentheses are standard error for at least 3 independent biological replicates at each sample time. A two-way ANOVA test comparing species, time and interactive (Species*Time) effects for each property are represented with significant *p*-values (< 0.05) in bold. The test results from a one-way ANOVA are shown using superscripted letters to identify the Bonferroni post-hoc analysis for significance between sample times (h). Letters indicate means that are statistically indistinguishable ($p < 0.05$; ANOVA).

Species	Sample time (h)	Growth irradiance (µmol photons m^{-2} s^{-1})	Cells mL^{-1} (x10^5)	Chl *a* $cell^{-1}$ (pg)	C $cell^{-1}$ (pg)	N $cell^{-1}$ (pg)	C:N	F_v/F_m	σ_{PSII}
Thalassiosira oceanica	1	70	18.85 (1.31)	0.51[a] (0.01)	14.83[a] (0.98)	3.07 (0.27)	4.90[a] (0.07)	0.71[a] (0.01)	275.07 (4.82)
	3	215	16.59 (1.06)	0.61 (0.02)	22.92[a] (2.41)	2.78 (0.07)	5.96[a] (0.33)	0.70[a] (0.01)	268.19 (4.76)
	6	400	17.26 (1.49)	0.66[b] (0.03)	28.17 (0.89)	2.96 (0.18)	6.51 (0.12)	0.65[b] (0.01)	275.91 (7.01)
	9	215	17.50 (1.40)	0.68[b] (0.03)	36.33[b] (0.91)	2.95 (0.26)	7.61[b] (0.51)	0.65[b] (0.01)	287.19 (5.94)
	11	70	17.99 (1.46)	0.66[b] (0.02)	40.38[b] (1.66)	2.89 (0.22)	7.84[b] (0.44)	0.66[b] (0.01)	289.16 (4.99)
Thalassiosira weissflogii	1	70	4.37 (0.10)	4.52 (0.53)	71.75[a] (1.84)	12.76[a] (1.84)	6.02 (0.93)	0.72 (0.01)	207.75 (5.66)
	3	215	4.31 (0.18)	4.93 (0.41)	74.24[a] (2.50)	14.35[a,b] (2.50)	5.62 (0.89)	0.72 (0.00)	202.91 (3.70)
	6	400	3.98 (0.21)	5.66 (0.29)	99.34[b] (3.87)	17.64[b,c] (3.20)	6.13 (0.92)	0.70 (0.02)	195.88 (4.34)
	9	215	4.52 (0.18)	5.64 (0.44)	107.23[b] (4.91)	18.20[c] (2.59)	6.19 (0.76)	0.69 (0.00)	201.27 (3.02)
	11	70	4.80 (0.11)	5.47 (0.46)	108.88[b] (4.02)	15.43[c] (1.98)	6.44 (0.39)	0.70 (0.00)	204.17 (2.56)
ANOVA (2-way)	Species		**<0.05**	**<0.05**	**<0.05**	**<0.05**	>0.05	**<0.05**	**<0.05**
	Time		>0.05	>0.05	**<0.05**	>0.05	>0.05	**<0.05**	>0.05
	Species*Time		>0.05	>0.05	**<0.05**	>0.05	>0.05	>0.05	>0.05

The light saturated intensity of PSII photochemistry, $E_{k,YII}$, from FRRf-derived YII values collected over a FLC, significantly varied over the day for both *T. oceanica* and *T. weissflogii* ($p < 0.0001$, Fig 3.1) suggesting dynamic photo-acclimation (S3.1 Table). Values of $E_{K,YII}$ were higher for *T. weissflogii* (~212-486 μmol photons m^{-2} s^{-1}) compared to *T. oceanica* (~131-270) at individual time points (2-way ANOVA of time*species, $p = 0.022$); however, overall diurnal trends in $E_{k,YII}$ variability were similar for both species. Maximal $E_{k,YII}$ values were obtained from the onset of light (i.e. 1 and 3 h) of ~267 and 471 μmol photons m^{-2} s^{-1} for *T. oceanica* and *T. weissflogii*, respectively. Conversely, $E_{k,YII}$ at 6 (maximal growth intensity), 9 and 11 h were on average approximately 2-fold lower than the values at the start of the photoperiod.

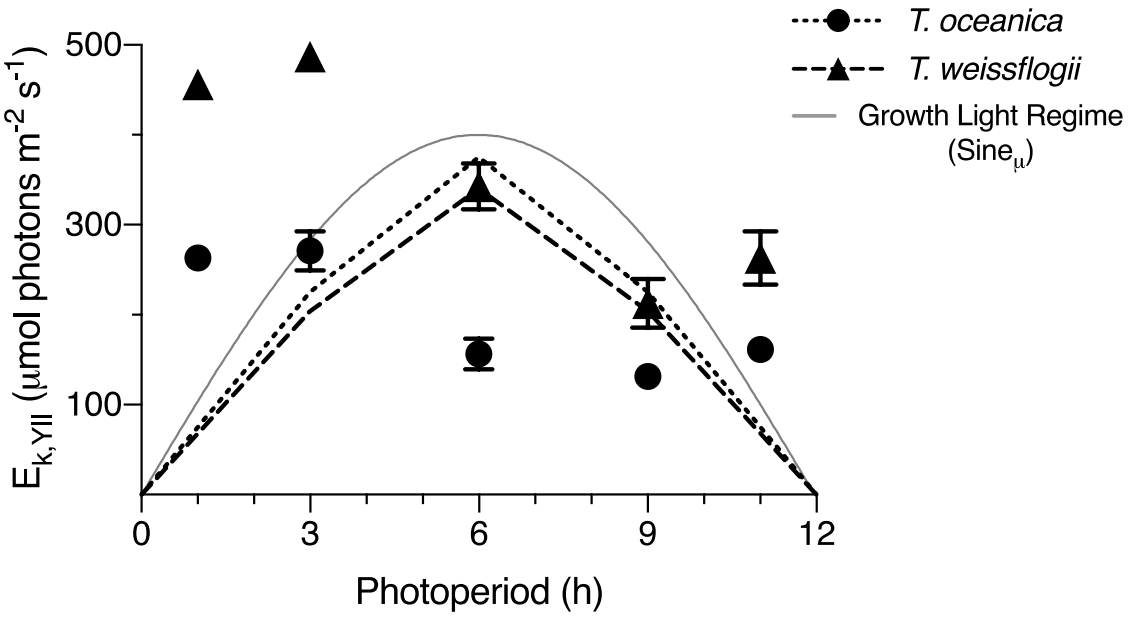

Figure 3.1. Changes in $E_{k,YII}$ for *T. oceanica* (circles) and *T. weissflogii* (triangles) acclimated to a 12:12 L:D cycle under sinusoidal light with max irradiance of 400 μmol photons m^{-2} s^{-1} (grey solid line). $E_{k,YII}$ was calculated using FRRf-derived YII values collected from a FLC. The spectrally corrected light intensities for FRRf-incubated samples are shown for *T. oceanica* (dotted line) and *T. weissflogii* (dashed line). Sampling occurred along the photoperiod at 1, 3, 6, 9 and 11 hours after the

onset of illumination. Error bars represent SE of the mean for at least 3 independent biological replicates.

3.4.2. Diurnal oxygen consumption

Respiration patterns in *T. oceanica* and *T. weissflogii* differed depending on actinic light exposure (R_{DARK}, $Sine_{\mu}$, $Sine_{HL}$) (Fig 3.2). In order to contrast species or environmental effects, respiration rate is commonly normalised to corresponding cellular properties (e.g. cell number (Chapter 2), C or Chl *a* content (Fisher & Halsey 2016, Manticki et al. 2017)) to relate respiratory activity with other cellular processes, such as carbon production. All of these various cellular properties differed between species but not between sampling times, with the exception of Chl *a* cell^{-1} at one timepoint (1 h) in *T. oceanica* (Table 3.2). However, regardless of normalisation property, the diurnal trends were ultimately markedly conserved (S3.3 Fig). Given the inherent differences in cell volumes of these two species (6-fold *T. weissflogii* > *T. oceanica*) that contributed to cell abundance, normalisation based on cell number was not the most meaningful to comparatively analyze respiration trends. Therefore, for subsequent analyses we normalised oxygen data to Chl *a*, as commonly reported in the wider literature for phytoplankton productivity measures.

Under Sineμ, the Chl *a*-specific total respiration rate (R_{TOTAL}, pmol O_2 (pg Chl *a* h)$^{-1}$; Eq 6) was at least two-fold higher in *T. oceanica* than *T. weissflogii*. R_{TOTAL} peaked with maximum light at 6 h in *T. weissflogii. T. oceanica* behaved similarly, except R_{TOTAL} remained high at 9 h (Fig 3.2). In both species, peaks in R_{TOTAL} followed decreases in $E_{k,YII}$ (Fig 3.1). The 2.4-fold increase in R_{TOTAL} between 3-6 h in *T. oceanica* under $Sine_{\mu}$ was primarily caused by increased LDR (~0.005 to 0.039 pmol O_2 (pg Chl *a* h)$^{-1}$), whereas R_{DARK} remained relatively constant (p = 0.09) (averaging 0.009 ± 0.0006 pmol O_2

(pg Chl *a* h)$^{-1}$) over the photoperiod. In contrast, R_{DARK} in *T. weissflogii* at $Sine_{\mu}$ increased 11-fold (ranging from 0.001 to 0.011 pmol O_2 (pg Chl *a* h)$^{-1}$), between 1 and 6 h, with less dramatic changes in LDR where significant differences were observed between 1, 3 h and 9 h ($p < 0.05$, Bonferroni corrected). The patterns exhibited by LDR and R_{DARK} in *T. oceanica* under $Sine_{\mu}$ exposure were equivalent to those exhibited under HL exposure ($Sine_{HL}$, $p = 0.33$), but differed in *T. weissflogii* ($p = 0.015$) (Fig 3.2).

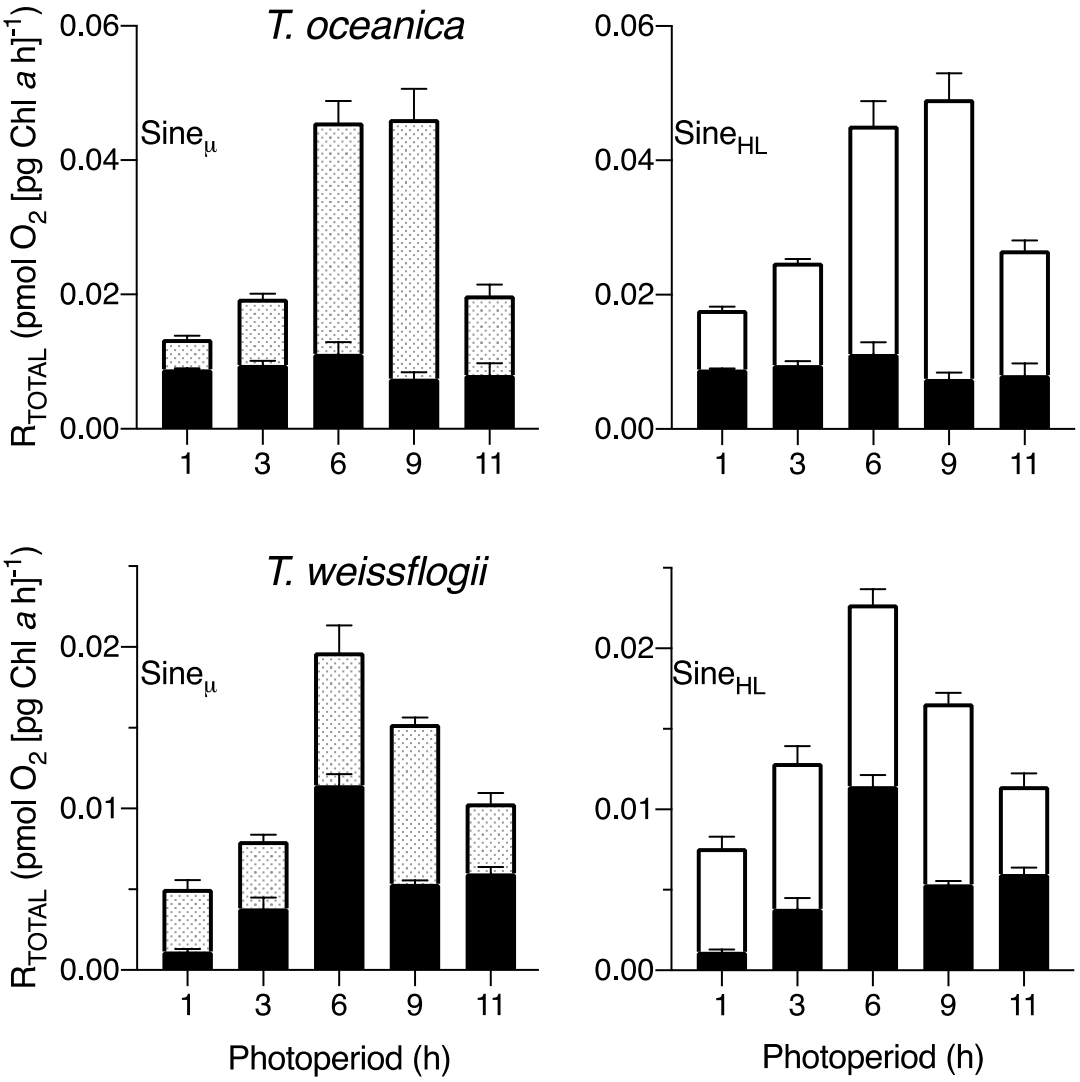

Figure 3.2. Total respiration (R_{TOTAL}, pmol O_2 [pg Chl *a* h]$^{-1}$) for *T. oceanica* and *T. weissflogii* acclimated to a sinusoidal light regime (maximum 400 μmol photons m^{-2} s^{-1}) at sample time points along the photoperiod. The light incubations representing variations in LDR ($Sine_{\mu}$ – dotted white, and $Sine_{HL}$ – solid white) were plotted separately and both included the dark respiration (R_{DARK} – black) for each corresponding timepoint. Error bars represent SE of the mean for at least three independent replicates. Note that the R_{DARK} value at each timepoint does not change between light incubation treatments but LDR values do reflect the response to light intensity shifts between treatments ($Sine_{\mu}$ and $Sine_{HL}$) and the y-axis scale is different between species.

The proportion of O_2 recycled through respiratory pathways, to in turn yield Net_{O2} from GP_{O2}, varied between *T. oceanica* and *T. weissflogii* (Fig 3.3). R_{TOTAL} as a % of GP_{O2} ranged from 5.1-29.4% in *T. oceanica* and from 2.6-12.3% in *T. weissflogii* under $Sine_{\mu}$ (Fig 3.3A,D). Both species exhibited a ca. 5-fold increase in R_{TOTAL}, propotional to GP_{O2}, from 1-3 h versus 9 h (5.8 and 4.6-fold in *T. oceanica* and *T. weissflogii*, respectively). The larger LDR values and diurnal variance observed in *T. oceanica* drove the greater disparity between GP_{O2} and Net_{O2} (Fig 3.3B,C) compared to *T. weissflogii* (Fig 3.3E,F). *T. oceanica* exhibited a marked decrease in Net_{O2} at 9 h to 68% ($p < 0.05$ pairwise comparisons for 1,3,11-9 h), whereas Net_{O2} remained at least 86% of GP_{O2} regardless of light treatment in *T. weissflogii*, similarly observed in a green alga (Halsey et al. 2011).

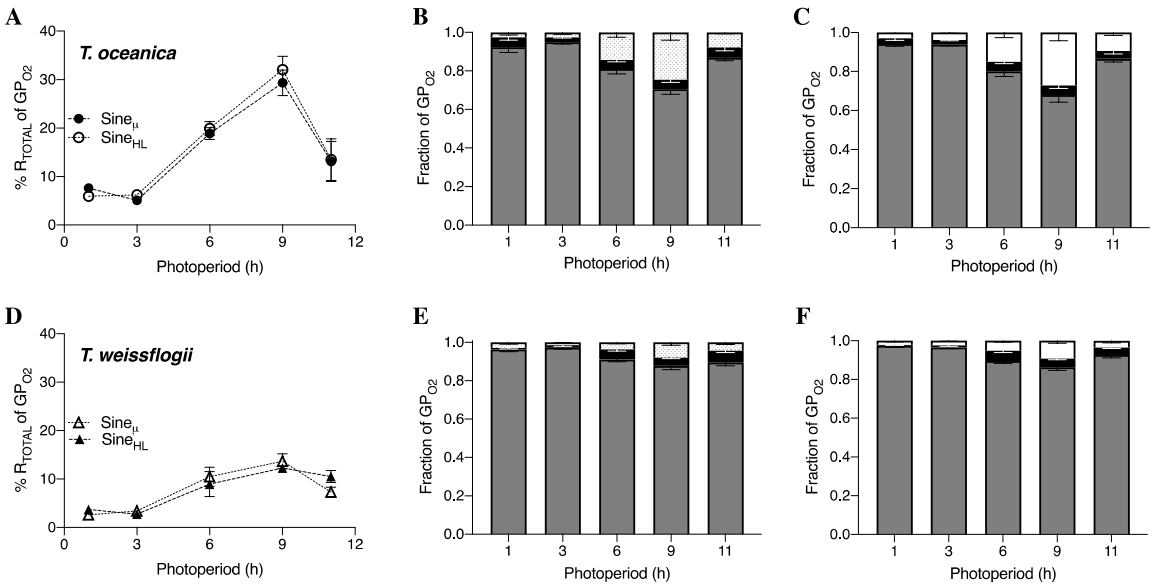

Figure 3.3. Respiratory components of gross oxygen production (GP_{O2}): (A,D) total respiration (R_{TOTAL}) as a percentage of gross O_2 production. GP_{O2} separated into the fraction of net oxygen production (Net_{O2}, grey), dark respiration (R_{DARK}, black) and light dependent respiration (LDR, white) under $Sine_{\mu}$ (B,D) and $Sine_{HL}$ (C,F) for *T. oceanica* (A-C) and *T. weissflogii* (D-F) sampled over the photoperiod. Error bars represent SE of the mean for at least three independent replicates.

3.4.3. Comparing MIMS- and fluorescence-based dynamics

PSII photochemical conversion efficiency (parameterised as YII, Eq. 3) negatively correlated with oxygen evolved at PSII (i.e. GP_{O2}) ($R^2 = 0.591$-0.856, $p < 0.0001$) for both species under $Sine_{\mu}$ and $Sine_{HL}$ exposures; S3.2 Table) (Fig 3.4), a result that support previous comparisons of GP_{O2} and YII using FRRf-based approaches in phytoplankton (e.g. Flameling & Kromkamp 1997; Suggett et al. 2003, 2009a). However, the regression slope differed between the two species and light treatments– but not with growth light intensity (S3.2 Table) – indicating species-specific differences in the photochemical conversion efficiency between absorbed light and gross O_2 evolution at PSII.

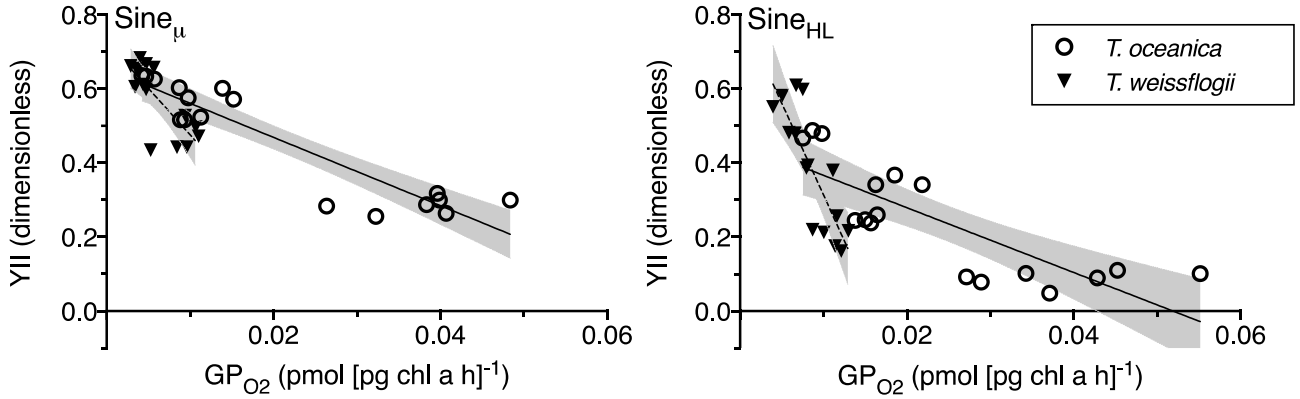

Figure 3.4. Pearsons correlations between YII (dimensionless) and GP_{O2} (pmol [pg Chl *a* h]$^{-1}$) for *T. oceanica* (circles, solid lines) and *T. weissflogii* (inverted triangles, dashed lines) for incubations at $Sine_{\mu}$ and $Sine_{HL}$ over the integrated photoperiod. Lines of best fit were generated using a simple linear regression model where the shaded areas represent the 95% confidence intervals for significant correlations ($p < 0.05$) only. Model parameters are displayed in S3.2 Table.

Pearson correlations between YII and GP_{O2} supported the approach to partition absorbed light into various energy sinks across the photoperiod, whereby, GP_{O2} was scaled to YII using proportions of LDR, R_{DARK} and Net_{O2} (Fig 3.3B,C,E,F) (as detailed in Chapter 2). Specifically, summing the energy flux yields (Eq. 2) of YII (photochemical conversion at PSII; Eq. 3), YNO (yield of nonregulated constitutive losses as fluorescence and heat; Eq. 4) and YNPQ (yield of regulated nonphotochemical quenching; Eq. 1) gives the total light energy that is absorbed at PSII (Eq. 2). YNO and YNPQ are energetic losses prior to photochemistry where their fates are related to subsequent photochemical processes and light-dependent repair pathways (Hughes et al. 2018a, Chapter 2). Thus, a more robust view of energy flux yields was possible by accounting for the light energy dissipated as well as used in photochemical conversion at PSII (YII). Net_{O2} is the fraction of YII that remains after both light

dependent (LDR) and independent (R_{DARK}) respiratory processes. YII fractions will not be specifically discussed here as they were scaled from GP_{O2} (see above; Fig 3.3).

Over the photoperiod both diatom species exhibited trade-offs between light energy dissipation (i.e. YNO and YNPQ) and light used for photochemical conversion (i.e. YII). With increasing light exposure during the first half of $Sine_{\mu}$, YII decreased from 0.63 to 0.25 in *T. oceanica* (all pairwise comparisons with time were significant except 1-11 h) and from 0.68 to 0.43 in *T. weissflogii* (significant pairwise comparisons except 1-11 h and 3,6-9 h). The decrease in YII in *T. oceanica* was balanced by increasing YNO from ~0.35 at 1 h to 0.72 at 6 h, but YNPQ remained relatively conserved throughout the diurnal cycle (~0.02-0.06; Friedman's test $p > 0.05$) (Fig 3.5). This pattern was similarly expressed in *T. oceanica* under $Sine_{HL,}$ but the transient exposure to 3x higher light caused YII to decrease ~3-fold by 6 h and YNPQ was 4-fold greater at 3 and 6 h (Fig 3.5). By contrast, in *T. weissflogii* under $Sine_{\mu}$, YNO instead remained relatively constant (0.31-0.45; no significant differences between any time points using Friedman's test), whereas YNPQ increased 110-fold from 0.001 at 1 h to 0.11 at 9 h. YNPQ was especially pronounced under $Sine_{HL}$ increasing to 0.48 at 9 h (Fig 3.5). These data show the interplay between YII, YNPQ and YNO that across the day was observed previously for these two species from a single discrete time point (Chapter 2).

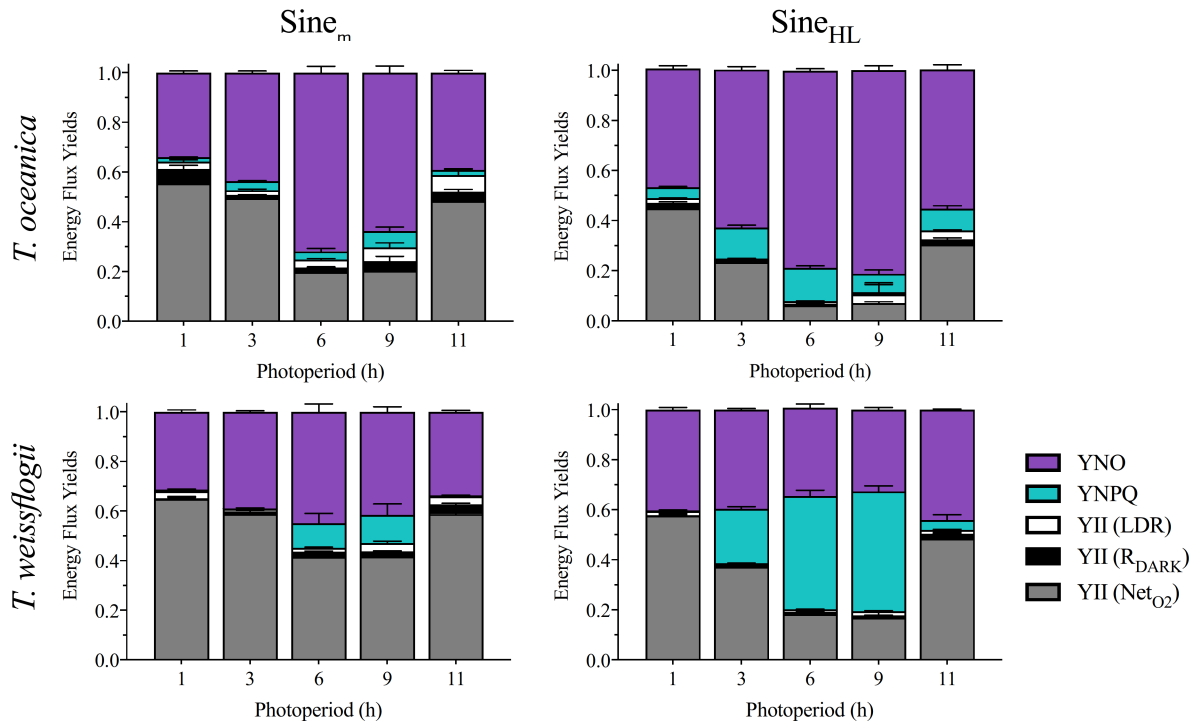

Figure 3.5. Energy flux yields for the sum of YNPQ (teal), YNO (purple) and YII, which was then further divided using GP_{O2} fractions of LDR (white), R_{DARK} (black) and Net_{O2} (grey) for *T. oceanica* and *T. weissflogii* exposed to $Sine_{\mu}$ and $Sine_{HL}$. Data averaged from at least 3 independent replicates with error bars representing SE of the mean.

Finally, given the close correspondence observed between YII and GP_{O2} (Fig 3.4), we subsequently explored whether significant and generalised relationships also existed between O_2 consumption parameters and fluorescence yields. Intriguingly, YII was also correlated with R_{TOTAL} (Fig 3.6A; S3.2 Table) – with patterns similar to those for YII versus GP_{O2} – and significant correlation coefficients were also observed for *T. weissflogii* between YNPQ and R_{TOTAL} at both light exposures ($R^2 = 0.593$, 0.744 for $Sine_{\mu}$ and $Sine_{HL}$, respectively, $p < 0.001$) and for *T. oceanica* at $Sine_{\mu}$ but not for *T. oceanica* under $Sine_{HL}$ ($p > 0.05$) (Fig 3.6B; S3.2 Table). YNO values observed in *T. oceanica* were further correlated with R_{TOTAL} under $Sine_{\mu}$ ($R^2 = 0.885$, $p < 0.0001$) and $Sine_{HL}$ ($R^2 = 0.774$, $p < 0.0001$) and

for *T. weissflogii* though the relationship flipped from positive under $Sine_{\mu}$ ($R^2 = 0.598$, $p < 0.001$) to negative under $Sine_{HL}$ ($R^2 = 0.335$, $p < 0.05$) (Fig 3.6C; S3.2 Table), in agreement with the higher YNPQ:YNO ratio (Fig 3.5).

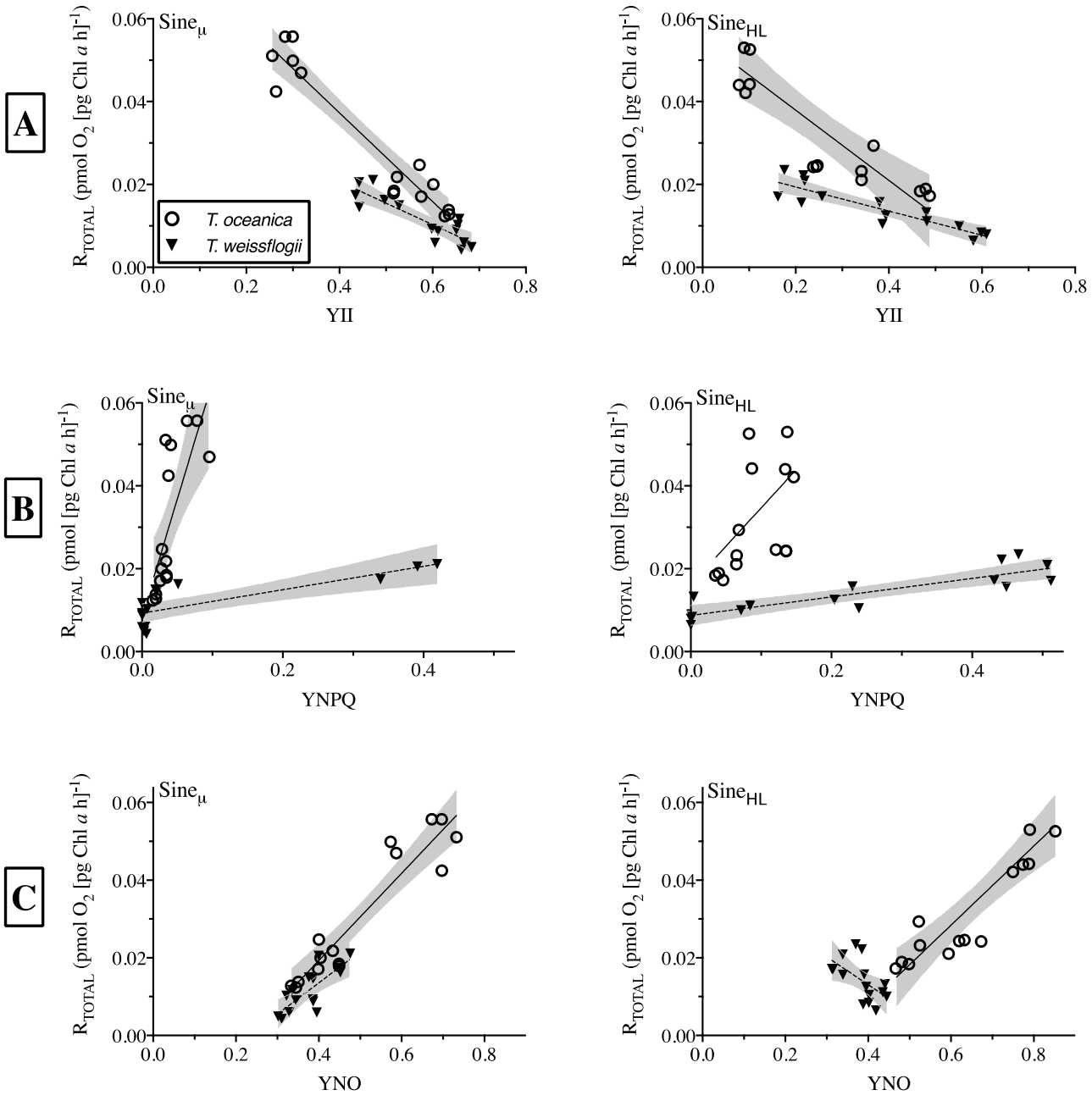

Figure 3.6. Pearson correlations between fluorescence- and oxygen-derived parameters for *T. oceanica*

(circles) and *T. weissflogii* (inverted triangles) at growth irradiance ($Sine_{\mu}$) and 3x growth irradiance ($Sine_{HL}$) collated over a 12-h photoperiod. Correlations included R_{TOTAL} to YII (Panel A), YNPQ (Panel B) and YNO (Panel C). Data points represent three individual replicate measures for each sample timepoint (1, 3, 6, 9, 11 h). Regression lines were included for both *T. oceanica* (solid line) and *T. weissflogii* (dashed line) and 95% CI (grey shaded area) displayed only for significant correlations ($p < 0.05$). Model parameters are displayed in S3.2 Table.

Significant coefficient correlations were observed between the photoacclimation index, $E_{k,YII}$, and cellular metabolic processes and biomass (C $cell^{-1}$) (S3.2 Table). Under $Sine_{\mu}$, high $E_{k,YII}$ values corresponded with lower R_{TOTAL} ($p < 0.05$) and greater Net_{O2} ($p < 0.01$) (Fig 3.7A,B; S3.2 Table). $E_{k,YII}$ and C $cell^{-1}$were negatively correlated for both species ($p < 0.005$) (Fig 3.7C,D; S3.2 Table).

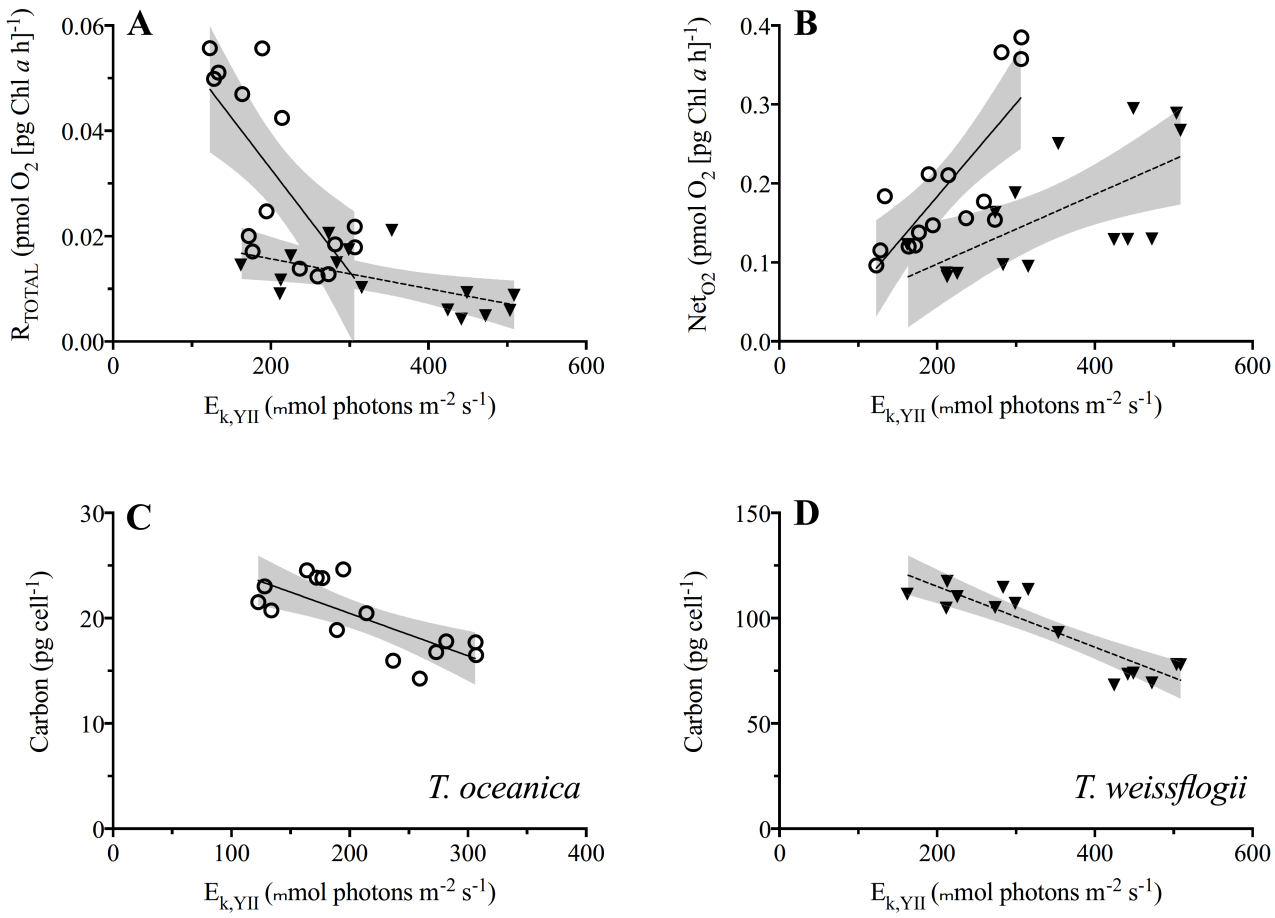

Figure 3.7. Pearson correlations between $E_{k,YII}$ and (A) R_{TOTAL}, (B) Net_{O2}, and (C,D) carbon (pg cell-1) for *T. oceanica* (circles) and *T. weissflogii* (inverted triangles). Regression lines with 95% CI (grey shaded area) are displayed only for significant correlations ($p < 0.05$). Model parameters are displayed in S3.2 Table.

3.5. Discussion

Respiration is a fundamental component of phytoplankton metabolism, yet is poorly understood relative to photosynthesis, especially in the context of oceanic carbon cycling – a knowledge gap that likely undermines the reliability of global primary productivity models (del Giorgio & Williams 2007; Williams & Lefèvre 2008). Indeed, whether and how phytoplankton respiration varies over space and

time can be reconciled with other dynamic processes has been rarely explicitly tested to date. We therefore examined variability in respiration over a diurnal period for two diatom species, with contrasting photo-protective capacities (i.e. nonphotochemical quenching), demonstrating temporal dynamics in respiration rates driven by species-specific physiological processes.

3.5.1. Respiration is not constant and LDR is a major contributor to total respiration

Studies to date have commonly observed daytime light-dependent oxygen uptake rates in cultivated microalgae upwards of 30-40% GP_{O2} (Weger et al. 1988, 1989; Lewitus & Kana 1995; Eriksen & Lewitus 1999; Suggett et al. 2008; Waring et al. 2010; Halsey et al. 2013; Broddrick et al. 2019); within such studies diatom respiration via light-dependent processes can comprise 15-19% of GP_{O2} (*T. weissflogii* - Weger et al. 1989; Halsey et al. 2013). Works specifically monitoring diatom responses to light have observed contributions of R_{TOTAL} to GP_{O2} similarly ranging between 15-49% (*Nitzschia epithemioides*, *T. pseudonana*, *T. oceanica* - Waring et al. 2010; Fisher & Halsey 2016; Chapter 2), although R_{DARK} can range between 6-63% of R_{TOTAL} depending on species and growth rate (Lewitus & Kana 1995; Halsey et al. 2010; Fisher & Halsey 2016). In our current work, the contribution of R_{TOTAL} to GP_{O2} varied over the sinusoidal photoperiod and increased up to 4.5-fold from the onset of light (Fig 3.3), from 5.1-29.4% of GP_{O2} in *T. oceanica* and from 2.6-12.3% GP_{O2} in *T. weissflogii* under $Sine_{\mu}$ (Fig 3.3A,D). However, notably the dynamic nature of R_{DARK} was not conserved between species, with *T. weissflogii* showing clear diurnal variability in R_{DARK} rates in both light treatments, in contrast to a temporally static R_{DARK} measured for *T. oceanica*. While R_{DARK} in the light has been considered to be only a minor process (Weger et al. 1989; Marra et al. 2014), we show it is clearly significant and variable. Such R_{DARK} variability has been proposed to be directly regulated by light (Weger et al.

1989), but to the best of our knowledge, no such regulation has yet been documented over a photoperiod.

LDR is commonly overlooked as a major respiratory pathway, even though LDR is well known to be regulated to optimise growth (Behrenfeld et al. 2008, Halsey et al. 2010). In our current study, LDR was observed to sometimes exceed R_{DARK}, in particular for *T. oceanica* (Figs 3.3 and 3.4), thus, measurements of R_{DARK} alone are far from representative of the full contribution of respiratory processes within cellular energy budgets. Light-dependent respiratory processes can be used as alternative pathways for energy dissipation (Allen et al. 2008; Mackey et al. 2008, Hughes et al. 2018), while simultaneously generating ATP through the consumption of electrons via O_2 reduction that consequently pumps protons into the lumen thus promoting proton motive force (Heber 2002; Wilhelm & Selmar 2011; Cardol et al. 2011; Raven et al. 2020). This consumption of electrons also alleviates excitation pressure within the photosynthetic electron transport chain which helps avoid damage to photosynthetic machinery (Eberhard et al. 2008; Wilhelm & Jakob 2011) and optimise linear electron flow that produces reductant that is used by the CBB cycle. The dynamic nature of LDR observed here with time of day under sinusoidal light (and change in $E_{K,YII}$) – increasing by as much as 56% between the time of 3 and 9 h – demonstrated the likely critical role of LDR in aiding energy and reductant flow to balance cellular processes, emphasising the limitations of relying on constant respiration values in energetic models (Behrenfeld et al. 1997; Lindemann et al. 2015).

3.5.2. Respiratory processes supporting growth

R_{DARK} is generally thought to positively correlate with growth rate (Laws & Wong 1978; Geider & Osborne 1989; Beardall et al. 2009) and thus biosynthesis (Falkowski et al. 1985). We observed that *T. oceanica* exhibited consistent R_{DARK} over the day, whereas *T. weissflogii* upregulated R_{DARK} that generally tracked light intensity (Fig 3.2), which in turn correlates with increased photosynthate production (Weger et al. 1989; Manticki et al. 2017). This indicates that, for *T. weissflogii*, catabolism of newly fixed carbon increased over the course of the day to supply energy and reductant for biosynthesis. The significant increase in N cell^{-1} at 6 h (Table 3.1), also when R_{DARK} is highest (Fig 3.2), is consistent with the notion that catabolism via R_{DARK} generates reductant and carbon skeletons required for NO_3^- assimilation, as has been previously hypothesised for green algae (Weger & Turpin 1989). Diatoms are thought to take up nutrients in excess of their immediate needs to facilitate synthesis of proteins and storage lipids (Elrifi & Turpin 1985; Lomas & Gilbert 2000; Litchman et al. 2007; Merz et al. 2020). Such "luxury" N-uptake is especially pronounced in larger species (Fawcett & Ward 2011), which aligns to *T. weissflogii* being 6-fold larger than *T. oceanica*. In fact, nitrate reductase (NR) activity was observed to increase in the light (Packard 1973; Martinez et al. 1987), at the expense of carbon fixation (Smith et al. 1992). For *T. weissflogii*, the modest 8% increase in C cell^{-1} concentrations from 6 to 9 h compared to the 25% increase observed from 3 to 6 h (Table 3.1) suggests that R_{DARK} was supporting N-uptake in lieu of C-uptake at midday. Conversely, *T. oceani*ca did not show this trade-off between C- and N-uptake over the photoperiod, but instead solely increased C-uptake to build reserves in preparation for respiratory needs during the night – the more widely accepted paradigm.

3.5.3. Photo-protective strategies as indicators of respiration dynamics

Photo-protection pathways, such as increased respiration in the light, are important regulators of the total energy yield in algae. Diatoms also have photo-protective mechanisms to dissipate excess light energy from PSII that is largely reflective of their ecological niche (Strzepek & Harrison 2004; Lavaud et al. 2007; Wilhelm et al. 2014; Lacour et al. 2020, Chapter 2). Centric *Thalassiosira* species in particular seem to have permanently modified their photosynthetic apparatus based on iron availability to maintain photosynthetic efficiency (Peers & Price 2006) such that open ocean species have higher PSII (lower iron content) to PSI (higher iron content) ratios compared to their estuarine and coastal counterparts. Nonphotochemical quenching requires structural modification of the PSII antennae that includes specific light harvesting pigment-protein complexes. Activation occurs via transthylakoid membrane proton motive force build-up that triggers epoxidation of xanthophyll cycle pigments from diadinoxanthin (Dd, light harvesting) to diatoxanthin (Dt, photo-protecting) (Demmig-Adams & Adams 2006; Lavaud & Goss 2014). *T. weissflogii* appears to relax nonphotochemical quenching slowly (Milligan et al. 2012) and thus avoids pre-emptive activation until reaching higher intensities by using LDR early in the day (by 1 h) when light is sub-saturating for photosynthesis to maximise NADPH and ATP generation by maintaining linear electron flow and pumping additional protons into the lumen, respectively. This proton pumping additionally serves to 'prime' the activation of nonphotochemical quenching (Grouneva et al. 2009; Raven et al. 2020) that requires an acidified lumen. The concerted use of LDR and nonphotochemical quenching in *T. weissflogii* led to YII values that were consistently higher over the diurnal cycle compared to *T. oceanica* (Fig 3.5).

Intriguingly, both YNO and YNPQ exhibited species-specific correlations with respiration rates, whereby higher YNO was associated with higher LDR and R_{TOTAL} over the day (i.e. *T. oceanica*) and

higher YNPQ was associated with lower R_{TOTAL}, but greater variability of R_{DARK} (i.e. *T. weissflogii*). In other words, there is a trade-off between energy dissipation as photons (i.e. YNO or YNPQ) and respiration whereby when YNPQ is activated (e.g. *T. weissflogii*) there is less reliance on dissipating energy as electrons along the ETC via oxygen consuming pathways (i.e. respiration). Conversely, when YNPQ is not utilised (e.g. *T. oceanica*), there is more excitation pressure within the ETC that must be safely dissipated, via LDR processes, to avoid damage to photosynthetic machinery and optimise photosynthetic efficiency. While YNPQ is considered an indication of photo-protection capacity, YNO describes the constitutive losses as heat and fluorescence of de-excitation reactions that do not lead to photochemical energy conversion at PSII and are not involved with the nonphotochemical quenching mechanism (Klughammer & Schreiber 2008). The impact of higher YNO:YNPQ in *T. oceanica* was previously evidenced by higher rates of photo-inactivation (K_{pi}) under high light compared to *T. weissflogii* and *T. pseudonana* (Chapter 2) that contributed to the lowest YII at 6 and 9 h (Figs 3.5 and 3.7). Lower YII indicates either (1) photo-inactivation or (2) a higher number of closed RCII because the PQ pool cannot oxidise as quickly as photo-oxidation is occurring at RCII (Perkins et al. 2018), thus causing the decrease in $E_{k,YII}$ from 6 h (Fig 3.1). Such a backlog of excitation energy within the electron transport chain did not result in a decrease in overall maximal photosynthetic efficiency of PSII (F_v/F_m) (Table 3.1), thus photo-inactivation is unlikely here. It appears that the photosynthetic generation of NADPH from LEF is not the rate limiting step for the CBB cycle (Raines 2003), which is clearly functioning optimally – presumably as expected under steady state growth conditions – even at maximal light from the significantly greater concentrations of C cell^{-1} at 6 and 9 h (Table 3.1).

3.5.4. Using fluorescence as an indicator of physiology

Another intriguing outcome of our assessment was the dynamic nature of $E_{k,YII}$ with time of day (Fig 3.1) – largely driven by changes in α (S3.1 Table) – which also correlated with changes in respiratory rate and carbon accumulation in biomass (Fig 3.7). E_k is generally considered to be a descriptor of the optimum light intensity for photosynthesis, balanced between modifications of light absorption versus downstream maximum photosynthesis rates (Falkwoski & Wirick 1981; Sakshaug et al. 1997; Behrenfeld et al. 1997). In the case of active fluorometry, $E_{k,YII}$ represents the balance between PSII light-harvesting and downstream electron turnover (Moore et al. 2006, Hughes et al. 2018a). E_k variability as a function of time of day is not commonly reported from photosynthesis studies (but see Aardema et al. 2019); however, it is not surprising that $E_{k,YII}$ would be dynamic given that many factors –operating over fast time scales – likely regulate changes in maximum electron turnover rate (Behrenfeld et al. 1998, Moore et al. 2006) compared to carbon-based E_k – operating over much slower time scales (e.g. Moore et al. 2006). Importantly, we observed declines in $E_{k,YII}$ from midday to end of day, while respiration rates peaked at midday and then declined. Ultimately, $E_{k,YII}$ positively correlated with Net_{O2} and negatively with R_{TOTAL}. This trend suggests that when optimum excitation pressure is reduced (i.e. $E_{k,YII}$ decreases), cells shunt electrons towards respiration that in turn decreases Net_{O2}. However, these respiratory processes could in some cases be essential to maintain electron turnover (Grouneva et al. 2009; Cardol et al. 2011, Alric & Johnson 2017). Corresponding high C cell^{-1} with lower $E_{k,YII}$ in the afternoon may largely reflect the maximum capacity of the CBB cycle to fix carbon. Here, lower $E_{k,YII}$ at higher light reflects a fully reduced PQ pool that prevents RCII from re-opening which causes more light energy to be dissipated – hence the lower fraction of YII at higher light. However, the continued increase in C cell^{-1} over the day indicates that PSII is not damaged, but instead rate-limited by the capacity of the CBB that causes the backlog of electrons along the photosynthetic

electron transport chain. Such dynamics are clearly critical and require further investigation to better resolve.

Using direct optical analyses of active chlorophyll *a* fluorescence yields of PSII has been pursued for decades as an alternative approach to measure GP_{O2} (Dubinsky et al. 1986; Genty et al. 1989; Flameling & Kromkamp 1997; Suggett et al. 2009a; Chapter 2; this study). Efforts are gaining traction to link fluorescence to primary production measures based on carbon (Robinson et al. 2014; Schuback et al. 2015, 2019; Zhu et al. 2017; Hughes et al. 2020 - for an extensive review see Hughes et al. 2018a), but to date these have not extended to exploring whether and how PSII fluorescence properties may also provide a means to describe O_2-consuming metabolic processes alongside GP_{O2}. In our study, $E_{k,YII}$ correlated well with both oxygen measures (R_{TOTAL} and Net_{O2}) and biomass (C $cell^{-1}$) for the two *Thalassiosira* species examined here. Similarly, YII and YNO provided good correlations with R_{TOTAL} while YNPQ did not reveal significant correlations for both species. YNO was a particularly useful indicator of energy dissipation trade-offs between YNPQ and YNO under $Sine_{HL}$ where a negative correlation was observed for *T. weissflogii* from higher YNPQ and a positive correlation for *T. oceanica* from lower YNPQ. Overall, YNO is a signal that is present even under moderate light (Chapter 2; this work) so it provides a baseline whereby under high light any deviations, as seen under high light (Fig 3.5), provide valuable information about species-specific photo-protective capacities, whereas YNPQ is not a parameter that can be applied to all species (i.e. those with low NPQ capacities; Fig 3.6B). While such co-variability between respiration rates and fluorescence quenching terms is not unreasonable to expect – for example where trade-offs in photochemical and nonphotochemical quenching align with operation of specific respiratory pathways (e.g. Hughes et al. 2018) – the underlying nature (and exact basis for) is not currently clear, but clearly warrants deeper investigation.

By examining these various fluorescence and metabolic components over the diel cycle for the first time, we demonstrate tantalising – and hitherto unexplored – potential for fluorometric measures to overcome existing limitations in describing the dynamic nature of phytoplankton respiration. Such an indirect assay approach for respiration is appealing due to the unparalleled scale and ease at which active fluorometry measurements can be acquired relative to incubation-based MIMS approaches that directly quantify respiration, and a fundamental determinant as to why fluorometry has increasingly become a "go to" tool for primary productivity studies. A critical next step should therefore be to examine the robustness of these relationships over a wider range of taxa and environments. Given the different respiration dynamics observed between species in this study, recent advances in taxonomic discrimination of phytoplankton by spectral fluorescence (Gorbunov et al. 2020) could further support the capacity of active fluorometry to overcome existing gaps in productivity models that currently parameterise respiration as a constant – and likely underestimated – value.

3.6. Conclusion

We have shown that simultaneous measures of oxygen consumption (LDR, R_{DARK}) and production (GP_{O2}, Net_{O2}) over a sinusoidal photoperiod can provide an increasingly more 'complete' view of energy flux budgets, and further reveal diverse metabolic strategies for energy production and dissipation that are intricately linked to support phytoplankton growth. For *T. weissflogii*, while R_{TOTAL} composed a lower portion of GP_{O2} over the day, the higher capacity for nonphotochemical quenching (i.e. YNPQ) with light intensity resulted in increased R_{DARK} to supplement energetic costs associated with this photo-protective mechanism. LDR is twofold used to (1) regulate pH of the lumen such that

nonphotochemical quenching is only activated when photolysis at PSII outpaces the capacity of the photosynthetic electron transport chain and (2) generate additional ATP. *T. oceanica* exhibits low capacity to photo-protect and compensates through a greater reliance on alternative electron pathways that flow to oxygen reduction (i.e. LDR). The results shown here suggest that the strategies employed by *T. oceanica* are less effective in maintaining higher YII, particularly at higher intensities, compared to *T. weissflogii*. Nevertheless, the equivalent growth rates exhibited by these species demonstrates that energy use strategies are initiated at the level of light absorption and should be considered in the context of ecological adaptation. Our data importantly demonstrates that assessing energy budgets and primary production *should not* rely on the assumption that respiration is constant either over the day or between species. The dynamic contributions of LDR and R_{DARK} to R_{TOTAL} over the diurnal cycle underscore the importance of accounting for all respiratory activities as they can provide useful insight into species-specific strategies for energy use including photo-protection that also relate to ecological niche. Such combined parameters could provide the basis for improving primary productivity models that can account for 'adaptive' dynamic (photo)physiological parameters based on ecological niche, or domains (Longhurst et al. 1995; Lindemann et al. 2015; Bouman et al. 2018), an outcome that will require more comprehensive assessments of respiration across taxonomic groups. The promising use of active chlorophyll fluorescence-derived measures of $E_{k,YII}$ to estimate phytoplankton biomass and net oxygen production also supports future work to investigate the potential generality of these findings.

3.7. Acknowledgments

Authors are grateful to the support provided by UTS research technical officers, especially Paul Brooks, Scott Allchin and Helen Price. NLF was supported by the UTS International Research Scholarship and President's Scholarship.

3.8. References

Aardema, H. M., Rijkeboer, M., Lefebvre, A., Veen, A., & Kromkamp, J. C. (2019). High-resolution underway measurements of phytoplankton photosynthesis and abundance as an innovative addition to water quality monitoring programs. *Ocean Science*, *15*(5), 1267–1285. https://doi.org/10.5194/os-15-1267-2019

Allen, A. E., LaRoche, J., Maheswari, U., Lommer, M., Schauer, N., Lopez, P. J., … Bowler, C. (2008). Whole-cell response of the pennate diatom Phaeodactylum tricornutum to iron starvation. *Proceedings of the National Academy of Sciences of the United States of America*, *105*(30), 10438–10443. https://doi.org/10.1073/pnas.0711370105

Allen, J. F. (2002). Photosynthesis of ATP - Electrons, Proton Pumps, Rotors and Poise. *Cell*, *110*(3), 273–276. Retrieved from https://reader.elsevier.com/reader/sd/pii/S009286740200870X?token=69B4D871A9EB11C29F20EB20A68EB3950616994DA872075D777357D6A4F191C1E7B6CBD0E617805306D727F12F4E444D

Alric, J., & Johnson, X. (2017). Alternative electron transport pathways in photosynthesis: a confluence of regulation. *Current Opinion in Plant Biology*, *37*(i), 78–86. https://doi.org/10.1016/j.pbi.2017.03.014

Ananda, M. M. A., & Weerahandi, S. (1997). Two-Way ANOVA with unequal cell frequencies and unequal variances. *Statistica Sinica*, *7*(3), 631–646.

Armbrust, E. V. (2009). The life of diatoms in the world's oceans. *Nature*, *459*(7244), 185–192. https://doi.org/10.1038/nature08057

Asada, K. (1999). The water-water cycle in chloroplasts: Scavenging of Active Oxygens and Dissipation of Excess Photons. *Annual Review of Plant Physiology and Plant Molecular Biology*, *50*(1), 601–639. https://doi.org/10.1146/annurev.arplant.50.1.601

Bailleul, B., Park, J., Brown, C. M., Bidle, K. D., Lee, S. H., & Falkowski, P. G. (2017). Direct measurements of the light dependence of gross photosynthesis and oxygen consumption in the ocean. *Limnology and Oceanography*, *62*(3), 1066–1079. https://doi.org/10.1002/lno.10486

Beardall, J., & Raven, J. A. (1990). Pathways and mechanisms of respiration in microalgae. *Mar Microb Food Webs*, *4*(1), 30.

Beardall, J., Burger-Wiersma, T., Rijkeboer, M., Sukenik, A., Lemoalle, J., Dubinsky, Z., & Fontvielle, D. (1994). Studies on enhanced post-illumination respiration in microalgae. *Journal of Plankton Research*, *16*(10), 1401–1410.

Beardall, J., Ihnken, S., & Quigg, A. (2009). Gross and net primary production: Closing the gap between concepts and measurements. *Aquatic Microbial Ecology*, *56*(2–3), 113–122. https://doi.org/10.3354/ame01305

Beckmann, K., Messinger, J., Badger, M. R., Wydrzynski, T., & Hillier, W. (2009). On-line mass spectrometry: Membrane inlet sampling. *Photosynthesis Research*, *102*(2), 511–522. https://doi.org/10.1007/s11120-009-9474-7

Behrenfeld, M. J., & Falkowski, P. G. (1997). A consumer's guide to phytoplankton primary productivity models. *Limnology and Oceanography*, *42*(7), 1479–1491. https://doi.org/10.4319/lo.1997.42.7.1479

Behrenfeld, M. J., Prasil, O., Kolber, Z. S., Babin, M., & Falkowski, P. G. (1998). Compensatory changes in photosystem II electron turnover rates protect photosynthesis from photoinhibition. *Photosynthesis Research*, *58*(3), 259-268.

Behrenfeld, M. J., Halsey, K. H., & Milligan, A. J. (2008). Evolved physiological responses of phytoplankton to their integrated growth environment. *Philosophical Transactions of the Royal Society B: Biological Sciences*, *363*(1504), 2687–2703. https://doi.org/10.1098/rstb.2008.0019

Bilger, W., & Björkman, O. (1990). Role of the xanthophyll cycle in photo-protection elucidated by measurements of light-induced absorbance changes, fluorescence and photosynthesis in leaves of Hedera canariensis. *Photosynthesis Research*, *25*(3), 173–185. https://doi.org/10.1007/BF00033159

Bouman, H. A., Platt, T., Doblin, M., Figueiras, F. G., Gudmundsson, K., Gudfinnsson, H. G., … Sathyendranath, S. (2018). Photosynthesis-irradiance parameters of marine phytoplankton: Synthesis of a global data set. *Earth System Science Data*, *10*(1), 251–266. https://doi.org/10.5194/essd-10-251-2018

Broddrick, J. T., Du, N., Smith, S. R., Tsuji, Y., Jallet, D., Ware, M. A., … Allen, A. E. (2019). Cross-compartment metabolic coupling enables flexible photo-protective mechanisms in the diatom Phaeodactylum tricornutum. *New Phytologist*, *222*(3), 1364–1379. https://doi.org/10.1111/nph.15685

Burlacot, A., Burlacot, F., Li-Beisson, Y., & Peltier, G. (2020). Membrane Inlet Mass Spectrometry: A Powerful Tool for Algal Research. *Frontiers in Plant Science*, *11*(September), 1–15. https://doi.org/10.3389/fpls.2020.01302

Cardol, P., Forti, G., & Finazzi, G. (2011). Regulation of electron transport in microalgae. *Biochimica et Biophysica Acta - Bioenergetics*, *1807*(8), 912–918. https://doi.org/10.1016/j.bbabio.2010.12.004

Del Giorgio, P., & Williams, P. (2007). Respiration in Aquatic Ecosystems. *Respiration in Aquatic Ecosystems*, 1–328. https://doi.org/10.1093/acprof:oso/9780198527084.001.0001

Demmig-Adams, B., & Adams III, W. W. (2006). Photo-protection in an ecological context: the remarkable complexity of thermal energy dissipation. *New Phytologist*, *172*(1), 11-21.

Du, N., Gholami, P., Kline, D. I., DuPont, C. L., Dickson, A. G., Mendola, D., … Greg Mitchell, B. (2018). Simultaneous quantum yield measurements of carbon uptake and oxygen evolution in microalgal cultures. *PLoS ONE*, *13*(6), 1–21. https://doi.org/10.1371/journal.pone.0199125

Dubinsky, Z., Falkowski, P. G., & Wyman, K. (1986). Light Harvesting and Utilization by Phytoplankton. *Plant and Cell Physiology*, *27*(7), 1335–1349. https://doi.org/10.1093/oxfordjournals.pcp.a077232

Eberhard, S., Finazzi, G., & Wollman, F. A. (2008). The dynamics of photosynthesis. *Annual Review of Genetics*, *42*, 463–515. https://doi.org/10.1146/annurev.genet.42.110807.091452

Elrifi, I. R., & Turpin, D. H. (1985). Steady-state luxury consumption and the concept of optimum nutrient ratios: A study with phosphate and nitrate limited Selenastrum minutum (chlorophyta). *Journal of Phycology*, *21*(4), 592-602.

Falkowski, P. G., & Wirick, C. D. (1981). A simulation model of the effects of vertical mixing on primary productivity. *Marine Biology*, *65*(1), 69–75. https://doi.org/10.1007/BF00397069

Falkowski, P. G., Dubinsky, Z., & Santostefano, G. (1985). Light-enhanced dark respiration in phytoplankton. *SIL Proceedings, 1922-2010*, *22*(5), 2830–2833. https://doi.org/10.1080/03680770.1983.11897784

Falkowski, P. G., Gan, R., & Wyman, K. (1985). *Growth-irradiance relationships in phytoplankton*. *30*(2), 311–321.

Falkowski, P. G., Katz, M. E., Knoll, A. H., Quigg, A., Raven, J. A., Schofield, O., & Taylor, F. J. R. (2004). The evolution of modern eukaryotic phytoplankton. *Science*, *305*(5682), 354–360. https://doi.org/10.1126/science.1095964

Falkowski, P., & Kiefer, D. A. (1985). Chlorophyll a fluorescence in phytoplankton: relationship to photosynthesis and biomass*. *Journal of Plankton Research*, *7*(5), 715–731. https://doi.org/10.1093/plankt/7.5.715

Fawcett, S. E., & Ward, B. B. (2011). Phytoplankton succession and nitrogen utilization during the development of an upwelling bloom. *Marine Ecology Progress Series*, *428*, 13-31.

Finazzi, G., Moreau, H., & Bowler, C. (2010). Genomic insights into photosynthesis in eukaryotic phytoplankton. *Trends in Plant Science*, *15*(10), 565–572. https://doi.org/10.1016/j.tplants.2010.07.004

Fisher, N. L., & Halsey, K. H. (2016). Mechanisms that increase the growth efficiency of diatoms in low light. *Photosynthesis Research*, *129*(2), 183–197. https://doi.org/10.1007/s11120-016-0282-6

Flameling, I. A., & Kromkamp, J. C. (1997). Photoacclimation of Scenedesmus protuberans (Chlorophyceae) to fluctuating irradiances simulating vertical mixing. *Journal of Plankton Research1*, *19*(8), 1011–1024.

Fratamico, A., Tocquin, P., & Franck, F. (2016). The chlorophyll a fluorescence induction curve in the green microalga Haematococcus pluvialis: further insight into the nature of the P–S–M fluctuation and its relationship with the "low-wave" phenomenon at steady-state. *Photosynthesis Research*, *128*(3), 271–285. https://doi.org/10.1007/s11120-016-0241-2

Gaarder, T., & Gran, H. H. (1927). Investigations on the primary production of plankton in the Oso Fjord. *Rapp. Cons. Explor. Mar*, *144*, 56-60.

Geider, R. J., & MacIntyre, H. L. (2002). Physiology and Biochemistry of Photosynthesis and Algal Carbon Acquisition. In *Phytoplankton Productivity* (pp. 44–77). https://doi.org/https://doi.org/10.1002/9780470995204.ch3

Genty, B., Briantais, J. M., & Baker, N. R. (1989). The relationship between the quantum yield of photosynthetic electron transport and quenching of chlorophyll fluorescence. *Biochimica et Biophysica Acta - General Subjects*, *990*(1), 87–92. https://doi.org/10.1016/S0304-4165(89)80016-9

Gorbunov, M. Y., Shirsin, E., Nikonova, E., Fadeev, V. V., & Falkowski, P. G. (2020). A multi-spectral fluorescence induction and relaxation (fire) technique for physiological and taxonomic analysis of phytoplankton communities. *Marine Ecology Progress Series*, *644*, 1–13. https://doi.org/10.3354/meps13358

Goss, R., & Lepetit, B. (2015). Biodiversity of NPQ. *Journal of Plant Physiology*, *172*, 13–32. https://doi.org/10.1016/j.jplph.2014.03.004

Grouneva, I., Jakob, T., Wilhelm, C., & Goss, R. (2009). The regulation of xanthophyll cycle activity and of non-photochemical fluorescence quenching by two alternative electron flows in the diatoms Phaeodactylum tricornutum and Cyclotella meneghiniana. *Biochimica et Biophysica Acta - Bioenergetics*, *1787*(7), 929–938. https://doi.org/10.1016/j.bbabio.2009.02.004

Guillard, R. L. (1975). Culture of phytoplankton for feeding marine invertebrates. In *Culture of Marine Invertebrate Animals* (pp. 29–60).

Halsey, K. H., & Jones, B. M. (2015). Phytoplankton Strategies for Photosynthetic Energy Allocation. *Annual Review of Marine Science*, *7*(1), 265–297. https://doi.org/10.1146/annurev-marine-010814-015813

Halsey, K. H., Milligan, A. J., & Behrenfeld, M. J. (2010). Physiological optimization underlies growth rate-independent chlorophyll-specific gross and net primary production. *Photosynthesis Research*, *103*(2), 125–137. https://doi.org/10.1007/s11120-009-9526-z

Halsey, K. H., Milligan, A. J., & Behrenfeld, M. J. (2011). Linking time-dependent carbon-fixation efficiencies in Dunaliella Tertiolecta (Chlorophyceae) to underlying metabolic pathways. *Journal of Phycology*, *47*(1), 66–76. https://doi.org/10.1111/j.1529-8817.2010.00945.x

Halsey, K. H., O'Malley, R. T., Graff, J. R., Milligan, A. J., & Behrenfeld, M. J. (2013). A common partitioning strategy for photosynthetic products in evolutionarily distinct phytoplankton species. *New Phytologist*, *198*(4), 1030–1038. https://doi.org/10.1111/nph.12209

Hennige, S. J., Smith, D. J., Perkins, R., Consalvey, M., Paterson, D. M., & Suggett, D. J. (2008). Photoacclimation, growth and distribution of massive coral species in clear and turbid waters. *Marine Ecology Progress Series*, *369*, 77–88. https://doi.org/10.3354/meps07612

Hoch, G., & Kok, B. (1963). A mass spectrometer inlet system for sampling gases dissolved in liquid phases. *Archives of Biochemistry and Biophysics*, *101*(1), 160–170. https://doi.org/10.1016/0003-9861(63)90546-0

Hughes, D. J., Campbell, D. A., Doblin, M. A., Kromkamp, J. C., Lawrenz, E., Moore, C. M., … Suggett, D. J. (2018a). Roadmaps and Detours: Active Chlorophyll- a Assessments of Primary Productivity Across Marine and Freshwater Systems. *Environmental Science and Technology*, *52*(21), 12039–12054. https://doi.org/10.1021/acs.est.8b03488

Hughes, D. J., Varkey, D., Doblin, M. A., Ingleton, T., Mcinnes, A., Ralph, P. J., … Suggett, D. J. (2018b). Impact of nitrogen availability upon the electron requirement for carbon fixation in Australian coastal phytoplankton communities. *Limnology and Oceanography*, *63*(5), 1891–1910. https://doi.org/10.1002/lno.10814

Hughes, D. J., Crosswell, J. R., Doblin, M. A., Oxborough, K., Ralph, P. J., Varkey, D., & Suggett, D. J. (2020). Dynamic variability of the phytoplankton electron requirement for carbon fixation in eastern Australian waters. *Journal of Marine Systems*, *202*(October 2019), 103252. https://doi.org/10.1016/j.jmarsys.2019.103252

Geider, R. J., & Osborne, B. A. (1989). Respiration and microalgal growth: a review of the quantitative relationship between dark respiration and growth. *New Phytologist*, *112*(3), 327–341. https://doi.org/10.1111/j.1469-8137.1989.tb00321.x

Jakob, T., Wagner, H., Stehfest, K., & Wilhelm, C. (2007). A complete energy balance from photons to new biomass reveals a light- and nutrient-dependent variability in the metabolic costs of carbon assimilation. *Journal of Experimental Botany*, *58*(8), 2101–2112. https://doi.org/10.1093/jxb/erm084

Jochem, F. J. (1999). Dark survival strategies in marine phytoplankton assessed by cytometric measurement of metabolic activity with fluorescein diacetate. *Marine Biology*, *135*(4), 721–728. https://doi.org/10.1007/s002270050673

Kana, T. M., Cornwell, J. C., Zhong, L., & Cornwell, J. (2006). Coastal and Estuarine Research Federation Determination of Denitrification in the Chesapeake Bay from Measurements of N 2

Accumulation in Bottom Water Determination of Denitrification in the Chesapeake Bay from Measurements of N2 Accumulation in Bottom Wa. *Source: Estuaries and Coasts Estuaries and Coasts*, *29*(2), 222–231. Retrieved from http://www.jstor.org/stable/3809708%0Ahttp://www.jstor.org/page/info/about/policies/terms.jsp%0Ahttp://www.jstor.org

Kana, T. M., Darkangelo, C., Hunt, M. D., Oldham, J. B., Bennett, G. E., & Cornwell, J. C. (1994). Membrane lnlet Mass Spectrometer for Rapid Environmental Water Samples. *Response*, *66*(23), 4166–4170. Retrieved from http://pubs.acs.org/doi/abs/10.1021/ac00095a009

Kana, T. M. (1993). Rapid oxygen cycling in Trichodesmium thiebautii. *Limnology and Oceanography*, *38*(1), 18–24. https://doi.org/10.4319/lo.1993.38.1.0018

Kana, T. M. (1992). Relationship between photosynthetic oxygen cycling and carbon assimilation in Synechococcus Wh7803 (cyanophyta). *Journal of Phycology*, *28*(3), 304-308.

Keller, B., Vass, I., Matsubara, S., Paul, K., Jedmowski, C., Pieruschka, R., … Muller, O. (2019). Maximum fluorescence and electron transport kinetics determined by light-induced fluorescence transients (LIFT) for photosynthesis phenotyping. *Photosynthesis Research*, *140*(2), 221–233. https://doi.org/10.1007/s11120-018-0594-9

Klughammer, C., & Schreiber, U. (2008). Complementary PS II quantum yields calculated from simple fluorescence parameters measured by PAM fluorometry and the Saturation Pulse method. *PAM Application Notes*, *1*(1), 27–35. https://doi.org/citeulike-article-id:6352156

Kolber, Z., & Falkowski, P. G. (1995). Variations in Chlorophyll fluorescence yields in phytoplankton in the World Oceans. *Australian Journal of Plant Physiology*, *22*, 341–355.

Kolber, Z. S., Prasil, O., & Falkowski, P. G. (1998). Measurements of variable chlorophyll fluorescence using fast repetition rate techniques: defining methodology and experimental protocols. *Biochimica et Biophysica Acta - Bioenergetics*, *1367*, 88–106. Retrieved from papers2://publication/uuid/C591C675-7666-49B5-AB3C-16E2C3FCFD57

Lacour, T., Babin, M., & Lavaud, J. (2020). Diversity in Xanthophyll Cycle Pigments Content and Related Nonphotochemical Quenching (NPQ) Among Microalgae: Implications for Growth Strategy and Ecology. *Journal of Phycology*, *56*(2), 245–263. https://doi.org/10.1111/jpy.12944

Langdon, C. (1993). The significance of respiration in production measurements based on oxygen. *ICES Mar. Sci. Symp.*, *197*, 69–78. Retrieved from https://www.researchgate.net/publication/230889097

Langner, U., Jakob, T., Stehfest, K., & Wilhelm, C. (2009). An energy balance from absorbed photons to new biomass for Chlamydomonas reinhardtii and Chlamydomonas acidophila under neutral and extremely acidic growth conditions. *Plant, Cell and Environment*, *32*(3), 250–258. https://doi.org/10.1111/j.1365-3040.2008.01917.x

Lavaud, J., & Goss, R. (2014). *The Peculiar Features of Non-Photochemical Fluorescence Quenching in Diatoms and Brown Algae*. https://doi.org/10.1007/978-94-017-9032-1_20

Lavaud, J., Strzepek, R. F., & Kroth, P. G. (2007). Photo-protection capacity differs among diatoms: possible consequences on the spatial distribution of diatoms related to fluctuations in the underwater light Climate. *Limnology and Oceanography*, *52*(3), 1188–1194. https://doi.org/10.2307/4499689

Laws, E. A., & Wong, D. C. (1978). Studies of carbon and nitrogen metabolism by three marine phytoplankton species in nitrate-limited continuous culture1, 2. *Journal of Phycology*, *14*(4), 406-416.

Laws, E. A., & Bannister, T. T. (1980). Nutrient- and light-limited growth of Thalassiosira fluviatilis in continuous culture, with implications for phytoplankton growth in the ocean. *Limnology and Oceanography*, *25*(3), 457–473. https://doi.org/10.4319/lo.2004.49.6.2316

Laws, E. A. (1991). Photosynthetic quotients, new production and net community production in the open ocean. *Deep Sea Research Part A. Oceanographic Research Papers*, *38*(1), 143-167.

Laws, E. A., McClellan, S. A., & Passow, U. (2020). Interactive Effects of CO2, Temperature, Irradiance, and Nutrient Limitation on the Growth and Physiology of the Marine Diatom Thalassiosira pseudonana (Coscinodiscophyceae). *Journal of Phycology*, 1–11. https://doi.org/10.1111/jpy.13048

Lewitus, A. J., & Kana, T. M. (1995). Light Respiration in Six Estuarine Phytoplankton Species: Contrasts Under Photoautotrophic and Mixotrophic Growth Conditions. *Journal of Phycology*, *31*(5), 754–761. https://doi.org/10.1111/j.0022-3646.1995.00754.x

Lindemann, C., Backhaus, J. O., & St John, M. A. (2015). Physiological constrains on Sverdrup's Critical-Depth-Hypothesis: The influences of dark respiration and sinking. *ICES Journal of Marine Science*, *72*(6), 1942–1951. https://doi.org/10.1093/icesjms/fsv046

Litchman, E. (2007). Resource competition and the ecological success of phytoplankton. In *Evolution of primary producers in the sea* (pp. 351-375). Academic Press.

Lomas, M. W., & Glibert, P. M. (2000). Comparisons of nitrate uptake, storage, and reduction in marine diatoms and flagellates. *Journal of Phycology*, *36*(5), 903-913.

Longhurst, A., Sathyendranath, S., Platt, T., & Caverhill, C. (1995). An estimate of global primary production in the ocean from satellite radiometer data. *Journal of Plankton Research*, *17*(6), 1245–1271. https://doi.org/10.1093/plankt/17.6.1245

Mackey, K. R. M., Paytan, A., Grossman, A. R., & Bailey, S. (2008). A photosynthetic strategy for coping in a high-light, low-nutrient environment. *Limnology and Oceanography*, *53*(3), 900–913. https://doi.org/10.4319/lo.2008.53.3.0900

Malviya, S., Scalco, E., Audic, S., Vincent, F., Veluchamy, A., Poulain, J., … Bowler, C. (2016). Insights into global diatom distribution and diversity in the world's ocean. *Proceedings of the National Academy of Sciences of the United States of America*, *113*(11), E1516–E1525. https://doi.org/10.1073/pnas.1509523113

Mantikci, M., Hansen, J. L. S., & Markager, S. (2017). Photosynthesis enhanced dark respiration in three marine phytoplankton species. *Journal of Experimental Marine Biology and Ecology*, *497*, 188–196. https://doi.org/10.1016/j.jembe.2017.09.015

Marra, J. F., Lance, V. P., Vaillancourt, R. D., & Hargreaves, B. R. (2014). Resolving the ocean's euphotic zone. *Deep-Sea Research Part I: Oceanographic Research Papers*, *83*, 45–50. https://doi.org/10.1016/j.dsr.2013.09.005

Martínez, E., Palacios, R., & Sanchez, F. (1987). Nitrogen-fixing nodules induced by Agrobacterium tumefaciens harboring Rhizobium phaseoli plasmids. *Journal of bacteriology*, *169*(6), 2828-2834.

Merz, E., Dick, G. J., Beer, D. De, Grim, S., Hübener, T., Littmann, S., … Klatt, J. M. (2020). Nitrate respiration and diel migration patterns of diatoms are linked in sediments underneath a microbial mat. *Environmental Microbiology*, *00*. https://doi.org/10.1111/1462-2920.15345

Milligan, A. J., Berman-Frank, I., Gerchman, Y., Dismukes, G. C., & Falkowski, P. G. (2007). Light-dependent oxygen consumption in nitrogen-fixing Cyanobacteria plays a key role in nitrogenase protection. *Journal of Phycology*, *43*(5), 845–852. https://doi.org/10.1111/j.1529-8817.2007.00395.x

Moore, C. M., Suggett, D. J., Hickman, A. E., Kim, Y.-N., Tweddle, J. F., Sharples, J., … Holligan, P. M. (2006). Phytoplankton photoacclimation and photoadaptation in response to environmental gradients in a shelf sea. *Limnol. Oceanogr*, *51*(2), 936–949. Retrieved from https://aslopubs.onlinelibrary.wiley.com/doi/pdf/10.4319/lo.2006.51.2.0936

Packard, T. T. (1973). The light dependence of nitrate reductase in marine phytoplankton 1. *Limnology and Oceanography*, *18*(3), 466-469.

Peers, G., & Price, N. M. (2006). Copper-containing plastocyanin used for electron transport by an oceanic diatom. *Nature*, *441*(7091), 341–344. https://doi.org/10.1038/nature04630

Perkins, R., Williamson, C., Lavaud, J., Mouget, J. L., & Campbell, D. A. (2018). Time-dependent upregulation of electron transport with concomitant induction of regulated excitation dissipation in Haslea diatoms. *Photosynthesis Research*, *137*(3), 377–388. https://doi.org/10.1007/s11120-018-0508-x

Platt, T. C., Bird, D. F., Sathyendranath, S., & Cushing, D. H. (1991). Critical depth and marine primary production. *Proceedings of the Royal Society of London. Series B: Biological Sciences*, *246*(1317), 205–217. https://doi.org/10.1098/rspb.1991.0146

Raines, C. A. (2003). The Calvin cycle revisited. *Photosynthesis research*, *75*(1), 1-10.

Raven, J. A. (1988). Acquisition of nitrogen by the shoots of land plants: its occurrence and implications for acid-base regulation. *New Phytologist*, *109*(1), 1–20. https://doi.org/10.1111/j.1469-8137.1988.tb00212.x

Raven, J. A., Beardall, J., & Quigg, A. (2020). Light-Driven Oxygen Consumption in the Water-Water Cycles and Photorespiration, and Light Stimulated Mitochondrial Respiration. In *Photosynthesis in Algae: Biochemical and Physiological Mechanisms* (pp. 161–178). https://doi.org/10.1007/978-3-030-33397-3_8

Ritchie, R. J. (2006). Consistent sets of spectrophotometric chlorophyll equations for acetone, methanol and ethanol solvents. *Photosynthesis Research*, *89*(1), 27–41. https://doi.org/10.1007/s11120-006-9065-9

Robinson, C., Suggett, D. J., Cherukuru, N., Ralph, P. J., & Doblin, M. A. (2014). Performance of Fast Repetition Rate fluorometry based estimates of primary productivity in coastal waters. *Journal of Marine Systems*, *139*, 299–310. https://doi.org/10.1016/j.jmarsys.2014.07.016

Sakshaug, E., Bricaud, A., Dandonneau, Y., Falkowski, P. ., Kiefer, D. ., Legendre, L., … Takahashi, M. (1997). Parameters of photosynthesis: Definitions, theory and interpretation of results. *Journal of Plankton Research*, *19*(11), 1637–1670. https://doi.org/10.1093/plankt/19.11.1637

Sarthou, G., Timmermans, K. R., Blain, S., & Tréguer, P. (2005). Growth physiology and fate of diatoms in the ocean: A review. *Journal of Sea Research*, *53*(1-2 SPEC. ISS.), 25–42. https://doi.org/10.1016/j.seares.2004.01.007

Schuback, N., Schallenberg, C., Duckham, C., Maldonado, M. T., & Tortell, P. D. (2015). Interacting effects of light and iron availability on the coupling of photosynthetic electron transport and CO2-assimilation in marine phytoplankton. *PLoS ONE*, *10*(7), 1–30. https://doi.org/10.1371/journal.pone.0133235

Schuback, N., & Tortell, P. D. (2019). Diurnal regulation of photosynthetic light absorption, electron transport and carbon fixation in two contrasting oceanic environments. *Biogeosciences*, *16*(7), 1381–1399. https://doi.org/10.5194/bg-16-1381-2019

Serôdio, J., Cruz, S., Vieira, S., & Brotas, V. (2005). Non-photochemical quenching of chlorophyll fluorescence and operation of the xanthophyll cycle in estuarine microphytobenthos. *Journal of Experimental Marine Biology and Ecology*, *326*(2), 157–169. https://doi.org/10.1016/j.jembe.2005.05.011

Silsbe, G. M., & Kromkamp, J. C. (2012). Modeling the irradiance dependency of the quantum efficiency of photosynthesis. *Limnology and Oceanography: Methods*, *10*(SEPTEMBER), 645–652. https://doi.org/10.4319/lom.2012.10.645

Smetacek, V. (2012). Making sense of ocean biota: How evolution and biodiversity of land organisms differ from that of the plankton. *Journal of Biosciences*, *37*(4), 589–607. https://doi.org/10.1007/s12038-012-9240-4

Smith, G. J., Zimmerman, R. C., & Alberte, R. S. (1992). Molecular and physiological responses of diatoms to variable levels of irradiance and nitrogen availability: Growth of Skeletonema costatum in simulated upwelling conditions. *Limnology and Oceanography*, *37*(5), 989–1007. https://doi.org/10.4319/lo.1992.37.5.0989

Strzepek, R. F., & Harrison, P. J. (2004). Photosynthetic architecture differs in coastal and oceanic diatoms. *Nature*, *431*(7009), 689. https://doi.org/10.1038/nature02954

Su, W., Jakob, T., & Wilhelm, C. (2012). The impact of nonphotochemical quenching of fluorescence on the photon balance in diatoms under dynamic light conditions. *Journal of Phycology*, *48*(2), 336–346. https://doi.org/10.1111/j.1529-8817.2012.01128.x

Suggett, D. J., Goyen, S., Pettay, D. T., Szabó, M., Warner, M. E., Evenhuis, C., & Ralph, P. J. (2015). Functional diversity of photobiological traits within the genus Symbiodinium appears to be governed by the interaction of cell size with cladal designation. *New Phytologist*, *208*(2), 370–381. https://doi.org/10.1111/nph.13483

Suggett, D. J., Macintyre, H. L., & Geider, R. J. (2004). Evaluation of biophysical and optical determinations of light absorption by photosystem II in phytoplankton. *Limnology and Oceanography: Methods*, *2*(10), 316–332. https://doi.org/10.4319/lom.2004.2.316

Suggett, D. J., MacIntyre, H. L., Kana, T. M., & Geider, R. J. (2009a). Comparing electron transport with gas exchange: Parameterising exchange rates between alternative photosynthetic currencies for eukaryotic phytoplankton. *Aquatic Microbial Ecology*, *56*(2–3), 147–162. https://doi.org/10.3354/ame01303

Suggett, D. J., Moore, C. M., Hickman, A. E., & Geider, R. J. (2009b). Interpretation of fast repetition rate (FRR) fluorescence: Signatures of phytoplankton community structure versus physiological state. *Marine Ecology Progress Series*, *376*, 1–19. https://doi.org/10.3354/meps07830

Suggett, D. J., Oxborough, K., Baker, N. R., Macintyre, H. L., Kana, T. M., & Geider, R. J. (2003). Fast repetition rate and pulse amplitude modulation chlorophyll a fluorescence measurements for assessment of photosynthetic electron transport in marine phytoplankton. *European Journal of Phycology*, *38*(4), 371–384. https://doi.org/10.1080/09670260310001612655

Sun, J., & Liu, D. (2003). Geometric models for calculating cell biovolume and surface area for phytoplankton. *Journal of Plankton Research*, *25*(11), 1331–1346. https://doi.org/10.1093/plankt/fbg096

Tortell, P. D. (2005). Dissolved gas measurements in oceanic waters made by membrane inlet mass spectrometry. *Limnology and Oceanography: Methods*, *3*(1), 24–37. https://doi.org/10.4319/lom.2005.3.24

Tozzi, S., Schofield, O., & Falkowski, P. (2004). Historical climate change and ocean turbulence as selective agents for two key phytoplankton functional groups. *Marine Ecology Progress Series*, *274*(Raven 1997), 123–132. https://doi.org/10.3354/meps274123

Tréguer, P., Nelson, D. M., Van Bennekom, A. J., Demaster, D. J., Leynaert, A., & Quéguiner, B. (1995). The silica balance in the world ocean: A reestimate. *Science*, *268*(5209), 375–379. https://doi.org/10.1126/science.268.5209.375

Wagner, H., Jakob, T., & Wilhelm, C. (2006). Balancing the energy flow from captured light to biomass under fluctuating light conditions. *New Phytologist*, *169*(1), 95–108. https://doi.org/10.1111/j.1469-8137.2005.01550.x

Wagner, H., Jakob, T., Lavaud, J., & Wilhelm, C. (2016). Photosystem II cycle activity and alternative electron transport in the diatom Phaeodactylum tricornutum under dynamic light conditions and nitrogen limitation. *Photosynthesis Research*, *128*(2), 151–161. https://doi.org/10.1007/s11120-015-0209-7

Waite, A. M., Thompson, P. A., & Harrison, P. J. (1992). Does energy control the sinking rates of marine diatoms? *Limnology and Oceanography*, *37*(3), 468–477. https://doi.org/10.4319/lo.1992.37.3.0468

Ware, M. A., Hunstiger, D., Cantrell, M., & Peers, G. (2020). A chlorophyte alga utilizes alternative electron transport for primary photo-protection. *Plant Physiology*, *183*(4), 1735–1748. https://doi.org/10.1104/pp.20.00373

Waring, J., Klenell, M., Bechtold, U., Underwood, G. J. C., & Baker, N. R. (2010). Light-induced responses of oxygen photoreduction, reactive oxygen species production and scavenging in two diatom species. *Journal of Phycology*, *46*(6), 1206–1217. https://doi.org/10.1111/j.1529-8817.2010.00919.x

Weger, H. G., Herzig, R., Falkowski, P. G., & Turpin, D. H. (1989). Respiratory losses in the light in a marine diatom: measuremetns by short-term mass spectrometry. *Limnology and Oceanography*, *34*(7), 1153–1161.

Wilhelm, C., & Jakob, T. (2011). From photons to biomass and biofuels: Evaluation of different strategies for the improvement of algal biotechnology based on comparative energy balances. *Applied Microbiology and Biotechnology*, *92*(5), 909–919. https://doi.org/10.1007/s00253-011-3627-2

Wilhelm, C., Jungandreas, A., Jakob, T., & Goss, R. (2014). Light acclimation in diatoms: From phenomenology to mechanisms. *Marine Genomics*, *16*(1), 5–15. https://doi.org/10.1016/j.margen.2013.12.003

Williams, P. J. l. B., & Lefèvre, D. (2008). An assessment of the measurement of phytoplankton respiration rates from dark 14 C incubations. *Limnology and Oceanography: Methods*, *6*(1), 1–11. https://doi.org/10.4319/lom.2008.6.1

Xue, X., Gauthier, D. A., Turpin, D. H., & Weger, H. G. (1996). Interactions between photosynthesis and respiration in the green alga Chlamydomonas reinhardtii. Characterization of light-enhanced dark respiration. *Plant Physiology*, *112*(3), 1005–1014. https://doi.org/10.1104/pp.112.3.1005

Zhu, Y., Ishizaka, J., Tripathy, S. C., Wang, S., Sukigara, C., Goes, J., … Suggett, D. J. (2017). Relationship between light, community composition and the electron requirement for carbon fixation in natural phytoplankton. *Marine Ecology Progress Series*, *580*, 83–100. https://doi.org/10.3354/meps12310

3.9. Supplementary Information

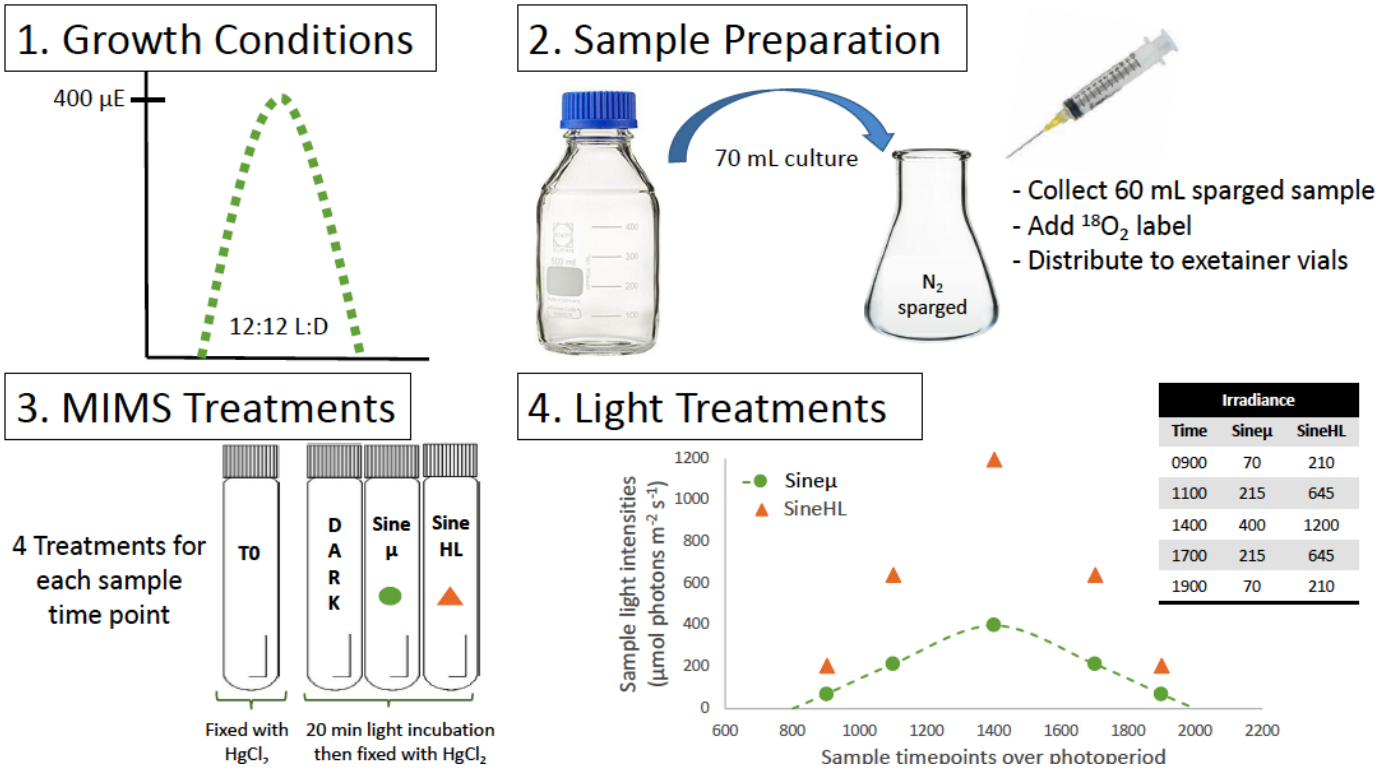

S3.1 Figure. Schematic of experimental design including (1) culture growth light regime, (2) sample preparation of sub-culture aliquots inoculated with labelled oxygen ($^{18}O_2$), (3) light treatments used to measure oxygen consumption and production using membrane inlet mass spectrometry (MIMS) and (4) sampling time points across the photoperiod with corresponding incubation irradiances for MIMS treatment samples ($Sine_{\mu}$ and $Sine_{HL}$).

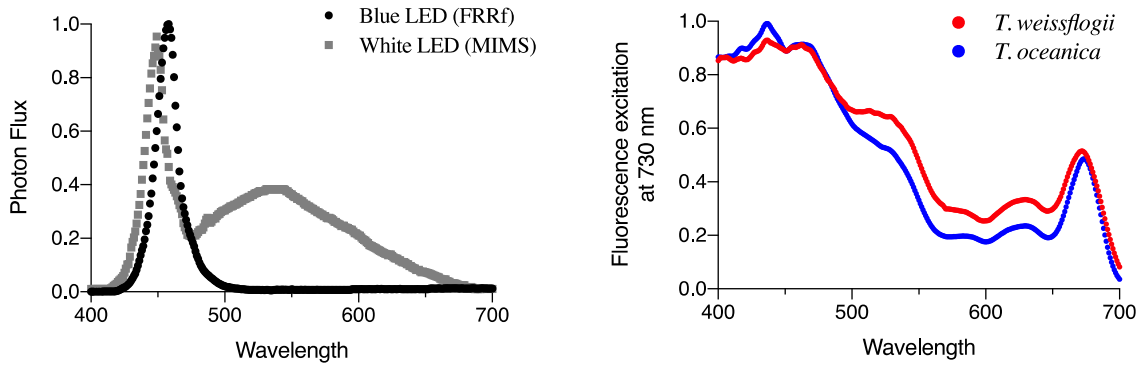

S3.2 Figure. Photon flux of light sources used for fluorescence (blue LED, black circles) and oxygen (white LED, grey squares) incubations and analyzed via FRRf and MIMS, respectively (left panel). Spectrally corrected fluorescence excitation detected at 730 nm of *T. weissflogii* (red dots) and *T. oceanica* (blue dots) weighting blue LED light to white LED light over photosynthetically active radiation (PAR, 400-700 nm) wavelengths (right panel). Note that the fluorescence excitation spectra for *T. weissflogii* and *T. oceanica* presented here were measured from cultures under different growth conditions than those described in Table 2.2.

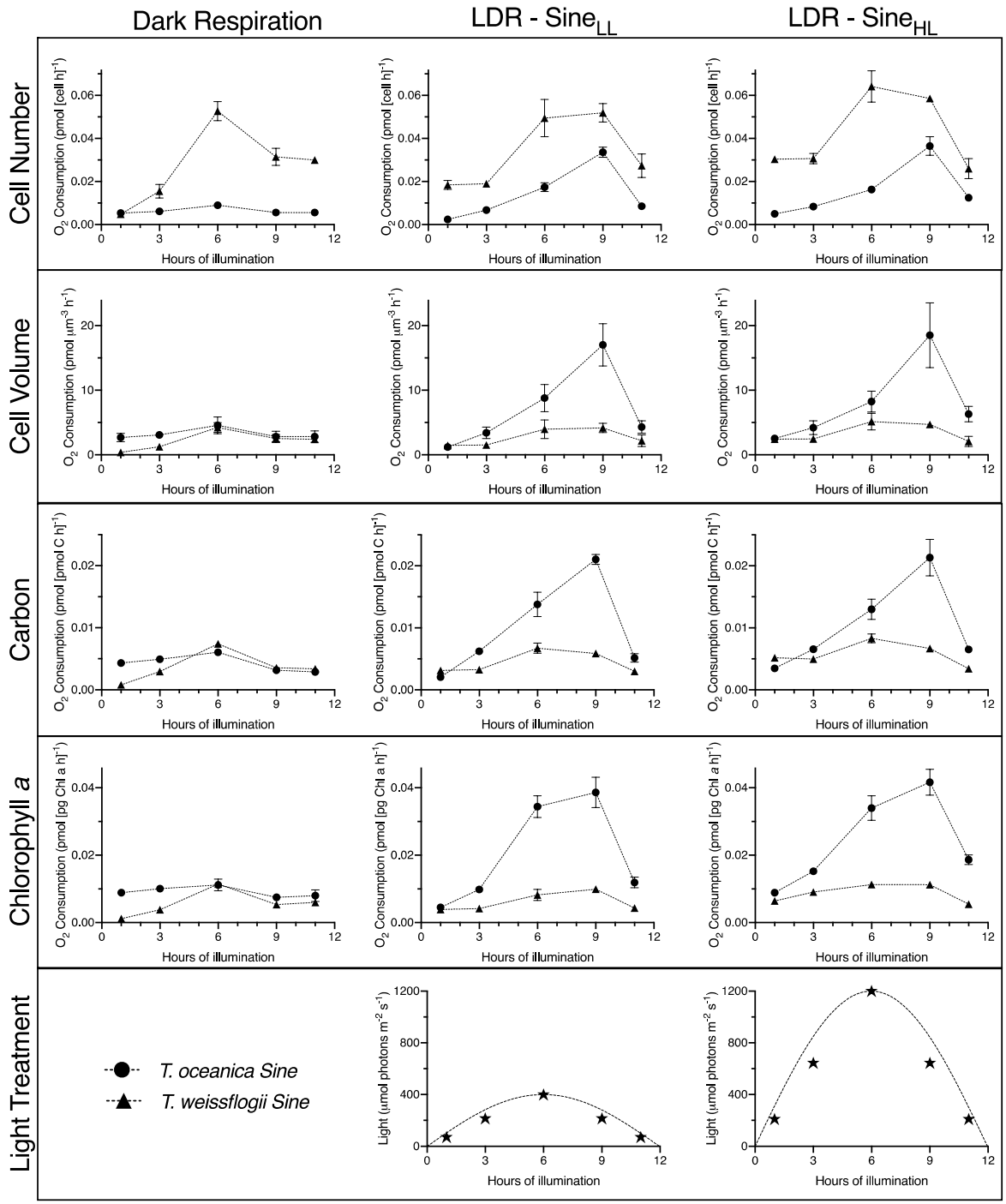

S3.3 Figure. Oxygen consumption in the dark and light by *T. oceanica* (circles) and *T. weissflogii* (triangles) acclimated to growth under 12 hours of sinusoidal light with a maximum intensity of 400 µmol photons m^{-2} s^{-1}. Dark respiration and LDR were measured over the photoperiod at 1, 3, 6, 9 and 11 hours. LDR measurements were completed at Sine$_{LL}$ and Sine$_{HL}$ light incubations for each timepoint

as denoted in the "Light Treatment" panel. Remaining panels ('cell number', 'cell volume', 'carbon' and 'chlorophyll *a*') show oxygen consumption measurements normalised to the corresponding parameter. Error bars for 'cell number', 'carbon' and 'chlorophyll *a*' panel graphs represent SEM while the error associated with 'cell volume' normalisations were calculated using the percentage of uncertainty to get the propagation of error for averages from at least three independent biological replicates.

S3.1 Table. PE curve parameters for *T. oceanica* and *T. weissflogii* grown over 12:12 L:D photoperiod following a sinusoidal light regime with a maximum irradiance of 400 μmol photons m^{-2} s^{-1}. PE curves were collected after 1, 3, 6, 9 and 11 hours following the onset of illumination. YII_{max}, is the maximum fluorescence-derived photochemical conversion at PSII, α is the light-limiting slope, $E_{k,YII}$ is the light saturation index calculated as YII_{max}/α and R^2 represents the goodness of fit. Values in parentheses represent the SE of the mean for at least three independent replicates.

PE Curve Parameter	Hours of Light	***T. oceanica***	***T. weissflogii***
YII_{max} (YII)	1	0.728 (0.005)	0.727 (0.006)
	3	0.723 (0.005)	0.729 (0.002)
	6	0.695 (0.009)	0.714 (0.017)
	9	0.685 (0.007)	0.724 (0.004)
	11	0.691 (0.008)	0.727 (0.003)
α ($x10^{-2}$)	1	0.278 (0.009)	0.160 (0.004)
	3	0.280 (0.032)	0.150 (0.003)
	6	0.475 (0.057)	0.214 (0.019)
	9	0.540 (0.051)	0.357 (0.043)

	11	0.439 (0.037)	0.287 (0.033)
$E_{k,YII}$	1	263.32 (9.90)	455.84 (12.37)
	3	270.92 (21.88)	486.78 (10.70)
	6	156.58 (17.29)	342.62 (25.52)
	9	131.48 (10.12)	212.58 (27.18)
	11	161.60 (12.75)	263.23 (29.49)
R^2	1	0.994 (0.001)	0.997 (0.001)
	3	0.988 (0.001)	0.996 (0.001)
	6	0.982 (0.004)	0.988 (0.002)
	9	0.984 (0.001)	0.987 (0.001)
	11	0.989 (0.001)	0.991 (0.000)

S3.2 Table. Pearson correlation parameters for various comparisons between measures of oxygen (GP_{O2}, R_{TOTAL}, LDR, Net_{O2}), fluorescence (YII, YNPQ, YNO, $E_{k,YII}$) and biomass (carbon, pg cell^{-1}) combining replicate (n=3) measurements for all time points over the photoperiod for *T. oceanica* and *T. weissflogii* under $Sine_{\mu}$ and $Sine_{HL}$. Significant correlations ($p < 0.05$) shown in bold. Values in parenthesis respresent SE of the mean (n=3).

Variable Comparisons	Pearson Correlation Parameters	*T. oceanica*		*T. weissflogii*	
		$Sine_{\mu}$	$Sine_{HL}$	$Sine_{\mu}$	$Sine_{HL}$
YII vs GP_{O2}	Slope	-9.213 (0.974)	-8.746 (1.614)	-25.11 (5.796)	-49.52 (8.873)
	Y-intercept	0.653 (0.025)	0.454 (0.045)	0.727 (0.039)	0.809 (0.080)
	R^2	0.856	0.662	0.591	0.706
	r	-0.925	-0.814	-0.769	-0.840

	p value	**<0.0001**	**<0.0001**	**0.0008**	**<0.0001**
YNPQ vs LDR	Slope	0.567 (0.124)	0.145 (0.092)	0.009 (0.005)	0.011 (0.002)
	Y-intercept	-0.002 (0.006)	0.010 (0.009)	0.005 (0.001)	0.006 (0.001)
	R^2	0.600	0.142	0.230	0.676
	r	0.775	0.377	0.479	0.822
	p value	**0.0004**	0.1358	0.0706	**<0.0001**
LDR vs GP_{O2}	Slope	-0.626 (1.215)	-3.850 (1.170)	-1.555 (7.203)	-4.899 (10.00)
	Y-intercept	0.234 (0.031)	0.355 (0.033)	0.181 (0.048)	0.276 (0.091)
	R^2	0.017	0.419	0.004	0.018
	r	-0.132	-0.648	-0.060	-0.135
	p value	0.614	**0.0049**	0.832	0.632
YII vs LDR	Slope	-0.055 (0.122)	0.191 (0.134)	-0.152 (0.217)	0.247 (0.157)
	Y-intercept	0.246 (0.059)	0.216 (0.038)	0.259 (0.126)	0.139 (0.065)
	R^2	0.013	0.119	0.036	0.160
	r	-0.115	0.345	-0.191	0.400
	p value	0.662	0.176	0.495	0.140
YII vs R_{TOTAL}	Slope	-0.107 (0.009)	-0.085 (0.015)	-0.052 (0.008)	-0.029 (0.004)
	Y-intercept	0.080 (0.004)	0.055 (0.004)	0.041 (0.005)	0.025 (0.002)
	R^2	0.917	0.724	0.773	0.808
	r	-0.958	-0.851	-0.879	-0.899
	p value	**<0.0001**	**<0.0001**	**<0.0001**	**<0.0001**

YNPQ vs R_{TOTAL}	Slope	0.564 (0.139)	0.185 (0.095)	0.028 (0.006)	0.022 (0.004)
	Y-intercept	0.009 (0.006)	0.016 (0.001)	0.009 (0.001)	0.009 (0.001)
	R^2	0.559	0.227	0.633	0.755
	r	0.748	0.477	0.796	0.869
	p value	**0.0014**	0.7787	**0.0004**	**<0.0001**
YNO vs R_{TOTAL}	Slope	0.112 (0.011)	0.102 (0.015)	0.081 (0.018)	-0.072 (0.028)
	Y-intercept	-0.026 (0.006)	-0.033 (0.010)	-0.019 (0.007)	0.042 (0.011)
	R^2	0.885	0.774	0.598	0.335
	r	0.941	0.880	0.773	-0.579
	p value	**<0.0001**	**<0.0001**	**0.0007**	**0.0238**
$E_{k,YII}$ vs R_{TOTAL}	Slope	1.96e-4 (5.15e-5)	n/a	-2.84e-5 (1.06e-5)	n/a
	Y-intercept	0.072 (0.011)	n/a	0.021 (0.004)	n/a
	R^2	0.526	n/a	0.354	n/a
	r	-0.725	n/a	-0.595	n/a
	p value	**0.0022**	n/a	**0.0193**	n/a
$E_{k,YII}$ vs Net_{O2}	Slope	1.18e-3 (2.62e-4)	n/a	4.41e-4 (1.39e-4)	n/a
	Y-intercept	-0.052 (0.058)	n/a	0.001 (0.050)	n/a
	R^2	0.608	n/a	0.435	n/a
	r	0.780	n/a	0.659	n/a
	p value	**0.0006**	n/a	**0.0075**	n/a
$E_{k,YII}$ vs C $cell^{-1}$	Slope	-0.040 (0.010)	n/a	-0.144 (0.020)	n/a

	Y-intercept	28.52 (2.217)	n/a	143.9 (7.289)	n/a
	R^2	0.551	n/a	0.797	n/a
	r	-0.742	n/a	-0.893	n/a
	p value	**0.0015**	n/a	**<0.0001**	n/a

S3.3 Table. Rates of oxygen production and consumption. MIMS analysis of gross oxygen production (GP_{O2}), light dependent respiration (LDR), dark respiration (R_{DARK}), and net oxygen production (Net_{O2}) for *T. weissflogii* and *T. oceanica* grown under a sinusoidal light regime with a maximum of 400 µmol photons m^{-2} s^{-1} ($Sine_{\mu}$) over a 12:12 L:D cycle. Rates were also collected from a transient exposure to high light that was 3x $Sine_{\mu}$ ($Sine_{HL}$) at the time of sampling. Samples were collected during the photoperiod at 1, 3, 6, 9 and 11 hours. Data averaged from at least 3 independent replicates. Values in parentheses are SE of the mean. For direct comparison with oxygen consumption/production rates from Chapter 2 see S2.1 Table.

Species + Growth Regime	Hours of Light	**pmol cell^{-1} h^{-1}**			
		R_{DARK}	**LDR**	**Net_{O2}**	**GP_{O2}**
$Sine_{\mu}$					
T. oceanica	1	0.005 (0.001)	0.002 (0.000)	0.087 (0.001)	0.097 (0.001)
	3	0.006 (0.000)	0.007 (0.001)	0.228 (0.006)	0.242 (0.007)
	6	0.009 (0.001)	0.017 (0.002)	0.116 (0.001)	0.144 (0.003)
	9	0.006 (0.001)	0.034 (0.002)	0.078 (0.003)	0.119 (0.003)
	11	0.006 (0.001)	0.009 (0.001)	0.097 (0.000)	0.131 (0.009)
T. weissflogii	1	0.005 (0.001)	0.018 (0.002)	0.504 (0.023)	0.529 (0.024)
	3	0.015 (0.003)	0.019 (0.002)	1.316 (0.055)	1.362 (0.059)
	6	0.053 (0.004)	0.049 (0.009)	1.153 (0.145)	1.250 (0.145)
	9	0.031 (0.004)	0.052 (0.004)	0.530 (0.044)	0.607 (0.040)
	11	0.030 (0.001)	0.027 (0.006)	0.514 (0.033)	0.576 (0.039)

	$Sine_{HL}$				
T. oceanica	1	-----	0.005 (0.000)	0.150 (0.006)	0.161 (0.007)
	3	-----	0.008 (0.001)	0.235 (0.006)	0.249 (0.006)
	6	-----	0.016 (0.001)	0.111 (0.004)	0.130 (0.005)
	9	-----	0.036 (0.004)	0.071 (0.005)	0.113 (0.002)
	11	-----	0.012 (0.001)	0.121 (0.005)	0.142 (0.001)
T. weissflogii	1	-----	0.030 (0.002)	1.108 (0.023)	1.150 (0.028)
	3	-----	0.031 (0.002)	1.640 (0.010)	1.710 (0.016)
	6	-----	0.064 (0.007)	1.183 (0.125)	1.295 (0.124)
	9	-----	0.059 (0.001)	0.511 (0.051)	0.595 (0.050)
	11	-----	0.026 (0.005)	0.914 (0.137)	0.975 (0.137)

Chapter 4

Light-dependent metabolic phenotype of the model diatom *Thalassiosira pseudonana*

Nerissa L. Fisher[1]*, Kimberly H. Halsey[2], David J. Suggett[1], Michelle Pombrol[2], Peter J. Ralph[1], Adrian Lutz[3a], Emilia M. Sogin[4b], Jennifer L. Matthews[1]*

[1] Climate Change Cluster, University of Technology Sydney, Ultimo 2007, NSW, Australia

[2] Department of Microbiology, Oregon State University, Corvallis, Oregon, USA

[3] Metabolomics Australia, University of Melbourne, Parkville 3052, VIC Australia

[4] Max Planck Institute for Marine Microbiology, Bremen, Germany

[a] Present address: Department of Microbiology & Immunology, the University of Melbourne, Parkville 3052, VIC Australia

*corresponding authors: nerissa.fisher@uts.edu.au, jennifer.matthews@uts.edu.au

Submitted for peer-review January 2020 to *Journal of Experimental Botany*

4.1. Abstract

'Omics'-based assessments are powerful tools to gain deeper insights into phytoplankton physiology. Light is a major factor altering phytoplankton physiology. Diatoms are especially responsive to dynamic light and are major producers of carbon and energy in aquatic ecosystems. We integrated independent transcriptomic and metabolomic datasets for the model centric diatom, *Thalassiosira pseudonana,* that was acclimated to high and low light intensities. These independent analyses merged to reveal key strategies used by *T. pseudonana* to shift carbon and energy fluxes depending on light-determined growth rate. The diatom relies on several regulated steps to shift central metabolism towards biosynthesis for rapid cell growth under high light or into pathways that conserve photosynthetic energy under low light. These pathways connected metabolic pools detected in the different treatments and helped reveal that low-light acclimated cells downregulated energy and carbon loss processes (e.g. glycolysis, TCA cycle) and instead utilised more conservative pathways (i.e. gluconeogenesis, glyoxylate cycle). These data highlight the value of combined metabolite and gene profiling to identify key metabolic switch points that may be leveraged in future cell-based models for predictions and manipulations of cell growth or bio-production.

4.2. Introduction

Diatoms are one of the most diverse (Mann & Vanormelinger 2013) and productive (Treguer et al. 1995, Armburst 2009) phytoplankton groups in aquatic systems, driving more net production than tropical rainforests or savannahs (Geider et al. 2001). In marine waters, diatoms thrive and bloom under physically complex conditions, particularly in coastal waters where nutrients are typically not the growth limiting factor (Tozzi et al. 2004) and light is highly dynamic (Richardson et al. 1983, MacIntyre et al. 2000). A wealth of research has helped explain how these factors regulate bloom

formation (Behrenfeld & Boss 2014), including diatom photo-physiological and/or biochemical responses to nutrient limitation (Behrenfeld et al. 2006; Kulk et al. 2013; Hughes et al. 2018) and light stress (Lavaud et al. 2007; Park et al. 2017) as well as corresponding energy allocation strategies/mechanisms employed/activated to sustain optimal fitness (Jakob et al. 2007; Wilhelm & Jakob 2011; Halsey & Jones 2015; Fisher & Halsey 2016; Wagner et al. 2006, 2017).

Rapid and high-throughput approaches that can capture (photo)physiological properties (e.g. bio-optics and active fluorometry, e.g. Moore et al. 2006; Behrenfeld et al. 2009; Suggett et al. 2009, 2010; Slisbe et al. 2015, 2016) have been useful to gain a first order understanding of how diatoms respond to dynamic environmental conditions. Photophysiology, particularly, for the sequenced model diatom *T. pseudonana*, under different light regimes to date has been largely examined through use of fluorescence-based assays of photosystem II (PSII) operation (e.g. Li & Campbell 2013; Li et al. 2017; Zhang et al. 2017; Chapter 2) and/or bulk cellular constituents (e.g. C and N allocation, Montagnes & Franklin 2001; Halsey et al. 2011, 2013, 2014). Emphasis on rapid moderations in electron flow through light harvesting or processing of electrons downstream of PSII has yielded useful insights into the changes in electron flow based on photosynthetic substrates (e.g. uptake of CO_2, NO_3 etc.) or products (e.g. O_2) (Fisher & Halsey 2016, Fisher et al. 2020). "Omics" platforms, particularly metabolomics, complement the wealth of current (photo)physiological knowledge for diatoms by providing information regarding the unique chemical fingerprints that arise in response to changing environments, which makes it possible to resolve the rapid and more complex metabolic processes at play. Research in recent years has focused on sequenced diatoms to connect "omics" platforms (e.g. genomics, transcriptomics and proteomics) to explain physiology (Monstant et al. 2007; McLean 2013; Levering et al. 2017) and elucidate the underlying function of targeted metabolites (Amin et al. 2015;

Johnson et al. 2016). Still, the emergent metabolic responses and underlying metabolic pathways underpinning responses to rapid changes in light availability that allow diatoms to maintain optimal fitness remains a black box.

Advances in 'omics' platforms – notably transcriptomics – have uncovered the regulatory pathways and networks responsible for fine-tuning diatom biology to changing environments (e.g. Ashworth et al. 2013, 2016; Smith et al. 2016; Cohen et al. 2018; Smith et al. 2019). Transcriptomics has indeed proven powerful (and most commonly employed to date), however, the fundamental nature by which phytoplankton appear to respond to rapid environmental changes is via post-translational modification of protein pools (Dyhrman et al. 2012; Launay et al. 2020) and metabolites (Bromke et al. 2013; Tan et al. 2019; Gauthier et al. 2020). While gene expression levels alone cannot predict phenotypes, metabolites are direct products of enzymatic reactions and thus provide a functional readout of the cellular networked response to an environment (Fernie et al. 2004). The model, sequenced diatom *Thalassiosira pseudonana* (Armburst et al. 2004) has been widely used in many omics-based studies, although studies exploring metabolomic responses in diatoms are limited to community interactions (Paul et al. 2013, Poulson-Ellestad et al. 2014), the exometabolome (Longnecker et al. 2017; Moore et al. 2020) and nutrient stress (Bromke et al. 2015, Heal et al. 2019) including salinity and pH (CO_2 concentration; Bromke et al. 2013). Together, these studies have improved understanding of the dynamic cellular processes of *T. pseduonana* but have largely overlooked the effect of light. Cross comparison of studies to date remains convoluted by the breadth of techniques (e.g. GC-MS, LC-MS, NMR) and sampling/extraction protocols used to assess the metabolome (Villas-Boas et al. 2007). To the best of our knowledge, there has yet to be a metabolomics-based study that has considered the role of light on the metabolite profile of *T. pseudonana* and, furthermore, none have considered whether

rapid photophysiological changes match dynamic reorganisation of the cell's metabolism (e.g. Lohr et al. 2019).

Here, we used metabolomics to examine how metabolic networks of *T. pseudonana* are altered under controlled manipulations of irradiance-driven steady state growth. We initially examined *T. pseudonana* grown under different constant light intensities to identify differences in gene expression and metabolites. We then compared the extent and nature of metabolite profile changes under light of the same intensity but delivered at half the daily total photon flux density dose (24:0 L:D constant vs. 12:12 L:D pulse). Together, our data provide a platform for conceptual integration (term coined by Cavill et al. 2016) of the genetic and molecular responses to light regime. Our work revealed fundamental shifts in central metabolism used to direct carbon and energy towards biosynthesis for rapid cell growth or into pathways that conserve photosynthetic energy to facilitate slow steady growth. Our data provide key metabolic switch points that may be leveraged in future cell-based models for predictions and manipulations of cell growth or bio-production.

4.3. Materials and methods

4.3.1. Culture conditions and maintenance

The diatom *Thalassiosira pseudonana* (CCMP 1335) was grown in a Multi-Cultivator (MC 1000-OD, Photon Systems Instrument (PSI), Drasov, Czech Republic), whereby light intensity and dose was altered across two different experiments (see "Light Treatments"). All cultures were maintained in exponential phase and optically thin (~10^6 cells mL^{-1}) via semi-batch dilutions as required at 20˚C using f/2+Si medium (Guillard 1975) supplemented with 0.17 µM Na_2SeO_3. Nitrate and phosphate

concentrations in the media reservoir were 250 and 50 µM, respectively (Laws & Bannister 1980) to avoid nutrient limitation. Small aliquots (3-4 mL) were drawn daily from each culture vessel for cell counts and photophysiology. Daily cell samples were preserved using glutaraldehyde (Sigma-Aldrich) until counted by chlorophyll fluorescence for 60 s at a rate of 30 µL min^{-1} via flow cytometry (CytoFlex S, Beckman Coulter, Miami, FL USA). Daily photophysiological assessment was performed on samples low light (<10 µmol photons m^{-2} s^{-1}) acclimated for 5 minutes (modified as per Suggett et al. 2015) before measuring fluorescence using a FastOcean Fast Repetition Rate fluorometer (FRRf; S/N: 12-8679-007) coupled to a bench-top FastAct unit (Chelsea Technologies Group Ltd., UK). The FRRf was programmed to deliver single turnover inductions consisting of 100 flashlets of 1.1 µs at 2.8 µs intervals to retrieve values of the maximum photochemical efficiency (F_v/F_m, dimensionless) and effective absorption cross section (σ_{PSII}, nm^2 $PSII^{-1}$) (e.g. Suggett et al. 2015) using the biophysical model of Kolber et al. (1998). A culture was considered to be in steady state growth for sampling when values of F_v/F_m and σ_{PSII} were consistent (<5% variance) across three consecutive days. Using this criterion, acclimation typically occurred over 2-5 weeks, depending on growth rate, to allow at least 7 generations. Once reaching steady state, samples were maintained at exponential growth phase via dilutions, and a minimum of four independent biological replicates per treatment were collected, with each replicate maintained as a semi-continuous batch culture over 2 months.

4.3.2. Light treatments

Two separate light-treatment experiments were performed by modifying the light delivered by the PSI Multicultivator LEDs (cool white light). First, cultures were grown in parallel under constant light (24:0 Light:Dark cycle) at three different light intensities, 200, 60, 5 µmol photons m^{-2} s^{-1}, referred to as HC, MC and LC, respectively. H, M, L signify light intensity as “high”, “medium”, “low”,

respectively, and C represents the light treatment "constant". In the second experiment, cultures were grown under pulse light (12:12 L:D cycle) at two light intensities, 200 and 5 µmol photons m^{-2} s^{-1}, referred to as HP and LP respectively, whereby P represents the "pulse" light treatment. Sampling was performed between 6-8 hours following the onset of light for the pulse treatment to standardise for time of day.

4.3.3. Chlorophyll and particulate organic carbon/nitrogen

Samples for chlorophyll were taken as 5 mL aliquots in duplicate from each biological replicate, each filtered onto a GF/F (Watmann, 25 mm) and extracted overnight at -20˚C in 90% acetone. Absorption was measured using a spectrophotometer (Aligent Technologies, Cary 60 UV-Vis) set at wavelengths 630, 657, 664, and 750 nm to calculate chlorophyll *a* concentration according to Ritchie (2006). Cellular particulate organic carbon (POC) and nitrogen (PON) were also measured in duplicate for each biological replicate, filtering 3-5 mL aliquots onto pre-combusted GF/F filters (Whatman, 25mm). Culture filtrate (5 mL) was also collected as background subtraction. Filters were stored at -20ºC until analysis on an elemental analyzer (LECO, Baulkham Hill, Australia).

4.3.4. Metabolomics sampling

To maintain cells acclimated to their steady state light environment, we gently filtered culture volumes under acclimated growth irradiance prior to immediate flash freezing. This was important to accommodate light-sensitive treatments and best capture the metabolic profile under a particular light regime, as opposed to the widely used current protocols where cultures are centrifuged (in the dark) to a pellet. For each sample, a volume of culture (for specific volumes and cell concentration per sample,

see S4.1 Table), was gently filtered under the respective experimental light intensity to minimise photoacclimatory changes from the growth light environment and concentrated down to 1 mL aliquots using a 2 µm polycarbonate membrane filter and a 47 mm GF/F backing filter. Cells maintained were in suspension during filtration for no more than 30 s by gently pipetting manually. The concentrated 1 mL culture was transferred to a 2 mL cryovial tube, immediately flash frozen in liquid nitrogen, and then stored at –80°C until extraction.

4.3.5. Metabolite extraction

Metabolite extraction followed in-house protocols adapted for marine algae (Metabolomics Australia, University of Melbourne). Each 1 mL concentrated sample was lyophilised overnight at -82°C under 0.1 mbar (Alpha 2-4 LDPlus, John Morris Scientific). To each dried sample, 450 µL 100% MeOH was added to extract the semi-polar metabolites and each sample vortexed. Cell slurry was transferred to clean 2 mL Eppendorf tube and an additional 450 µL 100% MeOH was used to rinse original tube and combined with sample. Samples were (1) vortexed, (2) sonicated (FX10 Ultrasonic Cleaner, Unisonics Pty Ltd, Australia) for 20 minutes at 4˚C to rupture the cells, (3) incubated at room temperature on a rotating platform at 1000 rpm for 30 min and finally (4) centrifuged for 10 min at 13000 rpm under 4°C to pellet cell debris. Supernatant was transferred and pellet re-suspended in 900 µL 50% MeOH to extract the polar metabolites. The re-suspended pellet mixture followed steps 1-4 outlined above. Again, the supernatant was transferred and added to the supernatant collected earlier. The combined supernatant was vortexed and centrifuged to avoid collecting cell debris. An aliquot of 850 µL of supernatant was added to 2 pre-weighed Eppendorf tubes, previously dried in a speedvac overnight. Both tubes with supernatant were dried in a speedvac (Eppendorf Concentrator 5301, Hamburg, Germany) overnight at 30˚C and re-weighed to determine a methanol extractable diatom metabolome

weight (i.e. ‘metabolite extract weight’). To prepare samples for GC-MS, individual extracts were derivatised following (Sogin et al. 2019), a protocol designed to measure metabolites from samples containing high concentrations of salts. All derivatised samples were processed within 1 day after derivatisation to avoid sample degradation and crystallisation of MeOX.

4.3.6. Metabolite analysis/GC-MS processing

Derivatised samples were analyzed using a GC (Agilent 7890B) coupled to a single quadrupole mass selective detector (Agilent 5944A) and an autosampler (Agilent 7693) as described in Sogin et al. (2019). The method was retention time locked using standard mixture of fatty acid methyl esters (Sigma Aldrich). Spectral components in a given sample were separated, detected and identified during deconvolution using AMDIS (http://chemdata.nist.gov/mass-spc/amdis/). Compound identification was based on an in-house library of MS spectra, with retention indices based on n-alkane and the standard mixes. Derivative peak areas from the GC-MS signal outputs were used to estimate relative abundance of individual metabolites. Data were then normalised to final area of the internal standard cholestane and then to sample ‘metabolite extract weight’.

4.3.7. Metabolite data normalisation

We chose to normalise our data by ‘metabolite extract weight’ (Raina et al. in review) instead of per cell or by, the more traditional normalisation metric, dry cellular biomass due to unforeseen circumstances using the sampling protocol of concentrating culture volume down to a 1 mL sample (see ‘*Metabolomics sampling*’ section above). Upon freeze drying, this 1 mL concentrated sample was subject to salt contamination, which ruled out the option to normalise by cell material dry weight. In

addition, normalisation per cell was not ideal since the cell density of LP was found to be significantly lower than all other light treatment samples ($p < 0.05$, see S4.2 Table for independent t-test comparisons) and subject to both biological and technological variation (De Livera et al. 2012). Therefore, normalising our data by 'metabolite extract weight' provided the most robust comparison across all light treatments.

4.3.8. Data processing and statistics

Statistical analyses of metabolomics data were processed using the software package MetaboAnalyst 4.0 (Chong et al. 2019). Normalised individual metabolites (using MetaboAnalyst) and physiological measurements (using IBM SPSS Statistics v26) were compared within and between light treatments using *t*-tests or ANOVAs set to a significance level of $p < 0.05$. Specifically, constant (HC, MC, LC) as well as HC, LC, HP, and LP light treatments were assessed using one-way ANOVAs followed by Tukey's multiple comparison test. To continue using these parametric tests, prerequisite assumptions of normality and homoscedasticity had to be satisfied, using Levene's and Shapiro-Wilk tests, respectively. If the assumption of normality was violated, data were either log or square-root transformed and the distribution of residuals re-tested. If either assumption continued to be violated despite transformation, differences between constant light treatments were instead evaluated using a non-parametric ANOVA on ranks (i.e. Kruskal-Wallis test), followed by Dunnett T3 post-hoc test. Pulse (HP and LP) light treatments were statistically assessed using Student's t-test. All statistical tests were set to a significance level of $p < 0.05$.

All data processed in MetaboAnalyst were log-transformed with no additional scaling. Principal component analysis (PCA) and partial least squares discriminant analysis (PLS-DA) were performed to assess information about sample groups via unsupervised and supervised methods, respectively. PLS-DA performance was assessed from ten-fold cross-validation based on Q^2 and goodness-of-fit (R^2) evaluated with permutation testing by prediction accuracy during training using 1000 iterations. To identify significant metabolites between treatments, significance analysis of microarray (SAM) plots with a false discovery rate (FDR) <10% were performed. SAM assigns a significance score to each metabolite based on relative changes to standard deviation between repeated measurements while FDR signifies the portion of metabolites found to be significant by chance. SAM was used to identify significant metabolites as it is better with high-dimensional data. ANOVA post-hoc comparisons were, subsequently, used to reveal significant differences between light treatments.

Assembling identified metabolites, especially those found to be significant, into metabolic pathways was completed using the software package VANTED (http://vanted.ipk-gatersleben.de, Junker et al. 2006) based on numerical identifiers from the Kyoto Encyclopedia of Gene and Genomes (KEGG) database (Kanehisa & Goto 2000).

4.3.9. Conceptual integration of metabolomes and transcriptomes from constant light treatments

While the focus of this experiment was to examine light-dependent metabolomic responses, we had the opportunity to also examine gene expression information for equivalent cultures grown under the constant light conditions. Here, cells were collected from cultures grown by the same operator (described in Fisher & Halsey 2016) under highly similar conditions. *T. pseudonana* CCMP 1335 was

grown to steady-state growth in continuous cultures at 200 and 5 μmol photons m^{-2} s^{-1} over a 24:0 L:D cycle. The slight culturing differences included temperature (18ºC) and light source (cool-white fluorescent tubes compared to LEDs). A 2ºC variation in the 18-20 ºC range gave similar physiological responses for *T. pseudonana* (Seehan et al. 2020). The spectral outputs for both light sources were compared. A spectral correction factor of 1.4 was used to weight the white LED light source to the cool-white fluorescent tube, and showed that light intensities experienced by *T. pseudonana* grown under high light ranged from 200 to 143 μmol photons m^{-2} s^{-1} and under low light ranged from 5 to 3.6 μmol photons m^{-2} s^{-1}; however, the magnitude of the growth irradiance differences between light treatments was the same. Cells were collected onto 0.2 μm filters, flash-frozen in liquid nitrogen, and stored at -80°C until RNA extraction and analysis using RNASeq-based transcriptomics to assess differences in gene expression. Given the independent nature of these experiments, we did not statistically compare across omics data sets but rather conceptually integrated (Cavill et al. 2016) patterns of metabolomic outcomes relative to transcriptional changes. Briefly, following established procedures (Dhyrman et al. 2012), total RNA was extracted from filters using a Qiagen RNeasy Midi Kit with the addition of silica beads (0.5 mm) to the lysis buffer, then reads were sequenced via Illumina HiSeq 3000 (see Supplementary information). Following quality trimming, sequence alignment, quality control measures and functional annotation, the results were compared between light treatments (equivalent to HC and LC metabolomics samples) using fold change (|FC|) cut-off of 2 with an adjusted *p*–value of 0.05.

All RNAseq data will be submitted to NCBI upon acceptance of this manuscript for publication.

4.4. Results

4.4.1. Physiological effects of light treatment

T. pseudonana at acclimated growth under constant and pulse light doses induced growth rates that significantly increased with light intensity, from ca. 0.12 - 0.18 to 1.12 - 1.17 d^{-1} (Table 4.1). Light intensities ranged from 5 to 200 μmol photons m^{-2} s^{-1} and growth rates were comparable between light dose treatments for the same intensity (i.e. HC vs. HP and LC vs. LP) despite the integrated daily photon dose for constant light being double that of the pulse light. Culture cell densities (mL^{-1}) between constant light treatments were not significantly different; however, there was a significant difference between pulse light treatments (Table 4.1) where the mean fold change in HP:LP cell density was 2.23.

For the constant light dose treatments, Chl *a* $cell^{-1}$ decreased, while both C $cell^{-1}$ and N $cell^{-1}$ increased, with increasing light intensity. The trends observed for pulse light were consistent with constant light for Chl *a* $cell^{-1}$, while, unexpectedly, C $cell^{-1}$ and N $cell^{-1}$ content was higher under lower light. Interestingly, regardless of light treatment (constant or pulse) the trend in the C:N ratio was higher under low light. Values for maximum photosynthetic efficiency (F_v/F_m, dimensionless) showed all treatments were highly efficient at harvesting light energy at PSII. Corresponding values of the effective cross section of PSII (σ_{PSII}, nm^2 $PSII^{-1}$) differed between constant and pulse light treatments. Under constant light, σ_{PSII} showed unexpected trends of decreasing under low light, whereas pulse light exhibited more expected trends whereby σ_{PSII} was higher under low light to maximise light capture. For statistical comparison of samples with matching average PFD across constant and pulse light dose treatments (HC-HP, LC-LP), an additional 2-way ANOVA was run to examine the influence of light

dose, light intensity and the interactive effect of light dose and light intensity (see S4.4 Table). All variables, except Chl *a* cell^{-1}, were significantly different for either light dose or light intensity and a significant interactive effect was revealed for C cell^{-1}, N cell^{-1} and F_v/F_m.

Table 4.1. Physiological characteristics of *Thalassiosira pseudonana* measured at the time of metabolomics sampling during steady-state acclimated growth to five different light regimes: Constant (high, medium, low), and Pulse (high, low) at 20°C. Values in parentheses represent SE of the mean for at least 3 independent biological replicates for specific growth rate (d^{-1}), cell density (mL^{-1}), Chl *a* ($cell^{-1}$), carbon (pg $cell^{-1}$), nitrogen (pg $cell^{-1}$), C:N, F_v/F_m and σ_{PSII} (nm^2 $PSII^{-1}$). ANOVA or Kruskal-Wallis (KW) test results are presented using F or H-values, respectively, for constant light treatments followed by Tukey post-hoc analysis with differences between individual cell characteristics and light intensity designated by superscripted letters and Student's *t* – test using t-values for pulse light treatments with significant *p* values ($p < 0.05$) in bold. For 2-way ANOVA test results for light treatments of equal PFD (HC-HP, LC-LP) see S4.4 Table.

Light Dose (L:D cycle)	Light Level Treatment	Avg PFD (µmol photons m^{-2} s^{-1})	Growth rate (d^{-1})	Cells mL^{-1} ($x10^6$)	Chl *a* $cell^{-1}$ (pg)	C $cell^{-1}$ (pg)	N $cell^{-1}$ (pg)	C:N	F_v/F_m	σ_{PSII} (nm^2 $PSII^{-1}$)
Constant (24:0)	High (HC)	**200**	**1.17^a** (0.08)	**2.35** (0.29)	**0.30^a** (0.04)	**14.61^a** (1.39)	**2.38^a** (0.28)	**6.16^a** (0.16)	**0.52^a** (0.00)	**3.82^a** (0.05)
	Med (MC)	**60**	**1.06^a** (0.03)	**2.16** (0.11)	**0.28^a** (0.01)	**10.23^b** (0.45)	**1.75^b** (0.12)	**6.00^a** (0.62)	**0.53^a** (0.00)	**3.91^a** (0.04)
	Low (LC)	**5**	**0.18^b** (0.00)	**1.59** (0.12)	**0.50^b** (0.03)	**10.32^c** (0.61)	**1.13^c** (0.10)	**9.34^b** (0.69)	**0.54^b** (0.00)	**3.45^b** (0.08)
	ANOVA or KW	F/H *p* value	H=8.38 **< 0.05**	F=3.92 > 0.05	F=17.64 **< 0.05**	F=74.06 **< 0.05**	F=15.65 **< 0.05**	H=9.10 **< 0.05**	F=6.23 **< 0.05**	F=14.26 **< 0.05**
Pulse (12:12)	High (HP)	**200**	**1.12** (0.10)	**1.77** (0.15)	**0.15** (0.01)	**8.87** (0.96)	**1.27** (0.16)	**7.55** (0.30)	**0.55** (0.00)	**3.28** (0.03)
	Low (LP)	**5**	**0.12** (0.01)	**0.80** (0.03)	**0.38** (0.03)	**17.70** (1.05)	**1.86** (0.18)	**9.80** (1.06)	**0.53** (0.00)	**3.47** (0.16)
	Student's *t*-test	t-value *p* value	3.52 **< 0.05**	7.18 **< 0.05**	6.92 **< 0.05**	15.30 **< 0.05**	8.81 > 0.05	14.07 **< 0.05**	166.29 > 0.05	39.78 **< 0.05**

4.4.2. Light-dependent effects on metabolic profiles

Distinctions in free metabolite pools, defined as those metabolites that are freely available in the cellular matrix, were evident between light intensity (i.e. constant) and light dose (i.e. pulse) treatments via spatial separation in the PCA plots (Fig 4.1A,B; S4.1A,B Fig). High (HC) and low (LC) constant light treatments exhibited no cluster overlap with one another, but both overlapped with the medium (MC) constant light, and together 38.2% and 21.5% of this variation was explained by PC1 and PC2, respectively (Fig 4.1A). High (HP) and low (LP) pulse light treatments exhibited slight overlap, with variation by PC1 and PC2 explained by 56 and 22.3%, respectively (S4.1A Fig). Directly comparing the high and low light intensities for constant (HC, LC) and pulse treatments (HP, LP) further revealed less distinct clusters via PCA (S4.1B Fig). However, PLS-DA analysis revealed spatial separation along 4 components ($Q^2 = 0.861$), which suggests high vs low light has an effect on the metabolite profiles, although larger sample sizes are required to validate the classification model fit (10-fold cross-validation; $p = 0.155$). Still, light regime (i.e. total daily integrated photon dose) appeared to exert a relatively consistent effect on the free metabolite pool, that was instead influenced more by the acclimated growth light intensity.

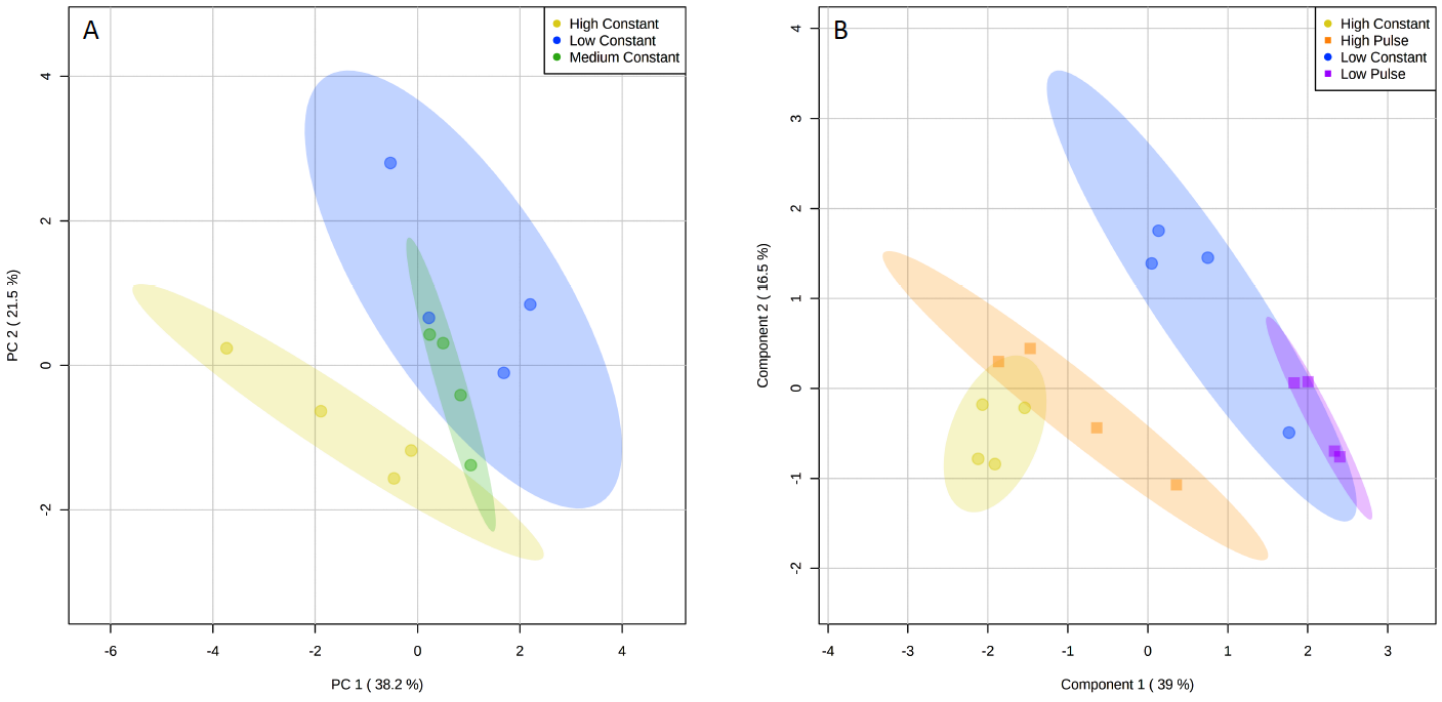

Figure 4.1. (A) PCA of relative metabolite abundances for constant light treatments (24:0 L:D) at high (yellow circles), medium (green circles) and low (blue circles) intensities. (B) PLS-DA of relative metabolite abundances for constant (high and low) and pulse (high – orange triangles, low – purple triangles) light treatments. Light intensities for high, medium and low are 200, 60 and 5 μmol photons m^{-2} s^{-1}, respectively. Data for relative metabolite abundances was normalised by internal standard then 'metabolite extract biomass'. Explained variances are shown as a percentage in brackets and shaded area is the 95% confidence region. Individual data points represent independent biological replicates (n=4).

Significant differences in metabolic profiles within and between light treatments were identified using SAM, supplemented by ANOVA generated Tukey post-hoc comparisons that represented significantly greater relative metabolite abundances. We first identified 9 metabolites that were significant within the constant light dose treatments (HC, MC, LC), whereby metabolite upregulation (i.e. higher relative concentration) varied between intensities (Fig 4.2). The metabolites identified were phytol, dihydroxybutyric acid (C4:1), eicosanioic acid (C20:0), threonic acid, furoic acid, fructose, aspartate, glyceryl-glycoside and lactate. Phytol, C20:0 and glyceryl-glycoside were more abundant at lower (MC, LC) light-acclimated intensities, C4:1 and fructose were more abundant at higher (MC, HC) light intensities, and threonic acid, furoic acid, aspartate and lactate were, specifically, more abundant in HC treatments (Fig 4.2). In the pulse light dose treatments (LP, HP), 11 metabolites were identified that significantly varied in relative abundance with light intensity (S4.2 Fig). Some of these metabolites were observed in both constant and pulse light dose treatments (e.g. C4:1, lactate, fructose, threonic acid, aspartate), but some metabolites identified by SAM were unique to pulse light dose treatments (e.g. arabinose, succinate, pentanoic acid (C5:0), myristic acid (C14:0), cycloartenol and anthraquinone) (S4.2 Fig) highlighting a potential time of day effect on metabolic profiles.

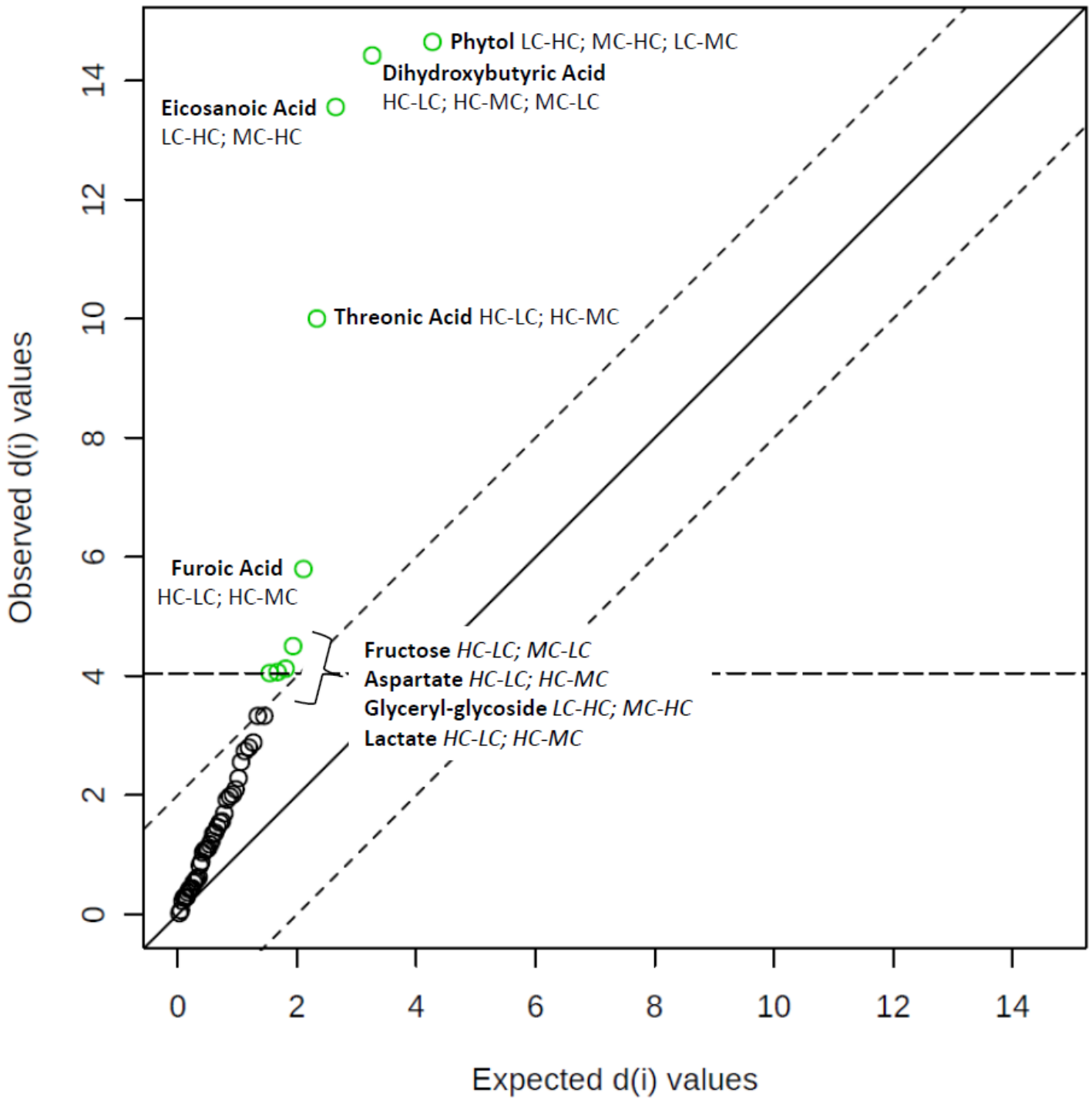

Figure 4.2. Significant metabolites (green circles) identified by SAM between constant light treatments (high - HC, medium - MC, low - LC). Significant metabolites determined from an ANOVA are distinguished in bold followed by Tukey post-hoc correlations in italics for a significance level of $p < 0.05$.

SAM-generated inter-comparisons between light treatments of equal average PFD but varying light dose (HC, HP, LC, LP) revealed 19 metabolites that significantly differed in relative abundance (Fig 4.3). Common significant metabolites with similar relationships to light intensity were identified included the 9 metabolites identified for the constant light intra-comparison (LC, MC, HC), except for glyceryl-glycoside, as well as the 11 metabolites identified for pulse light intra-comparison (LP, HP), except succinate (Table 4.2). Despite the aforementioned metabolite repeats, the inter-comparison of light treatments of equal average PFD did reveal new significant metabolites, including scyllo-inositol, ribose, trehalose, glucose, glycolic acid and butanoic acid (C4:0) (Fig 4.3, Table 4.2). Separating light dose treatments by light intensity highlighted that between low light intensity treatments, LC appeared to have larger pools of fructose, phytol, aspartate and glyceryl-glycoside compared to LP, whereas at high light intensities, fructose, C4:1, threonic acid, scyllo-inositol and furoic acid were present in higher amounts in HC compared to HP (Fig 4.3).

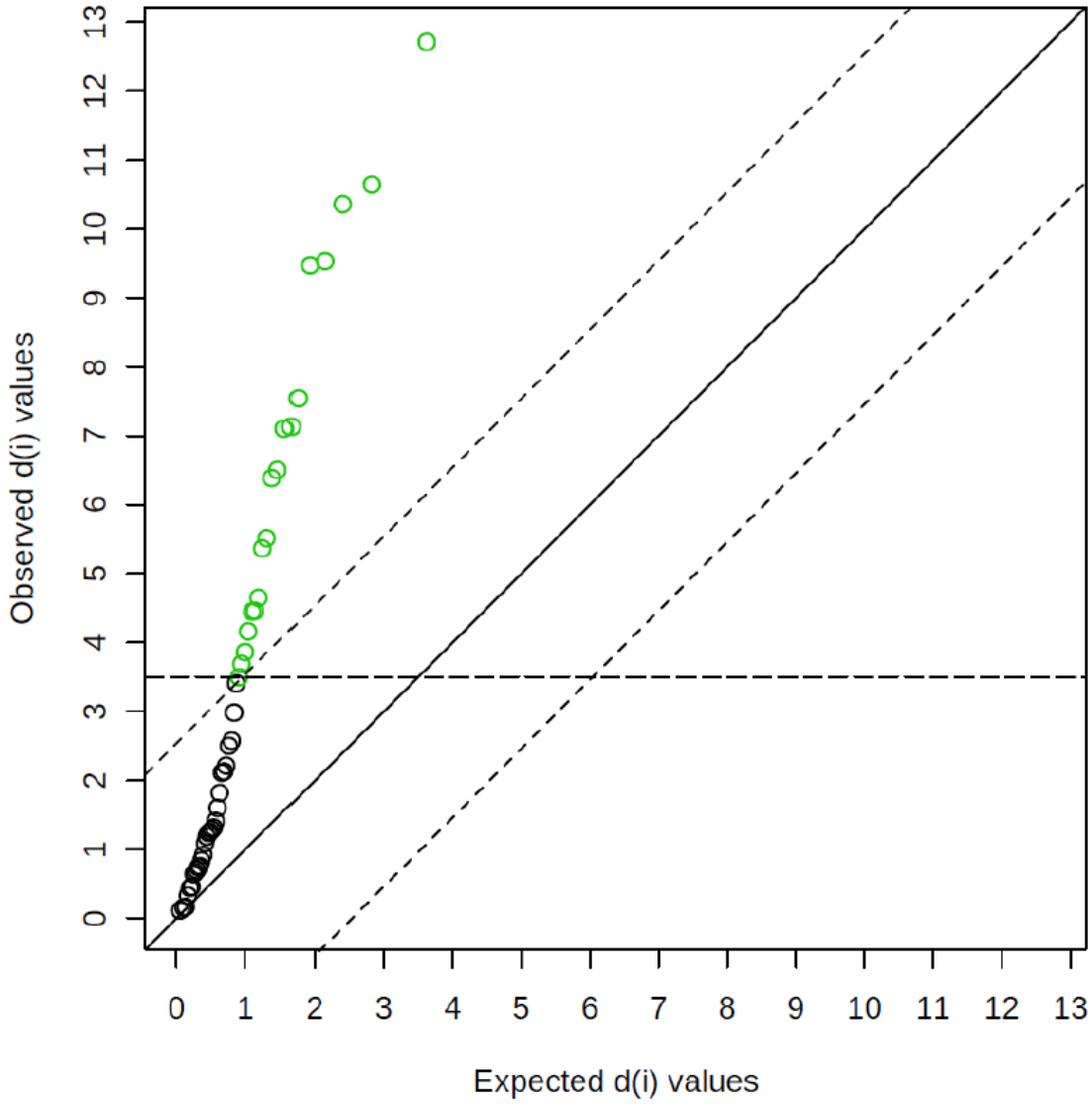

Fructose	HC - HP; HC - LC; HC - LP; HP - LP; LC - LP
Threonic acid	HC - HP; HC - LC; HC - LP; HP - LC; HP - LP
Dihydroxybutyric acid (C4:1)	HC - HP; HC - LC; HC - LP; HP - LC; HP - LP
Eicosanoic acid (C20:0)	LC - HC; LP - HC; LC - HP; LP - HP
Phytol	LC - HC; LP - HC; LC - HP; LC - LP
Anthraquinone	HC - LC; HC - LP; HP - LC; HP - LP; LC - LP
scyllo-Inositol	HC - HP; HC - LP; HP - LP; LC - LP
Aspartate	HC - LC; HC - LP; HP - LP; LC - LP
Lactate	HC - LC; HC - LP; HP - LC; HP - LP
Arabinose	HC - LC; HC - LP; HP - LP; LC - LP
Pentanoic acid (C5:0)	HC - LC; HC - LP; HP - LC; HP - LP
Butanoic acid (C4:0)	HC - LP; LC - HP; HP - LP; LC - LP
Myristic acid (C14:0)	HC - LP; HP - LP; LC - LP
Glycolic acid	HC - LC; HC - LP; HP - LP; LC - LP
Ribose	HC - LC; HC - LP; HP - LP
Lanosterol	HC - LP; HP - LP; LC - LP
Furoic acid	HC - HP; HC - LC; HC - LP
Trehalose	LC - HC; LC - HP
Glucose	HC - LP; HP - LP; LC - LP

Figure 4.3. Significant metabolites (green circles) identified by SAM between high and low constant and pulse light treatments (HC – high constant, HP – high pulse, LC – low constant, LP – low pulse). Significant metabolites are distinguished in bold followed by a Tukey post-hoc analysis generated from an ANOVA ($p < 0.05$).

Table 4.2. Compilation of SAM-identified significant metabolites for the various comparisons of light treatments – constant only (yellow), pulse only (green) and constant+pulse treatments of equal average PFD (blue).

Significant Metabolites	Constant (HC, MC, LC)	Pulse (HP, LP)	Constant+Pulse (HC, HP, LC, LP)
Butyric acid (C4:1)			
Threonic acid			
Fructose			
Aspartate			
Lactate			
Phytol			
Eicosanoic acid (C20:0)			
Furoic acid			
Glyceryl-glycoside			
Anthraquinone			
Lanosterol			
Myristic acid (C14:0)			
Pentaoic acid (C5:0)			
Succinate			
Arabinose			
scyllo-Inositol			
Ribose			
Trehalose			
Glucose			
Glycolate			
Butanoic acid (C4:0)			
TOTAL	**9**	**11**	**19**

Overall, lactate, aspartate, C4:1, fructose and threonic acid were the only metabolites that were statistically different for all comparisons of light intensity and light dose (Table 4.2). When comparing constant and pulse high and low light treatments, some metabolites were found to be exclusively significant on the basis of light intensity whereby lactate, C5:0 and ribose were consistently observed at high light intensities while C20:0 and

phytol were specific to low light intensities. Light intensity appeared to influence the specific metabolites identified as significant, but the relative abundances of those metabolites was seemingly more impacted by light dose (Fig 4.4).

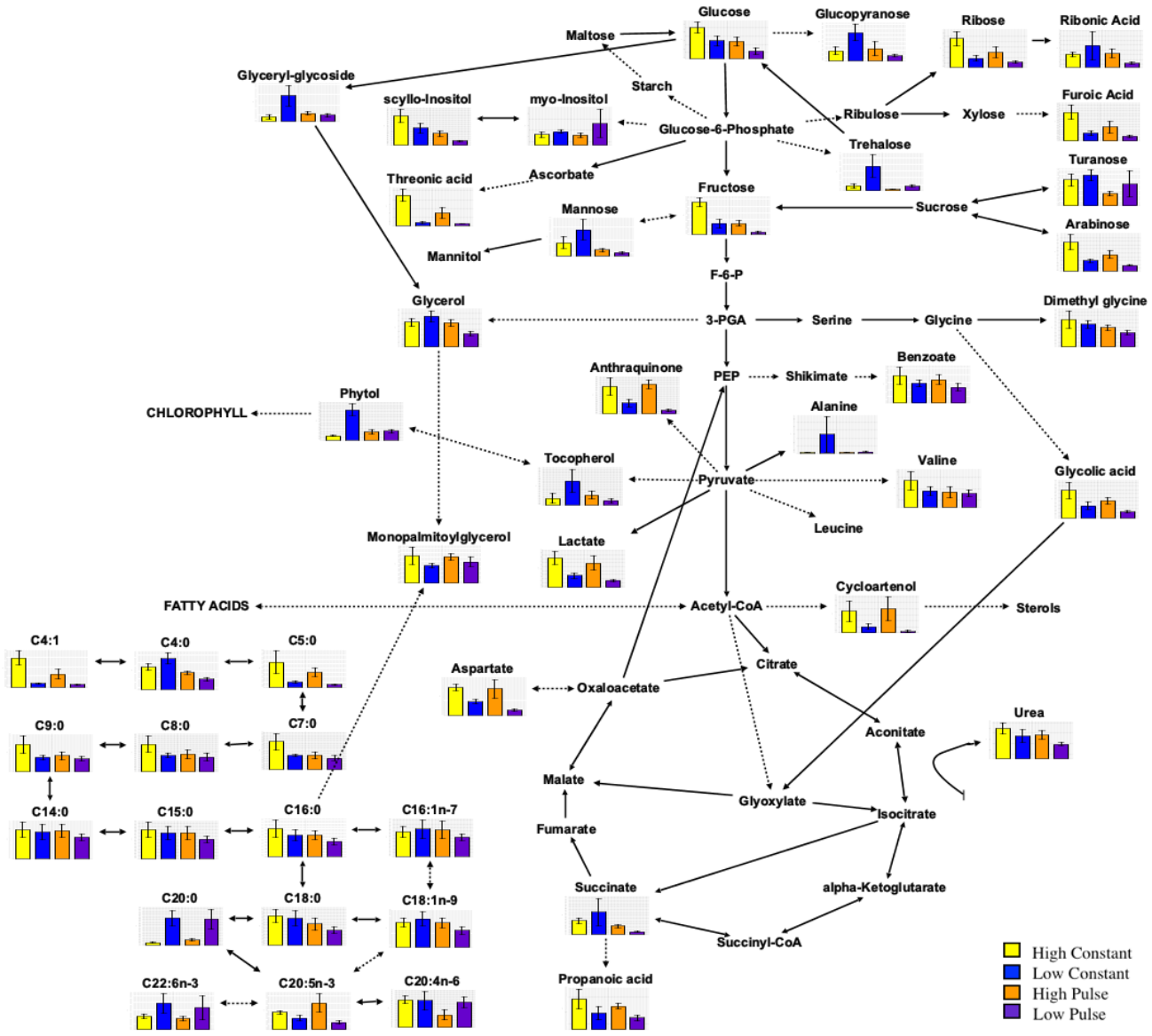

Figure 4.4. Summary metabolic pathway schematic of metabolites identified using GC-MS with overlaying plots of relative metabolite concentrations for high constant (HC, yellow bars), low constant (LC, blue bars), high pulse (HP, orange bars) and low pulse (LP, purple bars) light treatments. Solid lines indicate direct pathways between metabolites and dashed lines represent indirect pathways between metabolites.

4.4.3. Light-dependent gene expression of *T. pseudonana*

We next considered the metabolome responses in the context of differential gene expression observed in cells grown under HC and LC conditions. A total of 2904 genes (25% of the genome) were differentially expressed in HC compared to LC, using a |FC| > 2 cutoff (adjusted *p*-value <0.05). Of these genes, 1410 were upregulated in LC compared to HC and 1494 were downregulated in LC compared to HC. While the vast majority of the differentially expressed genes were unannotated in the KEGG database, many of the 86 genes upregulated in LC with annotated functions were associated with fatty acid metabolism, nucleotide sugar metabolism, and valine, leucine, and isoleucine degradation (S4.4 Table). Two of the most highly upregulated genes in LC had annotations involved in carbon metabolism: *PDK1_2* that encodes pyruvate-phosphate dikinase (PPDK, increased 6.65-fold) and *PCK1* that encodes phosphoenolpyruate carboxykinase (PCK1, increased 7.26-fold). Genes involved in processes associated with central carbon metabolism, such as the TCA cycle, the glyoxylate cycle and photorespiration, were also identified as differentially expressed. Although some of these genes fell below the |FC| > 2 cut-off, they remained significantly differentially expressed ($p < 0.05$) (S4.4 Table) and help explain observed metabolic profile differences between light-acclimated treatments (see below). Overall, the transcriptional profiles helped identify of pathways leading to the metabolites we retrieved, and support interpretations of the metabolic profile pattern differences observed between high and low light acclimated *T. pseudonana* (Fig 4.4).

4.5. Discussion

We applied metabolomics within the context of diatom photoacclimation, demonstrating that light intensity (High – 200 µmol photons m^{-2} s^{-1}, Low – 5 µmol photons m^{-2} s^{-1}) generally drove greater differences in metabolite expression for *T. pseudonana* compared to light dose (constant, pulse). The metabolites retrieved from GC-MS represent the compilation of free metabolites, or those present in the cellular matrix, under the

various light treatments at the time of sampling. In cells growing at steady state, a free metabolite could therefore indicate a metabolite that is (1) being actively produced in high quantities to meet high cellular demand or (2) used at a slower rate than it is consumed (i.e., has a slow turnover rate) under the current environmental conditions.

The light intensity-driven differences in metabolic profiles coupled with gene expression patterns reveal the careful metabolic balance required to maintain energy and carbon flux under widely ranging light conditions. Growth in high light led to the accumulation of metabolites indicative of cells capable of high energy and carbon investments. In low-light acclimated cells, free metabolites were associated with cellular maintenance activities. The combined differential metabolomic and gene expression data point to key pathway gating strategies that facilitate modest shifts in carbon flux that integrate to yield more than a five-fold change in growth rate.

Parallel (photo)physiological assessments of cellular functioning (Table 4.1) further support shotgun assessments of metabolites and other 'omics' data, including gene expression, to gain a systems-level understanding of growth and adaptation. Below we discuss how cells tune pathways from light-harvesting through central metabolism to achieve growth under widely varying light environments.

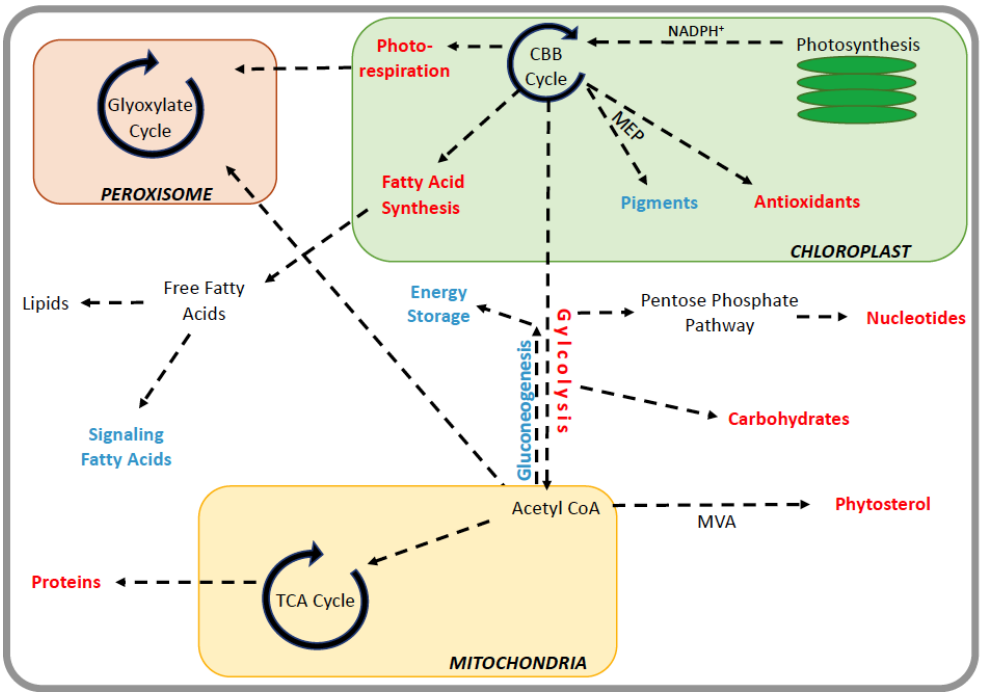

Associated significant metabolites upregulated under HIGH/LOW light	
Photorespiration	Glycolic Acid
Pigments	Phytol
Antioxidants	Anthraquinone
Fatty Acid Synthesis	C14:0, C4:0 , C4:1, C5:0
Signaling Fatty Acids	Eicosanoic Acid (C20:0)
Glycolysis	Glucose, Fructose, Lactate
Carbohydrates	Arabinose, Furoic Acid, Threonic Acid, scyllo-Inositol
Energy Storage	Trehalose
Proteins	Aspartate
Nucleotides	Ribose
Phytosterol	Cycloartenol

Figure 4.5. Schematic of the general metabolic changes for significant metabolites in *T. pseudonana* grown under high vs low light intensity for both constant and pulse light dose treatments. Blue indicates upregulation of relative metabolite concentrations for corresponding processes under lower light acclimation and red correlates to processes with associated significant metabolites that were upregulated under high light acclimation. Black indicates intermediary steps/processes that were not significantly up or down regulated according to the metabolites identified across all light treatments. Solid lines represent metabolic cycles and the dashed lines show the cellular pathways in which metabolites could be used within a cell.

4.5.1. Light harvesting and lipid biosynthesis → glycolysis

Higher concentrations of C14:0 (myristic acid or tetradecanoic acid), C16:0 (palmitic acid), and fatty acid intermediates needed for lipid biosynthesis were retrieved at generally higher concentrations in *T. pseudonana* under high light compared to low light. These fatty acid pools are associated with a greater Calvin-Benson-Bassham (CBB) cycle capacity (Dong et al. 2016). However, biomass production is not only determined by carbon production but also the overall energetic costs of cellular metabolism, including the biosynthesis and degradation of macromolecules (Shi et al. 2015; Wagner et al. 2017). Thus, while high light acclimated cells

maintained larger fatty acid pools facilitated by high rates of photosynthesis, low light acclimated cells maintained a lower "cost of living," in part by upregulating fatty acid degradation pathways, including genes encoding acyl-CoA dehydrogenase, glutaryl-CoA dehydrogenase, and a long-chain fatty acid CoA-ligase (S4.4 Fig).

Phytol, a constituent of chlorophyll *a* (Stonik & Stonik 2015), was significantly greater in low light treatments compared to high light treatments. The higher representation of metabolites associated with pigments can be attributed to an averaged two-fold (1.7 LC > HC and 2.5 LP > HP) greater concentration of chlorophyll *a* cell^{-1} under low light regardless of light dose (Table 4.1). In addition, higher concentrations of long chain poly-unsaturated fatty acids (e.g. oleic acid – C18:1n9 and docosahexaenoic acid – DHA, C22:6n3), though not statistically significant, were observed in low light treatments, suggesting a need for storage molecules that contain longer-lived energy in slow growing cells. A saturated fatty acid that had significantly higher concentrations in low light treatments was eicosanoic acid (C20:0), a signalling molecule (Matthews et al. 2017), that suggests a preparatory activity under low light that is less imperative under high light. However, given that our metabolic profiles were retrieved from free metabolite pools, the presence of C20:0 under low light could indicate that it accumulated in the cellular matrix because there was no cellular demand. Further research is required to resolve the upregulation of C20:0 in low light acclimated *T. pseudonana*.

High-light acclimated *T. pseudonana* showed higher relative abundances of sugar metabolites (e.g. glucose, fructose, arabinose, furoic acid threonic acid and scyllo-inositol). This collection of metabolites suggests that carbohydrate metabolism was upregulated to sustain higher energetic cellular demands. The bulk pools of carbohydrates and lipids are larger in diatoms grown under high light compared to low light (Fisher & Halsey 2016).

4.5.2. Glycolysis versus gluconeogenesis

In diatoms, glycolysis occurs in the cytosol to generate energy (ATP) and pyruvate, while gluconeogenesis works in opposition to glycolysis to produce carbon and energy storage molecules. We retrieved a collection of these storage metabolites, including storage sugars, trehalose and mannose (Michel et al. 2010; Obata et al. 2013; Villanova et al. 2017), in low light acclimated *T. pseudonana* (Fig 4.3). Complementing these results was the strong upregulation in low-light acclimated *T. pseudonana* of the genes encoding key enzymes, PPDK and PCK1. These enzymes increase flux through gluconeogenesis by catalyzing the conversion of pyruvate and oxaloacetate (OAA) to phosphoenolpyruvate (PEP) (S4.5 Table and S4.4 Fig). PPDK and PCK1 function as a primary hub that gates carbon flow through glycolysis or gluconeogenesis and into the tricarboxylic acid (TCA) cycle, fatty acid biosynthesis, and amino acid metabolism (Smith et al. 2012). The significantly larger pools of storage sugars in low-light acclimated cells are supported by upregulation of pathways leading through PEP into gluconeogenesis and away from pyruvate. In these slower growing cells, regulation of this critical hub appears to limit energy and carbon loss to rapid glycolytic activity. During low-light acclimated growth, low carbon fixation rates (Fisher & Halsey 2016) require mechanisms that prevent carbon depletion. The storage metabolites and transcripts identified in slow growing *T. pseudonana* provide evidence for a carefully tuned flux balance whereby a high rate of newly fixed carbon turnover is offset by upregulation of gluconeogenesis to yield sufficient carbon and energy reserves.

4.5.3. Glycolysis → acetyl CoA

Pyruvate has several metabolic fates: it can be fermented to lactate, converted to acetyl CoA and/or converted to OAA where the latter two compounds enter the TCA cycle in the mitochondria (Villanova et al. 2017). Lactate accumulation in high light treatments indicates fermentation of pyruvate that was induced by anaerobic-like conditions from increased rates of oxygen consumption by carbon respiration, photorespiration, and other alternative respiratory pathways (Bhatla & Lal 2018). Furthermore, lactate could be associated with lactate dehydrogenase activity, as was observed in nutrient-stressed *T. pseudonana* (Lin et al. 2017), resulting in the

oxidation of NADH to NAD^+ via the glyoxylate cycle in the peroxisomes (Winkler & Stabenau 1995) or TCA cycle (Roberts et al. 2007) regenerating NAD^+ to accommodate high glycolytic activity in fast growing cells.

Higher glycolytic activity in high light acclimated cells would also increase the production rate of acetyl-CoA for synthesis of cycloartenol. This key phytosterol is an essential structural component of cell membranes (Sachs & Kawka 2015) that are more abundant in rapidly dividing cells (Fabris et al. 2014; Jaramillo-Madrid et al. 2020).

In low light, genes involved in branched-chain amino acid (BCAA) and fatty acid degradation were upregulated. Both processes produce acetyl-CoA, which enters the glyoxylate and TCA cycles. Recent transcriptomic analyses of *P. tricornutum* have shown that genes involved in BCAA metabolism and the TCA cycle are co-regulated, suggesting their strong links to diatom central carbon metabolism (Smith et al. 2016; Levering et al. 2017; Broddrick et al. 2019).

Acetyl-CoA is a precursor for the TCA cycle in the mitochondria and the glyoxylate cycle in the peroxisome. Diatoms maintain favorable ATP:NADPH ratios in the chloroplast via transference of reducing equivalents to the mitochondria for ATP production and energy dissipation via oxygen consuming pathways (i.e. AOX; Vanlerberghe 2013) (Allen et al. 2008; Prihoda et al. 2012; Bailleul et al. 2015). Glycolic acid has been proposed to also participate in this inter-organelle transport (Davis et al. 2017), providing multiple mechanisms to maintain cellular energy balance.

4.5.4. TCA versus glyoxylate cycle

As discussed above, low-light acclimated cells appear to rely on mechanisms that prevent carbon depletion. This theme is also reflected in the adjustment of a set of genes involved in the glyoxylate cycle, TCA cycle and photorespiration. The glyoxylate cycle is a variant of the TCA cycle that takes place in the peroxisome and does not produce CO_2. This key difference is achieved via a two-step bypass. In the first step, isocitrate lyase converts isocitrate to succinate and glyoxylate; in the second step, malate synthase condenses glyoxylate and acetyl-CoA to form malate. Malate can replenish the glyoxylate cycle through the action of malate dehydrogenase, while succinate can be used to replenish the TCA cycle or serve as precursors for carbohydrate or amino acid biosynthesis (Kunze et al. 2006). Thus, the glyoxylate cycle links acetyl-CoA generation from fatty acid and amino acid catabolism with biosynthesis of carbohydrates or amino acids.

In our experiments, three genes encoding Pex transporters (Pex5, Pex1, and Pex19) were upregulated in low light relative to high light, suggesting slow growing cells increase flux through the glyoxylate cycle. Peroxisomes do not contain translational machinery; therefore, all peroxisomal enzymes must be imported from the cytosol (Kunze et al. 2006; Gonzalez et al. 2011). *P. tricornutum* uses one of two known peroxisomal targeting signals (PTS) in combination with a series of peroxins (Pex) that recognise these signals and transport cytosolically-synthesised proteins into the peroxisomal lumen (Williams & Stanley 2010; Cross et al. 2016).

Genes involved in the TCA and glyoxylate cycles were differentially expressed in cells growing in low or high light. All of the genes encoding enzymes involved in TCA cycle reactions that are bypassed by the glyoxylate cycle were downregulated with the exception of isocitrate dehydrogenase (S4.4 Table). The gene encoding malate synthase was upregulated in low-light grown cells, while malate dehydrogenase was downregulated in these cells. Taken together, a clear picture emerges whereby cells growing in low light increase flux through the glyoxylate cycle and decrease flux through the TCA cycle. Davis et al. (2017) proposed that cells use the

glyoxylate cycle to limit excess energy production, and here we directly show these shifts are dependent on light limited growth rate. In contrast, fast growing cells require a high functioning TCA cycle to support energy requirements for biosynthesis and growth. Aspartate is derived from OAA and was present in significantly higher amounts in high light acclimated cells.

Succinate was retrieved in the *T. pseudonana* metabolome but was not significantly different amongst light treatments. Nevertheless, the role of succinate as a fundamental intermediate in the glyoxylate and TCA cycles as well as a precursor to mediators of protein modification and redox-shuttling, makes this metabolite pool intriguing for further study, especially by flux-based analysis, which may help elucidate its regulatory role in growth rate modulation.

Photorespiration produces glycolic acid via RuBisCO's oxygenase activity. Glycolic acid was retrieved in greater amounts in high light-acclimated cells compared to low light cells. This result is consistent with higher rates of photorespiration with irradiance (Beardall 1989; Parker & Armbrust 2005). We propose that photorespiratory-generated glycolic acid under high light acclimated growth is initially repurposed in the mitochondria to prevent chloroplastic damage from overreduction, rather than immediately returned to the CBB cycle thus allowing simultaneous dissipation of energy and repurposing of carbon skeletons (Smith et al. 2019). Two photorespiratory genes, glycine decarboxylase p-protein (GDC) and serine hydroxymethyltransferase (SHMT) were downregulated in low-light acclimated cells compared to high light acclimated cells, confirming the role of this pathway in supporting rapid growth.

5.6. Conclusion

We observed metabolic profile differences that, in association with gene expression data, provided detailed information about carbon and energy partitioning strategies that are growth rate dependent. Low-light acclimated (i.e. slower growing) cells downregulated energy and carbon loss processes (e.g. glycolysis, TCA cycle) and instead utilised more conservative pathways (i.e. gluconeogenesis, glyoxylate cycle) that facilitate a slow but steady growth rate. The low retrieval of both metabolites and genes from low-light acclimated cells suggest that metabolic pools are rapidly turned over with few luxury stores.

Differences in metabolite abundances depending on light dose show that cells adjust metabolic pathways to accommodate light and dark periods and demonstrate the extraordinary metabolic plasticity used to optimise growth in dynamic natural assemblages. Our study adds a fundamental basis to the insights offered through 'omics' platforms for the model diatom, *T. pseudonana*, particularly highlighting the power of combined metabolite and gene profiling for unlocking "emergent" physiological characteristics (e.g. photo-physiology) that are shared across phytoplankton groups and used to understand broad scale growth and productivity and that can be leveraged for bio-production purposes.

4.7. Acknowledgments

The authors acknowledge Dr. Jean-Baptiste Raina (UTS) and N. Jayasinghe (Metabolomics Australia, University of Melbourne) for advice on extracting metabolomics samples and Samantha Bennett for help with culture maintenance. NLF was supported by the UTS International Research Scholarship and President's Scholarship. JLM was supported by a Human Frontier Science Programme Long-term Postdoctoral fellowship (LT000625/2018-L).

4.8. References

Allen, A. E., LaRoche, J., Maheswari, U., Lommer, M., Schauer, N., Lopez, P. J., … Bowler, C. (2008). Whole-cell response of the pennate diatom Phaeodactylum tricornutum to iron starvation. *Proceedings of the National Academy of Sciences of the United States of America*, *105*(30), 10438–10443. https://doi.org/10.1073/pnas.0711370105

Amin, S. A., Hmelo, L. R., Van Tol, H. M., Durham, B. P., Carlson, L. T., Heal, K. R., … Armbrust, E. V. (2015). Interaction and signalling between a cosmopolitan phytoplankton and associated bacteria. *Nature*, *522*(7554), 98–101. https://doi.org/10.1038/nature14488

Anders, S., Huber, W., Dobin, A., Davis, C. A., Schlesinger, F., Drenkow, J., … Bakhshi, S. (2010). Differential expression analysis for sequence count data via mixtures of negative binomials. *Advances in Environmental Biology*, *7*(10), 2803–2809.

Andrews, S. (2010). FastQC: a quality control tool for high throughput sequence data.

Armbrust, E. V., Berges, J. A., Bowler, C., Green, B. R., Martinez, D., Putnam, N. H., … Rokhsar, D. S. (2004). The genome of the diatom Thalassiosira Pseudonana: Ecology, evolution, and metabolism. *Science*, *306*(5693), 79–86. https://doi.org/10.1126/science.1101156

Armbrust, E. V. (2009). The life of diatoms in the world's oceans. *Nature*, *459*(7244), 185–192. https://doi.org/10.1038/nature08057

Ashworth, J., Coesel, S., Lee, A., Armbrust, E. V., Orellana, M. V., & Baliga, N. S. (2013). Genome-wide diel growth state transitions in the diatom Thalassiosira pseudonana. *Proceedings of the National Academy of Sciences of the United States of America*, *110*(18), 7518–7523. https://doi.org/10.1073/pnas.1300962110

Ashworth, J., Turkarslan, S., Harris, M., Orellana, M. V., & Baliga, N. S. (2016). Pan-transcriptomic analysis identifies coordinated and orthologous functional modules in the diatoms Thalassiosira pseudonana and Phaeodactylum tricornutum. *Marine Genomics*, *26*, 21–28. https://doi.org/10.1016/j.margen.2015.10.011

Bailleul, B., Berne, N., Murik, O., Petroutsos, D., Prihoda, J., Tanaka, A., … Finazzi, G. (2015). Energetic coupling between plastids and mitochondria drives CO 2 assimilation in diatoms. *Nature*, *524*(7565), 366–369. https://doi.org/10.1038/nature14599

Beardall, J. (1989). Photosynthesis and Photorespiration in Marine Organisms: Photosynthesis and photorespiration in marine phytoplankton. *Aquatic Botany*, *34*, 105–130.

Bhatla, S. C., & Lal, M. A. (2018). Chp. 7: Respiration. In *Plant Physiology, Development and Metabolism*.

Behrenfeld, M. J., & Boss, E. S. (2014). Resurrecting the Ecological Underpinnings of Ocean Plankton Blooms. *Annual Review of Marine Science*, *6*(1), 167–194. https://doi.org/10.1146/annurev-marine-052913-021325

Behrenfeld, M. J., Westberry, T. K., Boss, E. S., O'Malley, R. T., & Siegel, D. A. (2009). Satellite-detected fluorescence reveals global physiology of ocean phytoplankton. *Biogeosciences*, *6*(5), 779–794. https://doi.org/10.5194/bg-6-779-2009

Behrenfeld, M. J., Worthington, K., Sherrell, R. M., Chavez, F. P., Strutton, P., McPhaden, M., & Shea, D. M. (2006). Controls on tropical Pacific Ocean productivity revealed through nutrient stress diagnostics. *Nature*, *442*(7106), 1025–1028. https://doi.org/10.1038/nature05083

Broddrick, J. T., Du, N., Smith, S. R., Tsuji, Y., Jallet, D., Ware, M. A., … Allen, A. E. (2019). Cross-compartment metabolic coupling enables flexible photo-protective mechanisms in the diatom Phaeodactylum tricornutum. *New Phytologist*, *222*(3), 1364–1379. https://doi.org/10.1111/nph.15685

Bromke, M. A., Giavalisco, P., Willmitzer, L., & Hesse, H. (2013). Metabolic Analysis of Adaptation to Short-Term Changes in Culture Conditions of the Marine Diatom Thalassiosira pseudonana. *PLoS ONE*, *8*(6), 1–11. https://doi.org/10.1371/journal.pone.0067340

Bromke, M. A., Sabir, J. S., Alfassi, F. A., Hajarah, N. H., Kabli, S. A., Al-Malki, A. L., … Willmitzer, L. (2015). Metabolomic profiling of 13 diatom cultures and their adaptation to nitrate-limited growth conditions. *PLoS ONE*, *10*(10), 1–18. https://doi.org/10.1371/journal.pone.0138965

Cavill, R., Jennen, D., Kleinjans, J., & Briedé, J. J. (2016). Transcriptomic and metabolomic data integration. *Briefings in Bioinformatics*, *17*(5), 891–901. https://doi.org/10.1093/bib/bbv090

Chong, J., Wishart, D. S., & Xia, J. (2019). Using metaboanalyst 4.0 for comprehensive and integrative metabolomics data analysis. *Current protocols in Bioinformatics*. 68, e68. https://doi.org/10.1002/cpbi.86

Cohen, N. R., Gong, W., Moran, D. M., McIlvin, M. R., Saito, M. A., & Marchetti, A. (2018). Transcriptomic and proteomic responses of the oceanic diatom Pseudo-nitzschia granii to iron limitation. *Environmental Microbiology*, *20*(8), 3109–3126. https://doi.org/10.1111/1462-2920.14386

Cross, L. L., Ebeed, H. T., & Baker, A. (2016). Peroxisome biogenesis, protein targeting mechanisms and PEX gene functions in plants. *Biochimica et Biophysica Acta - Molecular Cell Research*, *1863*(5), 850–862. https://doi.org/10.1016/j.bbamcr.2015.09.027

Davis, A., Abbriano, R., Smith, S. R., & Hildebrand, M. (2017). Clarification of Photorespiratory Processes and the Role of Malic Enzyme in Diatoms. *Annals of Anatomy*, *168*(1), 134–153. https://doi.org/10.1016/j.protis.2016.10.005

De Livera, A. M., Dias, D. A., De Souza, D., Rupasinghe, T., Pyke, J., Tull, D., … Speed, T. P. (2012). Normalizing and integrating metabolomics data. *Analytical Chemistry*, *84*(24), 10768–10776. https://doi.org/10.1021/ac302748b

Dong, H. P., Dong, Y. L., Cui, L., Balamurugan, S., Gao, J., Lu, S. H., & Jiang, T. (2016). High light stress triggers distinct proteomic responses in the marine diatom Thalassiosira pseudonana. *BMC Genomics*, *17*(1), 1–14. https://doi.org/10.1186/s12864-016-3335-5

Dyhrman, S. T., Jenkins, B. D., Rynearson, T. A., Saito, M. A., Mercier, M. L., Alexander, H., … Heithoff, A. (2012). The transcriptome and proteome of the diatom thalassiosira pseudonana reveal a diverse phosphorus stress response. *PLoS ONE*, *7*(3). https://doi.org/10.1371/journal.pone.0033768

Fabris, M., Matthijs, M., Carbonelle, S., Moses, T., Pollier, J., Dasseville, R., … Goossens, A. (2014). Tracking the sterol biosynthesis pathway of the diatom Phaeodactylum tricornutum. *New Phytologist*, *204*(3), 521–535. https://doi.org/10.1111/nph.12917

Fernie, A. R., Trethewey, R. N., Krotzky, A. J., & Willmitzer, L. (2004). Metabolite profiling: From diagnostics to systems biology. *Nature Reviews Molecular Cell Biology*, *5*(9), 763–769. https://doi.org/10.1038/nrm1451

Fisher, N. L., Campbell, D. A., Hughes, D. J., Kuzhiumparambil, U., Halsey, K. H., Ralph, P. J., & Suggett, D. J. (2020). Divergence of photosynthetic strategies amongst marine diatoms. *PLoS ONE*, *15*(12), 1–27. https://doi.org/10.1371/journal.pone.0244252

Fisher, N. L., & Halsey, K. H. (2016). Mechanisms that increase the growth efficiency of diatoms in low light. *Photosynthesis Research*, *129*(2), 183–197. https://doi.org/10.1007/s11120-016-0282-6

Gauthier, L., Tison-Rosebery, J., Morin, S., & Mazzella, N. (2020). Metabolome response to anthropogenic contamination on microalgae: a review. *Metabolomics*, *16*(1), 1–13. https://doi.org/10.1007/s11306-019-1628-9

Geider, R. J., Delucia, E. H., Falkowski, P. G., Finzi, A. C., Philip Grime, J., Grace, J., … Ian Woodward, F. (2001). Primary productivity of planet earth: Biological determinants and physical constraints in terrestrial and aquatic habitats. *Global Change Biology*, *7*(8), 849–882. https://doi.org/10.1046/j.1365-2486.2001.00448.x

Gonzalez, N. H., Felsner, G., Schramm, F. D., Klingl, A., Maier, U. G., & Bolte, K. (2011). A single peroxisomal targeting signal mediates matrix protein import in diatoms. *PloS one*, *6*(9), e25316.

Guillard, R. L. (1975). Culture of phytoplankton for feeding marine invertebrates. In *Culture of Marine Invertebrate Animals* (pp. 29–60).

Halsey, K. H., & Jones, B. M. (2015). Phytoplankton Strategies for Photosynthetic Energy Allocation. *Annual Review of Marine Science*, *7*(1), 265–297. https://doi.org/10.1146/annurev-marine-010814-015813

Halsey, K. H., Milligan, A. J., & Behrenfeld, M. J. (2011). Linking time-dependent carbon-fixation efficiencies in Dunaliella Tertiolecta (Chlorophyceae) to underlying metabolic pathways. *Journal of Phycology*, *47*(1), 66–76. https://doi.org/10.1111/j.1529-8817.2010.00945.x

Halsey, K. H., O'Malley, R. T., Graff, J. R., Milligan, A. J., & Behrenfeld, M. J. (2013). A common partitioning strategy for photosynthetic products in evolutionarily distinct phytoplankton species. *New Phytologist*, *198*(4), 1030–1038. https://doi.org/10.1111/nph.12209

Halsey, K., Milligan, A., & Behrenfeld, M. (2014). Contrasting Strategies of Photosynthetic Energy Utilization Drive Lifestyle Strategies in Ecologically Important Picoeukaryotes. *Metabolites*, *4*(2), 260–280. https://doi.org/10.3390/metabo4020260

Heal, K. R., Kellogg, N. A., Carlson, L. T., Lionheart, R. M., & Ingalls, A. E. (2019). Metabolic Consequences of Cobalamin Scarcity in the Diatom Thalassiosira pseudonana as Revealed Through Metabolomics. *Protist*, *170*(3), 328–348. https://doi.org/10.1016/j.protis.2019.05.004

Hughes, D. J., Varkey, D., Doblin, M. A., Ingleton, T., Mcinnes, A., Ralph, P. J., … Suggett, D. J. (2018). Impact of nitrogen availability upon the electron requirement for carbon fixation in Australian coastal phytoplankton communities. *Limnology and Oceanography*, *63*(5), 1891–1910. https://doi.org/10.1002/lno.10814

Jakob, T., Wagner, H., Stehfest, K., & Wilhelm, C. (2007). A complete energy balance from photons to new biomass reveals a light- and nutrient-dependent variability in the metabolic costs of carbon assimilation. *Journal of Experimental Botany*, *58*(8), 2101–2112. https://doi.org/10.1093/jxb/erm084

Jaramillo-Madrid, A. C., Ashworth, J., Fabris, M., & Ralph, P. J. (2020). The unique sterol biosynthesis pathway of three model diatoms consists of a conserved core and diversified endpoints. *Algal Research*, *48*(October 2019), 101902. https://doi.org/10.1016/j.algal.2020.101902

Johnson, W. M., Kido Soule, M. C., & Kujawinski, E. B. (2016). Evidence for quorum sensing and differential metabolite production by a marine bacterium in response to DMSP. *ISME Journal*, *10*(9), 2304–2316. https://doi.org/10.1038/ismej.2016.6

Joshi, N. A., & Fass, J. N. (2011). Sickle: A sliding-window, adaptive, quality-based trimming tool for FastQ files (Version 1.33)[Software].

Junker, B. H., Klukas, C., & Schreiber, F. (2006). VANTED: A system for advanced data analysis and visualization in the context of biological networks. *BMC Bioinformatics*, *7*(109), 1–13. https://doi.org/10.1186/1471-2105-7-109

Kanehisa, M., & Goto, S. (2000). KEGG: Kyoto Encyclopedia of Genes and Genomes. *Nucleic Acids Research*, *28*(1), 27–30.

Kim, D., Langmead, B., & Salzberg, S. L. (2015). HISAT: A fast spliced aligner with low memory requirements. *Nature Methods*, *12*(4), 357–360. https://doi.org/10.1038/nmeth.3317

Kolber, Z. S., Prasil, O., & Falkowski, P. G. (1998). Measurements of variable chlorophyll fluorescence using fast repetition rate techniques: defining methodology and experimental protocols. *Biochimica et Biophysica Acta - Bioenergetics*, *1367*, 88–106. Retrieved from papers2://publication/uuid/C591C675-7666-49B5-AB3C-16E2C3FCFD57

Kulk, G., van de Poll, W. H., Visser, R. J. W., & Buma, A. G. J. (2013). Low nutrient availability reduces high-irradiance-induced viability loss in oceanic phytoplankton. *Limnology and Oceanography*, *58*(5), 1747–1760. https://doi.org/10.4319/lo.2013.58.5.1747

Kunze, M., Pracharoenwattana, I., Smith, S. M., & Hartig, A. (2006). A central role for the peroxisomal membrane in glyoxylate cycle function. *Biochimica et Biophysica Acta (BBA)-Molecular Cell Research*, *1763*(12), 1441-1452.

Launay, H., Huang, W., Maberly, S. C., & Gontero, B. (2020). Regulation of Carbon Metabolism by Environmental Conditions: A Perspective From Diatoms and Other Chromalveolates. *Frontiers in Plant Science*, *11*(July), 1–14. https://doi.org/10.3389/fpls.2020.01033

Lavaud, J., Strzepek, R. F., & Kroth, P. G. (2007). Photo-protection capacity differs among diatoms: possible consequences on the spatial distribution of diatoms related to fluctuations in the underwater light Climate. *Limnology and Oceanography*, *52*(3), 1188–1194. https://doi.org/10.2307/4499689

Laws, E. A., & Bannister, T. T. (1980). Nutrient- and light-limited growth of Thalassiosira fluviatilis in continuous culture, with implications for phytoplankton growth in the ocean. *Limnology and Oceanography*, *25*(3), 457–473. https://doi.org/10.4319/lo.2004.49.6.2316

Levering, J., Dupont, C. L., Allen, A. E., Palsson, B. O., & Zengler, K. (2017). Integrated Regulatory and Metabolic Networks of the Marine Diatom Phaeodactylum tricornutum Predict the Response to Rising CO2 Levels. *MSystems*, *2*(1), 1–12. https://doi.org/10.1128/msystems.00142-16

Li, G., & Campbell, D. A. (2013). Rising CO2 Interacts with Growth Light and Growth Rate to Alter Photosystem II Photo-inactivation of the Coastal Diatom Thalassiosira pseudonana. *PLoS ONE*, *8*(1). https://doi.org/10.1371/journal.pone.0055562

Li, G., Talmy, D., & Campbell, D. A. (2017). Diatom growth responses to photoperiod and light are predictable from diel reductant generation. *Journal of Phycology*, *53*(1), 95–107. https://doi.org/10.1111/jpy.12483

Li, H., Handsaker, B., Wysoker, A., Fennell, T., Ruan, J., Homer, N., … Durbin, R. (2009). The Sequence Alignment/Map format and SAMtools. *Bioinformatics*, *25*(16), 2078–2079. https://doi.org/10.1093/bioinformatics/btp352

Lin, Q., Liang, J. R., Huang, Q. Q., Luo, C. S., Anderson, D. M., Bowler, C., … Gao, Y. H. (2017). Differential cellular responses associated with oxidative stress and cell fate decision under nitrate and phosphate limitations in Thalassiosira pseudonana: Comparative proteomics. *PLoS ONE*, *12*(9), 1–27. https://doi.org/10.1371/journal.pone.0184849

Lohr, K. E., Camp, E. F., Kuzhiumparambil, U., Lutz, A., Leggat, W., Patterson, J. T., & Suggett, D. J. (2019). Resolving coral photoacclimation dynamics through coupled photophysiological and metabolomic profiling. *Journal of Experimental Biology*, *222*(8). https://doi.org/10.1242/jeb.195982

Longnecker, K., & Kujawinski, E. B. (2017). Mining mass spectrometry data: Using new computational tools to find novel organic compounds in complex environmental mixtures. *Organic Geochemistry*, *110*, 92–99. https://doi.org/10.1016/j.orggeochem.2017.05.008

Love, M. I., Anders, S., & Huber, W. (2014). Differential analysis of count data - the DESeq2 package. In *Genome Biology* (Vol. 15). Retrieved from http://biorxiv.org/lookup/doi/10.1101/002832%5Cnhttp://dx.doi.org/10.1186/s13059-014-0550-8

Luo, W., Pant, G., Bhavnasi, Y. K., Blanchard, S. G., & Brouwer, C. (2017). Pathview Web: User friendly pathway visualization and data integration. *Nucleic Acids Research*, *45*(W1), W501–W508. https://doi.org/10.1093/nar/gkx372

Macintyre, H. L., Kana, T. M., & Geider, R. J. (2000). The effect of water motion on short-term rates of photosynthesis by marine phytoplankton. *Trends in Plant Science*, *5*(1), 12–17. https://doi.org/10.1016/S1360-1385(99)01504-6

MacManes, M. D. (2014). On the optimal trimming of high-throughput mRNA sequence data. *Frontiers in Genetics*, *5*(JAN), 1–7. https://doi.org/10.3389/fgene.2014.00013

Mann, D. G., & Vanormelingen, P. (2013). An inordinate fondness? the number, distributions, and origins of diatom species. *Journal of Eukaryotic Microbiology*, *60*(4), 414–420. https://doi.org/10.1111/jeu.12047

Matthews, J. L., Crowder, C. M., Oakley, C. A., Lutz, A., Roessner, U., Meyer, E., ... & Davy, S. K. (2017). Optimal nutrient exchange and immune responses operate in partner specificity in the cnidarian-dinoflagellate symbiosis. *Proceedings of the National Academy of Sciences*, *114*(50), 13194-13199.

McLean, T. I. (2013). “Eco-omics”: A Review of the Application of Genomics, Transcriptomics, and Proteomics for the Study of the Ecology of Harmful Algae. *Microbial Ecology*, *65*(4), 901–915. https://doi.org/10.1007/s00248-013-0220-5

Michel, G., Tonon, T., Scornet, D., Cock, J. M., & Kloareg, B. (2010). Central and storage carbon metabolism of the brown alga Ectocarpus siliculosus: Insights into the origin and evolution of storage carbohydrates in Eukaryotes. *New Phytologist*, *188*(1), 67–81. https://doi.org/10.1111/j.1469-8137.2010.03345.x

Montagnes, D. J. S., & Franklin, D. J. (2001). Effect of temperature on diatom volume, growth rate, and carbon and nitrogen content: Reconsidering some paradigms. *Limnology and Oceanography*, *46*(8), 2008–2018. https://doi.org/10.4319/lo.2002.47.4.1272

Montsant, A., Allen, A. E., Coesel, S., Martino, A. De, Falciatore, A., Mangogna, M., … Bowler, C. (2007). Identification and comparative genomic analysis of signaling and regulatory components in the diatom Thalassiosira pseudonana. *Journal of Phycology*, *43*(3), 585–604. https://doi.org/10.1111/j.1529-8817.2007.00342.x

Moore, E. R., Davie-Martin, C. L., Giovannoni, S. J., & Halsey, K. H. (2020). Pelagibacter metabolism of diatom-derived volatile organic compounds imposes an energetic tax on photosynthetic carbon fixation. *Environmental Microbiology*, *22*(5), 1720–1733. https://doi.org/10.1111/1462-2920.14861

Moore, C. M., Suggett, D. J., Hickman, A. E., Kim, Y.-N., Tweddle, J. F., Sharples, J., … Holligan, P. M. (2006). Phytoplankton photoacclimation and photoadaptation in response to environmental gradients in a shelf sea. *Limnol. Oceanogr*, *51*(2), 936–949. Retrieved from https://aslopubs.onlinelibrary.wiley.com/doi/pdf/10.4319/lo.2006.51.2.0936

Obata, T., Schoenefeld, S., Krahnert, I., Bergmann, S., Scheffel, A., & Fernie, A. R. (2013). Gas-chromatography mass-spectrometry (GC-MS) based metabolite profiling reveals mannitol as a major storage carbohydrate in the coccolithophorid Alga Emiliania huxleyi. *Metabolites*, *3*(1), 168–184. https://doi.org/10.3390/metabo3010168

Park, J., Kuzminov, F. I., Bailleul, B., Yang, E. J., Lee, S. H., Falkowski, P. G., & Gorbunov, M. Y. (2017). Light availability rather than Fe controls the magnitude of massive phytoplankton bloom in the Amundsen Sea polynyas, Antarctica. *Limnology and Oceanography*, *62*(5), 2260–2276. https://doi.org/10.1002/lno.10565

Parker, M. S., & Armbrust, E. V. (2005). Synergistic effects of light, temperature, and nitrogen source on transcription of genes for carbon and nitrogen metabolism in the centric diatom Thalassiosira pseudonana (Bacillariophyceae). *Journal of Phycology*, *41*(6), 1142–1153. https://doi.org/10.1111/j.1529-8817.2005.00139.x

Paul, C., Mausz, M. A., & Pohnert, G. (2013). A co-culturing/metabolomics approach to investigate chemically mediated interactions of planktonic organisms reveals influence of bacteria on diatom metabolism. *Metabolomics*, *9*(2), 349–359. https://doi.org/10.1007/s11306-012-0453-1

Pertea, M., Pertea, G. M., Antonescu, C. M., Chang, T. C., Mendell, J. T., & Salzberg, S. L. (2015). StringTie enables improved reconstruction of a transcriptome from RNA-seq reads. *Nature Biotechnology*, *33*(3), 290–295. https://doi.org/10.1038/nbt.3122

Pertea, M., Kim, D., Pertea, G. M., Leek, J. T., & Salzberg, S. L. (2016). Transcript-level expression analysis of RNA-seq experiments with HISAT, StringTie and Ballgown. *Nature Protocols*, *11*(9), 1650–1667. https://doi.org/10.1038/nprot.2016.095

Poulson-Ellestad, K. L., Jones, C. M., Roy, J., Viant, M. R., Fernández, F. M., Kubanek, J., & Nunn, B. L. (2014). Metabolomics and proteomics reveal impacts of chemically mediated competition on marine plankton. *Proceedings of the National Academy of Sciences of the United States of America*, *111*(24), 9009–9014. https://doi.org/10.1073/pnas.1402130111

Prihoda, J., Tanaka, A., De Paula, W. B. M., Allen, J. F., Tirichine, L., & Bowler, C. (2012). Chloroplast-mitochondria cross-talk in diatoms. *Journal of Experimental Botany*, *63*(4), 1543–1557. https://doi.org/10.1093/jxb/err441

Quinlan, A. R., & Hall, I. M. (2010). BEDTools: A flexible suite of utilities for comparing genomic features. *Bioinformatics*, *26*(6), 841–842. https://doi.org/10.1093/bioinformatics/btq033

Raina. J.B., Bennett S. Lambert, Donovan H. Parks, Christian Rinke, Nachshon Siboni, Martin Ostrowski, Beth Signal, Adrian Lutz, Himasha Mendis, Francesco Rubino, Vicente I. Fernandez, Roman Stocker, Philip Hugenholtz, Gene W. Tyson, and Justin R. Seymour (In review) Chemotaxis shapes the microscale organization of the ocean's microbiome

Richardson, K., Beardall, J., & Raven, J. A. (1983). Adaptation of Unicellular Algae to Irradiance: an Analysis of Strategies. *New Phytologist*, *93*(2), 157–191. https://doi.org/10.1111/j.1469-8137.1983.tb03422.x

Ritchie, R. J. (2006). Consistent sets of spectrophotometric chlorophyll equations for acetone, methanol and ethanol solvents. *Photosynthesis Research*, *89*(1), 27–41. https://doi.org/10.1007/s11120-006-9065-9

Roberts, K., Granum, E., Leegood, R. C., & Raven, J. A. (2007). Carbon acquisition by diatoms. *Photosynthesis Research*, *93*(1–3), 79–88. https://doi.org/10.1007/s11120-007-9172-2

Sachs, J. P., & Kawka, O. E. (2015). The influence of growth rate on 2H/1H fractionation in continuous cultures of the coccolithophorid Emiliania huxleyi and the diatom Thalassiosira pseudonana. *PLoS ONE*, *10*(11), 1–27. https://doi.org/10.1371/journal.pone.0141643

Sheehan, C. E., Baker, K. G., Nielsen, D. A., & Petrou, K. (2020). Temperatures above thermal optimum reduce cell growth and silica production while increasing cell volume and protein content in the diatom Thalassiosira pseudonana. *Hydrobiologia*, *847*(20), 4233–4248. https://doi.org/10.1007/s10750-020-04408-6

Shi, D., Li, W., Hopkinson, B. M., Hong, H., Li, D., Kao, S. J., & Lin, W. (2015). Interactive effects of light, nitrogen source, and carbon dioxide on energy metabolism in the diatom Thalassiosira pseudonana. *Limnology and Oceanography*, *60*(5), 1805–1822. https://doi.org/10.1002/lno.10134

Silsbe, G. M., Behrenfeld, M. J., Halsey, K. H., Milligan, A. J., & Westberry, T. K. (2016). The CAFE model: A net production model for global ocean phytoplankton. *Global Biogeochemical Cycles*, *30*(12), 1756–1777. https://doi.org/10.1002/2016GB005521

Silsbe, G. M., Smith, R. E. H., & Twiss, M. R. (2015). Quantum efficiency of phytoplankton photochemistry measured continuously across gradients of nutrients and biomass in Lake Erie (Canada and USA) is

strongly regulated by light but not by nutrient deficiency. *Canadian Journal of Fisheries and Aquatic Sciences*, *72*(5), 651–660. https://doi.org/10.1139/cjfas-2014-0365

Smith, S. R., Dupont, C. L., McCarthy, J. K., Broddrick, J. T., Oborník, M., Horák, A., … Allen, A. E. (2019). Evolution and regulation of nitrogen flux through compartmentalized metabolic networks in a marine diatom. *Nature Communications*, *10*(1). https://doi.org/10.1038/s41467-019-12407-y

Smith, S. R., Gillard, J. T., Kustka, A. B., McCrow, J. P., Badger, J. H., Zheng, H., ... & Allen, A. E. (2016). Transcriptional orchestration of the global cellular response of a model pennate diatom to diel light cycling under iron limitation. *PLoS genetics*, *12*(12), e1006490.

Smith, S. R., Abbriano, R. M., & Hildebrand, M. (2012). Comparative analysis of diatom genomes reveals substantial differences in the organization of carbon partitioning pathways. *Algal Research*, *1*(1), 2-16.

Sogin, E. M., Puskas, E., Dubilier, N., & Liebeke, M. (2019). Marine metabolomics: A method for non-targeted measurement of metabolites in seawater by gas chromatography mass spectrometry. *MSystems*, *4*(6), 1–14. https://doi.org/10.1101/528307

Stonik, V. S., & Stonik, I. (2015). Low-molecular-weight metabolites from diatoms: Structures, biological roles and biosynthesis. *Marine Drugs*, *13*(6), 3672–3709. https://doi.org/10.3390/md13063672

Suggett, D. J., Moore, C. M., & Geider, R. J. (2010). Chlorophyll a Fluorescence in Aquatic Sciences: Methods and Applications. *Chlorophyll a Fluorescence in Aquatic Sciences: Methods and Applications*. https://doi.org/10.1007/978-90-481-9268-7

Suggett, D. J., Goyen, S., Pettay, D. T., Szabó, M., Warner, M. E., Evenhuis, C., & Ralph, P. J. (2015). Functional diversity of photobiological traits within the genus Symbiodinium appears to be governed by the interaction of cell size with cladal designation. *New Phytologist*, *208*(2), 370–381. https://doi.org/10.1111/nph.13483

Suggett, D. J., Moore, C. M., Hickman, A. E., & Geider, R. J. (2009). Interpretation of fast repetition rate (FRR) fluorescence: Signatures of phytoplankton community structure versus physiological state. *Marine Ecology Progress Series*, *376*, 1–19. https://doi.org/10.3354/meps07830

Tan, Y. H., Lim, P. E., Beardall, J., Poong, S. W., & Phang, S. M. (2019). A metabolomic approach to investigate effects of ocean acidification on a polar microalga Chlorella sp. *Aquatic Toxicology*, *217*(October). https://doi.org/10.1016/j.aquatox.2019.105349

Tenenbaum, D. (2016). KEGGREST: Client-side REST access to KEGG. *R package version*, *1*(1).

Tozzi, S., Schofield, O., & Falkowski, P. (2004). Historical climate change and ocean turbulence as selective agents for two key phytoplankton functional groups. *Marine Ecology Progress Series*, *274*(Raven 1997), 123–132. https://doi.org/10.3354/meps274123

Tréguer, P., Nelson, D. M., Van Bennekom, A. J., Demaster, D. J., Leynaert, A., & Quéguiner, B. (1995). The silica balance in the world ocean: A reestimate. *Science*, *268*(5209), 375–379. https://doi.org/10.1126/science.268.5209.375

Vanlerberghe, G. C. (2013). Alternative oxidase: a mitochondrial respiratory pathway to maintain metabolic and signaling homeostasis during abiotic and biotic stress in plants. *International journal of molecular sciences*, *14*(4), 6805-6847.

Villanova, V., Fortunato, A. E., Singh, D., Bo, D. D., Conte, M., Obata, T., … Finazzi, G. (2017). Investigating mixotrophic metabolism in the model diatom phaeodactylum tricornutum. *Philosophical Transactions of the Royal Society B: Biological Sciences*, *372*(1728). https://doi.org/10.1098/rstb.2016.0404

Villas-Boas, S.G., Nielsen, J., Smedsgaard, J., Hansen, M.A. and Roessner-Tunali, U., 2007. *Metabolome analysis: an introduction* (Vol. 24). John Wiley & Sons.

Wagner, H., Jakob, T., & Wilhelm, C. (2006). Balancing the energy flow from captured light to biomass under fluctuating light conditions. *New Phytologist*, *169*(1), 95–108. https://doi.org/10.1111/j.1469-8137.2005.01550.x

Wagner, H., Jakob, T., Fanesi, A., & Wilhelm, C. (2017). Towards an understanding of the molecular regulation of carbon allocation in diatoms: The interaction of energy and carbon allocation. *Philosophical Transactions of the Royal Society B: Biological Sciences*, *372*(1728). https://doi.org/10.1098/rstb.2016.0410

Wilhelm, C., & Jakob, T. (2011). From photons to biomass and biofuels: Evaluation of different strategies for the improvement of algal biotechnology based on comparative energy balances. *Applied Microbiology and Biotechnology*, *92*(5), 909–919. https://doi.org/10.1007/s00253-011-3627-2

Williams, C. P., & Stanley, W. A. (2010). Peroxin 5: A cycling receptor for protein translocation into peroxisomes. *The international journal of biochemistry & cell biology*, *42*(11), 1771-1774.

Williams, C. R., Baccarella, A., Parrish, J. Z., & Kim, C. C. (2016). Trimming of sequence reads alters RNA-Seq gene expression estimates. *BMC Bioinformatics*, *17*(1), 1–13. https://doi.org/10.1186/s12859-016-0956-2

Winkler, U., & Stabenau, H. (1995). Isolation and characterization of peroxisomes from diatoms. *Planta*, *195*(3), 403-407.

Zhang, R., Kong, Z., Chen, S., Ran, Z., Ye, M., Xu, J., … Yan, X. (2017). The comparative study for physiological and biochemical mechanisms of Thalassiosira pseudonana and Chaetoceros calcitrans in response to different light intensities. *Algal Research*, *27*(April), 89–98. https://doi.org/10.1016/j.algal.2017.08.026

4.9. Supplementary Information

S4.1 Table. Cell densities (mL^{-1}), volume of culture (mL) concentrated and preserved for metabolite extraction and the total cells (mL^{-1}) extracted for metabolomics analysis of technical replicates for three constant (high, medium, low) and two pulse (high, low) light treatments.

Light Dose (L:D)	Light Level (µmol photons m^{-2} s^{-1})	Replicate	Cell Density (mL^{-1}) ($x10^6$)	Culture Volume (mL)	Total Cells (mL^{-1}) ($x10^7$)
Constant (24:0)	High (200)	1	2.97	68	20.21
		2	2.68	73	19.55
		3	2.06	64	13.15
		4	1.69	70	11.85
	Medium (60)	1	1.91	68	12.96
		2	2.08	68	14.15
		3	2.24	79	17.69
		4	2.42	73	17.70
	Low (5)	1	1.31	75	9.83
		2	1.90	78	14.82
		3	1.61	71	11.44
		4	1.55	73	11.32
Pulse (12:12)	High (200)	1	1.83	60	10.98
		2	1.60	60	9.59
		3	2.17	75	16.30
		4	1.84	83	15.30
	Low (5)	1	0.77	69	5.34
		2	0.73	76	5.57
		3	0.90	68	6.10
		4	0.81	76	6.15

S4.2 Table. Fold change matrix of average total cell densities extracted for metabolomics analysis between light treatments (Constant – High [HC], Medium [MC], Low [LC] and Pulse – High [HP], Low [LP]) where n = 4 for independent biological replicates. Values in parentheses represent *p* values for independent t-tests.

	HC	**MC**	**LC**	**HP**	**LP**
HC	------				
MC	HC/MC = 1.04 (0.829)	------			
LC	HC/LC = 1.37 (0.138)	MC/LC = 1.32 (0.059)	------		
HP	HC/HP = 1.24 (0.21)	MC/HP = 1.20 (0.174)	LC/HP = 0.91 (0.556)	------	
LP	HC/LP = 2.80 **(0.003)**	MC/HC = 2.70 **(0.000)**	LC/LP = 2.05 **(0.001)**	HP/LC = 2.25 **(0.004)**	------

S4.3 Table. Physiological characteristics of *Thalassiosira pseudonana* during steady-state acclimated growth to four light regimes: Constant (high, low), and Pulse (high, low) at 20°C. Values in parentheses represent SE of the mean for at least 3 independent biological replicates for specific growth rate (d^{-1}), Chl *a* ($cell^{-1}$), carbon (pg $cell^{-1}$), nitrogen (pg $cell^{-1}$), C:N, F_v/F_m and σ_{PSII} (nm^2 $PSII^{-1}$). ANOVA or Kruskal-Wallis (KW) test results are presented using F or H-values, respectively, followed by Bonferroni or Dunnett T3 post-hoc analysis, respectively, with differences between individual cell characteristics and light treatment designated by superscripted letters and significant *p* values ($p < 0.05$) in bold.

Light Dose (L:D cycle)	Light Intensity	Avg PFD (µmol photons m^{-2} s^{-1})	Growth rate (d^{-1})	Chl *a* $cell^{-1}$ (pg)	C $cell^{-1}$ (pg)	N $cell^{-1}$ (pg)	C:N	F_v/F_m	σ_{PSII} (nm^2 $PSII^{-1}$)
Constant (24:0)	High (HC)	**200**	**1.17** (0.08)	**0.30** (0.04)	**14.61** (1.39)	**2.38** (0.28)	**6.16** (0.16)	**0.52** (0.00)	**3.82** (0.05)
	Low (LC)	**5**	**0.18** (0.00)	**0.50** (0.03)	**10.32** (0.61)	**1.13** (0.10)	**9.34** (0.69)	**0.54** (0.00)	**3.45** (0.08)
Pulse (12:12)	High (HP)	**200**	**1.12** (0.10)	**0.15** (0.01)	**8.87** (0.96)	**1.27** (0.16)	**7.55** (0.30)	**0.55** (0.00)	**3.28** (0.03)
	Low (LP)	**5**	**0.12** (0.01)	**0.38** (0.03)	**17.70** (1.05)	**1.86** (0.18)	**9.80** (1.06)	**0.53** (0.00)	**3.47** (0.16)
ANOVA (2-way)	*p* value	Light Dose	0.394	1.000	**0.000**	0.261	0.097	0.095	**0.027**
		Light Intensity	**0.000**	1.000	**0.000**	0.146	**0.004**	0.709	0.560
		Dose*Intensity	0.882	1.000	**0.000**	**0.000**	0.620	**0.005**	0.231

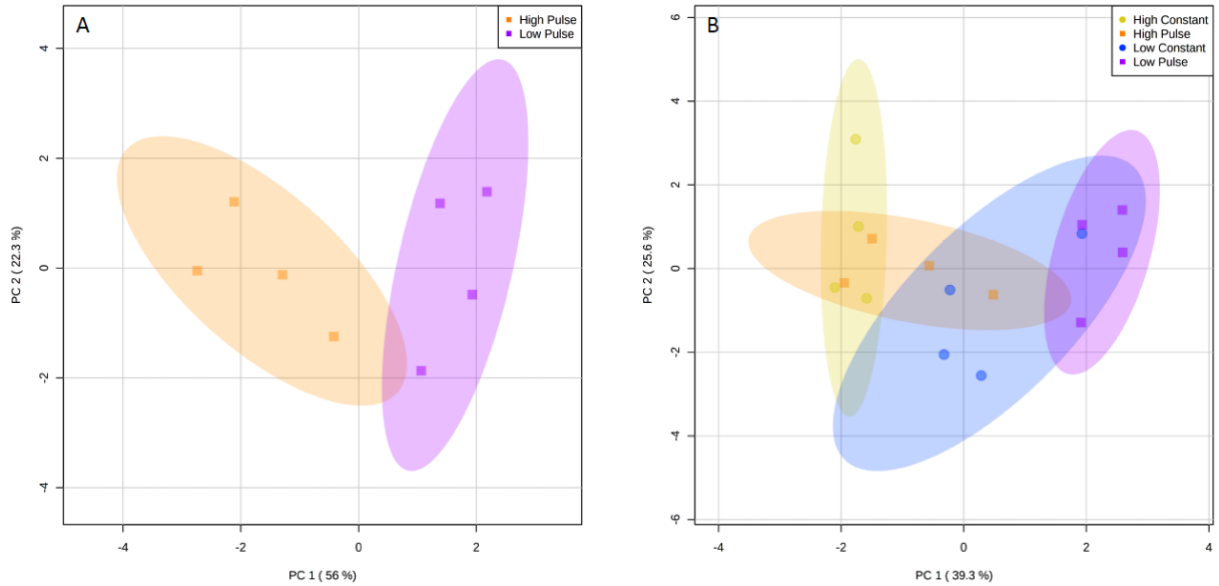

S4.1 Figure. PCAs of the relative metabolite abundances for (A) pulse (12:12 L:D) treatments at high (HP, 200 µmol photons m^{-2} s^{-1}) and low (LP, 5 µmol photons m^{-2} s^{-1}) light intensities and (B) for constant and pulse (HC – yellow circles, HP – orange squares, LC – blue circles, LP – purple squares) light treatments. Explained variances are shown as a percentage in brackets and shaded area is the 95% confidence region of individual treatment groups. Individual data points represent independent biological replicates (n=4).

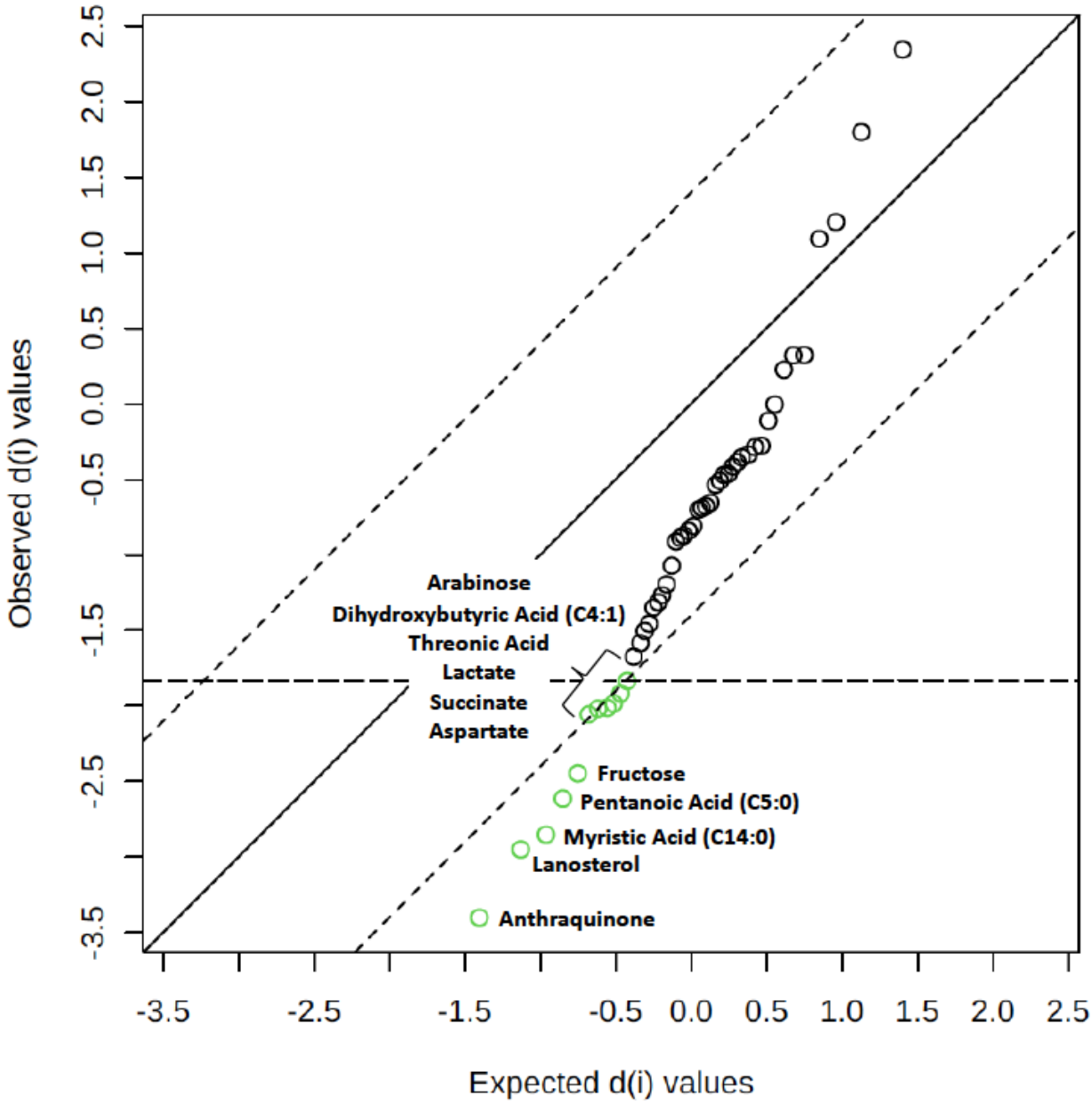

S4.2 Figure. Significant metabolites (green circles) identified by SAM between high and low pulse light treatments (HP – high pulse, LP – low pulse). Significant metabolites are distinguished in bold ($p < 0.05$) and a false detection rate (FDR) < 10%.

Supplemental Methods

RNA-Seq: Quality trimming and sequence alignment

FastQC (Andrews 2010) was used to check GC content and per-base quality scores in each sample. Raw reads were quality trimmed and filtered using Sickle v1.33 (Joshi & Fass 2011) with the options "-q 33 -l 50". The first option sets the quality score threshold for trimming to 33, while the second option discards all reads that are shorter than 50 base pairs after trimming. Sequencing adapters were not removed, as previous studies have shown that adapters do not significantly affect alignments to reference genomes and that aggressive trimming can lead to bias and poorer results (MacManes 2014; Williams et al. 2016). The *T. pseudonana* reference genome was obtained from NCBI in GFF format (accession number GCA_000149405.2) and converted to GTF using gffread. Reads were aligned to the reference genome using HISAT2 v2.1.0 (Kim et al. 2015) with the option "--dta". HISAT2 is a splice-aware aligner that generates alignments more quickly and using less memory than older alignment software such as BowTie or BWA (Pertea et al. 2016). The "--dta" option tells the program to report alignments in a format that is tailored to transcriptome assemblers like StringTie. HISAT2 created sequence alignment/map (SAM) files for each sample. These files contain the alignments in the order that that the sequences occurred in the input FASTQ files. SAMtools v1.3 (Li et al. 2009) was used to sort the alignments with respect to their genomic positions and then convert the files to binary alignment/map (BAM) files, which facilitate more rapid computation. Coverage depth of the genome was calculated using the "genomeCoverageBed" command with the "-ibam" option in BEDTools v2.25.0 (Quinlan & Hall 2010). StringTie v1.3.3 (Pertea et al. 2015) was used to assemble putative transcripts and generate counts tables for use in DESeq2. First, putative transcripts were assembled using the reference annotation file downloaded from NCBI. Then, data from all samples was merged into a single file using the command "stringtie --merge." Finally, "stringtie -eB" was used to calculate

transcript abundances and generate count tables structured for Ballgown (DESeq2 also accepts these counts tables as input). DESeq2 v1.20.0 (Love et al. 2014) was used to perform differential expression analysis and create exploratory visualisations.

Quality control and differential expression analysis

Prior to differential expression analysis, we transformed the count data to make it homoscedastic. We used the rlog transformation for downstream exploratory analyses and visualisations. DESeq2 (Anders & Huber 2010) tests for differential expression by 1) normalising sequencing depth between samples using an estimate of "size factors," 2) estimating dispersion across all samples, and 3) fitting a negative binomial generalised linear model. DESeq2 uses a Wald test to calculate a p-value for differential expression; these p-values are then adjusted for multiple testing using the Benjamini-Hochberg correction. DESeq2 also assigns $\log_2$ fold change values for each gene. Under the default parameters in DESeq2, the null hypothesis is that a gene is *not* differentially expressed between treatments. The alternative hypothesis is that a gene *is* differentially expressed between treatments. These default parameters were used to test for differential expression of genes between the high light and low light treatment groups. However, it cannot be assumed that genes with B-H adjusted p-values larger than our significance threshold are stably expressed. The parameters "altHypothesis = lessAbs" and "lfcThreshold = *x*" were added to the results function to test for stable expression. The parameter *x* defines the threshold for $\log_2$ fold change. Setting a $\log_2$ fold change threshold to 1 (fold change = 2) yielded 4,270 significant genes.

The Bioconductor package KEGGREST (Tenenbaum 2018) was used to access gene annotations from the KEGG database; functional annotation was limited to KEGG

pathways. Pathview Web (Luo et al. 2017) was used to visualise relative expression of genes within KEGG pathways.

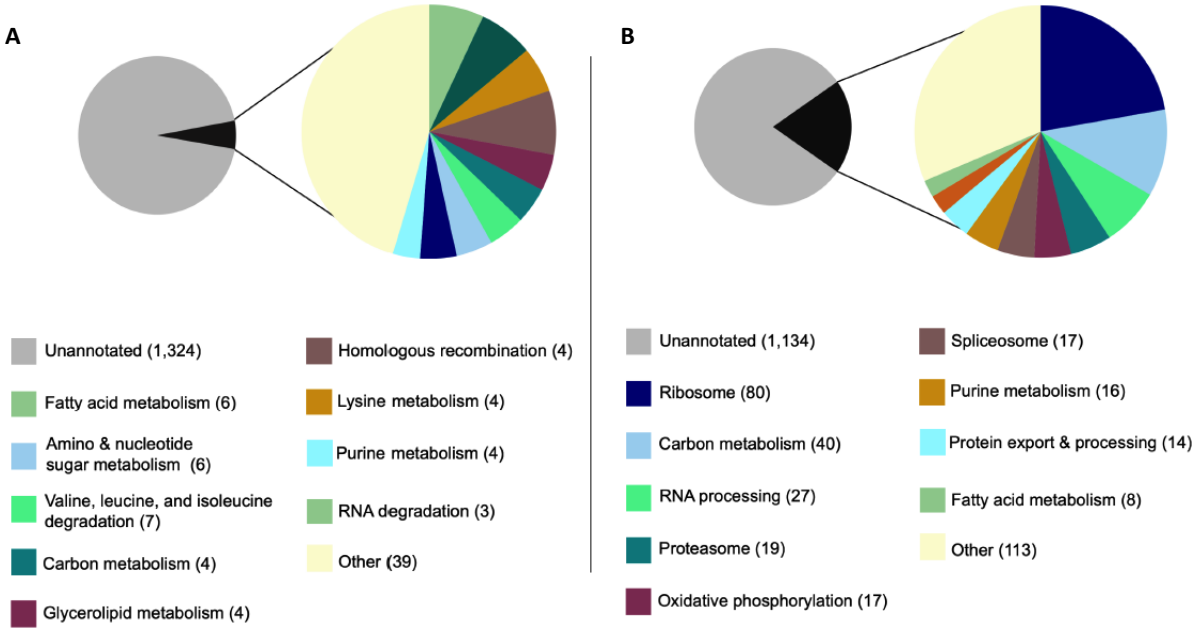

S4.3 Figure. Summary of annotated differentially expressed genes for those (A) downregulated in constant low light (LC, 5 µmol photons m^{-2} s^{-1}) relative to constant high light (HC, 200 µmol photons m^{-2} s^{-1}) and (B) upregulated in LC compared to HC. Differential expression was determined using the threshold $|FC| > 2$, $p < 0.05$ from three independent biological replicates.

S4.4 Table. Summary of differentially expressed genes involved in the glyoxylate cycle, TCA cycle, and related pathways. Genes with adjusted *p* value <0.05 in *T. pseudonana* grown at constant low light (LC, 5 µmol photons m^{-2} s^{-1}) compared to constant high light (HC, 200 µmol photons m^{-2} s^{-1}) conditions.

Gene Name	Function	Pathway	Fold Change	Adjusted *p*-value
THAPSDRAFT_795	2-oxoisovalerate E1 component alpha subunit	Valine, leucine and isoleucine degradation	19.8	1.25E-29
THAPSDRAFT_36291	2-oxoisovalerate E2 component	Valine, leucine and isoleucine degradation	10.3	4.88E-59
THAPSDRAFT_413	3-hydroxyisobutyrate dehydrogenase	Valine, leucine and isoleucine degradation	6.42	8.52E-20
THAPSDRAFT_25495	Malonate-semialdehyde dehydrogenase (acetylating)	Valine, leucine and isoleucine degradation	2.34	1.04E-04
THAPSDRAFT_32067	2-oxoisovalerate E1 component beta subunit	Valine, leucine and isoleucine degradation	2.08	8.46E-04
HCD1	3-hydroxyacyl-CoA dehydrogenase	Valine, leucine and isoleucine degradation	2.57	4.36E-06
PCB1	3-methylcrotonyl-CoA carboxylase beta subunit	Valine, leucine and isoleucine degradation	2.53	9.73E-04
KCT2	Acetyl-CoA acyltransferase	Valine, leucine and isoleucine degradation	-2.08	1.11E-05
ACD3	Acyl-CoA dehydrogenase	Fatty acid degradation; Valine, leucine and isoleucine degradation	5.29	4.94E-15
GCD1	Glutaryl-CoA dehydrogenase	Fatty acid degradation	2.29	5.07E-05
FCL1	Long-chain fatty acid CoA ligase	Fatty acid degradation	8.76	4.88E-20
THAPSDRAFT_262934	Probably malate synthase	Glyoxylate cycle	1.93	4.76E-02
MDH1	Malate dehydrogenase	TCA cycle	-3.36	3.01E-19
THAPSDRAFT_269718	Alpha-ketoglutarate dehydrogenase E1 component	TCA cycle	-1.46	1.73E-03

THAPSDRAFT_36971	Alpha-ketoglutarate dehydrogenase E2 component	TCA cycle	-1.78	9.27E-03
SDH1	Succinate dehydrogenase (ubiquinone) iron-sulfur subunit	TCA cycle	-1.29	2.40E-13
FUM1	Fumurate hydratase	TCA cycle	-2.45	1.80E-02
SCS1	Succinyl-CoA synthetase beta subunit	TCA cycle	-3.26	9.36E-19
IDH1	Putative isocitrate dehydrogenase	TCA cycle	-2.43	1.14E-10
PPC1	Phosphophenolpyruvate carboxylase	TCA cycle	-1.45	9.21E-03
THAPSDRAFT_269908	Pyruvate carboxylase	TCA cycle	-1.86	2.05E-06
THAPSDRAFT_264438	Peroxin 5	Peroxisomal transport	1.79	2.04E-04
THAPSDRAFT_261078	Peroxin 1	Peroxisomal transport	1.87	1.35E-03
THAPSDRAFT_37854	Peroxin 19	Peroxisomal transport	1.60	2.19E-02
GDCT	Glycine decarboxylase t-protein (GDC)	Photorespiration	-1.49	1.06E-02
GDCP	Glycine decarboxylase p-protein (GDC)	Photorespiration	-2.18	3.09E-05
THAPSDRAFT_26031	Serine hydroxymethyl-transferase (SHMT)	Photorespiration	-3.63	3.34E-18
PDK1_2	Pyruvate-phosphate dikinase (PPDK)	Gluco-neogenesis	6.65	6.96E-20
PCK1	Phosphoenolpyruvate carboxykinase	Gluco-neogenesis	7.26	4.82E-19
PYK1	Pyruvate kinase	Glycolysis	-6.47	6.63E-15
PYK2	Pyruvate kinase	Glycolysis	-2.27	8.83E-04

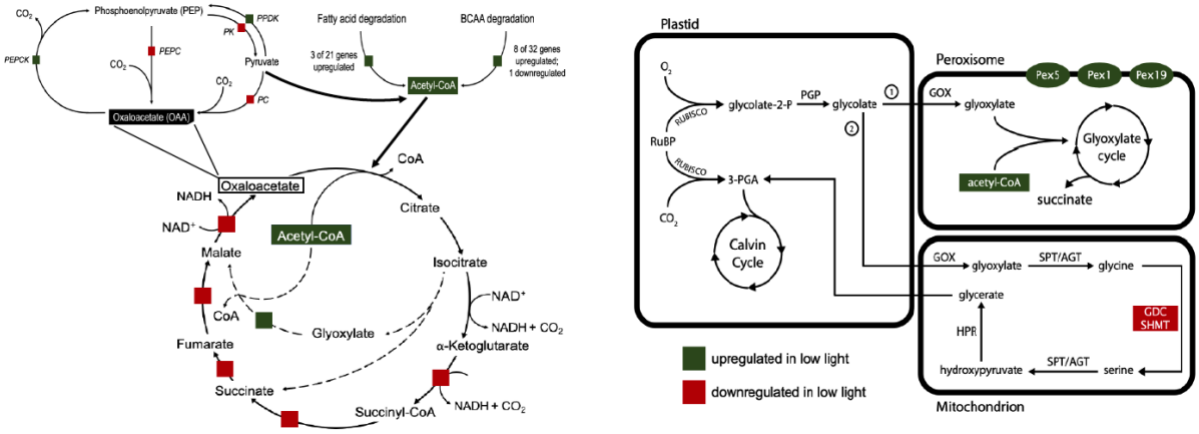

S4.4 Figure. Differentially expressed genes for *T. pseudonana* grown at constant low light (LC, 5 µmol photons m^{-2} s^{-1}) compared to constant high light (HC, 200 µmol photons m^{-2} s^{-1}) conditions showing upregulated (green) and downregulated (red) genes in LC. Right panel figure shows the interplay between processes occurring in the plastid, peroxisome and mitochondrion and left panel figures shows more detailed interactions between glycolysis, fatty acid and branched chain amino acid (BCAA) degradation and TCA cycle where dashed lines represent the glyoxylate cycle two-step bypass. PEPCK = PEP carboxykinase; PPDK = pyruvate-phosphate dikinase; PK = pyruvate kinase; PC = pyruvate carboxylase; PEPC = PEP carboxylase; Pex1,5,19 = peroxins that import proteins into the peroxisomes.

Chapter 5

General Discussion:

Synthesis of Results, Future Directions and Conclusion

5.1. Synthesis of results

In this final chapter, I consider how the knowledge gained from data Chapters 2-4 has helped bridge the current gaps in our understanding of diatom competitive fitness via alternative strategies of resource allocation; specifically, how different photo-protective capacities and downstream oxidase activities along the photosynthetic electron transport chain (PETC) interact to balance excess excitation pressure and maintain efficient productivity. My various research experiments incorporated fluorescence-, oxygen-, and 'omics'-based assessments of diatom responses to light when grown under constant (e.g. Chapters 2 and 4), pulse (e.g. Chapter 4) and sinusoidal (e.g. Chapter 3) regimes followed by a transient high light exposure (e.g. Chapters 2 and 3). This has enabled me to demonstrate new links between fluorescence and metabolic processes (i.e. oxygen consumption in the light and carbon retained in biomass), which in turn has highlighted implications to our current consideration of cellular energy budgets, including the lack of LDR processes. The novel insights gained have further provided a road map for key areas of future research needed to further improve primary productivity (PP) models.

5.1.1 Photophysiology is ecological niche-dependent

In the natural environment, where light climates are dynamic and often stochastic, phytoplankton need mechanisms to compensate for light availability where it continually fluctuates between doses that over- and under-saturate PETC capacity, notably to maintain linear electron flow (LEF). Diatoms, in particular, appear well equipped to maintain photosynthetic efficiency under fluctuating light where the most rapid and effective photo-protective mechanism is nonphotochemical quenching

(Lavaud & Lepetit 2013; Goss & Lepetit 2015). Evidence increasingly demonstrates that diatom photo-protective capacities – largely through evolved divergences in PSII light harvesting regulation – are associated with ecological niche (Strzepek & Harrison 2004; Lavaud et al. 2007; Dimier et al. 2009; van de Poll et al. 2010; Lavaud & Lepetit 2013; Barnett et al. 2015; Croteau et al. 2020). My work extends these previous works within a broader photosynthetic framework of adaptive differences by additionally balancing metabolic processes downstream of PSII light harvesting complexes (Chapter 2-4).

From an initial screening of photo-protective capacities amongst diverse diatom species, varying in size and shape (centric vs pennate), I observed a divergence of nonphotochemical quenching capacities that were largely consistent with the ecological niche from where isolates were originally sourced (although identifying such conserved patterns was not the original intention of this screening). Three general categories of photo-protective capacity emerged that confirmed observations made previously (Strzepek & Harrison 2004; Lavaud et al. 2007) whereby i) estuarine diatoms (e.g. *T. weissflogii*) exhibited a high capacity to rapidly initiate nonphotochemical quenching, (ii) oceanic diatoms (e.g. *T. oceanica*) had slower initiation of nonphotochemical quenching as light intensified and (iii) coastal diatoms (e.g. *T. pseudonana*) had an intermediate response (Chapter 2). Focusing on these representative centric *Thalassiosira* species of diatom photo-protective capacities, I subsequently combined active chlorophyll *a* fluorescence with membrane inlet mass spectrometry (MIMS)-based labelled oxygen isotope measurements, that provided the contributions of total (light and 'dark') respiration to GP_{O2} in the light. Remarkably, under optimal light and

nutrient-replete growth conditions, the photo-protective capacities and oxygen consumption rates of these three *Thalassiosira* diatoms were nearly identical (MacIntyre et al. 2002; Lavaud et al. 2007; Chapter 2). In contrast, species-specific differences were observed under transient exposure to high light that revealed midstream oxidase (MOX) activities (i.e. LDR) were upregulated in the oceanic species to compensate for their lower capacities to initiate nonphotochemical quenching compared to the estuarine species that initiated nonphotochemical quenching rapidly thus decreasing reliance on MOXs to alleviate pressure along the PETC. (Chapter 2; Fig 5.1).

Disparities in energy dissipation, as observed in Chapter 2, largely reflect photo-adaptive responses to ecological niche – via compensatory light harvesting *versus* light utilisation – whereby pelagic waters are characterised by a more stable light environment that are often iron-limited compared to coastal and estuarine waters (MacIntyre et al. 2000; Lavaud et al. 2007). Photosynthetic machinery has thus adapted and evolved according to the conditions of the environment, such that, even under controlled laboratory conditions today, these divergent strategies remain evolutionarily conserved (Strzepek & Harrision 2004; Peers & Price 2006; Suggett et al. 2015), providing a sound basis with which laboratory observations (Fig 5.1) can be applied to field-relevant scenarios.

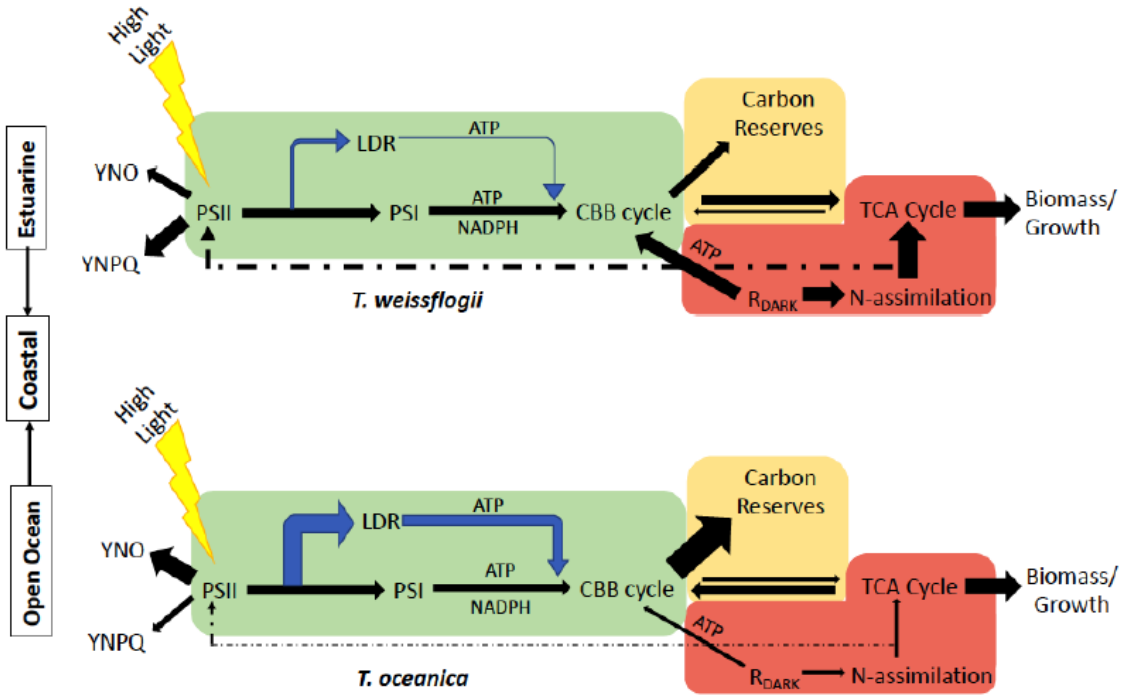

Figure 5.1 Schematic of diatom responses to high light from species found in open ocean (*T. oceanica*) and estuary (*T. weissflogii*) in which coastal diatoms exhibit an intermediate response. The main flow of energy involves light energy harvested at photosystem II (PSII) where excitons are passed along the linear electron transport chain to PSI where NADPH is generated to fuel, in addition to ATP, the Calvin-Benson-Bassham (CBB) cycle. Products generated from the CBB cycle enter the cytoplasm (yellow box) to glycolysis which feeds into the tricarboxylic acid cycle (TCA) cycle in the mitochondria (red box) to build macromolecules to support growth. Alternatively, gluconeogenesis diverts energy away from TCA cycle to build carbon reserves. Sources of energy dissipation from high light before reaching PSII are the yield of constitutive losses via fluorescence and heat (YNO) and the yield of regulated thermal dissipation via nonphotochemical quenching (YNPQ) Once photolysis occurs at the PSII reaction centre, electrons can enter processes of light-dependent respiration (LDR) via oxidase activity within the chloroplast (green box) which can be a way to dissipate excess electrons or generate additional ATP. Additionally, mitochondrial

respiration (R_{DARK}) can supplement ATP demands via the catabolism of carbon molecules to supply to the CBB cycle or assimilation of nutrients (i.e. nitrogen, N). Nitrogen is particularly essential to build pigments and proteins that are fundamental components of the nonphotochemical quenching mechanism. The arrow thickness correlates to the upregulation of pathways by these diatoms under high light as observed in Chapters 2 and 3.

5.1.2. The dynamic nature of respiration

Chapter 2 demonstrated the importance of MOX activity (i.e. LDR) for some species from a discrete, short-term measurement under transient high light exposure. This finding raised many questions as to how a gradual – and predictable – change in light (i.e. sinusoidal) over time would alter diatom-dependency on MOX activity versus photo-protective mechanisms, and whether any patterns observed between species are consistent with known differences in ecological niche (Chapter 3). My work showed that respiration dynamics are both temporally driven and species-specific, which challenges current generalised assumptions of respiration as a "constant" 10% of GP_{O2} (Falkowski & Owens 1978; Burris 1980; Langdon 1993) and therefore current models of PP (where a respiration parameter is included) (Behrenfeld & Falkowski 1997). Similarly, light-dependent oxidase activity cannot be equated – e.g. via some constant – to more easily measured mitochondrial ('dark') respiration – as both processes were independently influenced by time of day and were species-specific.

The outcomes of Chapter 3 provided new insight into respiratory dependencies in the light that were indeed consistent with the expression of divergent light (energetic)

utilisation pathways by distinct ecological niche separation. Specifically, where species evolved to higher nitrogen availability (typical in estuarine and coastal systems, i.e. in this case *T. weissflogii*), I observed an increase in cellular nitrogen over the day (Chapter 3), presumably to build light-harvesting pigment-protein structures (nitrogen-rich compounds) that are constituents of nonphotochemical quenching (Goss & Lepetit 2015; Fig 5.1). The energetic demands for N-assimilation was provided by R_{DARK}, which increased with light intensity (Chapter 3). However, at the onset of light, *T. weissflogii* exhibited proportionally more LDR to 'prime' nonphotochemical activation by maintaining LEF that produces NADPH and pumping protons into the lumen which functions two-fold to acidify the lumen – required to de-epoxidase xanthophyll cycle pigments – and optimise ATP generation via transthylakoid proton motive force (Chapter 3). In contrast, oceanic species that evolved to lower nutrient (e.g. iron) availability (i.e. in this case *T. oceanica*) increased reliance on LDR to dissipate excess excitation pressure along the PETC and building carbon reserve over the day in preparation for night-time respiration (Chapter 3). Ultimately, measures of respiration in the light (both R_{DARK} and LDR) are dynamic and simply using a respiration rate that occurs independent of photosynthesis (i.e. in the dark) does not accurately reflect the contributions of respiratory processes occurring in the light, which in the latter case are clearly significant and important for dynamic resource allocation. Such lack of knowledge with which respiration rates in the light vary over space and time is clearly a major factor currently limiting our ability to better understand – and predict – PP budgets.

5.1.3. Respiration is misrepresented in current considerations of primary productivity

Energetic budgets governing PP over the last two decades have rested on bridging the gap of resource transformation between light harvesting and carbon uptake in the oceans. In particular, fluorescence lifetimes are used to track the efficiency of light absorption (Lin et al. 2016) where active fluorescence induction track the subsequent efficiency by which excitation energy is converted to more conventional measures of photosynthesis (O_2 release, CO_2 uptake) (Lawrenz et al. 2013; Hughes et al. 2018). Given the vast majority of PP measures to date are carbon-based, efforts have – perhaps unsurprisingly – remained focussed on tracking conversion between fluorescence and carbon PP measures (Behrenfeld et al. 2008; Hughes et al. 2018), yet this has resulted in masking the critical roles of oxygen, including O_2 cycling, in balancing cellular resource requirements (Behrenfeld et al. 2008; Halsey et al. 2013; Halsey & Jones 2015). While it has been argued that measures of O_2 dynamics are actually a better parameter than CO_2 uptake to assess productivity (Williams et al. 2013), it is still rare to find studies that integrate measures of photo-physiology/active fluorometry and O_2 measures, especially that simultaneously measure O_2 consumption in the light via LDR and R_{DARK} (Chapters 2 and 3). I have shown that respiration processes in the light are dynamic over the photoperiod and are species-specific, sometimes representing ~30% of GP_{O2} (Chapter 3), which means the measures of GP_{O2} acquired in previous studies were underestimated from using true dark respiration rates that inherently underestimate respiratory processes happening in the light (e.g. Wagner et al. 2006; Jakob et al. 2007; Su et al. 2012). Importantly, use of alternate respiration pathways to sustain cellular functioning not only impacts the relationships between fluorescence, O_2 evolution and CO_2 uptake ("currencies", e.g. Suggett et al. 2009), but also re-route the metabolic pathways with which energy and reductant are processed via different carbon

skeletons (Raven 1997; Raven et al. 2012). In fact, arguably fluorescence, O_2 and CO_2 "currencies" are the 'emergent' signatures with which different metabolic pathways are employed. Thus, identifying specific metabolites that are involved in respiratory and photosynthetic pathways – in parallel to PP measures – should provide more powerful insights into energetic trade-offs based on environmental conditions. Such insights justified the work of Chapter 4 which provided the first overview of light-driven metabolic profiles changes in a model diatom, *Thalassiosira pseudonana*, to assess what metabolites play a role in the ecological success of diatoms under various light climates. Given the novelty of this work, it was necessary to use constant and pulse light regimes to (1) provide a foundation for future metabolic profiles achieved under dynamic light and (2) use light regimes that matched previous physiological (Fisher & Halsey 2015) and transcriptomic (Pombrol thesis) assessment of *T. pseudoana* to build a comprehensive cellular network driven by light.

5.1.4. An 'omics' insight into physiology

Metabolomics is an emergent platform to elucidate physiological responses to changing environments. Importantly, metabolomics provides a snapshot of the cellular metabolome to growth conditions at any one time, and thus a powerful complementary tool to provide diagnostic biomarkers that explain photo-physiology and metabolic pathways (i.e. photosynthesis and respiration). To the best of my knowledge, a metabolomics-based study solely looking at the response of diatoms to light (Chapter 4) had not been previously achieved, which was surprising given that we commonly measure the light-driven responses of emergent properties of metabolism (O_2, CO_2) to explain phytoplankton fitness (Wagner et al. 2006, 2017; Jakob et al 2007; Su et al.

2012; Fisher & Halsey 2016; Du et al. 2018; Joy-Warren et al. 2019; Henderikx Freitas et al. 2020; Chapter 2 and 3) that is, in turn, used to parameterise PP. Here, I combined transcriptomics (samples and analysis completed separately) and metabolomics to explain the well-documented physiological responses of the model diatom, *Thalassiosira pseudonana*, to varying light-acclimated growth based on intensity and dose (Chapter 4). I found evidence of energetic pathway gating whereby under high light there was an upregulation energy and carbon consumption pathways that supported higher growth rates (i.e. glycolysis and TCA cycle) and under low light pathways that conserved energy and carbon were favoured (i.e. gluconeogenesis and the glyoxylate cycle). Such metabolic insights from Chapter 4 complement photophysiology measurements (e.g. Chapters 2 and 3) by highlighting the cellular pathways that utilise photosynthetically generated energy.

Metabolomics, and other 'omics'-techniques, provide the additional advantage of elucidating cellular compounds that cannot be attained by traditional physiological measurements which offers greater insight and new perspectives on metabolic processes influenced by the environment, especially from diatoms (Longnecker & Kujawinski 2017). From the metabolic profile of *T. pseudonana*, I observed an interesting metabolite that was markedly abundant in low light acclimated cultures, a signalling metabolite – eicosanoic acid (C20:0), that could trigger cellular metabolic adjustments required to respond to rapid light fluctuations. It is also possible that this signalling molecule is associated with the tightly connected network between diatoms and their specific bacterial consortia (Amin et al. 2012) to facilitate complex exchanges of nutrients or molecules (Amin et al. 2015). Such findings spark many questions and

provide a foundation for future research into how specific metabolites can be used to trigger metabolic responses under more dynamic light regimes that elucidate mechanisms enabling diatom success in dynamic environments, including their relationship to other microorganisms (Seymour et al. 2017). Also, it raises the question if metabolic profiles observed in diatoms are conserved across algal groups and how the metabolome changes under non-steady state growth. Additionally, such advanced insights into metabolic profile shifts within diatoms based on growth condition manipulations can be useful for bioproduction of targeted metabolites (Fernie et al. 2012) that are useful for optimizing lipid production for biofuels (Chisti 2008; Levitan et al. 2014), discovering alternative ecofriendly antifoulants (Réveillon et al 2019) and providing a foundation for nanotechnological innovations from the diatom biomineral exoskeleton (Kröger & Poulsen 2008).

As technological advances continue to improve and provide higher resolution into cellular composition, having a sound mechanistic understanding of metabolic processes will be paramount to connect traditional and emergent techniques to assess PP and also make accurate cellular networks of energy fluxes that allow survival in challenging environments. The novelty of my work (e.g. Chapter 4) created a framework whereby light-driven metabolic profile differences provided insight into key metabolites that served as diagnostic biomarkers for (photo)physiological responses – currently retrieved via fluorescence, oxygen and carbon measures (as seen in Chapters 2 and 3) – that can ultimately lead to more comprehensive and informative energy budget models.

5.1.5. Energy budgets: steady vs non-steady state assessments

Assessing productivity involves measuring cellular currencies (e.g. fluorescence, oxygen and carbon) where the balancing of energy between production and consumption processes can be organised using an energy budget model (Fig 5.2). Historically, energy budgets have accounted for, at most, two cellular currencies, primarily carbon and oxygen while fluorescence – hence light energy flux yields – have not been included (Halsey et al. 2010, 2013; Shi et al. 2015; Fisher & Halsey 2016). The carbon fraction remaining as biomass is then, at times, further fractionated into macromolecular pools of lipids, carbohydrates and proteins to gain insight into the reduced state of carbon that is ultimately retained in biomass (Halsey et al. 2011; Bittar et al. 2013; Inomura et al. 2020). Rarely is this biofractionation of macromolecules included in the overall energy budget schematic (Fig 5.2A). Current energy budgets, from my work, incorporate the fluorescence-derived measures of light energy allocation where YNO and YNPQ are the yields of light energy dissipated via constitutive fluorescence/heat and regulated heat, respectively (Fig 5.2B). The remaining light energy is used for photochemical conversion (YII; Chapters 2 and 3) that can be allocated to cellular metabolic processes (Chapter 4), involving oxygen and carbon, resulting in biomass (i.e. net primary production). Here, metabolomics was used to gain deeper insight into specific allocations of photosynthetically generated energy to carbon metabolites opposed to generalised biofractionation of macromolecules. Yet, key metabolites observed between light treatments (Chapter 4) were not included in the overall energy budget model thus for a more comprehensive energy budgets, future works should aim to include energy fluxes via fluorescence, oxygen and metabolites (Fig 5.2C)

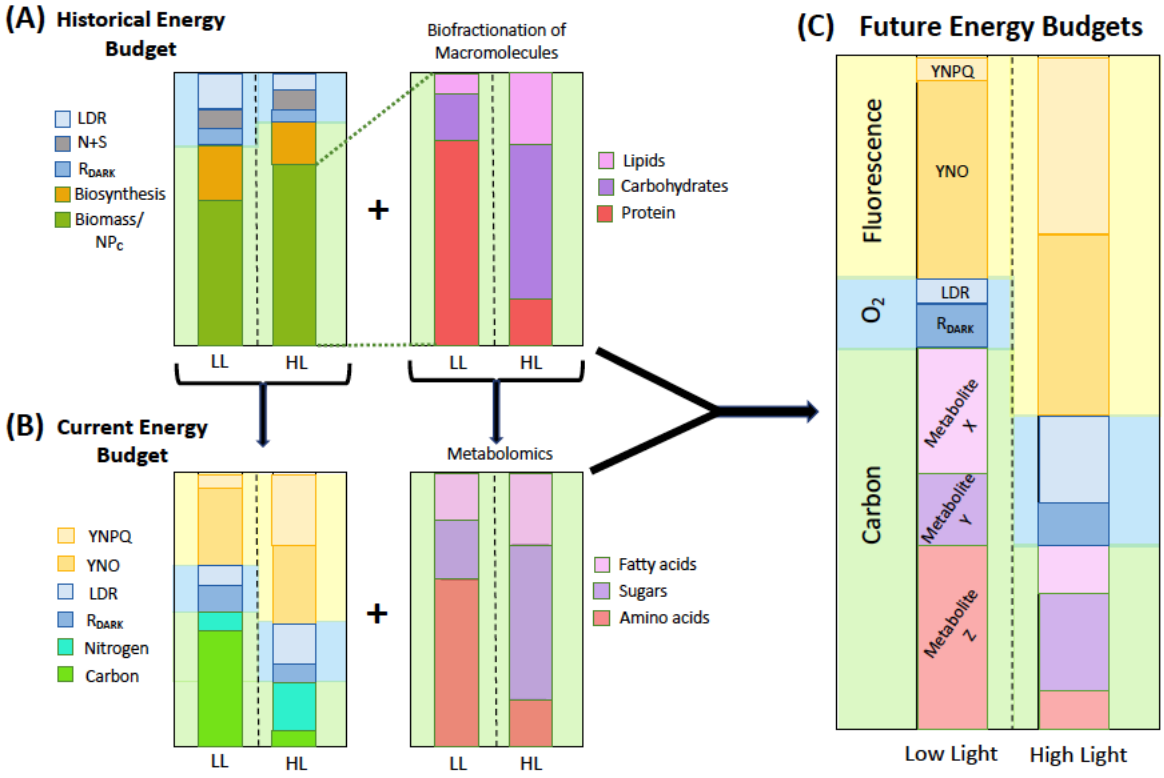

Figure 5.2 Development of energy budget models using cellular currencies – carbon (green background), oxygen (blue background) and fluorescence (yellow background) – from (A) historical, (B) current to (C) proposed future models. Historical energy budget models typically include two cellular currencies and a separate biofractionation of macromolecules. Current energy budgets account for the three cellular currencies but does not include that deeper carbon insight gained from metabolomics. Future energy budgets models could integrate all cellular currencies including the information gained from further partitioning of carbon molecules (e.g. metabolites). Such comprehensive energy budgets will provide more accurate accounting of energy that ultimately is retained in biomass under various environmental stressors. Data was adapted from (A) Fisher & Halsey (2016) and (B) Chapters 2 and 3 where sub-fractionations within cellular currencies are measurements that were collected from diatoms in response to light.

Importantly, the energy budgets available to date, including the work of my thesis, are largely based on growth under steady-state conditions where the information gained reflects acclimation to regular resource supply (even if these resources are limiting). Steady-state experiments offer a foundation from which data collected from non-steady state growth can improve insights into physiological adjustments that are more representative of natural assemblages. Thus, having energy budget models from cultures grown under non-steady state growth can reveal the complexities of assessing cellular processes that contribute to competitive performance in natural environments that are ever-changing (Moore et al. 2013).

5.1.6. Towards improving energy budgets and primary productivity models

The foundation of energy budget and PP models are attributed to measures of cellular currencies such as carbon (most common), oxygen and fluorescence (emerging). Since the introduction of fluorescence to assess photophysiology, our understanding of phytoplankton light harvesting capacity has greatly improved whereby concomitant physiological assessments of metabolic processes have revealed correlations between light harvesting and processes downstream of PSII (Chapters 2 and 3). Particularly, over the past two decades efforts have focused on connecting fluorescence to derive carbon uptake rates and, while the results thus far are mixed, the ability to retrieve accurate estimates of PP in real-time is invaluable (Moore et al. 2003; Lawrenz et al 2013; Gorbunov & Falkowski 2021). Efforts to link fluorescence-derived electron transfer from PSII (ETR_{PSII}) and carbon-uptake rates remain focussed on this goal (Moore et al. 2006; Shuback et al. 2017; Hughes et al. 2018). Photoacclimation status –

routinely parameterised as E_k (the light saturation index of photosynthesis) – is most commonly derived from PE curves of carbon uptake and have been used extensively in models to derive productivity (Behrenfeld et al. 2004; Moore et al. 2006); intriguingly, fluorometric-derived values E_k have received much less attention.

From the novel use of fluorescence-derived photoacclimation (i.e. $E_{k,YII}$), I showed a strong correlation with carbon retained in biomass between both diatoms studied (Chapter 3, Fig 3.7C,D). Additionally, I found $E_{k,YII}$ correlated well with measures of oxygen production and consumption, opening the potential to use $E_{k,YII}$ to assess multiple metabolic processes contributing to PP. Such insight is particularly intriguing where new algorithms are emerging that can 'instantaneously' capture $E_{k,YII}$ from individual induction measures – and without the need for time consuming fluorescence light response curves (e.g. Gorbunov & Falkowski 2021), potentially providing an extremely high throughout means to examine dynamic metabolic reorganisation. Still, such notions are preliminary and rest on future validation of the application of $E_{k,YII}$ in natural aquatic ecosystems, and how this factor can describe changes in respiratory and carbon storage metrics.

5.2. Future Directions

The culmination of my work has provided a foundation for future research to combine fluorometric assessment of photo-protective capacities with metabolic processes via simultaneous measures of oxygen consumption/production and metabolic profiles. Additionally, my work has raised new questions and highlighted gaps in the literature on whether and how metabolic processes linked to fluorescence are conserved with

ecological niche amongst other diatom species of varying size and shape (Blommaert et al. 2018) as well as across other algal groups (Ware et al. 2020). There are several key research priorities that will progress our current mechanistic understanding of energetic fluxes using cellular currencies that will ultimately lead to improved energy budget and PP models:

- Increased research that focuses on photo-protective capacities to include all phytoplankton groups and determine the extent by which nonphotochemical quenching responses are conserved with ecological niche. Knowledge of conserved photo-protective capacities amongst algal groups with ecological niche would allow interpretations of fluorescence data to be generalised based on location. Indeed, the accuracy of future models of PP would improve with knowledge that fluorescence signals are linked to metabolic processes than can be correlated with specific regions of ocean. Such regions of the ocean that could be considered include generalized regions (e.g. oceanic, coastal, estuarine) as well as regions distinguished by latitudes – specifically high latitudes in regard to climate change impact and dominance of diatoms – and biogeochemical signatures.
- Respiration is critical for modelling PP in marine systems (Platt et al. 1991), thus a more comprehensive dataset of oxygen-based measures that account for both light-dependent (LDR) and -independent (R_{DARK}) respiration during the day needs to be collected. With this knowledge, the use of constant dark respiration rates, that underestimate rates in the light, can be replaced by more accurate respiratory O_2 consumption contributions occurring simultaneously with photosynthetic O_2 evolution to improve energy budget models. Currently,

there are roadblocks to compiling datasets of respiratory contributions in the light that need to be addressed. An expensive labelled oxygen isotope is essential to measure simultaneous oxygen production and consumption in the light, via MIMS – an instrument that is bulky, expensive and tedious to operate (Falkowski & Raven 2013). As such, the number of MIMS in laboratories worldwide is limited, thus requiring the community invest efforts to making this instrument pool more readily accessible. Additionally, having standardised protocols for sample collection (incubation vs real-time measures), handling and processing would further expedite compiling datasets across research groups.

- Metabolomics is a powerful tool providing a snap-shot of metabolic profiles that are specific to the current growth conditions. Cellular processes are continually adjusting to balance energetic needs based on environmental conditions to optimise growth. From laboratory-controlled environments, I found unique light-driven metabolic profiles; however, as this was the first metabolomics study on the effect of light in diatoms, more research is needed to validate my findings. Specifically, I found metabolites involved in photorespiration which is intriguing as photorespiration in diatoms is often considered to be a minor process given the presence of carbon concentration mechanisms (CCMs, Giordano et al. 2005). Metabolomics could thus provide diagnostic biomarkers that are indicative of respiratory processes and carbon gating pathways. The ultimate aim for future research is to identify key metabolites that can provide direct insight into metabolic processes that influence energy budgets and PP models especially in the natural environment were change occurs – and is occurring – rapidly.

- Fluorescence, respiration and metabolomics provide useful insights of (photo)physiology but independently cannot provide a complete accounting of energy fluxes that optimise cellular growth. Future research will need to use a more integrated framework of photobiology (fluorescence) and metabolism (respiration, metabolic profiles) to better capture empirical relationships that can collectively improve model foundations. Indeed, respiration remains a poorly understood and quantified process such that this incomplete knowledge of respiration dynamics prevents a deeper understanding of PP (Williams & del Giorgio 2005, Bailleul et al. 2017), but it is not enough to focus on just one cellular currency. Fluorescence and carbon (metabolomics) data must be concomitantly collected with oxygen measures before we can solely depend on a single parameter (e.g. fluorescence) to achieve accurate estimates of global PP.

Overall, I have shown associations between fluorometric-derived photo-protective capacities and metabolic process (e.g. respiration) with the potential to use key metabolites as biomarkers of photo(physiology). Laboratory and field-based studies would greatly benefit from exploiting the rapid, real-time and *in situ* capacity with which active chlorophyll fluorescence can describe the highly dynamic variability of PP (Kolber & Falkowski 1995, Suggett et al. 2009; Du et al. 2018). Future studies should aim to incorporate concomitant measure of fluorescence, oxygen and carbon when generating energy budgets. Adaptive models are beginning to emerge that account for dynamic physiological processes (i.e. respiration) (Lindemann et al. 2015) that have largely to-date been assumed to be a constant determined from measures of

respiration in the dark, which I have proven is simply not sufficient (Chapter 3). Global assessments of PP could be separated into domains (Longhurst et al. 1995; Rothstein et al. 2006) where ecological niche-dependent (photo)physiologies can be the guiding factor. Indeed, a model is only as good as the mechanistic understanding of physiological processes and supporting quality laboratory- and field-based datasets.

5.3. Conclusion

In a world where change is happening at unprecedented rates via anthropogenic activity, developing a more a robust mechanistic understanding of energy fluxes that will allow for more accurate assessments of PP is of utmost importance to monitor, predict and ultimately manage ocean health and the energy available for higher trophic levels (i.e. food security). Especially, given phytoplankton are the base of aquatic food webs, if the mixed layer within the water column shallows thus exposing phytoplankton to higher light intensities for longer durations (Behrenfeld 2014) and the flux of nutrients to surface waters decreases, it is likely to disrupt the current balance of ocean ecosystems. Such abiotic changes are already showing an impact on phytoplankton in Antarctic (Petrou & Ralph 2011; Joy-Warren et al. 2019; Bozzato et al. 2019) and Arctic (Lacour et al. 2018; Croteau et al. 2020) waters, where the increase in irradiance may actually improve PP for some species (Lewis et al. 2020); although, how marine ecosystems as a whole will ultimately appear and function remains uncertain (Boyd et al. 2010; Post et al. 2013; Gao et al. 2018; Oziel et al. 2020). Imbalances within phytoplankton PP influence ocean health that will ultimately lead to cascading global impacts, to an extent we cannot predict with confidence.

For over a century, members of the scientific community have attempted to empirically model estimates of PP but our mechanistic understanding - and associated datasets – of fundamental metabolic processes is not robust to support the rapid pace of model development. Since the introduction of fluorescence, the possibility to derive measures of PP using such methods has been the driving force behind much research, particularly for oceanographers (Behrenfeld et al. 2005; Bouman et al. 2019). The ability to replace incubation-based carbon uptake and oxygen measures of productivity with an incubation-free and non-invasive method is game changing, especially when fluorescence can be derived from satellites (Behrenfeld et al. 2009). Efforts towards this goal have increasingly gained traction yielding substantially more published works aiming to connect fluorescence to get to PP; however, future progress is contingent on improvements made in datasets for metabolic process, including both photosynthesis and respiration.

The culmination of this thesis has shown that (in)accuracy of energy budgets and PP models can be evidenced by deeper insight into evolved adaptive (photo)physiological strategies of diatoms, whereby trade-offs between photo-protective capacities and dependence on oxidase activity reflect ecological niche. My work incorporated fluorescence-, oxygen-, and 'omics'-based assessments of diatom responses to light whereby fundamental gaps in knowledge were addressed to resolve the contribution of light-dependent respiratory processes to GP_{O2} that I found were closely associated with photo-protective capacity. The mechanistic understanding that is gained from monitoring changes over a day allow for better, and more accurate, integration of the contributions with various metabolic processes alter cellular energy budgets.

Respiration in the light can no longer be ignored given the species-specific and light-dependent contributions to GP_{O2} I found (Chapters 2 and 3) or considered an acceptable equivalent to arbitrary measures of dark respiration. Connecting fluorescence with metabolic processes offers a promising solution to provide robust estimate of PP in real-time; however, this work is preliminary. Building on the dataset collected from this thesis, future works can start to fill the fundamental gaps in knowledge that is stunting progress towards more accurate productivity measures that are ultimately indicative of ocean health.

References

Amin, S. A., Parker, M. S., & Armbrust, E. V. (2012). Interactions between Diatoms and Bacteria. *Microbiology and Molecular Biology Reviews*, *76*(3), 667–684. https://doi.org/10.1128/mmbr.00007-12

Amin, S. A., Hmelo, L. R., Van Tol, H. M., Durham, B. P., Carlson, L. T., Heal, K. R., … Armbrust, E. V. (2015). Interaction and signalling between a cosmopolitan phytoplankton and associated bacteria. *Nature*, *522*(7554), 98–101. https://doi.org/10.1038/nature14488

Bailleul, B., Park, J., Brown, C. M., Bidle, K. D., Lee, S. H., & Falkowski, P. G. (2017). Direct measurements of the light dependence of gross photosynthesis and oxygen consumption in the ocean. *Limnology and Oceanography*, *62*(3), 1066–1079. https://doi.org/10.1002/lno.10486

Barnett, A., Méléder, V., Blommaert, L., Lepetit, B., Gaudin, P., Vyverman, W., … Lavaud, J. (2015). Growth form defines physiological photo-protective capacity in intertidal benthic diatoms. *ISME Journal*, *9*(1), 32–45. https://doi.org/10.1038/ismej.2014.105

Behrenfeld, M. J. (2014). Climate-mediated dance of the plankton. *Nature Climate Change*, *4*(10), 880–887. https://doi.org/10.1038/nclimate2349

Behrenfeld, M. J., Boss, E., Siegel, D. A., & Shea, D. M. (2005). Carbon-based ocean productivity and phytoplankton physiology from space. *Global Biogeochemical Cycles*, *19*(1), 1–14. https://doi.org/10.1029/2004GB002299

Behrenfeld, M. J., & Falkowski, P. G. (1997). A consumer's guide to phytoplankton primary productivity models. *Limnology and Oceanography*, *42*(7), 1479–1491. https://doi.org/10.4319/lo.1997.42.7.1479

Behrenfeld, M. J., Halsey, K. H., & Milligan, A. J. (2008). Evolved physiological responses of phytoplankton to their integrated growth environment. *Philosophical Transactions of the Royal Society B: Biological Sciences*, *363*(1504), 2687–2703. https://doi.org/10.1098/rstb.2008.0019

Behrenfeld, M. J., Prasil, O., Babin, M., & Bruyant, F. (2004). In search of a physiological basis for covariations in light-limited and light-saturated photosynthesis. *Journal of Phycology*, *40*(1), 4–25. https://doi.org/10.1046/j.1529-8817.2004.03083.x

Behrenfeld, M. J., Westberry, T. K., Boss, E. S., O'Malley, R. T., & Siegel, D. A. (2009). Satellite-detected fluorescence reveals global physiology of ocean phytoplankton. *Biogeosciences*, *6*(5), 779–794. https://doi.org/10.5194/bg-6-779-2009

Bittar, T. B., Lin, Y., Sassano, L. R., Wheeler, B. J., Brown, S. L., Cochlan, W. P., & Johnson, Z. I. (2013). Carbon allocation under light and nitrogen resource gradients in two model marine phytoplankton1. *Journal of Phycology*, *49*(3), 523–535. https://doi.org/10.1111/jpy.12060

Blommaert, L., Lavaud, J., Vyverman, W., & Sabbe, K. (2018). Behavioural versus physiological photo-protection in epipelic and epipsammic benthic diatoms. *European Journal of Phycology*, *53*(2), 146–155. https://doi.org/10.1080/09670262.2017.1397197

Bouman, H. A., Platt, T., Doblin, M., Figueiras, F. G., Gudmundsson, K., Gudfinnsson, H. G., … Sathyendranath, S. (2018). Photosynthesis-irradiance parameters of marine phytoplankton: Synthesis of a global data set. *Earth System Science Data*, *10*(1), 251–266. https://doi.org/10.5194/essd-10-251-2018

Boyd, P. W., Strzepek, R., Fu, F., & Hutchins, D. A. (2010). Environmental control of open-ocean phytoplankton groups: Now and in the future. *Limnology and Oceanography*, *55*(3), 1353–1376. https://doi.org/10.4319/lo.2010.55.3.1353

Bozzato, D., Jakob, T., & Wilhelm, C. (2019). Effects of temperature and salinity on respiratory losses and the ratio of photosynthesis to respiration in representative Antarctic phytoplankton species. *PLoS ONE*, *14*(10), 1–19. https://doi.org/10.1371/journal.pone.0224101

Burris, J. E. (1980) Respiration and Photorespiration in Marine Algae. In: Falkowski P.G. (eds) Primary Productivity in the Sea. Environmental Science Research, vol 19. Springer, Boston, MA. https://doi.org/10.1007/978-1-4684-3890-1_23

Chisti, Y. (2008) Biodiesel from microalgae beats bioethanol. *Trends Biotechnol*. 26, 126–131

Croteau, D., Guérin, S., Bruyant, F., Ferland, J., Campbell, D. A., Babin, M., & Lavaud, J. (2020). Contrasting nonphotochemical quenching patterns under high light and darkness aligns with light niche occupancy in Arctic diatoms. *Limnology and Oceanography*, 1–15. https://doi.org/10.1002/lno.11587

Dimier, C., Brunet, C., Geider, R., & Raven, J. (2009). Growth and photoregulation dynamics of the picoeukaryote Pelagomonas calceolata in fluctuating light. *Limnology and Oceanography*, *54*(3), 823–836. https://doi.org/10.4319/lo.2009.54.3.0823

Du, N., Gholami, P., Kline, D. I., DuPont, C. L., Dickson, A. G., Mendola, D., … Greg Mitchell, B. (2018). Simultaneous quantum yield measurements of carbon uptake and oxygen evolution in microalgal cultures. *PLoS ONE*, *13*(6), 1–21. https://doi.org/10.1371/journal.pone.0199125

Falkowski, P., & Owens, T. (1978). Effects of light intensity on photosynthesis and dark respiration in six species of marine phytoplankton. *Marine Biology*, *45*(4), 289–295.

Falkowski, P. G., & Raven, J. A. (2013). *Aquatic photosynthesis*. Princeton University Press.

Fernie, A. R., Obata, T., Allen, A. E., Araújo, W. L., & Bowler, C. (2012). Leveraging metabolomics for functional investigations in sequenced marine diatoms. *Trends in Plant Science*, *17*(7), 395–403. https://doi.org/10.1016/j.tplants.2012.02.005

Fisher, N. L., & Halsey, K. H. (2016). Mechanisms that increase the growth efficiency of diatoms in low light. *Photosynthesis Research*, *129*(2), 183–197. https://doi.org/10.1007/s11120-016-0282-6

Gao, G., Shi, Q., Xu, Z., Xu, J., Campbell, D. A., & Wu, H. (2018). Global warming interacts with ocean acidification to alter PSII function and protection in the diatom Thalassiosira weissflogii. *Environmental and Experimental Botany*, *147*(October 2017), 95–103. https://doi.org/10.1016/j.envexpbot.2017.11.014

Giordano, M., Beardall, J., & Raven, J. A. (2005). CO 2 concentrating mechanisms in algae: mechanisms, environmental modulation, and evolution. *Annu. Rev. Plant Biol.*, *56*, 99-131.

Goss, R., & Lepetit, B. (2015). Biodiversity of NPQ. *Journal of Plant Physiology*, *172*, 13–32. https://doi.org/10.1016/j.jplph.2014.03.004

Gorbunov, M. Y., & Falkowski, P. G. (2021). Using chlorophyll fluorescence kinetics to determine photosynthesis in aquatic ecosystems. *Limnology and Oceanography*, *66*, 1–13. https://doi.org/10.1002/lno.11581

Gorbunov, M. Y., Shirsin, E., Nikonova, E., Fadeev, V. V., & Falkowski, P. G. (2020). A multi-spectral fluorescence induction and relaxation (fire) technique for

physiological and taxonomic analysis of phytoplankton communities. *Marine Ecology Progress Series*, *644*, 1–13. https://doi.org/10.3354/meps13358

Halsey, K. H., & Jones, B. M. (2015). Phytoplankton Strategies for Photosynthetic Energy Allocation. *Annual Review of Marine Science*, *7*(1), 265–297. https://doi.org/10.1146/annurev-marine-010814-015813

Halsey, K. H., O'Malley, R. T., Graff, J. R., Milligan, A. J., & Behrenfeld, M. J. (2013). A common partitioning strategy for photosynthetic products in evolutionarily distinct phytoplankton species. *New Phytologist*, *198*(4), 1030–1038. https://doi.org/10.1111/nph.12209

Halsey, K. H., Milligan, A. J., & Behrenfeld, M. J. (2011). Linking time-dependent carbon-fixation efficiencies in Dunaliella Tertiolecta (Chlorophyceae) to underlying metabolic pathways. *Journal of Phycology*, *47*(1), 66–76. https://doi.org/10.1111/j.1529-8817.2010.00945.x

Halsey, K. H., Milligan, A. J., & Behrenfeld, M. J. (2010). Physiological optimization underlies growth rate-independent chlorophyll-specific gross and net primary production. *Photosynthesis Research*, *103*(2), 125–137. https://doi.org/10.1007/s11120-009-9526-z

Henderikx Freitas, F., White, A. E., & Quay, P. D. (2020). Diel Measurements of Oxygen- and Carbon-Based Ocean Metabolism Across a Trophic Gradient in the North Pacific. *Global Biogeochemical Cycles*, *34*(11). https://doi.org/10.1029/2019GB006518

Hughes, D. J., Campbell, D. A., Doblin, M. A., Kromkamp, J. C., Lawrenz, E., Moore, C. M., … Suggett, D. J. (2018). Roadmaps and Detours: Active Chlorophyll- a Assessments of Primary Productivity Across Marine and Freshwater Systems. *Environmental Science and Technology*, *52*(21), 12039–12054. https://doi.org/10.1021/acs.est.8b03488

Inomura, K., Omta, A. W., Talmy, D., Bragg, J., Deutsch, C., & Follows, M. J. (2020). A Mechanistic Model of Macromolecular Allocation, Elemental Stoichiometry, and Growth Rate in Phytoplankton. *Frontiers in Microbiology*, *11*(February), 1–22. https://doi.org/10.3389/fmicb.2020.00086

Jakob, T., Wagner, H., Stehfest, K., & Wilhelm, C. (2007). A complete energy balance from photons to new biomass reveals a light- and nutrient-dependent variability in the metabolic costs of carbon assimilation. *Journal of Experimental Botany*, *58*(8), 2101–2112. https://doi.org/10.1093/jxb/erm084

Joy-Warren, H. L., van Dijken, G. L., Alderkamp, A. C., Leventer, A., Lewis, K. M., Selz, V., … Arrigo, K. R. (2019). Light Is the Primary Driver of Early Season Phytoplankton Production Along the Western Antarctic Peninsula. *Journal of Geophysical Research: Oceans*, *124*(11), 7375–7399. https://doi.org/10.1029/2019JC015295

Kolber, Z., & Falkowski, P. G. (1995). Variations in Chlorophyll fluorescence yields in phytoplankton in the World Oceans. *Australian Journal of Plant Physiology*, *22*, 341–355.

Kröger, N. & Poulsen, N. (2008) Diatoms - from cell wall biogenesis to nanotechnology. *Annu. Rev. Genet*. 42, 83–107

Lacour, T., Larivière, J., Ferland, J., Bruyant, F., Lavaud, J., & Babin, M. (2018). The role of sustained photo-protective non-photochemical quenching in low temperature and high light acclimation in the bloom-forming arctic diatom Thalassiosira gravida. *Frontiers in Marine Science*, *5*(OCT). https://doi.org/10.3389/fmars.2018.00354

Langdon, C. (1993). The significance of respiration in production measurements based on oxygen. *ICES Mar. Sci. Symp.*, *197*, 69–78. Retrieved from https://www.researchgate.net/publication/230889097

Lavaud, J., & Lepetit, B. (2013). An explanation for the inter-species variability of the photo-protective non-photochemical chlorophyll fluorescence quenching in diatoms. *Biochimica et Biophysica Acta - Bioenergetics*, *1827*(3), 294–302. https://doi.org/10.1016/j.bbabio.2012.11.012

Lavaud, J., Strzepek, R. F., & Kroth, P. G. (2007). Photo-protection capacity differs among diatoms: possible consequences on the spatial distribution of diatoms related to fluctuations in the underwater light Climate. *Limnology and Oceanography*, *52*(3), 1188–1194. https://doi.org/10.2307/4499689

Lawrenz, E., Silsbe, G., Capuzzo, E., Ylöstalo, P., Forster, R. M., Simis, S. G. H., … Suggett, D. J. (2013). Predicting the Electron Requirement for Carbon Fixation in Seas and Oceans. *PLoS ONE*, *8*(3). https://doi.org/10.1371/journal.pone.0058137

Lewis, K. M., Van Dijken, G. L., & Arrigo, K. R. (2020). Changes in phytoplankton concentration now drive increased Arctic Ocean primary production. *Science*, *369*(6500), 198–202. https://doi.org/10.1126/science.aay8380

Lin, H., Kuzminov, F. I., Park, J., Lee, S. H., Falkowski, P. G., & Gorbunov, M. Y. (2016). Phytoplankton: The fate of photons absorbed by phytoplankton in the global ocean. *Science*, *351*(6270), 264–267. https://doi.org/10.1126/science.aab2213

Lindemann, C., Backhaus, J. O., & St John, M. A. (2015). Physiological constrains on Sverdrup's Critical-Depth-Hypothesis: The influences of dark respiration and sinking. *ICES Journal of Marine Science*, *72*(6), 1942–1951. https://doi.org/10.1093/icesjms/fsv046

Longhurst, A., Sathyendranath, S., Platt, T., & Caverhill, C. (1995). An estimate of global primary production in the ocean from satellite radiometer data. *Journal of plankton Research*, *17*(6), 1245-1271.

Longnecker, K., & Kujawinski, E. B. (2017). Mining mass spectrometry data: Using new computational tools to find novel organic compounds in complex environmental mixtures. *Organic Geochemistry*, *110*, 92–99. https://doi.org/10.1016/j.orggeochem.2017.05.008

Macintyre, H. L., Kana, T. M., Anning, T., & Geider, R. J. (2002). Photoacclimation of photosynthesis irradiance response curves and photosynthetic pigments in microalgae and cyanobacteria. *Journal of Phycology*, *38*(1), 17–38. https://doi.org/10.1046/j.1529-8817.2002.00094.x

Macintyre, H. L., Kana, T. M., & Geider, R. J. (2000). The effect of water motion on short-term rates of photosynthesis by marine phytoplankton. *Trends in Plant Science*, *5*(1), 12–17. https://doi.org/10.1016/S1360-1385(99)01504-6

Moore, C. M., Suggett, D. J., Hickman, A. E., Kim, Y.-N., Tweddle, J. F., Sharples, J., … Holligan, P. M. (2006). Phytoplankton photoacclimation and photoadaptation in response to environmental gradients in a shelf sea. *Limnol. Oceanogr*, *51*(2), 936–949. Retrieved from https://aslopubs.onlinelibrary.wiley.com/doi/pdf/10.4319/lo.2006.51.2.0936

Moore, C. M., Suggett, D., Holligan, P. M., Sharples, J., Abraham, E. R., Lucas, M. I., … Hydes, D. J. (2003). Physical controls on phytoplankton physiology and production at a shelf sea front: a fast repetition-rate fluorometer based study. *Marine Ecology Progress Series*, *259*, 29–45. Retrieved from papers://64c875cb-35e9-49cc-86a7-69f7bda703f6/Paper/p9

Moore, C. M., Mills, M. M., Arrigo, K. R., Berman-Frank, I., Bopp, L., Boyd, P. W., … Ulloa, O. (2013). Processes and patterns of oceanic nutrient limitation. *Nature Geoscience*, *6*(9), 701–710. https://doi.org/10.1038/ngeo1765

Oziel, L., Baudena, A., Ardyna, M., Massicotte, P., Randelhoff, A., Sallée, J. B., … Babin, M. (2020). Faster Atlantic currents drive poleward expansion of temperate phytoplankton in the Arctic Ocean. *Nature Communications*, *11*(1), 1–8. https://doi.org/10.1038/s41467-020-15485-5

Peers, G., & Price, N. M. (2006). Copper-containing plastocyanin used for electron transport by an oceanic diatom. *Nature*, *441*(7091), 341–344. https://doi.org/10.1038/nature04630

Petrou, K., & Ralph, P. J. (2011). Photosynthesis and net primary productivity in three Antarctic diatoms: Possible significance for their distribution in the Antarctic marine ecosystem. *Marine Ecology Progress Series*, *437*, 27–40. https://doi.org/10.3354/meps09291

Platt, T. C., Bird, D. F., Sathyendranath, S., & Cushing, D. H. (1991). Critical depth and marine primary production. *Proceedings of the Royal Society of London. Series B: Biological Sciences*, *246*(1317), 205–217. https://doi.org/10.1098/rspb.1991.0146

Post, E., Bhatt, U. S., Bitz, C. M., Brodie, J. F., Fulton, T. L., Hebblewhite, M., … Walker, D. A. (2013). Ecological Consequences of Sea-Ice Decline. *Science*, *341*(6145), 519–524. https://doi.org/10.1126/science.1235225

Raven, J. A., Giordano, M., Beardall, J., & Maberly, S. C. (2012). Algal evolution in relation to atmospheric CO2: carboxylases, carbon-concentrating mechanisms and carbon oxidation cycles. *Philosophical Transactions of the Royal Society B: Biological Sciences*, *367*(1588), 493-507.

Raven, J. A. (1997). Inorganic carbon acquisition by marine autotrophs. *Advances in botanical research*, *27*, 85-209.

Réveillon, D., Tunin-Ley, A., Grondin, I., Othmani, A., Zubia, M., Bunet, R., … Briand, J. F. (2019). Exploring the chemodiversity of tropical microalgae for the discovery of natural antifouling compounds. *Journal of Applied Phycology*, *31*(1), 319–333. https://doi.org/10.1007/s10811-018-1594-z

Rothstein, L. M., Cullen, J. J., Abbott, M., Chassignet, E. P., Denman, K., Doney, S. C., … Yoder, J. (2006). Modeling Ocean Ecosystems: The PARADIGM Program. *Oceanography*, *19.1*, 22–51. https://doi.org/10.5670/oceanog.2006.89

Schuback, N., Hoppe, C. J., Tremblay, J. É., Maldonado, M. T., & Tortell, P. D. (2017). Primary productivity and the coupling of photosynthetic electron transport and carbon fixation in the Arctic Ocean. *Limnology and Oceanography*, *62*(3), 898-921.

Seymour, J. R., Amin, S. A., Raina, J. B., & Stocker, R. (2017). Zooming in on the phycosphere: The ecological interface for phytoplankton-bacteria relationships. *Nature Microbiology*, *2*(May). https://doi.org/10.1038/nmicrobiol.2017.65

Shi, D., Li, W., Hopkinson, B. M., Hong, H., Li, D., Kao, S. J., & Lin, W. (2015). Interactive effects of light, nitrogen source, and carbon dioxide on energy metabolism in the diatom Thalassiosira pseudonana. *Limnology and Oceanography*, *60*(5), 1805–1822. https://doi.org/10.1002/lno.10134

Strzepek, R. F., & Harrison, P. J. (2004). Photosynthetic architecture differs in coastal and oceanic diatoms. *Nature*, *431*(7009), 689. https://doi.org/10.1038/nature02954

Su, W., Jakob, T., & Wilhelm, C. (2012). The impact of nonphotochemical quenching of fluorescence on the photon balance in diatoms under dynamic light conditions. *Journal of Phycology*, *48*(2), 336–346. https://doi.org/10.1111/j.1529-8817.2012.01128.x

Suggett, D. J., Goyen, S., Pettay, D. T., Szabó, M., Warner, M. E., Evenhuis, C., & Ralph, P. J. (2015). Functional diversity of photobiological traits within the genus Symbiodinium appears to be governed by the interaction of cell size with cladal designation. *New Phytologist*, *208*(2), 370–381. https://doi.org/10.1111/nph.13483

Suggett, D. J., Moore, C. M., Hickman, A. E., & Geider, R. J. (2009). Interpretation of fast repetition rate (FRR) fluorescence: Signatures of phytoplankton community structure versus physiological state. *Marine Ecology Progress Series*, *376*, 1–19. https://doi.org/10.3354/meps07830

van de Poll, W. H., Buma, A. G. J., Visser, R. J., Janknegt, P. J., Villafane, V. E., & Helbling, E. W. (2010). Xanthophyll cycle activity and photosynthesis of Dunaliella tertiolecta (Chlorophyceae) and Thalassiosira weissflogii (Bacillariophyceae) during fluctuating solar radiation. *Phycologia*, *49*(3), 249–259.

Wagner, H., Jakob, T., & Wilhelm, C. (2006). Balancing the energy flow from captured light to biomass under fluctuating light conditions. *New Phytologist*, *169*(1), 95–108. https://doi.org/10.1111/j.1469-8137.2005.01550.x

Wagner, H., Jakob, T., Fanesi, A., & Wilhelm, C. (2017). Towards an understanding of the molecular regulation of carbon allocation in diatoms: The interaction of energy and carbon allocation. *Philosophical Transactions of the Royal Society B: Biological Sciences*, *372*(1728). https://doi.org/10.1098/rstb.2016.0410

Ware, M. A., Hunstiger, D., Cantrell, M., & Peers, G. (2020). A chlorophyte alga utilizes alternative electron transport for primary photo-protection. *Plant Physiology*, *183*(4), 1735–1748. https://doi.org/10.1104/pp.20.00373

Williams, P. L. B., & del Giorgio, P. A. (2005). Respiration in aquatic ecosystems: history and background. *Respiration in aquatic ecosystems*, 1-17.

Williams, P. J. L. B., Quay, P. D., Westberry, T. K., & Behrenfeld, M. J. (2013). The oligotrophic ocean is autotrophic. *Annual Review of Marine Science*, *5*, 535–549. https://doi.org/10.1146/annurev-marine-121211-172335